UNIVERSIDAD COMPLUTENSE DE MADRID

FACULTAD DE CIENCIAS BIOLÓGICAS

Departamento de Bioquímica y Biología Molecular I

TESIS DOCTORAL

Implicación de AMPK en la señalización intracelular inducida por CCR_7 en las células dendríticas

MEMORIA PARA OPTAR AL GRADO DE DOCTOR

PRESENTADA POR

Pilar López-Cotarelo García de Diego

Director

José Luis Rodríguez Fernández

Madrid, 2017

Universidad complutense de Madrid

Facultad de Ciencias Biológicas

Dpto de Bioquímica y Biología Molecular I

IMPLICACIÓN DE AMPK EN LA SEÑALIZACIÓN INTRACELULAR INDUCIDA POR CCR7 EN LAS CÉLULAS DENDRÍTICAS

Tesis Doctoral

Pilar López-Cotarelo García de Diego

UNIVERSIDAD COMPLUTENSE DE MADRID

FACULTAD DE CIENCIAS BIOLÓGICAS

DPTO. DE BIOQUÍMICA Y BIOLOGÍA MOLECULAR I

IMPLICACIÓN DE AMPK EN LA SEÑALIZACIÓN INTRACELULAR INDUCIDA POR CCR7 EN LAS CÉLULAS DENDRÍTICAS

MEMORIA PARA OPTAR AL GRADO DE DOCTOR PRESENTADO POR

PILAR LÓPEZ-COTARELO GARCÍA DE DIEGO

BAJO LA DIRECCIÓN DEL DOCTOR

JOSÉ LUIS RODRÍGUEZ FERNÁNDEZ

MADRID, 2016

El Dr. José Luis Rodríguez Fernández

CERTIFICA

Que el trabajo titulado "**Implicación de AMPK en la señalización intracelular inducida por CCR7 en las células dendríticas**" que presenta Pilar López-Cotarelo García de Diego para la obtención del grado de Doctor por la Universidad Complutense de Madrid, ha sido realizado bajo mi dirección y reúne la calidad y contenidos suficientes para que se presentado ante el tribunal correspondiente.

Para que así conste a los efectos oportunos se expide el presente certificado en Madrid a 30 de Septiembre del 2016.

AGRADECIMIENTOS

Por supuesto no hubiera logrado llegar hasta aquí sin la ayuda de muchas personas, a las que quiero dar las gracias:

José Luis, gracias por darme la oportunidad de realizar este proyecto, por guiarme, enseñarme y contagiarme de tu pasión por la investigación, y por hacerlo siempre con generosidad y comprensión.

Gracias a mis compañeros de laboratorio: Laura y Cris, sin vosotras no hubiera superado los malos momentos, fuisteis mi apoyo y mi fuerza; Carol y Olga, por tantas horas de discusiones científicas y, sobre todo, las no científicas, y por vuestra inestimable ayuda en la corrección, no será fácil volver a encontrar unas compañeras como vosotras; Bea y Bego, por todos esos cafés y momentos de desconexión tan necesarios para no acabar volviéndome loca del todo; Génesis, Alex y Cristina, los tres aportasteis vuestro granito de arena para que esta empresa llegase a buen puerto. Gracias a todos por tantas risas y buenos recuerdos.

Alvaro, Robb y Oleg, cada uno me abristeis la puerta en diferentes momentos y me permitisteis incorporarme a vuestros equipos. Gracias por ayudarme a aprender, crecer y enriquecerme profesional y personalmente.

Y mis otros compañeros, ahora en la distancia: Dieke, Elaine, Caroline y todos los demás que me acogisteis y me ayudasteis allí donde lo necesité.

Por último mi familia, gracias por el apoyo incondicional que me habéis dado cada día, y en especial a los dos grandes culpables de que hoy esté aquí; y Dani, por creer siempre en mí, especialmente cuando yo no he sido capaz de hacerlo.

ÍNDICE

SUMMARY

Dendritic cells (DCs) are professional antigen presenting cells capable of initiating the immune response by activating naive T lymphocytes. In their last phase of differentiation called mature CD (mDCs), these cells present antigens captured in the areas of inflammation to lymphocytes in the lymph nodes. To carry out this role, mCDs must migrate through the afferent lymphatics to the lymph nodes. The chemokine receptor CCR7, which is expressed by mDCs, is key to direct these cells to the lymph nodes. Before, it has been shown that CCR7 relays intracellular signaling resulting in the extension of the survival of mDCs. However, the mechanisms used by this receptor to promote survival are not completely understood.

AMPK (AMP-dependent Kinase) is a sensor of energy status that can detect changes in the AMP/ATP ratio. This enzyme responds to increased levels of AMP by inducing activation of catabolic and inhibition of anabolic pathways. In this thesis, it was investigated whether AMPK plays a role in CCR7-dependent regulation of survival in DCs.

We first analyzed whether AMPK kinase played a pro-apoptotic or a pro-survival role in DCs. Reduction of AMPK levels using siRNA increases the survival of human mDCs. We suggest that AMPK induces specifically apoptosis because it promotes morphological and biochemical changes associated with this type of cell death. In this regard, AMPK induces nuclear pyknosis and fragmentation and as well as a caspase-dependent cell death that involves the specific activation of caspase-3. Activation of AMPK also induces apoptosis of DCs *in vivo*, as shown in experiments where apoptosis was analyzed in popliteal lymph nodes. The data presented indicate that AMPK may induce apoptosis in DCs through two mechanisms. First, AMPK may induce translocation of the transcription factor FOXO1 from the cytoplasm to the nucleus. Once in the nucleus, FOXO1 activates the transcription of the pro-apoptotic Bcl2 family member Bim. Second, AMPK inhibits the activity of the pro-survival kinase complex mTORC1.

We also investigated the mechanism whereby CCR7 regulates AMPK activity in mat DCs. The data obtained show that CCR7 stimulation induced a rapid phosphorylation of AMPK at Ser485, a residue that inhibits the activity of this enzyme. The inhibition of AMPK activity was also supported by the decrease in the phosphorylated/activated form of the AMPK target Acetyl-CoA carboxylase. Studies using pharmacological inhibitors show that downstream of CCR7, Gαi and Gβγ subunits of protein G mediate AMPK inhibition. Although it has been shown that the

kinases Akt, S6k and PKA are able to directly phosphorylate AMPK at Ser485 in several cell types, we show that these kinases are not involved in CCR7-dependent phosphorylation of AMPK in DCs. Instead, it was found that downstream of CCR7, MEK1/2 and ERK1/2 are the key kinases inducing, phosphorylation of AMPK on Ser485. Co-immunoprecipitation experiments showed that ERK and AMPK may be components of a signaling complex that induces phosphorylation/inhibition of AMPK. Proximity ligation assays (PLA) indicate that CCR7 stimulation of DCs induces proximity between ERK and AMPK (≤40 nm), consistent with the possibility of interaction between these molecules.

In conclusion, the data presented, suggest that CCR7 uses the MEK/ERK/AMPK signaling pathway, in addition to the Akt pathway, as a complementary mechanism to switch-off pro-apoptotic signaling and to promote survival in DCs. Taken together, the data show that AMPK may be a new potential target to modulate the function of mat DC in the immune system.

RESUMEN EN ESPAÑOL

Las células dendríticas son células presentadoras de antígenos profesionales capaces de activar a los linfocitos T vírgenes e iniciar la respuesta inmune adaptativa. En su fase final de diferenciación, denominada fase de CD maduras (CDms), estos leucocitos pueden migrar a través de los vasos linfáticos aferentes hasta los ganglios linfáticos, donde presentan los antígenos capturados en las áreas de inflamación a los linfocitos T. Las CDms maduras expresan el receptor de quimioquinas CCR7 que es fundamental para que estas células se dirijan a los ganglios linfáticos. En trabajos previos se mostró que la activación de CCR7 aumenta la supervivencia de las CDms, aunque los mecanismos de señalización que regulan este proceso no se conocen por completo.

AMPK (AMP-dependent Kinase) es una molécula considerada un "guardián energético" celular debido a que es capaz de detectar cambios en la proporción AMP/ATP. En respuesta a un aumento de los niveles de AMP, AMPK activa las rutas de señalización catabólicas e inhibe las anabólicas. En esta tesis se estudia la posible implicación de AMPK en la regulación de la supervivencia de las CDs mediada por CCR7.

En primer lugar, analizamos si AMPK tiene un papel inductor de la supervivencia o de la apoptosis en las CDs. La reducción de los niveles de AMPK con un siRNA provoca un aumento de la supervivencia de las CDms, lo que indica que AMPK induce muerte en las CDs. Se sugiere que la activación de AMPK provoca una muerte de tipo apoptótico porque morfológicamente implica procesos de picnosis y de fragmentación del núcleo y bioquímicamente depende de caspasas, implicando específicamente a la caspasa-3. Los experimentos en los que se analizó la supervivencia de las células en los ganglios linfáticos mostraron que AMPK induce apoptosis de las CDs *in vivo*. Además, los resultados obtenidos indican que AMPK induce la apoptosis de las CDs mediante al menos dos mecanismos. Primero, la activación de AMPK induce la translocación del factor de transcripción FOXO1 del citoplasma al núcleo. Una vez en el núcleo, FOXO1 activa la transcripción de la proteína pro-apoptótica Bim, miembro de la familia Bcl2. Segundo, la activación de AMPK inhibe la actividad del complejo pro-supervivencia mTORC1 en las CDs.

También investigamos los mecanismos empleados por CCR7 para regular la actividad de AMPK en las CDms. Los resultados muestran que la estimulación de CCR7 induce una rápida fosforilación de AMPK en la Ser485, un residuo que inhibe la actividad de la enzima. Además, la estimulación de CCR7 también induce una

disminución en los niveles de fosforilación de AMPK en la Thr172 (posición activadora) y una disminución en la forma fosforilada/inhibida de la Acetil-CoA carboxilasa, una diana de AMPK. Además, los estudios con inhibidores farmacológicos muestran que la inhibición de AMPK está mediada por las subunidades Gαi y Gβγ de la proteína G.

Aunque se ha descrito en diferentes tipos celulares que las quinasas Akt, S6k y PKA fosforilan directamente a AMPK en la Ser485, mostramos que tras la estimulación de CCR7, ninguna de estas tres quinasas está implicada en la fosforilación de AMPK. En su lugar, los resultados indican que son MEK1/2 y ERK1/2 las quinasas clave en la inducción de la fosforilación de AMPK en la Ser485. En este sentido, los experimentos de co-inmunoprecipitación muestran que ERK y AMPK pueden ser componentes de un mismo complejo de señalización que induce la inhibición de AMPK. Además, los ensayos de ligación por proximidad (PLA) indican que la estimulación de CCR7 en las CDs induce la aproximación entre ERK y AMPK (≤40 nm), lo que es consistente con la posibilidad de que estas dos moléculas interaccionen directamente.

En resumen, la información presentada sugiere que CCR7 emplea, además de la ruta de Akt, también la ruta de señalización de MEK/ERK/AMPK como mecanismo complementario para apagar la señalización pro-apoptótica y promover la supervivencia de las CDs. En su conjunto, los resultados presentados muestran que AMPK puede ser una posible diana terapéutica para modular la función de las CDms y la respuesta inmune.

INTRODUCCIÓN

INTRODUCCIÓN

1- LAS CÉLULAS DENDRÍTICAS

La respuesta inmune y las células dendríticas

El sistema inmune (SI) constituye un sistema de defensa encargado de proteger al organismo frente a amenazas externas (e.g. bacterias, hongos, parásitos o virus) e internas (e.g. células tumorales).

Clásicamente se distinguen dos tipos de inmunidad en el sistema inmune, la inmunidad innata y la adaptativa. La función principal de la inmunidad innata es responder ante cualquier patógeno de manera rápida y relativamente inespecífica. En cambio, el sistema inmune adaptativo (linfocitos T y B) proporcionan una respuesta que se caracteriza por ser específica y por generar una memoria inmunológica que permite responder en futuros encuentros con patógenos similares de manera más rápida y eficaz [1]. De esta manera, la inmunidad innata representa una primera línea de defensa del organismo que actúa capturando los antígenos, favoreciendo la reparación de la zona dañada y, en caso de ser necesario, activando a la inmunidad adaptativa mediante la presentación de los correspondientes antígenos. Recientemente se ha observado que existen células del sistema inmune innato que pueden poseer memoria inmunológica, lo que implica que la separación entre el sistema inmune innato y el adaptativo no es tan estricta como se pensaba [2, 3]. Aunque la mayoría de las células del sistema inmune innato y algunos tipos de células epiteliales son capaces, en mayor o menor medida, de presentar antígenos a las células del sistema inmune adaptativo, las células dendríticas (CDs) son las presentadoras más eficaces y especializadas [1].

Las CDs actúan como centinelas del organismo, distinguen entre antígenos propios y no propios, y son capaces de presentar aquellos antígenos que suponen una amenaza para el organismo y activar a los componentes de la inmunidad adaptativa. Por tanto, las CDs constituyen un vínculo que conecta la inmunidad innata y la adaptativa [1].

Ciclo biológico de las CDs

Las CDs derivan de progenitores hematopoyéticos presentes en la medula ósea (**Figura 1**). Las CDs que se ubican en los tejidos periféricos se encuentran en un estado de diferenciación denominado "inmaduro", de ahí que se las denomine CD inmaduras (CDi). En estas regiones, las CDis desempeñan una labor de "centinela"

frente a diferentes "señales de peligro" para el organismo, como patógenos o citoquinas producidas en respuesta a traumas o daños tisulares. Al mismo tiempo, las CDis mantienen la tolerancia inmune frente a las proteínas propias, impidiendo que las células del sistema inmune ataquen elementos del propio organismo [4]. Las CDs captan señales de peligro mediante receptores específicos como los Toll-like Receptors (TLRs) y otros receptores que son capes de detectar DAMPS (danger-associated molecular patterns) en las zonas de inflamación.

Las CDis también presentan receptores de quimioquinas inflamatorios (CCR1, CCR2, CCR5, CCR6 y CXCR1) que dirigen a estas células hacia el foco de la infección donde se expresan las quimioquinas inflamatorias [5, 6]. Además, las CDis poseen una elevada capacidad para internalizar y procesar antígenos procedentes de patógenos que capturan mediante macropinocitosis, fagocitosis o endocitosis mediada por receptores [7].

Para que las CDs puedan promover la activación de los linfocitos T y, por tanto, el inicio de la respuesta inmune adaptativa deben experimentar un proceso de diferenciación denominado maduración. Este proceso que convierte a las CDis en CDs maduras (CDm) confiere a estas últimas células unas características fenotípicas que les permiten activar con gran eficiencia a los linfocitos T [8, 9].

Los TLRs que captan las señales de peligro en el entorno de las CDis, también promueven su maduración. A medida que las CDs maduran pierden la expresión de los receptores de quimioquinas inflamatorios y la capacidad fagocítica, aunque mantienen la capacidad endocítica mediada por receptores [10]. Por el contrario, incrementan los niveles de las moléculas presentadoras de antígenos MHC-I y MHC-II (HLA-I y HLA-II en humanos), de las moléculas coestimuladoras (CD40, CD80 y CD86) y del receptor de quimioquinas CCR7 [5, 6, 11, 12]. Este receptor promueve la migración de las CDms hacia los ganglios linfáticos guiadas por un gradiente de sus ligandos: las quimioquinas CCL21 y CCL19 [13 14]. Una vez en los ganglios las CDms se dirigen hacia las zonas T donde presentan los antígenos capturados en las zonas periféricas a los linfocitos T vírgenes. Aquellos linfocitos cuyo TCR reconozca el antígeno presentado por la CDm, interaccionará con la CD formando una estructura de contacto denominada sinapsis inmunológica que induce la activación del linfocito T [15]. Una vez activado, el linfocito experimenta un proceso de proliferación seguido de su migración hacia la zona de daño o infección donde la CD captó originalmente el antígeno.

2- APOPTOSIS

La apoptosis es un tipo de muerte celular programada que se observa en los procesos de desarrollo y envejecimiento y de manera homeostática en las células de los diferentes tejidos del organismo [16]. La apoptosis también se induce como respuesta frente a diferentes agresiones incluyendo procesos infecciosos, daño celular o intoxicaciones por agentes externos.

Durante la primera fase de la apoptosis se producen cambios morfológicos en la célula que incluyen una reducción del tamaño celular, la formación de protuberancias ("blebs") en la membrana plasmática y condensación y fragmentación nuclear [17]. En una segunda fase se forman cuerpos apoptóticos, que son trozos de citoplasma rodeados por un fragmento de membrana plasmática que mantiene su integridad e impide que su contenido se vierta al exterior. En el interior de los cuerpos apoptóticos se empaquetan orgánulos y en ocasiones fragmentos de ADN. Estos cuerpos finalmente son captados y eliminados por células fagocíticas como los macrófagos. Debido a que durante el proceso apoptótico el contenido citoplásmico no se libera al exterior la muerte celular no conduce a un proceso inflamatorio como es el caso, en cambio, de la necrosis [18, 19].

Desde un punto de vista bioquímico la destrucción celular que supone la apoptosis requiere de la activación de un grupo de cistein proteasas denominadas caspasas. Estas proteasas son sintetizadas en forma de precursor o zimógeno, que carece de capacidad enzimática, y que debe ser proteolizado para que adquiera actividad enzimática. La activación de los zimógenos puede llevarse a cabo por otras caspasas ya activadas o, como en el caso de la caspasas 8 y 9, por proximidad y dimerización de varias moléculas de zimógenos [20].

Tipos de apoptosis

En función de la naturaleza del estímulo inductor de la apoptosis, ésta puede ser clasificada como intrínseca o extrínseca.

La apoptosis extrínseca es aquella inducida por señales extracelulares que se transmiten a través de receptores de membrana. Estas señales pueden ser ligandos como FASL o TNFα que inducen muerte [21]. Este tipo de apoptosis lleva a una activación de las caspasas -8, 9 ó 10 (caspasas iniciadoras), que son capaces de autoactivarse y que inician una cascada que termina con la activación de las caspasas efectoras -3, -6 o -7. Finalmente, las caspasas efectoras llevan a cabo la proteolisis de múltiples sustratos (**figura 1**).

La apoptosis intrínseca (o mitocondrial), en cambio, es el resultado de un proceso de estrés intracelular que puede ser provocado por daño en el ADN, estrés

oxidativo, exceso de calcio citosólico o la acumulación de proteínas plegadas de manera anómala, entre otros, que impactan sobre la mitocondria.

Los diferentes estímulos pro-apoptóticos resultan en diferentes cascadas de señalización que confluyen en la mitocondria y que pueden conducir a la permeabilización de la membrana externa mitocondrial (MOMP) [22]. Del mismo modo, existe otra amplia red de rutas de señalización de supervivencia que también convergen a nivel de la mitocondria y previenen la formación del MOMP. De esta manera, el destino final de la célula será el resultado del balance entre ambos tipos de señalización, desencadenándose aquel tipo de respuesta, pro- o anti-apoptótica, que sea predominante [21]. En caso de prevalecer las señales pro-apoptóticas el proceso prosigue con el MOMP, que provoca la anulación del potencial de membrana mitocondrial y por tanto la detención de la síntesis de ATP mitocondrial. La permeabilización de la membrana externa mitocondrial también desencadena la liberación del componentes del espacio intermembrana de la mitocondria, como el citocromo c al citosol [22]. El citocromo c en el citosol activa a la proteína APAF1 y junto a ella participa en la formación del apoptosoma, un complejo multiproteico que incluye a la caspasa 9 que, al oligomerizar, induce su activación [23]. La activación de esta caspasa iniciadora da lugar finalmente a la activación de las caspasas efectoras, entre las que se incluyen la caspasa 3. Además del citocromo c, la permeabilización mitocondrial libera otras proteínas como la endonucleasa G que puede fragmentar el DNA y mediar una apoptosis independiente de caspasas [24].

Muchas de las rutas de la apoptosis intrínseca que confluyen en la mitocondria están mediadas por proteínas de la familia Bcl-2. Hasta la fecha se han descrito unos 25 miembros de esta familia que se dividen funcionalmente en dos grandes grupos dependiendo de si inhiben la apoptosis (pro-apoptóticas) o la inducen (anti-apoptóticas). Los miembros anti-apoptóticos de esta familia suelen encontrarse en el citoplasma, y entre ellos destacan Bcl-2 y Bcl-xl. En cambio, los componentes pro-apoptóticos de la familia suelen encontrarse asociados a membrana y entre ellos se encuentran Bim, Bad, Bax y Bak.

El grupo de las proteínas anti-apoptóticas lleva a cabo su función mediante la inhibición de los componentes pro-apoptóticos [25]. A su vez, los miembros pro-apoptóticos pueden actuar promoviendo directamente la apoptosis al aumentar la permeabilidad de la membrana mitocondrial o bien uniéndose a las proteínas anti-apoptóticas e impidiendo que éstas lleven a cabo su función. Bim, por ejemplo, actúa úniendose a Bax y desplazando a Bcl-xl que se encuentra inhibiendolo. Además Bim provoca en Bax un cambio conformacional que permite su translocación del citosol a la mitocondria e inserción en la membrana externa donde es capaz de oligomerizar y formar poros que induncen la permeabilización de la membrana mitocondrial[26].

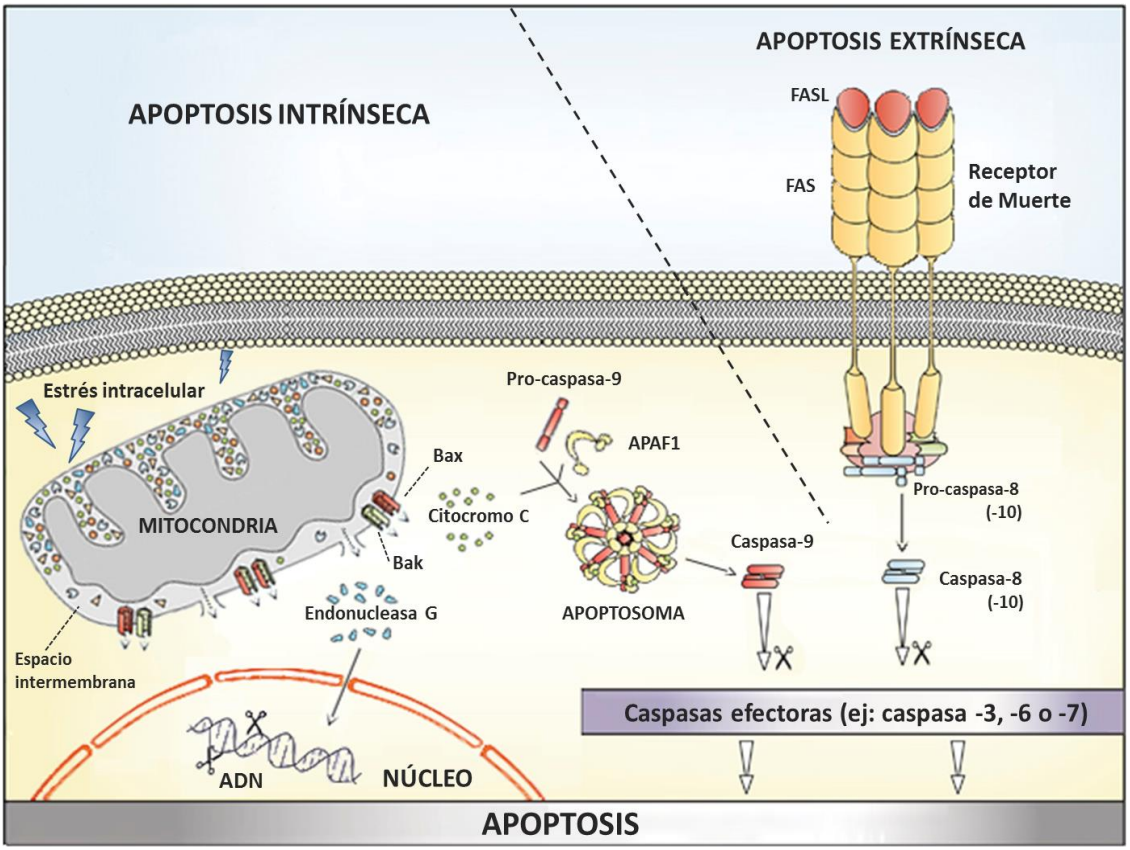

Figura 1: Tipos de apoptosis. La apoptosis puede ser de tipo intrínseco (mitocondrial) o extrínseco (dependiente de receptores de muerte) en función de la naturaleza de los estímulos que la activan. La apoptosis intrínseca se desencadena en respuesta a un estrés intracelular que provoca una alteración en el equilibrio de las proteínas de la familia Bcl-2, produciéndose una inhibición de los componentes anti-apoptóticos y favoreciendose la actividad de los componentes pro-apoptóticos. Los miembros pro- y anti-apoptóticos de la familia Bcl2 impactan sobre Bax y Bak que controlan la integridad de la membrana mitocondrial. Cuando Bax y Bak son activados se translocan a la membrana externa mitocondrial donde forma poros que favorecen la permeabilización de dicha membrana y la inhibición del potencial transmembrana mitocondrial. Como consecuencia de la permeabilización mitocondrial se libera al citoplasma el contenido del espacio intermembana que incluye el citocromo c y la endonucleasa G. La endonucleasa G se transloca al núcleo donde promueve un tipo de apoptosis independiente de caspasas mediante la fragmentación del ADN. La liberación de citocromo c induce un tipo de apoptosis dependiente de caspasas al promover la formación del apoptosoma que culmina con la activación de la caspasa iniciadora -9 y la posterior cascada de caspasas efectoras. La apoptosis extrínseca se produce en respuesta a la señalización de ligandos externos a través de los receptores transmembrana de la célula. Tanto la apoptosis intrínseca como la extrínseca son dependientes de caspasas en la que la activación del receptor induce rápidamente la activación de una caspasa iniciadora (-8, -9 o -10) y posteriormente de las caspasas efectoras que culminan con la muerte celular. Figura modificada a partir de Galluzzi et all 2012

Apoptosis en CDs

La longevidad de las células dendríticas juega un papel fundamental en la respuesta inmune. La vida media de las CDs suele ser relativamente corta, aunque se observan diferencias entre los diferentes subtipos a otros [27, 28]. A pesar de que todavía se desconoce el significado de estas diferencias, se sabe que, en general, a medida que aumenta la vida media de las CDs mejora la respuesta inmune [29, 30]. Su supervivencia está altamente regulada ya que el incremento de su vida media, incrementar la probabilidad de los encuentros con los linfocitos en el ganglio y por tanto la inmunidad adaptativa. Sin embargo, la longevidad de las Ds debe mantenerse dentro de ciertos límites ya que se ha observado que tanto la falta de CDs maduras como la presencia de CDs con vidas artificialmente prolongadas llevan a la aparición de procesos de autoinmunidad [29, 31-34]. Por un lado, se han detectado deficiencias en la apoptosis de las CDs de algunos pacientes con síndrome linfoproliferativo humano autoinmune y por otro, la inmunosupresión inducida por sepsis se ha visto asociada a procesos de apoptosis en CDs mediados por caspasa 3, tanto en humano como en ratón [35, 36]. Además, se ha descrito que en la inmunoterapia antitumoral con CDs, solo el 5-6% de las CDs inyectadas a los pacientes llegan finalmente a los ganglios linfáticos, mientras que no está claro el destino del otro 95%, que probablemente mueren en la zona de inyección donde podrían estar induciendo tolerancia [37]. Todo ello sugiere que el estudio de los mecanismos que regulan la supervivencia de las CDm puede ser de gran utilidad para el desarrollo de estrategias que permitan modular la longevidad de estas células y mejorar así la respuesta inmunitaria.

3- QUIMIOQUINAS

Las quimioquinas son una superfamilia de citoquinas quimiotácticas (Mr 7,5-10 KDa) que incluye a unos 50 miembros en humanos y que tienen una gran importancia en la regulación del tráfico leucocitario [38]. Las quimioquinas presentan una estructura terciaria altamente conservada consistente en un extremo N-terminal flexible que contiene cuatro cisteinas que forman dos puentes disulfuro, seguido de tres laminas β antiparalelas y una α-hélice en el extremo C-terminal [39].

En función del papel que desempeñan en la respuesta inmune las quimioquinas se pueden dividir entre inflamatorias, que son inducidas y se expresan en situaciones de inflamación, y las homeostáticas, que se sintetizan de manera constitutiva y en condiciones de homeostasis. Además, existen quimioquinas que presentan una doble función y pueden producirse de manera homeostática en algunos contextos e inducirse en condiciones inflamatorias.

También se pueden clasificar atendiendo a criterios estructurales basándose en la posición relativa de las dos primeras cisteínas del extremo N-terminal. Se han descrito cuatro clases de quimioquinas: CC, CXC, XC y CX3C; donde C hace referencia a un residuo de cisteina conservado y X puede ser cualquier otro aminoácido. Las quimioquinas de tipo CC tienen las dos cisteínas consecutivas mientras que las de tipo CXC y CX3C poseen uno o tres aminoácidos entre ambas cisteínas respectivamente. Por último, las quimioquinas de tipo XC solo tienen dos de las cuatro cisteinas que se corresponden con la segunda y la cuarta de los otros grupos. Basándose en este sistema de clasificación en 2001 se introdujo un sistema de nomenclatura que emplea el grupo al que pertenece la quimioquina, seguido por una L (de ligando) y un número [40].

Las quimioquinas pueden formar monómeros, dímeros y oligómeros. Algunas, son funcionales tanto en su estado monomérico como en su estado dimérico, mientras que otras solo son funcionales en una de las dos situaciones. Además, las quimioquinas también pueden formar heterodímeros [38].

Las quimioquinas CCL19 y CCL21

Como se mencionó anteriormente las CDs migran hasta los ganglios linfáticos en respuesta a gradientes de las quimioquinas homeostáticas CCL19 y CCL21, cuyo receptor es CCR7.

CCL21 tiene un peso molecular de 14,5 KDa y se caracteriza por tener seis cisteínas en vez de las cuatro que tienen típicamente las quimioquinas. Además posee una cola polibásica en su extremo C-terminal que le permite unirse a glicosaminoglicanos y formar un gradiente quimiotáctico estacionario sobre la

matriz extracelular [41]. En ratón, como consecuencia de una duplicación génica existen dos variantes funcionales de CCL21 que se diferencian en el aminoácido presente en la posición 65 de la proteína: CCL21-Leu y CCL21-Ser. CCL21-Leu contiene una leucina en dicha posición y se expresa en los vasos linfáticos de los órganos no linfoides como son el corazón o la piel [42]. Por el contario, CCL21-Ser (con una serina en la posición 65) se expresa en las vénulas del endotelio alto, en las células estromales del área T de los ganglios linfáticos y en las células epiteliales de la médula del timo [43] En humanos, CCL21 tiene un patrón de expresión parecido al del ratón, con la diferencia de que CCL21 no se expresa en las vénulas del endotelio alto y sólo existe el gen que codifica para la forma CCL21-Leu [42, 44].

CCL19 posee un peso molecular más reducido que CCL21 (11 KDa) con el que comparte un 32% de homología en su secuencia peptídica, pero carece de la extensión polibásica del extremo C-terminal. En homeostasis CCL19 se expresa sólo en las células reticulares del área T de los ganglios y en las células epiteliales de la médula del timo. CCL19 también puede ser sintetizada por las CDs maduras que llegan a los ganglios, por lo que potencialmente podría servir de fuente adicional de CCL19, que podría incrementar el número de CDs que llegan a los ganglios linfáticos [45]. Sin embargo, experimentos realizados con CDs obtenidas de ratones KO para CCL19, indican que la ausencia de CCL19 no afecta a la migración o maduración de las CDs [46]**.** Se ha sugerido que CCL19 pudiera regular la migración quimiotáctica en el ganglio frente a CCL21 que, debido a su capacidad para unirse a los glycosaminao glicanos, podría regular adhesión y migración haptotáctica [47].

El patrón de expresión de CCL19 y CCL21 permite que las CDs que expresan CCR7 puedan migrar con eficiencia hacia los ganglios linfáticos. Tras alcanzar la zona T de los ganglios linfáticos, las CDs llevan a cabo su función de presentación antigénica y activación de los linfocitos T.

CCL19 y CCL21 son también ligandos de un segundo receptor decoy: CCR11 (también llamado CCx-CKR1) que es expresado por las células reticulares de los ganglios linfáticos, las células epidérmicas y las células epiteliales del timo [48]. Este receptor secuestra sus ligandos para limitar su accesibilidad a otros receptores y parece tener un papel importante en el desarrollo y selección de los linfocitos T o durante procesos inflamatorios en los que se incrementan los niveles de CCL19 o CCL21 [48, 49].

4- CCR7

Estructura

CCR7 pertenece a la superfamilia de los receptores transmembrana heptahelicoidales acoplados a proteínas G. Como todos los miembros de esta superfamilia, CCR7 contiene siete dominios transmembrana, con su región N-terminal y tres bucles hacia el exterior de la célula y la región C-terminal y otros tres bucles hacia el citoplasma. Al igual que ocurre con las quimioquinas, los receptores acoplados a proteínas G también pueden encontrarse en forma dimérica [38]. Cuando estos receptores son activados interaccionan con las proteínas G y las activan.

Las proteínas G son proteínas heterotrímericas que están formadas por las subunidades α, β y γ. Existen 21 isoformas de la subunidad α que se clasifican agrupándolas en cuatro familias (αs, αi, αq/11 y α12/13), 6 isoformas de la subunidad β y 12 de la subunidad γ que se pueden combinar entre sí [50]. La subunidad α tiene actividad GTPasa y en su estado inactivo se encuentra unida a las subunidades β y γ, al mismo tiempo que une una molécula de GDP. La activación de la proteína G provoca que la subunidad α libere el GDP y una GTP, así como su disociación de las subunidades β y γ, que forman un dímero muy estable que actúa como una única unidad funcional independiente de la subunidad α [51]. Tras este proceso tanto la subunidad α, por un lado, como el dímero de subunidades βγ, por otro, actúan de manera independiente para regular la señalización intracelular desde el receptor.

Los receptores de quimioquinas reciben su nombre según la subfamilia de quimioquinas que unen (C, CC, CXC, CX3C) seguido de la letra "R" y un número que se asignó atendiendo al orden cronológico en que fue identificado [40].

La actividad de los receptores acoplados a proteínas G puede ser regulada a través de un proceso de desensibilización. Este mecanismo que se desencadena en respuesta a una exposición prolongada y/o repetida a su ligando se produce mediante la fosforilación del receptor en su extremo C-terminal por las proteínas GRK (G-receptor coupled kinase), PKA o PKC. Esta fosforilación promueve la unión de β-arrestina impidiendo su interaccion con la proteína G y la posterior señalización intracelular [52]. El complejo formado por el receptor unido a la arrestina es dirigido hacia vesículas de clatrina, donde es internalizado y puede ser redirigido hacia los lisosomas para ser degradado o puede ser reciclado, mediante su desfosforilación, y redirigido de nuevo a la membrana [53, 54].

Aunque CCL19 y CCL21 se unen con afinidades parecidas a CCR7, se ha comprobado que pueden regular algunas funciones de manera diferente. Por ejemplo, estudios con células HEK293 muestran como la estimulación del receptor CCR7 con CCL19 induce la fosforilación, mediada por GRK3 y GRK6, del receptor y, posteriormente,

su internalización y desensibilización. La estimulación con CCL21 en cambio induce la fosforilación sólo por GRK6 [55].

En condiciones homeostáticas CCR7 se expresa en células del sistema inmunitario. Además de en las CDs maduras, se expresa en linfocitos B vírgenes, varias poblaciones de linfocitos T (timocitos dobles negativos y dobles positivos, linfocitos T vírgenes, T reguladores y una subpoblación de memoria central), macrófagos, neutrófilos y la población $CD16^-$ de linfocitos NK [43, 56, 57]. Además, en algunos tipos de cánceres como el melanoma y el cáncer de mama es común encontrar altos niveles de CCR7 que se asocian con metástasis y un peor pronóstico de la enfermedad [58, 59].

Papel en el organismo:

En ratones knockout (KO) de CCR7 se han detectado numerosas alteraciones, entre las que se incluyen:

Arquitectura aberrante de los órganos linfoides.

Deficiencias en la migración hacia los ganglios linfáticos de las CDs y de varias poblaciones de linfocitos T que expresan CCR7.

Desarrollo de estructuras linfoides ectópicas, sobre todo en zonas de mucosa. Debido a que las células no migran eficientemente hacia los ganglios linfáticos, se acumulan en los tejidos periféricos y formar estructuras ectópicas [60].

Retraso en la inducción de la respuesta inmune adaptativa. Como ya se explicó previamente, para que se desencadene una respuesta inmune adaptativa completa y eficiente es necesario que las CDs migren a los ganglios linfáticos y lleven a cabo la presentación antigénica y la activación los linfocitos T vírgenes [61].

Problemas en la diferenciación y la maduración de los linfocitos. CCR7 juega un papel importante a diferentes niveles de la diferenciación de los linfocitos. En ausencia de CCR7 se produce un bloqueo en el desarrollo de los timocitos en su estado DN1-DN2 y un proceso de selección negativa defectuoso[62].

Disminución de la tolerancia central y periférica. La pérdida de tolerancia central se puede deber a los problemas en la selección negativa de los linfocitos. La tolerancia periférica, se ve afectada entre otros motivos porque los linfocitos T reguladores ven disminuida su capacidad de inducción de tolerancia [63]

Autoinmunidad espontánea. Los problemas de tolerancia central y periférica, junto con la acumulación de células inmunológicas en la periferia, da lugar a un aumento de la incidencia de enfermedades autoinmunes en estos ratones [64].

Todos estos efectos señalan el importante papel de CCR7 durante la respuesta inmune.

5- RUTAS DE SEÑALIZACIÓN REGULADAS POR CCR7

Además de activar la quimiotaxis, la estimulación de CCR7 CCR7 aumenta la velocidad migratoria, regula la citoarquitectura celular, activa la endocitosis, induce supervivencia y potencia la maduración de las CDs [65-69]. Durante los últimos años nuestro laboratorio ha estudiado las rutas de señalización empleadas por CCR7 para regular la supervivencia, la endocitosis, la citoarquitectura, la quimiotaxis, y la velocidad migratoria. Como se puede ver en la **figura 2** estas rutas de señalización se agrupan en módulos aparentemente independientes entre sí.

Módulo de regulador de la dinámica de la actina

La endocitosis, la velocidad migratoria y la citoarquitectura están degulados por un módulo que controla la dinámica de la actina. CCR7 activa este módulo a través de las proteínas G de la subfamilia Gαi que activa a la quinasa MST1 y posteriormente a la GTPasa RhoA, $G_{\alpha 13}$ también media la activación de RhoA (**figura 2**). RhoA a su vez controla las quinasas ROCK y PYK2. ROCK, una vez activado, fosforila y activa directamente a la MLC e inhibe a la fosfatasa MLCP. Por otro lado ROCK también puede mediar la fosforilación/inhibición de la cofilina a través de LIMK, aunque la cofilina también es inhibida por la quinasa PYK2 [65, 70].

Módulo regulador de la supervivencia

Este módulo está regulado por la proteína G Gαi, la quinasa de lípidos PI3K y la Ser-Thr quinasa Akt [69]. Akt regula viarias vías, por un lado, inhibe las rutas pro-apoptóticas de la CDs, fosforilando/inhibiendo a la quinasa proapoptótica GSK3 y el factor de transcripción pro-apoptótico FoxO [71]. Por otro lado, Akt también estimula la supervivencia activando al factor de transcripción inductor de supervivencia NF-κB que induce la transcripción de Bclxl, que promueve supervivencia [69]. Por último, Akt activa otra ruta a través de mTORC1 que regula la actividad de 4EBP1 y S6K, que promueven la síntesis de proteínas y, por tanto, la supervivencia celular (**figura 2**).

- PI3K (PhosphoInositide 3-Kinase) engloba a una familia de quinasas que se caracterizan por ser capaces de fosforilar fosfoinosítidos (PIs) en la posición 3' OH de su anillo de inositol [72]. Los PIs susceptibles de ser fosforilados por PI3K son PI, PI(4)P y $PI(4,5)P_2$ que generan PI(3)P, $PI(3,4)P_2$ o $PI(3,4,5)P_3$ respectivamente. Los PIs fosforilados actúan como segundos mensajeros puesto que constituyen nuevos sitios de unión para aquellas proteínas que poseen dominios PH, FYVE o PX entre otros [73].

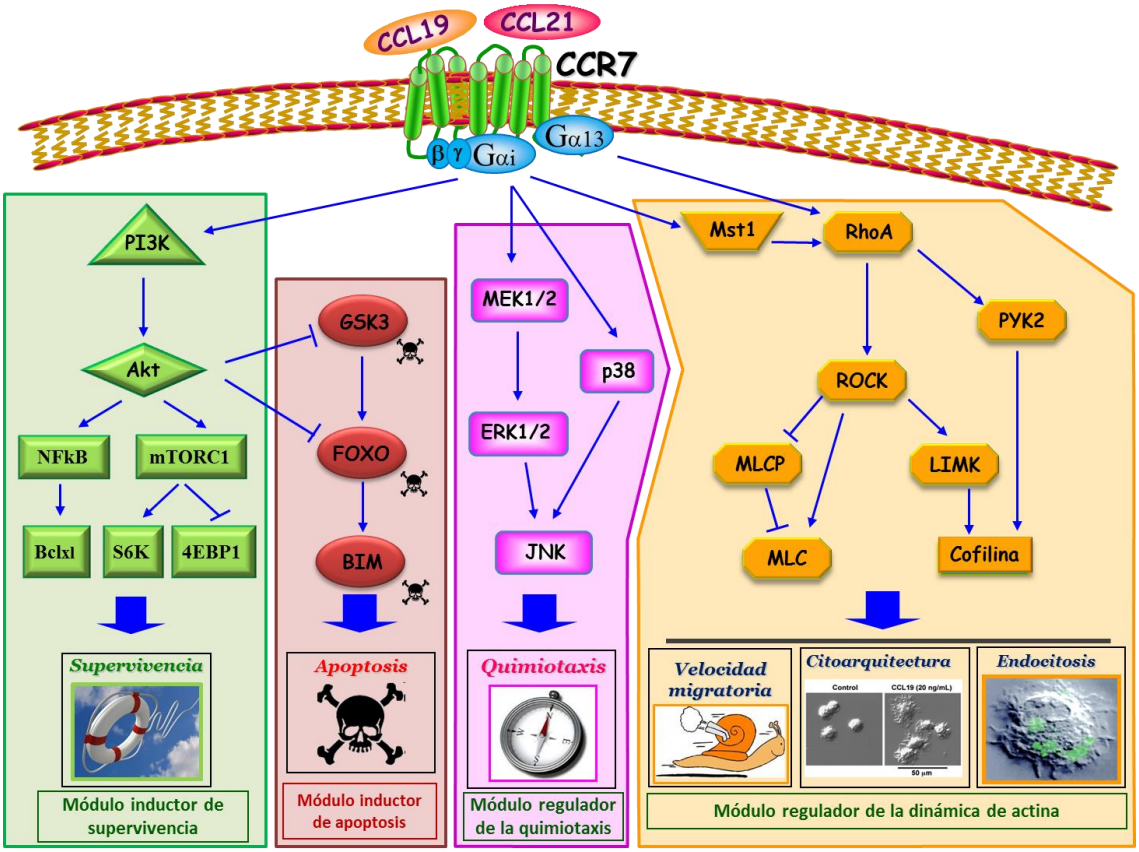

Figura 2. CCR7 y sus rutas de señalización. Las rutas de señalización activadas por CCR7 se agrupan en módulos aparentemente independientes entre sí para regular diferentes funciones. El módulo de supervivencia está controlado por la ruta de PI3K, Akt, NF-kB y mTORC1 que se encuentran inhibiendo a su vez al módulo de apoptosis compuesto por GSK3, FoxO y Bim. El módulo de regulación de la quimiotaxis incluye la ruta de las MAPK con p38 por un lado y MEK1/2 y ERK ½ por otro. Por último, el módulo de regulación de la dinámica de la actina está controlado por Mst1, RhoA, PYK2, cofilina y MLC que regulan la velocidad migratoria, la citoarquitectura y la endocitosis.

- Akt (también conocida como PKB) es una serina/treonina quinasa que posee un extremo N-terminal con un dominio PH de unión a PI(3,4)P2 y a PI(3,4,5)P3. Se activa por fosforilación de dos residuos, uno próximo a la región responsable de actividad catalítica (Thr308) y otro en el extremo C-terminal (Ser473) [74]. La presencia del dominio PH, permite que Akt se acumule en la membrana en las zonas de activación de PI3K lo que favorece su activación de dos maneras. Por un lado, la unión de Akt a los PIs fosforilados de la membrana provoca un cambio conformacional que expone los dos residuos susceptibles de fosforilación. Por otro, la fosforilación en la Thr308 se lleva a cabo por la quinasa PDK1, que también posee un dominio PH, y por tanto también se acumula en las zonas de activación de PI3K, lo que posibilita la proximidad entre PDK1 y Akt [75].Además. para que Akt complete su activación es necesario que

también sea fosforilada en la Ser473 por el complejo mTORC2 [76]. Aunque las fosforilaciones en la Ser473 y la Thr308 son las más conocidas y estudiadas recientemente se han descrito fosforilaciones en otras posiciones que también pueden incrementar la actividad de Akt. Por ejemplo, la fosforilación en la Tyr176 permite que Akt se una a los ácidos fosfatídicos de la membrana plasmática y de esta manera permite la activación de Akt de manera independiente de PI3K. Además, Akt también puede ser fosforilada en las tirosinas 215, 315, 326 y 474 [77].

- GSK3 (glycogen synthase kinase 3) es una de las múltiples dianas de Akt. Existen dos isotipos de GSK3 (GSK3α y GSK3β) que presentan un alto grado de homología pero que difieren en su funcionalidad. La quinasa GSK3β se encuentra basalmente activada en mamíferos, debido a que en estado basal la enzima se encuentra fosforilada en la posición activadora Tyr216. Por otro lado, GSK3 puede ser inhibida mediante su fosforilación en la Ser9 por Akt, PKA, PKC, p70S6K (S6K) o p90RSK (RSK) [78] [79].

- FoxO (Forkhead bOX O) constituye una familia de factores de transcripción que en mamíferos posee cuatro representantes (FoxO1, FoxO3, FoxO4 y FoxO6) que poseen en común un motivo "winged hélix" de unión a DNA. FoxO puede encontrarse tanto en el citoplasma como en el núcleo a donde transloca para regular la transcripción de diferentes dianas. La translocación núcleo-citoplasma de FoxO está regulada por fosforilación. Una de las modificaciones más estudiadas es la fosforilación en la Ser256 de FoxO1, mediada por AKT, que provoca su translocación al citoplasma y su posterior ubiquitinación y degradación en el proteasoma [80, 81]. La familia de proteínas FoxO regula procesos celulares tan variados como la diferenciación, el crecimiento, el metabolismo, el ciclo celular y la supervivencia. FoxO regula la supervivencia actuando a dos niveles; por un lado, modula la expresión de algunos ligandos de receptores de muerte (por ejemplo FasL) que actúan induciendo apoptosis de manera paracrina [82, 83]. Por otro lado, FoxO también puede regular la expresión de proteínas de la familia Bcl-2, como la proteína pro-apoptótica Bim [84].

- NF-κB (Nuclear Factor-κB) es el nombre general que reciben los factores de transcripción formados por proteínas de unión a DNA de la familia Rel. En mamíferos esta familia incluye a cinco miembros, RelA (p65), RelB, c-Rel, NFκB1 (p105/p50) y NF-κB2 (p100/p52); que comparten un dominio RHD (Rel homology domain) que les permite asociarse entre sí para formar homo- y heterodímeros [85]. En su estado inactivo los dímeros de NF-κB se encuentran en el citoplasma unidos a IκB. En respuesta a una señal activadora IκB es fosforilado,

ubiquitinado y degradado en el proteasoma. Una vez libres, los dímeros de NF-κB translocan al núcleo donde regulan la transcripción de sus genes diana. La actividad de NF-κB también se regula por fosforilación. Aunque NF-κB puede ser fosforilado en múltiples posiciones, la fosforilación más estudiada es la que está mediada por PKA y MSK1 en la Ser276, que tiene un efecto inhibitorio sobre la transcripción de muchas de las dianas de NF-κB [86, 87]. NF-κB está implicado en multitud de procesos como la proliferación, el ciclo celular, la diferenciación o la apoptosis gracias a que regula la expresión de un gran número de genes que incluyen a las proteínas anti-apoptóticas Bcl-2 y Bcl-xl.

- mTORC1 (mechanistic target of rapamycin complex 1) es una de las dianas de Akt claves en la regulación del metabolismo. La quinasa mTOR puede funcionar como componente de dos complejos multiproteicos distintos denominados mTORC1 y mTORC2 que difieren en su composición, regulación y función [88]. El complejo mTORC1 incluye, además de mTOR, Raptor, mLST8 y dos inhibidores endógenos del propio complejo, PRAS40 y DEPTOR [89-92]. A través de sus dianas S6K (p70 ribosomal s6 kinase) y 4E-BP (eukaryotic translation initiation factor 4E-Binding Protein 1), mTORC1 estimula la síntesis de proteínas, lípidos y ácidos nucleicos, así como promueve la producción de ATP, e induce supervivencia[88, 93, 94].

Módulo regulador de la quimiotaxis

Esta ruta intracelular está mediada por la proteína $G_{\alpha i}$ que activa dos rutas de MAPK (Mitogen-activated protein kinases), una a través de MEK1/2 y ERK1/2 y otra a través de p38 que controlan conjuntamente la actividad de JNK [65] (**figura 2**).

- MEK (Mitogen/Extracellular signal-regulated Kinase) también conocido como MKKK (MAP kinase kinase kinase) constituye una familia de 7 enzimas con un peso molecular de entre 43 y 50 KDa y una actividad quinasa dual capaz de fosforilar residuos de tirosina y treonina. De entre todas ellas MEK1 y MEK2 (MEK1/2) destacan por su alto grado de homología (80% de homología total y un 90% de homología en el dominio quinasa) y están compuestas por 393 y 400 aminoácidos respectivamente. Se trata de dos enzimas muy selectivas ya que tienen dos únicos sustratos conocidos, las quinasas ERK1 y ERK2 (ERK1/2). MEK1/2 poseen una región N-terminal de unos 70 aminoácidos multifuncional que posee un segmento de interacción con su sustrato, una secuencia de exportación nuclear y un segmento auto-regulador que estabiliza la conformación inactiva de la enzima; un dominio quinasa de unos 290 residuos que contiene la región de activación de la proteína y un extremo C-terminal de

unos 30 aminoácidos [95]. Además, MEK1/2 tienen la capacidad de asociarse entre sí formando homo- y heterodímeros [96, 97].

La actividad de MEK1/2 se regula fundamentalmente mediante fosforilaciones. La activación de la variante humana de MEK1 requiere que ésta sea fosforilada por Raf en la Ser218 y la Ser222 (Ser222 y 226 en MEK2) [98, 99]. Cuando estas dos fosforilaciones van acompañadas de la fosforilación en la Thr298 por PAK1 (p-21-activated kinase-1) se promueve la asociación de MEK1 con ERK1/2, favoreciendo la activación de este último [100, 101].

También se han descrito una serie de fosforilaciones inhibitorias como son la Thr286 y la Thr292, ambas sustratos de Cdc2 y de ERK [102, 103]. La fosforilación de la Thr292 por ERK bloquea la fosforilación activadora en la Thr298 de MEK1 por PAK1, al mismo tiempo que dificulta la capacidad de MEK1/2 para formar heterodímeros lo que afecta negativamente a la actividad de MEK1/2 [97, 104]. De esta manera se establece un mecanismo de regulación por retroalimentación negativa entre ERK1/2 y MEK1. A pesar de que la Thr292 está presente sólo en MEK1, la regulación a través de la fosforilación de esta posición afecta también a la actividad de MEK2. La fosforilación de MEK1 en la Thr292 también reduce la actividad de MEK2, mientras que la ausencia de MEK1 provoca una activación prolongada de MEK2 y ERK1/2 [97]. Por último, es importante comentar que para que MEK1/2 puedan interaccionar con sus proteínas reguladoras y con sus proteínas diana necesita la presencia de proteínas adaptadoras como KSR1/2.

Existe una amplia gama de inhibidores frente MEK1/2. En esta tesis se emplean dos: PD0325901 y UO126. Ambos tienen capacidad de atravesar la membrana plasmática de las células y destacan por su alta especificidad. Inhiben a MEK1/2 de manera no-competitiva impidiendo que se produzca la fosforilación de su diana ERK1/2.

- ERK1/2 (extracellular signal-regulated kinase 1 y 2) forman parte de la familia de las MAP quinasas. Se trata de una familia de serina/treonina quinasas que incluyen a las ERK (ERK1-8), JNK (JNK1-3) y p38 MAP quinasas (p38α/β/γ/δ). ERK1 y ERK2 se expresan ubicuamente, comparten la mayor parte de sus funciones y tienen un 84% de homología, difiriendo principalmente en su región N-terminal donde ERK1 posee una inserto de 17 aminoácidos [105]. Además, se trata de dos proteínas muy conservadas filogenéticamente, de hecho, las dos isoformas difieren más entre sí que con sus homólogos de rata o ratón. De las dos isoformas ERK2 es la más estudiada.

  ERK2 posee 350 aminoácidos y, al igual que la mayoría de los miembros de la familia de las quinasas, presenta una estructura bilobulada (**figura 3**). El lóbulo

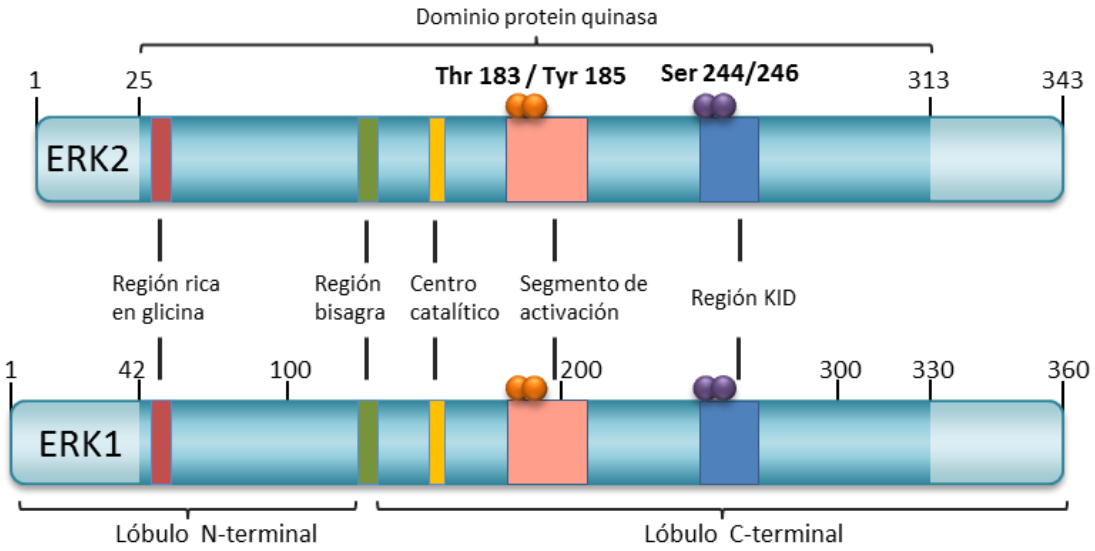

Figura 3: Estructura de ERK1/2. ERK1 y ERK2 tienen un 84% de homología y un peso de unos 350 KDa. Ambas quinasas poseen una estructura bilobular en la que el lóbulo N-terminal de ERK1 tiene una inserción de 17 aminoácidos que no está presente en ERK2. El lóbulo C-terminal (de mayor tamaño) posee el centro catalítico, un segmento de activación y una región KID. ERK1/2 pueden ser fosforilados en varias posiciones. Las fosforilaciones en la treonina 183 y en la tirosina 185 del segmento de activación son activadoras (en naranja) mientras que las fosforilaciones en las serinas 244 y 246 de la región KID no afectan a la actividad de la enzima sino a su localización celular (en morado). Figura modificada a partir de Roskoski et. al., 2012.

N-terminal es el más pequeño de los dos y contiene una región rica en prolina de unión a ATP. El lóbulo C-terminal, de mayor tamaño, contiene el sitio de unión al sustrato, el centro catalítico, el bucle de activación que contiene dos residuos fosforilables (Thr183 y Tyr185) y el dominio KID (Kinase Insert Domain) que también puede ser fosforilado en las Ser244 y Ser246 [105].

Las fosforilaciones de la Thr183 y la Tyr185 del bucle de activación se llevan a cabo por MEK1/2 y son fundamentales para que ERK1/2 adquieran su conformación activa. Esta activación se lleva a cabo en el citoplasma y permite que ERK1/2 homodimericen (los heterodímeros son inestables) y que sean fosforilados en las Ser244/246 [106]. La fosforilación de estas dos posiciones a su vez facilita la translocación de ERK1/2 al núcleo mediada por la importina 7, aunque alternativamente parte del ERK1/2 activado puede permanecer en el citoplasma [106, 107]. La desfosforilación de ERK se lleva cabo por las fosfatasas de especificidad dual DUSPs [108].

La actividad de ERK también se regula a través de su localización, ya que tanto su retención artificial en el citoplasma como su envío forzado al núcleo producen alteraciones en diferentes funciones celulares como la progresión del

ciclo celular o la extensión de neuritas [109, 110]. La localización celular de ERK se regula, además de por su estado de mono- o dimerización, por la presencia de proteínas adaptadoras. Estas proteínas además de facilitar la interacción entre ERK, sus sustratos y las quinasas que se encuentran por encima en su ruta, pueden intervenir en muchos casos en la localización final de ERK. Entre estas proteínas adaptadoras se encuentra por ejemplo MP-1 (MEK Partner-1) que por un lado favorece la interacción entre MEK1/2 y ERK1/2, al mismo tiempo que las dirige hacia los endosomas [111, 112]. Otro ejemplo es PEA-15, que parece actuar de proteína adaptadora entre ERK y su sustrato RSK2 y que además actúa reteniendo a ERK en el citoplasma [113, 114].

Además de estar implicado en la progresión del ciclo celular y la formación de neuritas, se han descrito otras muchas funciones de ERK1/2 que incluyen: proliferación, citoquinesis, transcripción, diferenciación celular, muerte celular, senescencia, reordenamiento del citoesqueleto de actina y tubulina, formación de uniones GAP, adhesión celular y quimiotaxis (como es en el caso de las CDs en respuesta a la estimulación de CCR7). También se han descrito mutaciones y alteraciones de ERK1/2 que están asociadas con diferentes patologías como son la diabetes, problemas cardiovasculares y múltiples tipos de cáncer [115].

Los inhibidores específicos de ERK son mucho más recientes que los de MEK. El primero que se describió fue el FR180, un inhibidor competitivo de ERK que se identificó en el año 2005. En esta tesis, además del FR180, también se ha empleado otros dos inhibidores: Un inhibidor competitivo de ERK compuesto por un grupo pirazolilpirrol (CAYMAN) y un péptido de 13 aminoácidos que se corresponde con la región N-terminal de MEK y que se une reversiblemente a ERK impidiendo su asociación con MEK (péptido inhibidor de ERK). Aunque todos estos péptidos han sido testados frente a múltiples quinasas como JNK, y p38 no son tan específicos como PD0325901 y UO126 por lo que se hace necesario analizar simultáneamente más de uno para confirmar los resultados obetinodos.

6- AMPK

Estructura

AMPK (AMP-activated protein kinase) pertenece a la familia de las serina/treonina quinasas. Es una proteína heterotrimérica compuesta por una subunidad α-catalítica y dos subunidades reguladoras β y γ. Se han descrito dos isoformas de la subunidad α, dos de la subunidad β y tres de la subunidad γ [116-118]. Todas ellas están codificadas por distintos genes que pueden combinarse entre sí, lo que permite que haya hasta 12 combinaciones posibles de la enzima completa.

Las subunidades α1 y α2 son bastante similares entre sí. Están formadas por aproximadamente 550 aminoácidos, con un extremo N-terminal muy conservado donde se encuentra el dominio catalítico y un extremo C-terminal divergente. Los patrones de expresión de ambas subunidades difieren de unas especies a otras ya que por ejemplo en el caso del hígado humano la subunidad mayoritaria parece ser la α1, mientras que en el caso de la rata parece predominar la subunidad α2 [119].

Las subunidades β1 y β2 tienen 270 y 272 residuos respectivamente. Ambas contienen una región de miristilación en su extremo N-terminal y aunque difieren bastante en los primeros 65 aminoácidos poseen un 71% de homología global [116, 120]. Al igual que ocurre con las isoformas de la subunidad α, su distribución parece variar de unas especies a otras [119].

A diferencia de las subunidades α y β, la diferentes isoformas de la subunidad γ presentan una gran variedad de tamaños (γ1 331 residuos, γ2 569 residuos, y γ3 489 residuos). Las mayores divergencias entre las 3 isoformas se encuentran en el extremo N-terminal mientras que comparten un extremo C-terminal con cuatro dominios cistationina β-sintasa consecutivos bastante conservados, cada uno de los cuales contiene un bolsillo de unión a nucleótidos [121, 122]. Además de diferir en longitud estas tres isoformas también presentan patrones muy diferentes de expresión.

Regulación

La actividad de AMPK es regulada mediante mecanismos alostéricos y de modificación covalente (**figura 4**).

AMP es un regulador alostérico que se une a los dominios cistationina β-sintasa de la subunidad γ e induce la activación de la enzima mediante al menos dos mecanismos [123]. . Por un lado, provoca un cambio conformacional que estimula la capacidad de LKB1 de fosforilar a AMPK en la Thr172 de la subunidad α. Aunque hay estudios que sugieren que este efecto está también mediado por el ADP, estos resultados no han

podido ser validados [124, 125]. Por otro lado, el AMP también favorece el estado activo de AMPK al dificultar la desfosforilación de la Thr172 por fosfatasas [124, 126]. A diferencia de lo que ocurre en el caso anterior, este bloqueo de la defosforilación es mimetizada por el ADP, aunque con una eficacia 10 veces menor [125, 127].

La fosforilación en diferentes residuos de AMPK regula covalentemente la actividad de esta quinasa (**figura 4**). Como ya se ha dicho, una de las formas mediante las cuales el AMP activa a AMPK es promoviendo su fosforilación en la Thr172, que se localiza dentro del llamado bucle de activación ("activation loop") de la subunidad α. Esta fosforilación, que es necesaria para que la enzima sea activa, puede estar mediada a cabo por LKB1, CAMKK2 y TAK1 [128-130].

La subunidad α también es susceptible de ser fosforilada en su extremo C-terminal. Dentro de ese segmento se encuentra la Ser485 (Ser492 en la subunidad α2) cuya fosforilación produce un efecto inhibitorio sobre la enzima [131, 132]. El estudio de su estructura cristalográfica sugiere que este efecto inhibitorio podría llevarse a cabo debido a que la Ser485 se encuentra situada cerca de la Thr172 desde donde podría inhibir su fosforilación al bloquear físicamente el acceso de LKB1, CaMKK2 y TAK1 [133, 134]. Además de la autofosforilación de AMPKα en la Ser485, Se han descrito otras tres quinasas capaces de fosforilarla en este residuo: AKT, PKA y S6K [135]. Por último, PKA también es capaz de fosforilar a la subunidad α en la Ser173 (adyacente a la Thr172), lo que también parece inhibir la actividad de la enzima [136].

AMPKβ también es susceptible de fosforilación en múltiples residuos. Las serinas 24, 25 y 108 de la subunidad β1 son autofosforiladas por AMPKα y, mientras que la 108 provoca un incremento en la actividad de AMPK, la fosforilación de las Ser 24/25 no parece afectar a la actividad de la enzima. En cambio, son necesarias para la localización citoplásmica de AMPK, ya que evitan que la subunidad sea translocada al núcleo. La Ser182 de la subunidad β1 también es susceptible de ser fosforilada y parece tener un papel similar al de las Ser24/25 aunque en este caso todavía no se ha identificado a ninguna quinasa responsable de su fosforilación [137, 138]. Por último, la subunidad β2 carece de las Ser24/25 por lo que solo es fosforilada en las serinas 108 y 182 [139].

Función

Debido a que AMPK es sensible a la relación AMP/ATP tradicionalmente se le ha considerado un sensor del estado energético y nutricional de las células eucariotas. Cuando esta relación aumenta debido a un déficit energético, AMPK actúa para restaurar la homeostasis energética activando las vías catabólicas que producen ATP y apagando las rutas anabólicas.

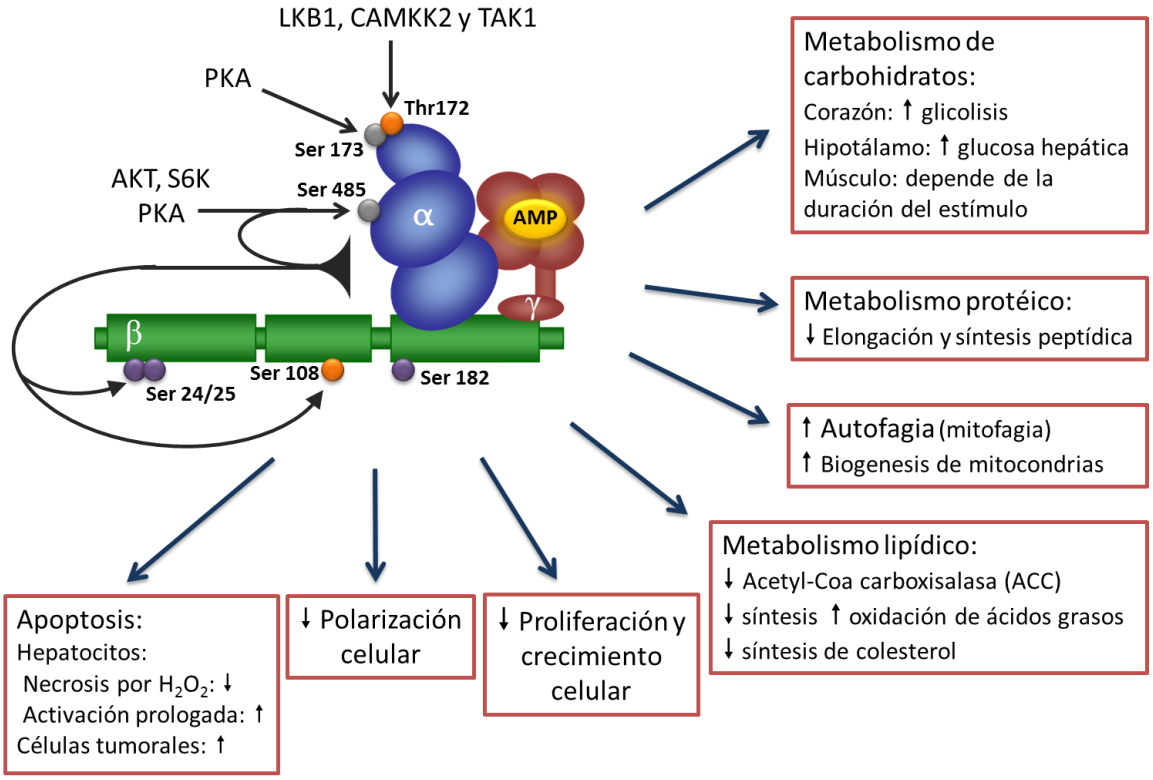

Figura 4: Estructura y función de AMPK. AMPK es un trímero formada por una subunidad α catalítica y dos subunidades reguladoras β y γ. AMPK puede ser activada alostéricamente por la unión de AMP a la subunidad γ o por fosforilaciones en las subunidades α y β. Las fosforilaciones en la treonina 172 de la subunidad α y en la serina 108 de la subunidad β son activadoras (en naranja) mientras que las fosforilaciones en las serinas 173 y 485 de la subunidad α son inhibitorias (en gris). Por último, las fosforilaciones en las serinas 24, 25 y 182 de la subunidad β no afectan a la actividad de la enzima sino a su localización celular (en morado). También se muestran las quinasas descritas hasta la fecha responsables de dichas fosforilaciones y las principales funciones celulares reguladas por AMPK.

Estas rutas de regulación parecen haber surgido tempranamente en la evolución ya que existen genes ortólogos de AMPK en todo tipo de organismos eucariotas. De esta manera, estudios genéticos en eucariotas no mamíferos sugieren que originalmente AMPK jugaba un papel en la respuesta a la escasez de fuentes de carbono. En levaduras, snf1, la quinasa ortóloga de AMPK, es necesaria para cambiar de un metabolismo glicolítico a uno oxidativo cuando hay escasez de glucosa o cuando se produce el catabolismo de otras fuentes de carbón fermentables [140]. Otro ejemplo es SnRK1, su homóloga en plantas, que es necesaria para la biosíntesis de almidón [141].

En mamíferos AMPK no solo regula las rutas metabólicas sino que está implicada en todo tipo de procesos celulares. La primera manera a través de la cual AMPK puede actuar en respuesta a desequilibrios energéticos es a través de las rutas del metabolismo de carbohidratos. En el corazón se ha observado que la activación de

AMPK provoca tanto un aumento de la captación de glucosa mediante un incremento de la translocación a la membrana de los receptores GLUT4, como un incremento de la glicolisis [142, 143]. En el músculo esquelético AMPK estimula la formación de glucosa al inhibir directamente a la glucógeno sintasa [144], pero su activación crónica acaba provocando un aumento de los niveles de glucosa-6-fosfato que tiene capacidad de activar a la glucógeno sintasa [145].

La respuesta a la escasez de ATP también incluye la regulación del metabolismo lipídico a varios niveles. AMPK fosforila e inhibe a la Acetyl-CoA carboxilasa (ACC), que cataliza la conversión de acetil-CoA en malonil-CoA y que es comúnmente empleada como medida del estado de activación de AMPK *in vivo* [146]. Mediante la inhibición de esta enzima, AMPK inhibe la síntesis de ácidos grasos y activa su oxidación en la mitocondria [147, 148]. Además, la activación de AMPK conduce a un aumento de la captación de ácidos grasos en músculo y corazón y a una inhibición de la síntesis de colesterol [148-150] .

Otra manera que tiene AMPK de regular los niveles de ATP es a través del metabolismo proteico. AMPK de inhibe la elongación peptídica mediante la activación de la quinasa eEF-2 [151]. Además puede inhibir la síntesis proteica modulando la vía de mTORC1 a través de TSC1/TSC2 y de Raptor [152, 153].

AMPK también controla la polarización celular. Varios estudios han demostrado que AMPK regula la polarización en neuronas y en líneas celulares derivadas de riñón, donde además es esencial para la formación de las uniones estrechas celulares [154-156].

En condiciones de escasez de nutrientes, AMPK actúa como un punto de control metabólico que inhibe el crecimiento celular y la proliferación al mismo tiempo que activa la autofagia. Se ha sugerido que uno de los mecanismos involucrados pudiera ser el bloqueo del ciclo celular en la fase G1/S, lo que provoca, entre otros fenomenos, que AMPK juegue un papel muy importante en la formación de tumores [157]. Por otro lado, como AMPK inhibe al complejo mTORC1, además de actuar directamente sobre la síntesis de proteínas, también induce activación de la autofagia. Dentro de los mecanismos generales de autofagia, AMPK es capaz de regular específicamente la mitofagia al mismo tiempo que estimula la biogénesis de nuevas mitocondrias [158, 159]. De esta manera, el resultado final de la acción de AMPK sería el reemplazo de las mitocondrias defectuosas por mitocondrias nuevas y funcionales [160].

Hace algo más de una década comenzaron a aparecer estudios que mostraban como AMPK jugaba un papel importante en la decisión entre supervivencia o muerte celular [128]. Su papel parece depender del contexto ambiental y de la duración de los estímulos. Estudios en hepatocitos (necrosis inducida por H_2O_2) y

fibroblastos (apoptosis inducida por privación de suero) muestran que la activación de AMPK induce supervivencia [161, 162]. Por el contario, otros estudios muestran que la activación prolongada de AMPK induce apoptosis en hepatocitos (activando a c-jun) y en células tumorales (promoviendo la translocación de FOXO3 al núcleo) [163, 164]. Es más, en el caso de las neuronas AMPK tiene un papel protector en caso de déficit energético, mientras que su activación prolongada induce apoptosis [165].

Activadores e inhibidores:

Existen múltiples agentes capaces de activar a AMPK, entre los más comúnmente empleados se encuentran PT1, AICAR y A769662. AICAR es un nucleósido usado para activar a AMPK tanto de cultivos celulares, como de tejidos y de animales *in vivo*. Una vez incorporado al interior celular AICAR es fosforilado y convertido en ZMP, un nucleótido que mimetiza al AMP y que, por tanto, es capaz de activar alostéricamente a AMPK sin alterar los niveles intracelulares de AMP ni modificar la relación AMP:ATP [166]. Sin embargo varios estudios han demostrado recientemente que AICAR no solo actúa sobre AMPK sino que tiene más dianas como son las enzimas glucoquinasa, glucógeno fosforilasa, fosfofructoquinasa o Hsp90 [167].

A769662 es un activador de AMPK específico de los complejos que contienen la subunidad β1, pero no la β2 y presenta una mayor especificidad por el AMPK que AICAR [168]. Se une a la enzima a través de un punto situado entre el dominio catalítico de la subunidad α y la subunidad β, inhibiendo la desfosforilación de la Thr172 [169-171] . Sin embargo, este no parece ser su mecanismo de acción primario ya que, de manera dependiente de la fosforilación de la subunidad β1 en la Ser108, también puede activar a AMPK alostéricamente en ausencia de fosforilación en la Thr172 [172] .

Entre los inhibidores de AMPK se encuentran el compound C y el araA, sin embargo ambos se caracterizan por su baja especificidad por AMPK. Entre las quinasas activadas potente e inespecíficamente por el Compund C se encuentran ERK8, MNK1 y Src entre otras, además de dar lugar a una producción de ceramidas que induce apoptosis [173, 174]. AraA, por otro lado, además de inhibir a AMPK parece inhibir la adenilato ciclasa y activar a la familia de las ERK [175].

MATERIALES Y METODOS

MATERIALES Y MÉTODOS

Reactivos generales

Las quimioquinas CCL19 y CCL21, así como el TNFα son de Peprotech (Rocky Hill, NJ). Las citoquinas GM-CSF e IL4 se compraron a ImmunoTools. El colorante fluorescente carboxyfluorescein diacetato succinimidyl ester (CFSE) se obtuvo de Molecular Probes y el SR-FLIVO de Immunochemistry Technologies.

El Hoechst 33342, el yoduro de propodio, la poliornitina, el LPS, el inhibidor de Akt1/2 (Akti, usado a 5 μM), el inhibidor de PI3K (LY294002, usado 100μM) el inhibidor de Gαi (toxina pertussis, usada a 100 ng/ml) y los activadores de PKA (dibutiril-cAMP y Bromo-cAMP usados a 500 nM y a 200 μM, respectivamente) se compraron a Sigma. El inhibidor de caspasas (Z-VAD-FMK, usado a 10 μg/ml) es de Enzo (Life Science). El inhibidor de AMPK (Compound C, usado a 20μM), los inhibidores de MEK (UO126 y PD0325901 usados a 2,5 μM y a 1 μM, respectivamente) y el inhibidor de ERK (péptido inhibidor de la activación de ERK, usado a 50μM) se obtuvieron de Calbiochem (Nottingham, UK). El segundo de los inhibidores de ERK (CAYMAN10561, usado a 20 μM) es de Cayman Chemicals (Ann Harbor, MI). El tercer inhibidor de ERK (FR180204, usado a 100 μM), el inhibidor de mTORC1 y mTORC2 (KU0063794, usado a 500 nM), el inhibidor de mTORC1 (rapamicina, usada a 100 nM), el inhibidor de Gβγ (galleina, usada a 500 μM) y los activadores de AMPK (A769662 y AICAR, usados a 25 μM y 1 mM, respectivamente) se compraron a Tocris Bioscience (Bristol, UK).

El anticuerpo anti-Bim es de Affinity Bioreagents (Golden, CO). Los anticuerpos anti-MEK1, anti-β-actina, anti-4E-BP1, anti-ERK1, anti-ERK2 y anti-AMPKα1 se obtuvieron de Santa Cruz Biotechnology Inc. (Santa Cruz, CA). Los anticuerpos anti-Akt, anti-Bcl-xl, anti-AMPKα, anti-mTOR, anti-fosfo-MEK1/2 (Ser-217/221), anti-fosfo-ERK1/2 (Thr-202/Tyr-204 en ERK1, Thr-185/Tyr-187 en ERK2), anti-fosfo-Akt1 (Ser-473), anti-fosfo-AMPKα1 (Ser-485), anti-fosfo-AMPKα (Thr-172), anti-phospho-4EBP1 (Thr-37/46), anti-fosfo-p70-S6K (Thr-389) y anti-p70-S6K son de Cell Signaling Technology (Beverly, MA). El anticuerpo anti-fosfo-Acetil CoA-carboxilasa (Ser-79) se obtuvo de Millipore, el anti-Caspasa 3 de Biorbyt (Cambrifge, UK) el anti-Caspasa 8 de BD (San Diego, CA) y el anti-α-tubulina de Rockland Inc. (Limerick, PA).

Ratones

Para los experimentos con ratones se emplearon machos de la cepa C57BL/6 que tenían entre 8 y 10 semanas de edad. Estos animales se mantuvieron en el animalario del Centro de Investigaciones Biológicas y fueron tratados en condiciones libres de patógenos de acuerdo con las directrices establecidas por el comité de ética del Centro de Investigaciones Biológicas sobre el uso y cuidado de los animales de experimentación.

Cultivos celulares

Obtención de CDs de ratón

Para obtener las CDs de ratón se extrajeron y se disgregaron los bazo de los ratones en PBS con 5 mM EDTA. La suspensión obtenida fue filtrada con filtros con un tamaño de poro de 100 µm (BD, San Diego, CA). A continuación, las CDs se marcaron en buffer MACS (2 mM EDTA, 0,5 BSA en PBS) con anticuerpos anti-CD11c acoplados a bolas magnéticas conforme a las especificaciones del fabricante (Miltenyi Biotech, Alemania). Las CDs marcadas fueron purificadas empleando columnas LS (Miltenyi Biotech, Alemania) y finalmente fueron cultivadas en RPMI con 10% FBS a 10^6 CDs/ml. Por último, las CDs se maduraron en presencia de LPS (1 µg/ml) durante 12 horas a 37ºC con un 5% de CO_2.

Obtención de CDs humanas

Las CDs humanas empleadas fueron derivadas de monocitos de sangre periférica. Los monocitos se obtuvieron a partir de "Buffy coats" de donantes de sangre sanos (Centro de Transfusiones de la Comunidad de Madrid). El contenido de los buffy coats se separó mediante un gradiente de Lymphoprep (Nycomed, Noruega) del que se extrajo la capa de células mononucleares. Estas células se lavaron con PBS para retirar los restos de Lymphoprep y se resuspendieron en buffer MACS. Los monocitos se aislaron marcándolos con anticuerpos anti-CD14 acoplados a bolitas magnéticas (Miltenyi Biotech, Alemania) y se cultivaron en RPMI con 10% FBS a 8 x 10^5 células/ml. Para diferencias los monocitos en CDs se mantuvieron en cultivo durante siete días en presencia de GM-CSF (1000 U/ml) e IL4 (1000 U/ml), que se añadían cada 48 horas. De esta manera se obtuvieron CDs inmaduras que finalmente se maduraron añadiendo GM-CSF (1000 U/ml), IL4 (1000 U/ml) y TNFα (50 ng/ml) durante otros 3 días.

Inmunofluorescencias

Las CDs se adhirieron sobre cristales previamente recubiertos con poliornitina (20 µg/ml) durante 45 min, a 37° C, 5% de CO_2 en RPMI con 0,1% BSA. Pasado ese tiempo las células fueron estimuladas o no con CCL21 (15 nM) durante 5 minutos y posteriormente fueron fijadas con 4% paraformaldehido (Santa Cruz, CA), durante 15 minutos, a temperatura ambiente. Una vez fijadas las muestras se permeabilizaron con metanol frío durante 10 minutos, se lavaron con PBS, se bloquearon durante 10 min con IGg humana y se marcaron con los anticuerpos primarios (anti-ERK1, anti-MEK1 o anti-AMPKα1) durante una hora y con una mezcla del correspondiente anticuerpo secundario y Hoechst 33342 (5 µg/ml) durante otra hora. Finalmente, las muestras se lavaron, se montaron con medio de montaje DAKO (Dakocytomation) y se analizaron con un Microscopio Láser Confocal espectral (CLSM) Leica TCS SP5. Las imágenes se analizaron con el software de Adobe Photoshop CS3 versión 10.0.

PLA

Las CDs se adhirieron sobre cristales de poliornitina y se fijaron del mismo modo que en el caso de las inmunofluorescencias. A continuación, las CD se permeabilizaron con 0,2% Triton x100 (Sigma) y se marcaron con los anticuerpos primarios. Después, en lugar de emplear anticuerpos secundarios se realizó la técnica PLA (Proximity Ligation Assay) siguiendo las instrucciones del fabricante (Duolink II in situ PLA detection kit, Sigma) (**Figura 5**) [176]. Brevemente, las muestras se incubaron con anticuerpos secundarios conjugados con sondas de ADN (sondas PLUS y MINUS). A continuación, estas sondas se hibridaron con oligos de secuencias complementarias y se ligaron con una enzima ligasa. Finalmente, se añadió una solución de detección que contiene una polimerasa que amplifica el ADN, así como unas sondas fluorescentes que pueden ser detectadas por microscopía de fluorescencia. Las muestras se montaron empleando una solución de montaje suministrada por la casa comercial que incluye DAPI para marcar los núcleos. Las muestras se analizaron por microscopia confocal empleando el mismo microscopio y software que para las inmunofluorescencias.

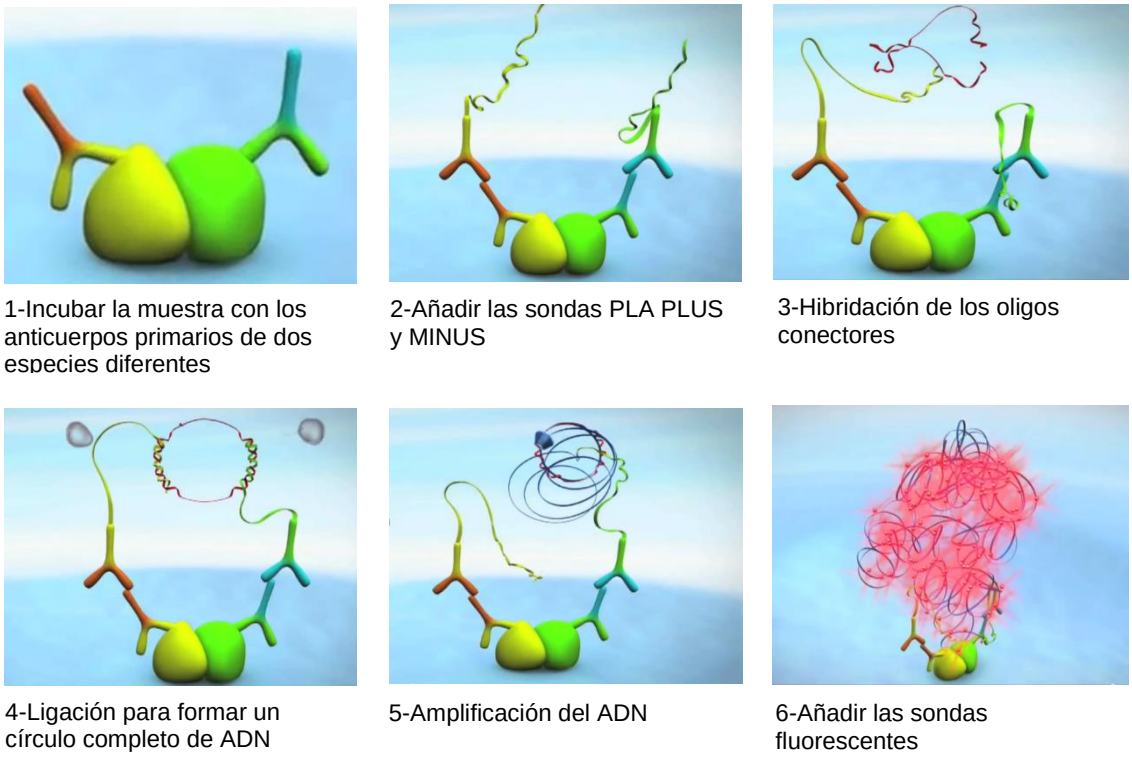

Figura 5: Esquema del fundamento de la técnica PLA. En primer lugar, la muestra se incuba con los anticuerpos primarios que se unen a las proteínas de interés. Después se añaden los anticuerpos secundarios conjugados con oligonucleótidos (sonda PLA MINUS y sonda PLA PLUS). A continuación, se añade la solución de ligación que contiene dos oligonucleótidos (en rojo) y la enzima ligasa. Estos dos oligonucleótidos son complementarios a los que se encuentran conjugados con los anticuerpos secundarios, por lo que hibridan con estos últimos. Si las proteínas de interés se encuentran lo suficientemente juntas la enzima ligasa los une permitiendo que formen un círculo. Por último, se añade la solución de amplificación que contiene nucleótidos (no se muestran), la enzima polimerasa y nuevos oligonucleótidos marcados fluorescentemente. Si los oligonucleótidos de los anticuerpos secundarios han sido ligados y circularizados en el paso anterior la polimerasa podrá llevar a cabo una reacción de amplificación circular que genera un producto concatenado al que se pueden unir los oligonucleótidos fluorescentes que generarán una señal visible con un microscopio de fluorescencia. Imagen adaptada de http://www.sigmaaldrich.com/video/life-science/duolink.html

Análisis de la apoptosis

Análisis de la apoptosis in vitro.

Los experimentos de análisis de la apoptosis en las CDs humanas in vitro se realizaron induciendo la apoptosis mediante la privación de suero. Para ello, el mismo número de CDs vivas (cuantificadas mediante exclusión de la tinción con Azul Tripán) se mantuvieron durante los tiempos indicados en cada experimento en RPMI con 0,1% de BSA. En el caso de los experimentos de cuantificación de la

apoptosis en CDs de ratón los experimentos se realizaron en con 10% FBS RPMI, ya que estás células tienen una vida media mucho menor y experimentan apoptosis incluso en presencia de suero. A continuación, se estudió la apoptosis de las CDs analizando los núcleos, mediante microcopia de fluorescencia, o analizando la fragmentación del ADN, por citometría.

Para el análisis por microscopía de fluorescencia las CDs fueron adheridas sobre cristales de poliornitina del mismo modo que se hizo para las inmunofluorescencias. A continuación, las CDs se fijaron con paraformaldehido al 4% durante 15 minutos, a temperatura ambiente, y posteriormente se permeabilizaron con metanol frío durante 10 minutos. Las muestras se lavaron, se marcaron durante una hora con Hoechst 33342 (5 µg/ml) en PBS con 0,1% BSA y se montaron de igual modo que en el caso de las inmunofluorescencias. Las tinciones se analizaron usando un microscopio Axioplan Universal de Zeiss con una cámara CCD Digital Leica DFC 350 FX con un objetivo 63x ó 100x de inmersión en aceite (Leica Microsystems, Mannheim). Finalmente se cuantificó el porcentaje de núcleos pignóticos o fragmentados presentes en cada preparación.

Para los experimentos de análisis de la fragmentación del DNA las CDs se permeabilizaron durante 30 minutos a 4ºC con etanol al 70%. Las CDs se lavaron y se marcaron con 5 µl de una solución de IP con RNasa (Inmunostep, Salamanca) durante 15 minutos a temperatura ambiente. El marcaje de las CDs se analizó con un citómetro de flujo EPICS (Coulter Electronics) equipado con un láser de Argón sintonizado a 488 nm.

Análisis de la apoptosis en los ganglios poplíteos

Este procedimiento se realizó siguiendo el protocolo descrito previamente por Gómez-Cabañas et al. [177]. Se emplearon CDs de ratón inmaduras que se marcaron con CFSE (2,5 µM) en PBS con 0,1% de BSA a una concentración de 10^7 CDs/ml durante 30 minutos a 37ºC. A continuación, 2 x 10^6 de estas CDs se resuspendieron en 20 µl de RPMI y se inyectaron de manera subcutánea en las almohadillas de cada una de las patas traseras de nuevos ratones receptores. Pasadas 36 horas, tiempo suficiente para que las CDs migren mayoritariamente a los ganglios poplíteos, se inyectó, de manera intraperitoneal, el activador de AMPK A769662 (3,6 mg disuelto en DMSO /25 g de ratón) o el mismo volumen de DMSO en los ratones control. Tras otras 4 horas y media, se inyectó de manera intravenosa el marcador de caspasas SR-FLIVO (8 µg/25 g de ratón; λ_{abs} 565 nm, λ_{em} > 600 nm). Este compuesto contiene un grupo FLIVO^{TM} con un péptido inhibidor de caspasas (Val-Ala-Asp) conjugado a una sulforrodamina B que proporciona la fluorescencia y a un grupo fluorometil

cetona (FMK) que se une covalentemente a una cisteína del centro activo de las caspasas. Una hora después de haber inyectado el (SR)-FLIVO los animales fueron sacrificados y sus ganglios poplíteos fueron extraídos, fijados con paraformaldehido al 4% durante 1 hora a 4°C y montados. Finalmente, las preparaciones se analizaron por microscopia multifotón realizando fotos cada 2 µm con un microscopio de barrido láser confocal y multifotón LSM710 y LSM510 acoplados a un microscopio invertido AxioObserver y uno vertical AxioImager M1 (Zeiss), respectivamente. Las imágenes se analizaron empleando la versión FIJI del software de Image J.

Análisis por Western Blot

Para reducir la actividad basal de las moléculas señalizadoras y para conseguir que sólo el receptor CCR7 sea el responsable de la señalización de las CDs, estas células (100 x 10^3 células por punto) se mantuvieron en RPMI, sin suero y en presencia de 0,1% BSA durante 30 minutos antes de ser estimuladas con CCL21 (15 nM). La estimulación se detuvo solubilizando las células en buffer de carga 2×SDS-PAGE (200 mM Tris-HCl, pH 6,8, 0,1 mM ortovanadato de sodio, 6% SDS, 1 mM EDTA, 4% β-mercaptoetanol, 10% glicerol y azul de bromofenol). Las muestras se hirvieron durante 10 minutos y las proteínas se separaron mediante electroforesis en gel de poliacrilamida con dodecilsulfato sódico (polyacrylamide gel electrophoresis-SDS, PAGE-SDS) y posteriormente se transfirieron a una membrana de nitrocelulosa (BIO-RAD). Las membranas se bloquearon durante 2 horas con una mezcla de 5% de leche desnatada en TBST (TBS que incluye 0,1% Tween 20, pH 7.5) y posteriormente se incubaron durante 18 horas a 4°C en agitación con los anticuerpos primarios y 1 hora a temperatura ambiente con el anticuerpo secundario conjugado a peroxidasa (1:5000 en TBST, Santa Cruz Biotechnology, Santa Cruz, CA). Por último, para revelar las bandas inmunoreactivas, las membranas se incubaron durante 2 minutos con ECL (Pierce). La densitometría de los blots se analizó con el software Multigauge de Fujifilm.

Immunoprecipitación

Las CDs (30 x 10^6 por condición) se mantuvieron en RPMI con 0,1% BSA durante 30 minutos antes de ser estimuladas o no con CCL21 durante 5 minutos (15 nM). A continuación, las CDs se disolvieron en buffer de lisis (que incluye un cocktail de inhibidores de proteasas (Sigma), 1% Nonidet P-40, 100 mM NaCl, 1 mM EDTA, 0.5 µM vanadato y 20 mM Hepes, pH 7.4) y se mantuvieron en agitación durante 30 horas a 4° C. Las muestras se centrifugaron durante 90 minutos a velocidad máxima,

a 4°Cpara retirar los restos de membranas y de ADN. El sobrenadante se incubó durante 15 horas con bolitas de Ig-agarosa a 4°C (TrueBlotTM, eBioscience, San Diego, CA) y se centrifugó durante 30 minutos a velocidad máxima para retirar las moléculas de la muestra que se unían inespecíficamente a las bolas. De nuevo se conservó el sobrenadante que se incubó durante 4 horas en agitación a 4° C con el anticuerpo anti-AMPKα, tiempo tras el cual se añadieron nuevas bolas de Ig-agarosa durante otras 2 horas. Por último, las bolas con los anticuerpos unidos se lavaron 5 veces en buffer de lisis y se hirvieron en buffer de carga 2×SDS-PAGE suplementado con 50 mM de ditiotreitol. Las muestras se analizaron normalmente por SDS-PAGE con la diferencia de que en este caso se empleó un anticuerpo secundario que reconoce únicamente los anticuerpos en su conformación nativa, por lo que no detecta las inmunoglobulinas empleadas para realizar la inmunoprecipitación (TrueBlotTM, eBioscience).

Nucleofecciones

Las CDs maduras (3 x 10^6 CDs por condición) fueron nucleofectadas, según el experimento, con 5 µg de los plásmidos FOXO-GFP o GFP-Control (regalo de Terry Unterman, VA Chicago Healthcare System) o con 0,8 µg del siRNA de AMPK o el siRNA control (Santa Cruz Biotechnology Inc., Santa Cruz, CA). La nucleofección se realizó utilizando el nucleofector y el kit de nucleofección de CDs de Amaxa Biosystems siguiendo las instrucciones del fabricante. Finalmente, las CDs se cultivaron en 3 ml de RPMI con 10% FBS suplementado con GM-CSF (1000 U/ml) e IL4 (1000 U/ml) y se mantuvieron en cultivos durante 36 horas antes de emplearlas para realizar los experimentos.

Estadística

Los datos representados en los gráficos muestran la media ± la desviación estándar. El análisis estadístico se realizó con el test t de Student para muestras pareadas considerando que las diferencias eran significativas cuando el valor p era menor de 0,05 (excepto el análisis de los datos de la apoptosis in vivo en el que se empleó el test para muestras no pareadas.). “ns” indica diferencias no significativas entre dos tratamientos, “n” hace referencia al número de experimentos independientes realizados.

OBJETIVOS

OBJETIVOS

1- Analizar si AMPK juega algún papel en la regulación de la supervivencia de las CDs

2- Describir el mecanismo que emplea AMPK en la regulación de la apoptosis o la supervivencia de las CDs.

3- Estudiar si CCR7 regula la actividad de AMPK en las CDs.

4- Usar un modelo in vivo para confirmar el papel de AMPK en la regulación de la supervivencia de las CDs

5- Analizar los mecanismos de señalización intracelular que emplea CCR7 para regular la actividad de AMPK.

RESULTADOS

RESULTADOS

1- AMPK induce apoptosis en células dendríticas maduras in vitro.

AMPK puede inducir apoptosis o supervivencia dependiendo del tipo celular y del estímulo [164, 165, 178], por tanto, nuestro primer objetivo fue analizar si AMPK promueve o inhibe la apoptosis en las CDs humanas derivadas de monocitos. Para ello empleamos dos activadores farmacológicos de AMPK: AICAR y A769662. Las CDs maduras se mantuvieron en RPMI-BSA en presencia o ausencia de uno de los dos activadores y posteriormente analizamos mediante Western Blot el grado de activación de AMPK. Como se puede ver en la **figura 6A** las, CDs tratadas con AICAR ó A769662 presentan una potente fosforilación tanto de un residuo de AMPK que

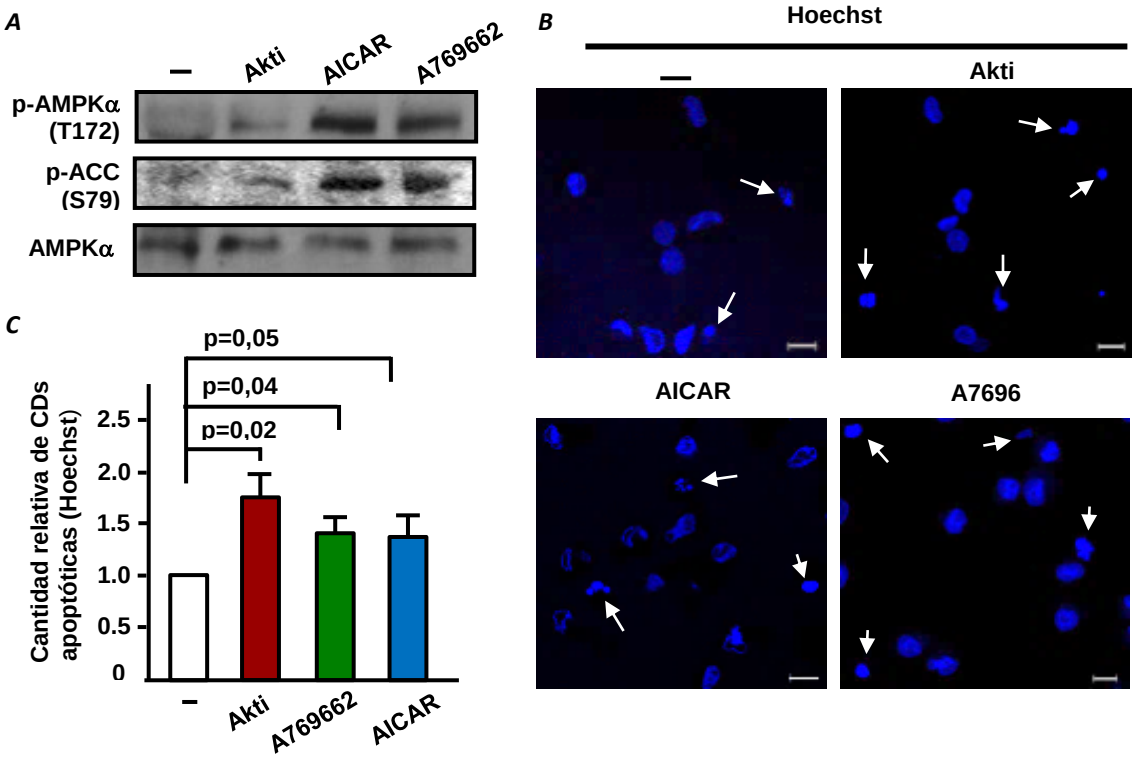

Figura 6: La activación de AMPK induce picnosis nuclear en las CDs humanas. A: CDs humanas maduras se mantuvieron durante 24 h en RPMI /0,1% BSA, en presencia o ausencia de Akti (5 µM), AICAR (1 mM) o A769662 (25 µM). Posteriormente las células se analizaron mediante Western Blot con anticuerpos anti fosfo-AMPKα (Thr172), fosfo-ACC (Ser79) y AMPKα total. **B:** Se muestran fotos representativas de CDs tratadas como en el apartado A y teñidas con Hoechst 33342. Las flechas señalan núcleos condensados o fragmentados que se corresponden con células muertas. **C:** Cuantificación del número de CDs apoptóticas que tratadas como en el apartado B. Se representa el incremento del número de células apoptóticas con respecto al control, CDs en RPMI con un 10% de FBS y sin inhibidores. Los resultados muestran el valor de la media ± SD. (n=6)

indica que esta molécula se encuentra activada (Thr172) como de su diana en la enzima Acetil-CoA Carboxilasas (ACC) que es fosforilada específicamente por AMPK en la Ser79 [146, 179].

Una vez comprobada la eficacia de los activadores se procedió a realizar un ensayo de apoptosis, cuantificando mediante microscopía de fluorescencia el porcentaje de CDs con núcleos picnóticos. Se trataron las células con AICAR ó A769662 y se empleó el inhibidor de AKT (Akti) como control positivo de apoptosis. Como se puede ver en las **figuras 6B y 6C,** los dos activadores inducen un aumento de la proporción de núcleos picnóticos con respecto al control, aunque sin llegar a una cantidad tan alta como la del control positivo.

También se midió la apoptosis estudiando la fragmentación del ADN [180]. Para este fin se analizó por citometría la incorporación de yoduro de propidio en el núcleo de las células. En estos experimentos tanto AICAR como A769662 indujeron un aumento de más del doble de fragmentación del ADN comparado con el control, aunque muy por debajo del control positivo con el inhibidor de Akt (**figura**

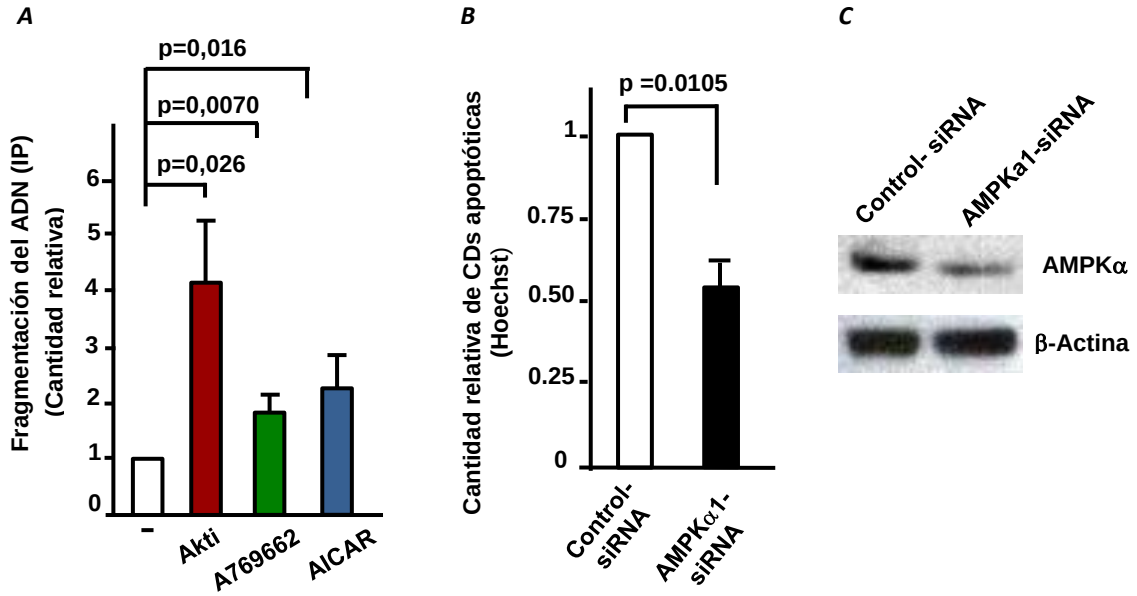

Figura 7: La muerte celular inducida por AMPK provoca fragmentación del ADN. **A:** CDs humanas maduras se mantuvieron durante 24 h en RPMI /10% FBS sin tratamiento o en presencia de Akti (5 µM), AICAR (1 mM) o A769662 (25 µM). Las células se tiñeron con yoduro de propidio (IP) y el grado de fragmentación del DNA fue analizado por citometría. La grafica muestra valores estandarizados con respecto al control de CDs sin tratamiento. **B:** CDs humanas maduras fueron nucleofectadas con un siRNA control o con un siRNA específico para AMPK. Pasadas 36 horas las CDs se pusieron en RPMI en presencia de 0,1% de BSA durante otras 24 h, periodo tras el cual se cuantificó el número de CDs apoptóticas para cada uno de los tratamientos. **C:** Una alícuota de CDs transfectadas como en el apartado B se analizó mediante Western Blot con anticuerpos anti AMPKα total y anti β-actina. Los resultados muestran el valor de la media ± SD (n=3).

7A).También se confirmó el papel de AMPK en la supervivencia de las CDs reduciendo la actividad de AMPK mediante la transfección de las CDs con un siRNA control o un siRNA de AMPKα. En línea con los resultados anteriores se observó que la reducción de los niveles de AMPK iba acompañado de una disminución de la muerte celular (**figuras 7B y 7C**).

Por último, puesto que la apoptosis requiere la activación de caspasas, se analizó si estas proteasas estaban implicadas en el tipo de muerte inducida por AMPK [21]. Para este fin las CD se pre-trataron con el inhibidor de caspasas Z-VAD-FMK y posteriormente se expusieron a los activadores de AMPK. Los resultados muestran que el pre-tratamiento bloquea por completo la apoptosis inducida por AICAR y A769662 (**figura 8A**), lo que indica que la activación de AMPK da lugar a una apoptosis dependiente de caspasas. Además, se analizó la activación de la caspasa 3 en respuesta a la activación de AMPK con AICAR y A769662. En la **figura 8B** se puede ver como el tratamiento induce un aumento en los niveles del fragmento *p17* de la caspasa 3, resultado de la proteólisis que tiene lugar tras la activación de esta

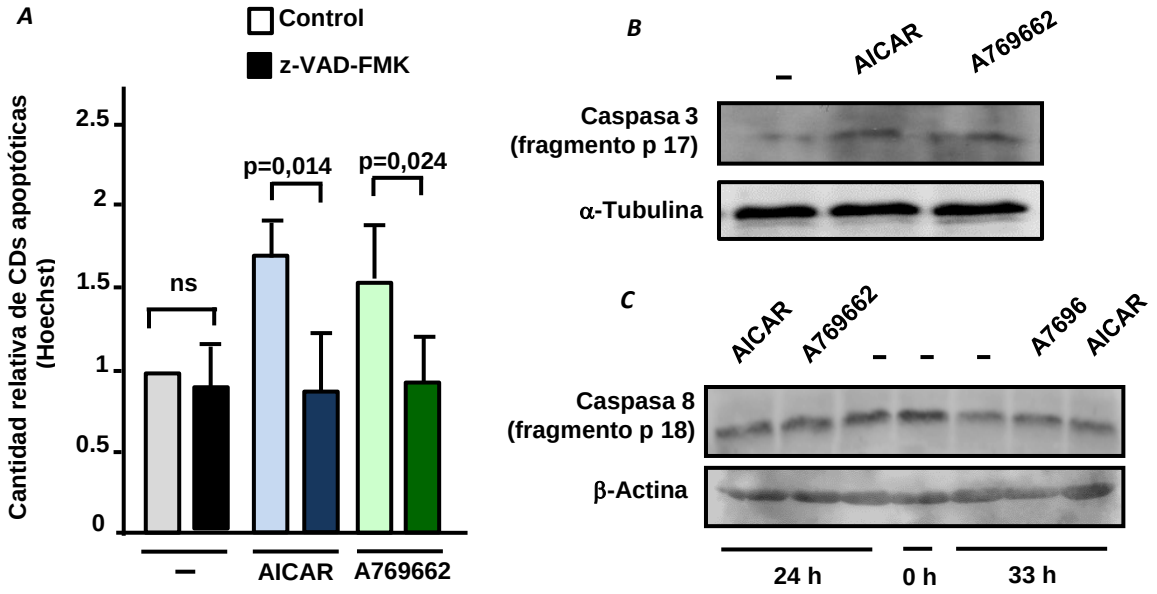

Figura 8: La muerte celular inducida por AMPK es de tipo intrínseco y dependiente de caspasas. **A:** CDs humanas maduras se mantuvieron durante 40 h en RPMI /0,1% BSA o el mismo medio suplementado con AICAR (1 mM) o A769 (25 µM) combinado o no con el inhibidor de caspasas z-VAD-FMK (10 µg/ml). Las CDs se tiñeron con Hoechst 3342 y, posteriormente se cuantificó el número de CDs apoptóticas. Se representa el incremento relativo del número de células apoptóticas (en ausencia o presencia de inhibidores de caspasas) con respecto al control de células sin tratar. Se muestra el valor de la media ± SD (n=5). **B:** Las CDs humanas se mantuvieron 33 h en RPMI con 0,1% BSA exclusivamente o este mismo medio suplementado con AICAR (1 mM) o A769 (25 µM). Posteriormente se analizaron los niveles del fragmento de activación p17 de la caspasa 3. Se presentan los niveles α-tubulina para mostrar la carga de todos los carriles. **C:** Las CDs humanas se mantuvieron 24 o 33 h en las mismas condiciones que en el apartado A. Posteriormente se analizaron los niveles del fragmento p18 de la caspasa 8y de β-actina.

caspasa.

A continuación, quisimos confirmar que la apoptosis inducida por AMPK era una apoptosis intrínseca y no una apoptosis extrínseca inducida por receptores de muerte. Para ello analizamos el nivel de activación de la caspasa 8, que es la caspasa iniciadora implicada en la apoptosis extrínseca, mediante el análisis de los niveles su fragmento p18. Sin embargo, como se puede ver en la **figura 8C**, no observamos activación de esta caspasa, por lo que descartamos que se tratara de una apoptosis extrínseca.

2- AMPK induce apoptosis estimulando la translocación de FOXO1 al núcleo

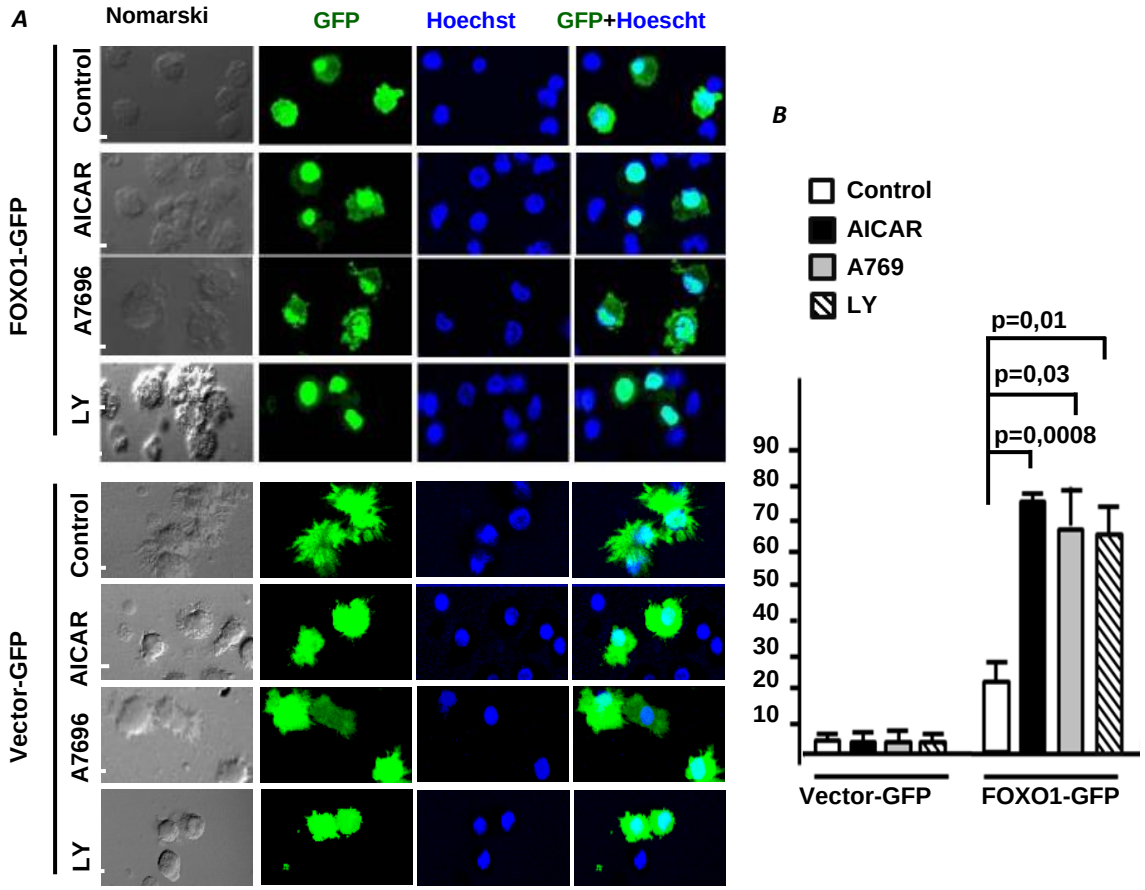

Figura 9: AMPK promueve la translocación de FOXO1 al núcleo. A: CDs humanas maduras se transfectaron con un plásmido control (vector) o con el plásmido FOXO1-GFP. Pasadas 6 h las CDs se dejaron sin tratar o se trataron durante otras 2,5 h con AICAR (1 mM), A769662 (25 µM), o con LY294002 (LY, 100 µM). A continuación, las CDs se colocaron sobre cristales recubiertos de poliornitina y se tiñeron con Hoechst 33342. Por último, se analizó la localización de FOXO con un microscopio de fluorescencia. La escala equivale a 20 µM. **B:** Cuantificación del porcentaje de células transfectadas que presentan la señal GFP concentrada en el núcleo. Se muestra el valor de la media ±SD (n=3)

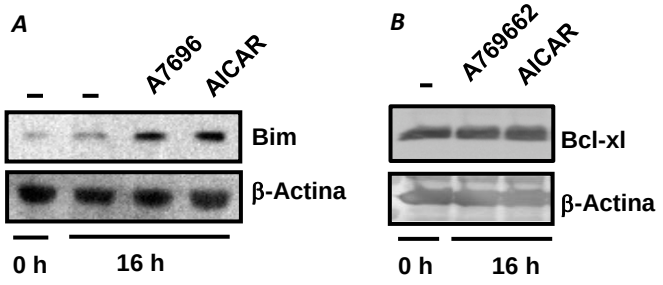

Figura 10: La activación de AMPK genera un aumento de expresión de Bim pero no afecta a los niveles de Bcl-xl. A: CDs humanas se mantuvieron 16 h en RPMI/ 0,1% BSA o en este mismo medio en presencia de AICAR (1 mM) o A769662 (25 µM). A continuación, se analizaron los niveles BIM mediante Western Blot. **B:** Análisis de los niveles de Bcl-xl de CDs tratadas como en el apartado A.

e inhibiendo al complejo mTORC1.

Una vez confirmado el papel pro-apoptótico de AMPK en las CDs, nos propusimos caracterizar los mecanismos involucrados en la inducción de la apoptosis. Para ello, analizamos posibles dianas entre las moléculas para las que ya se conocía su implicación en la regulación de la supervivencia inducida por CCR7 (**figura 2**), como el factor de transcripción FOXO, que promueve la apoptosis en las CDs.

La actividad de FOXO puede ser analizada estudiando su localización celular, ya que su localización nuclear se asocia con su estado activo y su localización citoplásmica con su estado inactivo. Para analizar el posible papel de FOXO1 como diana de AMPK se transfectaron CDs maduras con un plásmido FOXO1-GFP o con un plásmido GFP control. A continuación, estas células se trataron o no con AICAR, A769662 o el inhibidor de PI3K LY, que se usó como control positivo y posteriormenete se analizó por microscopía de fluorescencia la localización celular de FOXO1. Como se puede ver en las **figuras 9A y 9B**, la activación de AMPK induce la translocación de FOXO1 al núcleo.

Para confirmar estos resultados, se analizaron los niveles de expresión de la proteína pro-apoptótica BIM, un miembro de la familia Bcl2 cuya expresión está bajo el control de FOXO. En la **figura 10A** se puede ver cómo tras 16 horas de activación de AMPK se produce un aumento de los niveles de BIM.

Analizamos también si AMPK inhibe al factor de transcripción NF-κB, que es un componente molecular de la ruta inducida por CCR7 que promueve la supervivencia (**figura 2**, página 22). Para ello se analizaron los niveles de la proteína anti-apoptótica Bcl-xl, cuya expresión está regulada por NFκB. Sin embargo, se observó que sus niveles se mantuvieron constantes y no cambiaron cuando las células fueron tratadas con los dos activadores de AMPK (**figura 10B**).

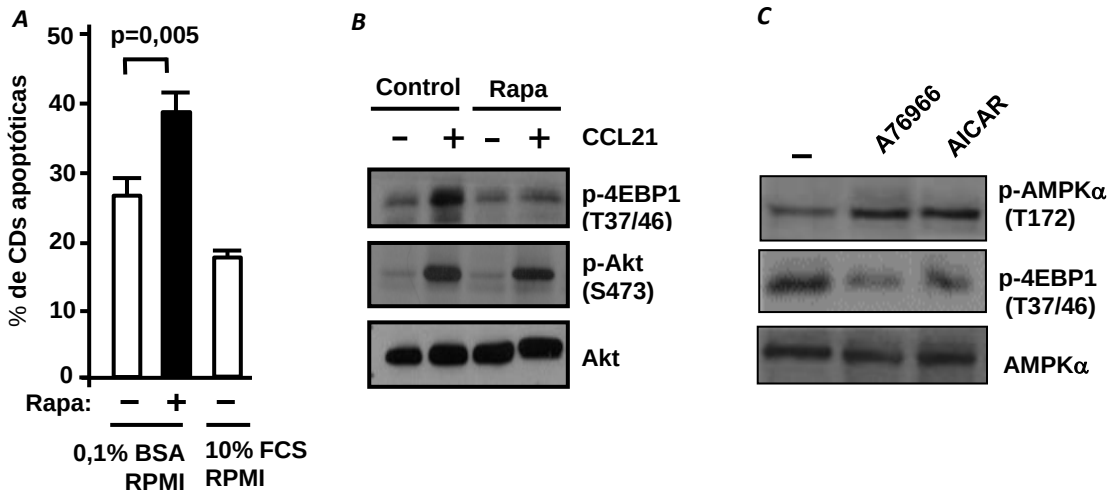

Figura 11: AMPK inhibe al complejo promotor de supervivencia mTORC1. A: CDs humanas se mantuvieron 40 h en RPMI/0,1% BSA en ausencia o en presencia de Rapamicina (RAPA, 100 nM). Como control negativo se emplearon CDs en RPMI con 10% de FBS. A continuación, las CDs se adhirieron sobre cristales con poliornitina, se fijaron, se permeabilizaron y se tiñeron con Hoechst 33342 para cuantificar el porcentaje de células apoptóticas. Los resultados muestran el valor de la media ± SD. (n=3). **B:** Se extrajeron alícuotas de CDs control y de CDs tratadas con RAPA del apartado A y se estimularon o no 5 min con CCL21. Posteriormente, se analizaron por Western Blot los niveles de fosfo-4EBP1 (Thr37/39), fosfo-Akt (Ser473) y AKt total. **C:** Las CDs humanas se mantuvieron durante 60 min en RPMI /10% de FBS en ausencia o en presencia de AICAR (1 mM) o A769662 (25 µM). Alícuotas de cada uno de los tratamientos se extrajeron y se analizaron por Western Blot con anticuerpos anti fosfo-AMPKα (Thr172), fosfo-4EBP1 (Thr37/39) y AMPKα total.

Por último, decidimos analizar el papel de mTORC1, un complejo cuya actividad también está regulada por la ruta de supervivencia inducida por CCR7. En primer lugar, confirmamos que mTORC1 promueve la supervivencia de las CDs. Para ello se trataron las CDs maduras con el inhibidor rapamicina, cuyo efecto inhibitorio sobre mTORC1 se puede analizar siguiendo los niveles de fosforilación de su diana 4EBP1. En las **figuras 11A y 11B** se puede ver como la inhibición de mTORC1 da lugar a un incremento de la apoptosis de las CDs, lo que confirma su papel como molécula anti-apoptótica. Para comprobar que mTORC1 era una diana de AMPK, analizamos también la actividad de mTORC1 analizando la fosforilación de su diana 4EBP1 en CDs, que fueron tratadas o no, con los dos activadores de AMPK. Como se obsrva en la **figura 11C** la activación de AMPK provoca una inhibición de mTORC1.

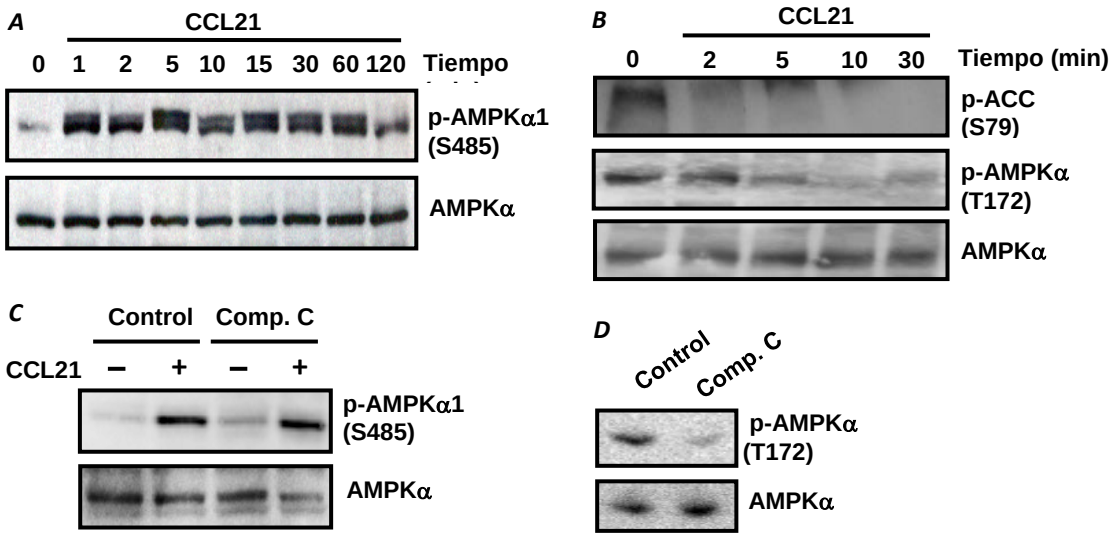

Figura 12: La estimulación de CCR7 induce la fosforilación e inhibición de AMPK: A: CDs humanas mantenidas en RPMI/0,1% BSA fueron estimuladas con CCL21 durante diferentes tiempos. A continuación, las células fueron lisadas y analizadas por Western Blot con anticuerpos anti fosfo-AMPK (Ser485) o AMPK total. **B:** Análisis de CDs tratadas como en el apartado A y analizadas con anticuerpos anti fosfo-ACC (Ser79), fosfo-AMPK (Thr172) o AMPKα total. **C:** Análisis de CDs tratadas como en el apartado A pero a las que se pretrataron o no durante 1 h con Compound C (Comp. C, 20μM). Posteriormente los lisados se analizaron con anticuerpos anti fosfo-AMPK (Ser485) o AMPK total. **D:** Análisis con anticuerpos anti fosfo-AMPK (Thr172) y AMPKα total de alícuotas de las muestras del apartado C.

3- La estimulación de CCR7 induce la fosforilación e inhibición de AMPK.

Como CCR7 induce supervivencia en las CDs, nos planteamos la posibilidad de que este receptor pudiera promover señalización intracelular que inhibiera la actividad de AMPK, como mecanismo adicional de control de la supervivencia. Para estudiar si CCR7 regula la actividad de AMPK, las CDs humanas se estimularon con CCL21. A continuación, se examinó el estado de activación de AMPK analizando el nivel de fosforilación en la Ser485 (fosforilación inhibitoria), en la Thr172 (fosforilación activadora) y el nivel de fosforilación de la diana ACC.

Como se puede observar en las **figuras 12A y 12B** la estimulación de las CDs con CCL21 induce una rápida fosforilación de AMPK en la Ser485, que va acompañada de una bajada de los niveles de fosforilación de AMPK en la Thr172 y de ACC en la Ser79.

Esta descrito que AMPK tiene capacidad de autofosforilarse en la Ser485 [132]. Para saber si CCR7 estaba induciendo la fosforilación inhibitoria de AMPK directamente o si estaba activando a AMPK para que se autofosforilara en esta posición usamos el Compound C, un inhibidor de AMPK. El proceso de autofosforilación se descartó debido a que los experimentos mostraron que las CDs estimuladas con CCL21

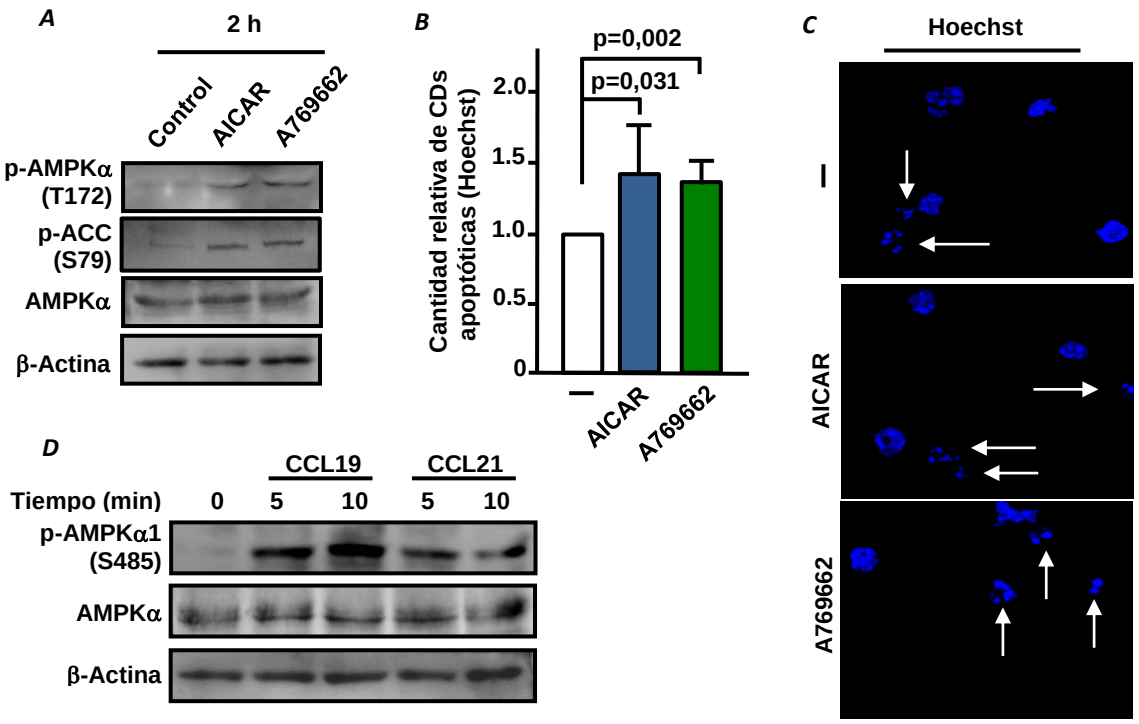

Figura 13: La activación de AMPK induce apoptosis en CDs de ratón. A: CDs de ratón se mantuvieron durante 2 h en RPMI/0,1 % BSA en ausencia o presencia de AICAR (1 mM) o A769662 (25 µM). Una alícuota de cada uno de los tratamientos se extrajo y se analizó por Western Blot con anticuerpos anti fosfo-AMPKα (Thr172), fosfo-ACC (Ser79), AMPKα total y β-actina. **B:** Incremento relativo del número de células apoptóticas de CDs tratadas como en el apartado A y adheridas sobre cristales recubiertos de poliornitina y teñidas con Hoechst 33342. Los resultados muestran el valor de la media ± SD. (n=6). **C:** Fotos representativas de CDs tratadas como en el apartado B. Las flechas señalan núcleos condensados o fragmentados que se corresponden con células muertas. **D:** Las CDs en RPMI con un 0,1 % de BSA fueron estimuladas con CCL21 o CCL19 durante 5 ó 10 min. A continuación, fueron lisadas y analizadas por Western Blot con anticuerpos anti fosfo-AMPK (Ser485), AMPK total y β-actina.

presentaban el mismo grado de fosforilación en la Ser485 en presencia y ausencia de Compound C, a pesar de que este inhibidor bloqueó por completo la actividad de AMPK (**figura 12C y 12D**).

4- La activación de AMPK induce apoptosis in vivo en CDs de ratón en los ganglios linfáticos.

Los resultados obtenidos acerca del papel pro-apoptótico de AMPK en las CDs fueron obtenidos in vitro. Quisimos replicar estos resultados en un modelo in vivo. Para ellos usamos un modelo de ratón en el que se analiza la apoptosis de las CDs en los ganglios poplíteos [177]. Sin embargo, antes de realizar este experimento

comprobamos primero que los resultados obtenidos in vitro acerca del efecto de AMPK sobre las CDs humanas eran reproducibles en ratón.

En primer lugar, analizamos la eficacia de nuestros activadores farmacológicos en las CDs de ratón. Para ello, tratamos las CDs maduras de ratón con AICAR ó A769662 y analizamos primero su capacidad de activar a AMPK y, después, si la activación de AMPK también induce apoptosis en las CDs de ratón. Como se muestra en la **figura 13A**, los activadores son capaces de inducir una activación eficiente de AMPK cuando se mide la fosforilación de AMPK en la Thr172. Además, al igual que ocurre con las CDs humanas, cuando se cuantifican los núcleos picnóticos de las CDs de ratón tratadas o no con los activadores se aprecia un aumento de

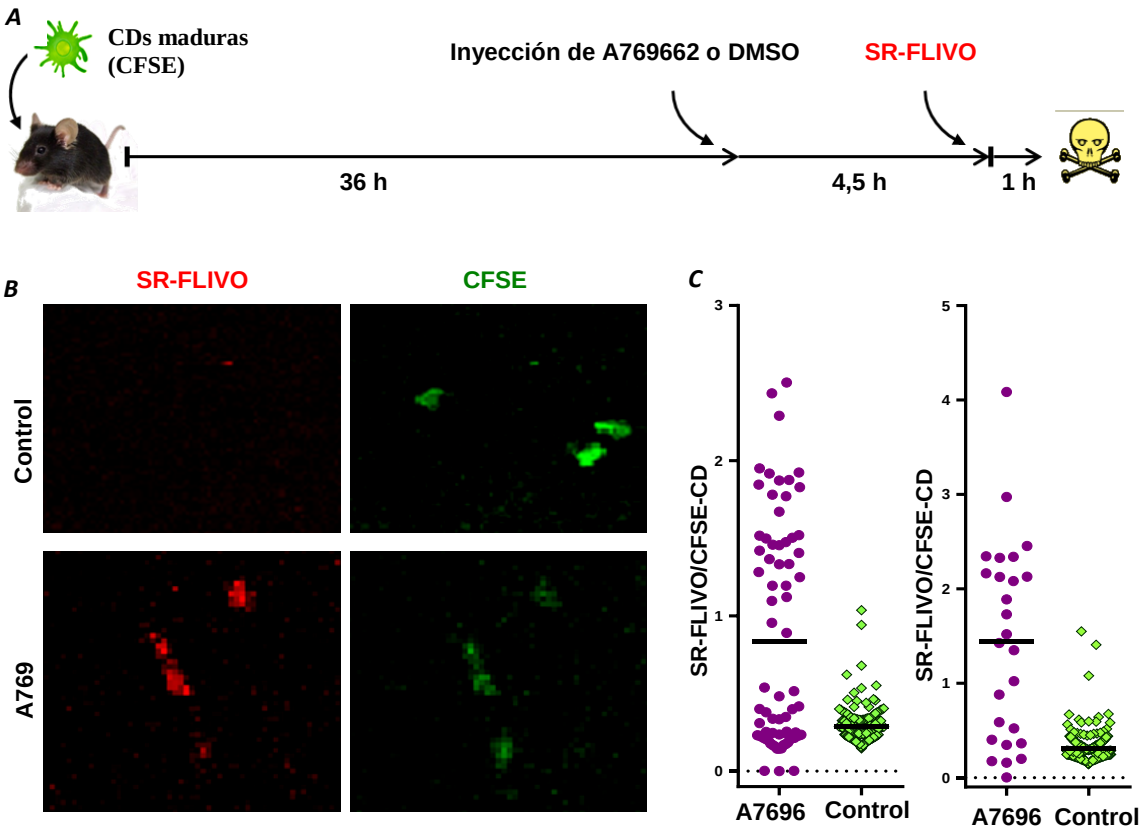

Figura 14: La activación de AMPK induce apoptosis en CDs in vivo. A: Esquema del protocolo experimental. Se inyectaron 2 x 10^6 CDs marcadas con CFSE en las almohadillas de las patas traseras de los ratones receptores. Después de 36 h se inyectaron de manera intraperitoneal 100 µmol de A769662 o un volumen equivalente del solvente (DMSO) a los ratones. Pasadas otras 4,5 h se inyectó el SR-FLIVO de manera intravenosa. Tras 1 h los ratones fueron sacrificados y se les extrajeron los ganglios poplíteos que fueron fijados y analizados con un microscopio confocal multifotón. **B:** Imágenes representativas del marcaje con SR-FLIVO y CFSE de CDs de ganglios de animales tratados con A769662 o con DMSO. **C:** Cuantificación de la fluorescencia de las CDs. Se muestran los valores de amplitud máxima del SR-FLIVO sobre la amplitud máxima del CFSE de las CDs de dos experimentos independientes.

células apoptóticas (**figuras 13B y 13C**). Por lo tanto, se puede concluir que AMPK es una molécula pro-apoptótica también en las CDs de ratón en cultivo. Asimismo, observamos que, al igual que ocurre con las CDs humanas, la estimulación de CCR7 en las CDs murinas también induce inhibición de AMPK mediante su fosforilación en la Ser485 (**figura 13D**).

Una vez comprobado que los resultados obtenidos in vitro sobre el papel de AMPK en las CDs humanas y de ratón eran equivalentes, procedimos a realizar los experimentos in vivo. La **figura 14A** muestra el esquema resumen del protocolo experimental que usamos. Brevemente: $2x10^6$ CDs de ratón marcadas con el colorante intravital CFSE se inyectaron en las patas traseras de ratones C57BL6. Pasadas 36 horas (tiempo suficiente para que las CDs alcancen los ganglios) se inyectó intraperitonealmente A769662 ó su solvente (DMSO) a los ratones [65]. Se dejaron pasar otras 4,5 horas para que el activador farmacológico hiciera efecto sobre las CDs y se inyectó de manera intravenosa el inhibidor fluorescente de caspasas SR-FLIVO. Una hora después, los animales fueron sacrificados y se extrajeron sus ganglios poplíteos que se analizaron por microscopia multifotón. En las **figuras 14B** y **14C** se muestra el resultado de la cuantificación de las imágenes obtenidas, en las que se aprecia como las CDs de los ganglios tratados con A769 tienen de media una intensidad máxima de fluorescencia del SR-FLIVO mayor que las CDs de los ganglios de los ratones control. Por tanto, AMPK también juega un papel pro-apoptótico en las CDs in vivo.

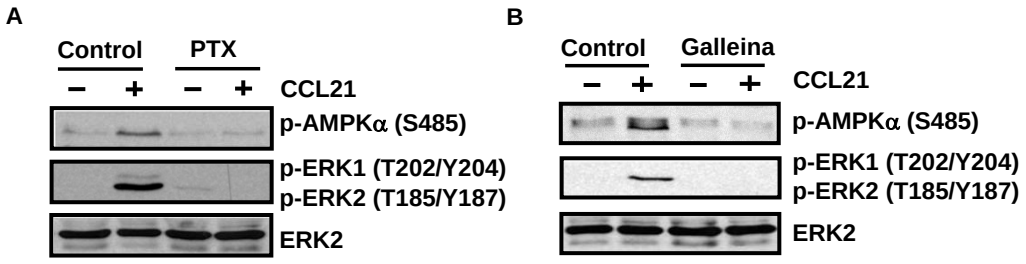

Figura 15: La fosforilación inhibitoria de AMPK inducida por CCR7 está mediada por las subunidades Gαi y Gβγ de la proteína G. A: CDs humanas en RPM/0,1% BSA fueron tratadas o no con la toxina pertussis (PTX, 100 ng/ml, 3 h) y estimuladas o no 5 min con CCL21. A continuación, las células fueron lisadas y analizadas por Western Blot con anticuerpos anti fosfo-AMPK (Ser485), fosfo ERK1/2 (Thr-202/Tyr-204 ERK1; Thr-185/Tyr-187 ERK2) o anti ERK2 total. **B:** CDs tratadas o no con Galleina (500 µM, 15 min) fueron estimuladas con CCL21 como en el apartado A y analizadas con anticuerpos anti fosfo-AMPK (Ser485), fosfo ERK1/2 (Thr-202/Tyr-204 ERK1; Thr-185/Tyr-187 ERK2) o ERK2 total. En ambos casos se muestra un experimento representativo de 3 realizados.

5- La inhibición de AMPK inducida por CCR7 está mediada por Gαi, Gβγ, MEK y ERK.

Nuestro siguiente objetivo fue caracterizar la ruta de señalización empleada por CCR7 para inhibir a AMPK. Comenzamos por intentar identificar la familia de la subunidad α de la proteína G responsable de transmitir la señal desde CCR7, para lo que se empleó la toxina Pertussis que actúa inhibiendo específicamente a las proteínas de la familia Gαi. Se realizaron experimentos pretratando las CDs o no con la toxina Pertussis y estimulándolas posteriormente con CCL21, para analizar a continuación el grado de fosforilación en la Ser485 de AMPK. Como control de la actividad del inhibidor se comprobaron los niveles de fosforilación de ERK1/2, cuya actividad se sabe que está regulada por Gαi [65]. Como se puede ver en la **figura 15A,** la inhibición de la actividad de la subunidad Gαi va acompañada de un bloqueo casi completo de la estimulación de p-AMPK Ser485.

Una vez comprobada la implicación de Gαi en la transmisión de la señal inhibitoria desde CCR7 hasta AMPK, analizamos el papel de las otras dos subunidades de las proteínas G: las subunidades β y γ. Para ello, pretratamos las CDs humanas con Galleina, un inhibidor específico de estas dos subunidades y, posteriormente, estimulamos las CDs con CCL21. Como se sabe que la fosforilación de ERK1/2 también es dependiente de la actividad de Gβγ, nuevamente analizamos esta quinasa como control de la correcta actividad del inhibidor [65]. En la **figura 15B** se muestra cómo la estimulación de la fosforilación en la Ser485 de AMPK también es dependiente de la actividad de las subunidades βγ de la proteína G.

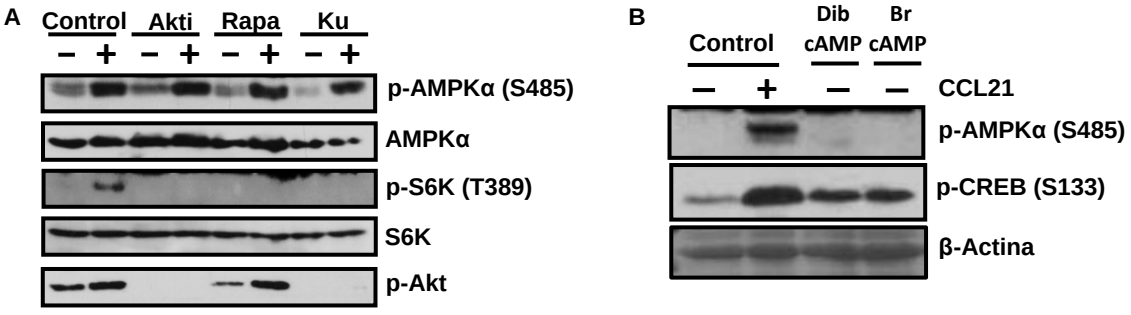

Figura 16: La fosforilación inhibitoria de AMPK inducida por CCR7 no está mediada por Akt, S6k ni PKA. A: CDs humanas en RPMI/0,1% BSA fueron pretratadas o no con Akti (5 μM), RAPA (10 nM), or KU0063794 (Ku, 500 nM) durante 60 min y, posteriomente fueron, estimuladas o no 5 min con CCL21. A continuación, las CDs fueron lisadas y analizadas por Western Blot con anticuerpos anti fosfo-AMPK (Ser485), AMPK total, fosfo-S6K (thr389), S6K total y fosfo-Akt (Ser473). **B:** CDs estimuladas con CCL21 (15 nM, 5 min), o tratadas con dibutiril-cAMP (Dib cAMP, 500 nM) o con bromo-cAMP (Br cAMP, 200 μM) durante 60 min fueron lisadas y analizadas por Western Blot con anticuerpos anti fosfo-AMPK (Ser 485), fosfo-CREB (Ser133) y AMPK total.

A continuación, analizamos las moléculas implicadas en la inhibición de AMPK por debajo de la proteína Gαi. Hasta la fecha se han descrito tres quinasas capaces de llevar a cabo la fosforilación de AMPK en la Ser485: Akt, S6K y PKA [132, 136, 181]. En el laboratorio habíamos descrito previamente la implicación de Akt y S6k en el módulo inductor de supervivencia que se activa en respuesta a la estimulación de CCR7 en las CDs (**figura 2**, página 22) [69]. Además, la actividad de Gαi y de Gβγ son esenciales para la activación de dicho módulo. Por ello, Akt y S6k eran nuestras principales candidatas para ser las responsables de la fosforilación de AMPK y decidimos comenzar por estudiar a estas dos quinasas.

Para examinar la implicación de Akt empleamos un inhibidor específico de Akt1 y Akt2 (Akti). Se realizó un pretratamiento de las CDs seguido de su estimulación con CCL21, comprobándose posteriormente el efecto del inhibidor mediante el análisis los niveles de fosforilación de Akt en la Ser473 (fosforilación activadora). En la **figura 16A** se muestra como el bloqueo de la activación de Akt no afecta a la estimulación de la fosforilación de AMPK en la Ser485.

Analizamos si S6K pudiera ser la responsable de fosforilar e inhibir a AMPK. Para ellos inhibimos a S6K mediante el bloqueo con dos agentes farmacológicos de las quinasa mTORC1, que regula la actividad de S6K.: Rapamicina o KU0063794. Para comprobar que estos agentes farmacológicos bloqueaban a S6K empleamos anticuerpos contra una forma activa y fosforilada (Thr389) de S6K. Tras la estimulación de CCR7 los dos inhibidores farmacológicos inhibieron por completo la activación de S6K, pero no afectaron a la fosforilación de AMPK (**figura 16A**).

Descartadas las quinasas Akt y S6K como responsables de la fosforilación de AMPK quedaba PKA como candidata. Para comprobar si PKA era la quinasa reguladora de AMPK sometimos a las CDs a un tratamiento con dos activadores de PKA análogos del AMP cíclico (cAMP): dibutiril-cAMP y bromo-cAMP. Como control positivo de la activación de PKA y de AMPK estimulamos a las CDs con CCL21 y analizamos el grado de activación de PKA empleando anticuerpos frente a una de sus dianas, el factor de transcripción CREB (**figura 16B**). De esta manera pudimos observar cómo

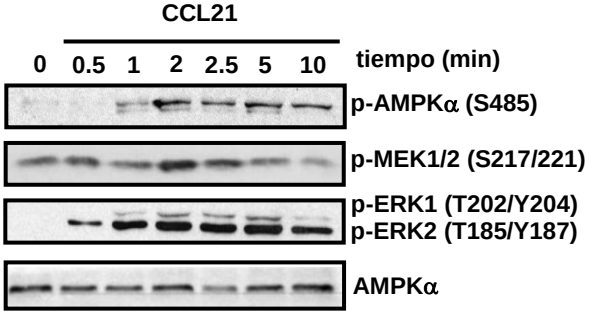

Figura 17: Cinéticas de fosforilación de AMPK, MEK1/2 y ERK1/2: A: CDs humanas mantenidas en RPMI con 0,1% BSA fueron estimuladas con CCL21 durante diferentes tiempos. A continuación, fueron lisadas y analizadas por Western Blot con anticuerpos anti fosfo-AMPK (Ser485), fosfo-MEK1/2 (Ser-217/221), fosfo-ERK1/2 (Thr-202/Thr-204 ERK1; Thr-185/Tyr-187 ERK2) y AMPKα total.

la fosforilación de AMPK en la Ser485 aumentaba en respuesta a la estimulación de CCR7, pero no en respuesta al tratamiento con los activadores de PKA. Estos resultados sugieren que PKA no media los efectos de CCR7 sobre AMPK.

Para tratar de encontrar la vía de señalización implicada en la inhibición de AMPK, decidimos seguir buscando candidatos entre las moléculas ya descritas en las rutas de señalización activadas en respuesta a la activación de CCR7 (**figura 2**). Puesto que no habíamos observado ningún efecto sobre la inducción de la fosforilación de AMPK en la Ser485 con los inhibidores de Akt, descartamos las moléculas del módulo regulador de supervivencia y decidimos continuar buscando entre las proteínas implicadas en el módulo regulador de la quimiotaxis.

Para ello comenzamos por estudiar a MEK1/2 y ERK1/2, dos de las quinasas claves implicadas en el módulo regulador de la quimiotaxis **(figura 2**, página 22**)**. Realizamos un estudio comparando las cinéticas de fosforilación de AMPK, MEK1/2 y ERK1/2 en respuesta a la estimulación de CCR7 con CCL21. Como muestra la **figura 17**, se observó activación de ERK1/2 muy rápidamente, desde los primeros 30 segundos,

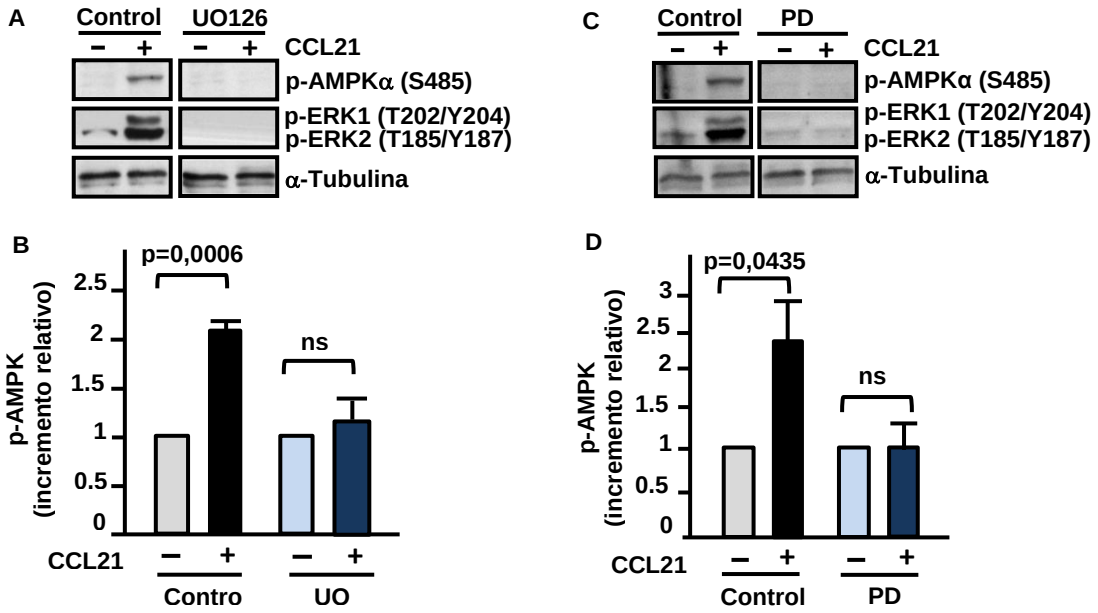

Figura 18: La fosforilación inhibitoria de AMPK inducida por CCR7 está mediada por MEK1/2. **A**: CDs humanas en RPMI/0,1 % BSA fueron tratadas o no con UO126 (2,5 µM, 60 min) y estimuladas 5 min con CCL21. A continuación, fueron lisadas y analizadas por Western Blot con anticuerpos anti fosfo-AMPK (Ser485), fosfo-ERK1/2 (Thr-202/Tyr-204 ERK1; Thr-185/Tyr-187 ERK2) o tubulina **B:** Cuantificación del incremento en la fosforilación de AMPK (Ser485) de CDs tratadas como en el apartado A. **C**: CDs en RPMI/0,1% de BSA fueron tratadas o no con PD325901 (PD, 1 µM, 60 min) y estimuladas con CCL21 (5 min) y lisadas como en el apartado A. A continuación, fueron analizadas por Western Blot con anticuerpos anti fosfo-AMPK (Ser485), fosfo-ERK1/2 (Thr-202/Tyr-204 ERK1/Thr-185/Tyr-187 ERK2) o α-tubulina. **D:** Cuantificación del incremento en la fosforilación de AMPK (Ser485) de CDs tratadas como en el apartado C. Los resultados muestran el valor de la media ± SD. ns, indica diferencias no significativas.

alcanzándose el máximo de activación a los 2 minutos. Esta cinética es compatible con la observada para la fosforilación de AMPK en la Ser485 que empieza a ser detectable a partir del primer minuto y alcanza el máximo a los 2 minutos. Por tanto, la cinética de la activación de la ruta de MEK1/2 y ERK1/2 parece preceder a la de la fosforilación de AMPK y ello es compatible con la hipótesis de que MEK1/2 y ERK1/2 estén regulando la actividad de AMPK.

A continuación, analizamos directamente la implicación de MEK1/2 en la

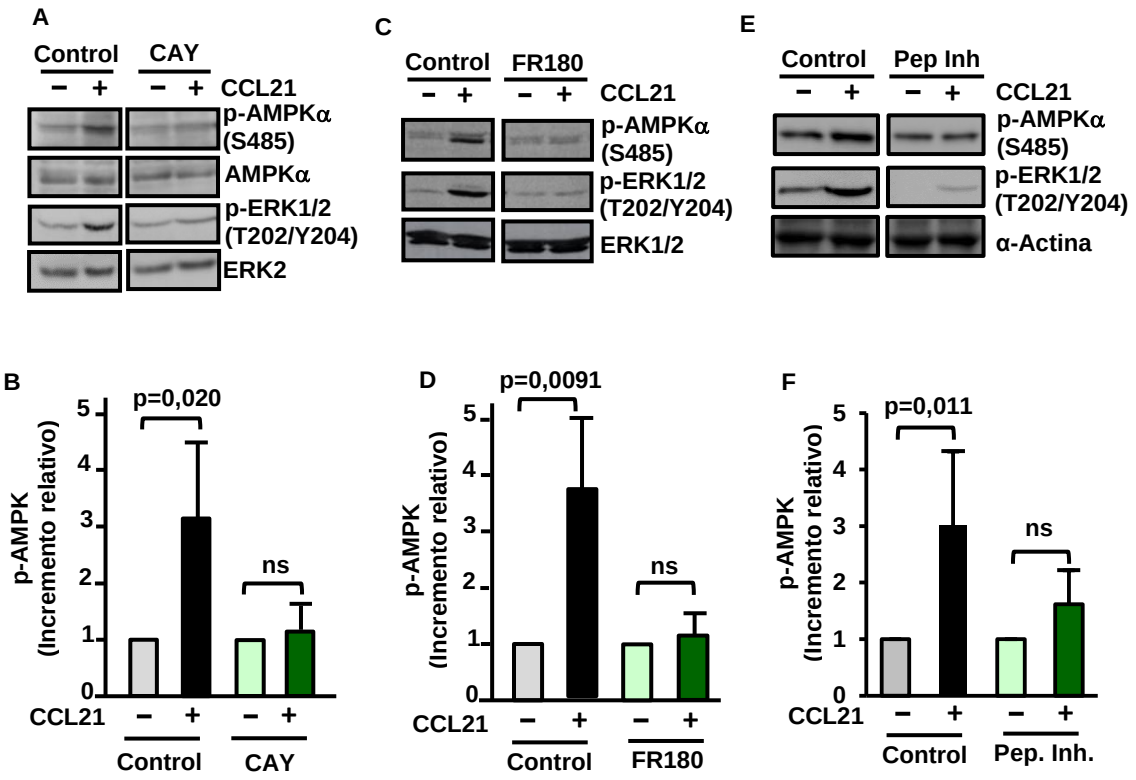

Figura 19: La fosforilación inhibitoria de AMPK inducida por CCR7 está mediada por ERK1/2. A: CDs humanas en RPMI/0,1% BSA fueron tratadas o no con el inhibidor CAYMAN (CAY, 20 µM, 2,5 h) y estimuladas o no 5 min con CCL21. A continuación, fueron lisadas y analizadas por Western Blot con anticuerpos anti fosfo-AMPK (Ser485), AMPK total, fosfo-ERK1/2 (Thr-202/Tyr-204 ERK1; Thr-185/Tyr-187 ERK2) o ERK2 total. **B:** Cuantificación del incremento en la fosforilación de AMPK (Ser485) de CDs tratadas como en el apartado A. **C:** CDs en RPMI/0,1% de BSA fueron tratadas o no con FR180 (100 µM, 60 min), estimuladas con CCL21 y lisadas como en el apartado A. A continuación, fueron analizadas por Western Blot con anticuerpos anti fosfo-AMPK (Ser485), fosfo-ERK1/2 (Thr-202/Tyr-204 ERK1; Thr-185/Tyr-187 ERK2) o α-ERK1/2 total. **D:** Cuantificación del incremento en la fosforilación de AMPK (Ser485) de CDs tratadas como en el apartado C. **E:** CDs tratadas como en el apartado A salvo por el inhibidor empleado que fue el péptido inhibidor (Pep. Inh., 50µM, 60 min). A continuación, fueron analizadas por Western Blot con anticuerpos anti fosfo-AMPK (Ser 485), fosfo-ERK1/2 (Thr-202/Tyr-204 ERK1/Thr-185/Tyr-187 ERK2) o α-actina. **F:** Cuantificación del incremento en la fosforilación de AMPK (Ser485) de CDs tratadas como en el apartado E. Los resultados muestran el valor de la media ± SD (n=5), ns indica diferencias estadísticamente no significativas.

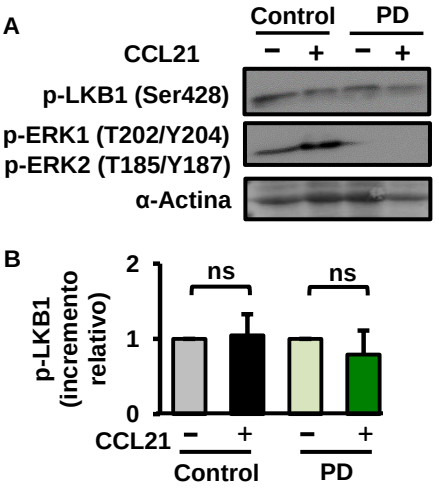

Figura 20: ERK1/2 no inhibe a AMPK mediante la inhibición de LKB1. A: CDs humanas en RPMI / 0,1% BSA fueron tratadas o no con PD325901 (PD, 1µM) durante 60 min y estimuladas 5 min con CCL21. A continuación, fueron lisadas y analizadas por Western Blot con anticuerpos anti fosfo-LKB1 (Ser428), fosfo-ERK1/2 (Thr-202/Tyr-204 ERK1;Thr-185/Tyr-187 ERK2) o α-actina. **B:** Cuantificación del incremento en lafosforilación de LKB1 (Ser428) de CDs tratadas como en el apartado A. Los resultados muestran el valor de la media ± SD (n=5), ns indica diferencias estadísticamente no significativas.

fosforilación de AMPK en la Ser485 mediante el uso de PD325901 y UO126, dos inhibidores selectivos de MEK1/2. Para analizar la eficacia de estos inhibidores sobre MEK1/2 estudiamos el nivel de fosforilación en las Ser217/221 de su diana ERK1/2 en respuesta a la estimulación de las CDs con CCL21. En la **figura 18** se puede ver como ambos inhibidores no solo bloquean eficazmente la activación de MEK1/2 inducida por CCR7, sino que también anulan completamente la fosforilación de AMPK en la Ser485.

Hasta la fecha, ERK1/2 es el único sustrato descrito de MEK1/2. Por lo tanto, si MEK1/2 está implicado en la inhibición de AMPK inducida por CCR7 era de esperar que también lo estuviera ERK1/2. Para comprobarlo realizamos experimentos en los que analizamos los niveles de fosforilación de AMPK tras reducir los niveles de ERK1 o ERK2 con siRNAs. Sin embargo, aunque probamos varios siRNAs que presentaban una gran eficacia reduciendo los niveles de ERK1 y ERK2 en células HL60, no conseguimos reducir los niveles de estas dos quinasas cuando los empleamos sobre las CDs. De esta manera, decidimos cambiar de estrategia y llevar a cabo los experimentos con tres inhibidores farmacológicos de Erk: CAYMAN, FR180 y el péptido inhibidor de ERK. Las CDs fueron pretratadas con cada uno de estos inhibidores y posteriormente fueron estimuladas con CCL21 durante 5 minutos. En los tres casos la inhibición de ERK1/2 estuvo acompañada de la inhibición de la fosforilación de AMPK en la Ser485 (**figura 19**).

Se ha descrito que tanto ERK1/2 como su sustrato RSK son capaces de fosforilar e inhibir a LKB1 en la Ser428 [182] . Para comprobar si ese era nuestro caso y ERK1/2 pudiera estar inhibiendo a la quinasa activadora de AMPK, como mecanismo complementario a la inhibición directa de AMPK analizamos si la inhibición de MEK1/2 y Erk1/2 podría regular la fosforilación de LKB1. Para este fin realizamos experimentos de inhibición en presencia de PD325901 y analizamos los niveles de fosforilación de LKB1. Sin embargo, ni los niveles de fosforilación en la Ser428 de

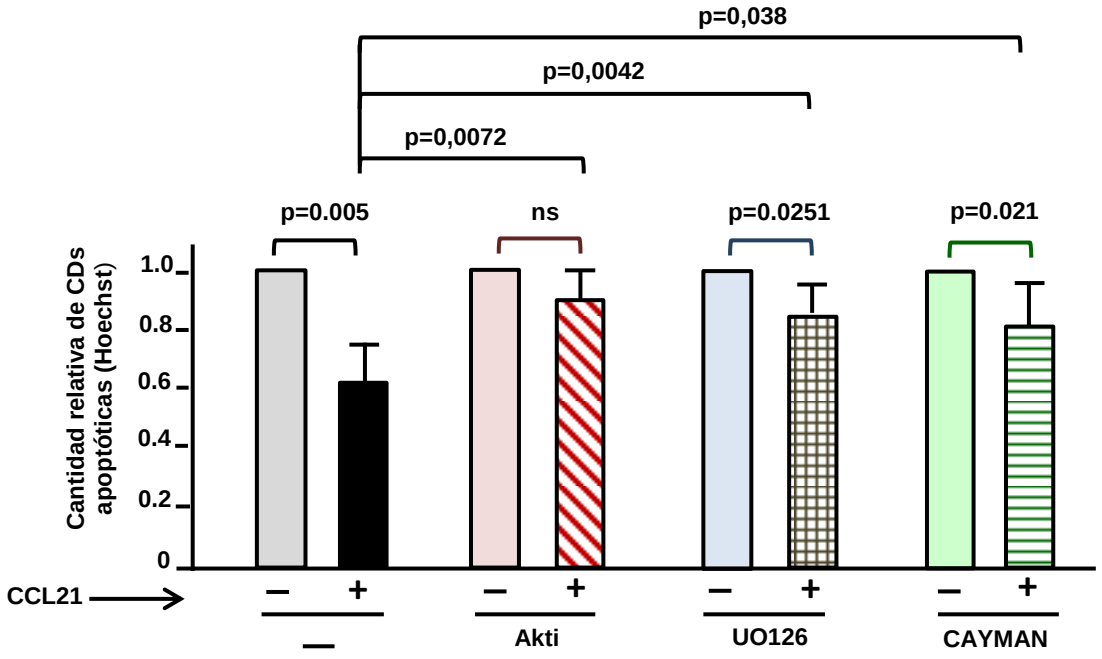

Figura 21: MEK1/2 y ERK1/2 median parcialmente la supervivencia de las CDs inducida por CCR7. **A:** CDs humanas maduras se mantuvieron en RPMI/10% FBS solas o en presencia del inhibidor de Akt, Akti (5 µM), de MEK1/2, o de ERK ½, UO126 (1 µM) o CAYMAN (20 µM) y estimuladas o no con CCL21. Pasadas 30 h las CDs se adhirieron a cristales recubiertos de poliornitina, se fijaron, permeabilizaron y tiñeron con Hoechst 33342. Se representa la reducción del número de células apoptóticas con respecto al control de CDs en RPMI/0,1% de BSA y sin ningún tratamiento suplementario. Los resultados muestran el valor de la media ± SD (n=5).

LKB1 variaban al estimular las CDs con CCL21 ni tampoco parecían alterarse tras el tratamiento con el inhibidor de MEK1/2, por lo que no parece probable que ERK pueda bloquear la activación de AMPK como mecanismo complementario a la inhibición (**figura 20).**

Para confirmar los resultados bioquímicos obtenidos con los inhibidores decidimos analizar también, a nivel funcional, el efecto de la inhibición de MEK1/2 y ERK1/2, ya que si, efectivamente, MEK1/2 y ERK1/2 mediaban los efectos inhibitorios sobre AMPK también debían inhibir la apoptosis. Para confirmar esta hipótesis, analizamos si la inhibición de MEK1/2-ERK1/2 podría reducir los efectos promotores de la supervivencia de CCR7. Analizamos la apoptosis de las CDs tras 30 horas de estimulación con CCL21 en presencia o ausencia de un inhibidor de MEK1/2 (UO126), un inhibidor de ERK1/2 (CAYMAN) o de un inhibidor de Akt (Akti), que fue empleado como control positivo de inducción de apoptosis. Estos experimentos mostraron que tanto el inhibidor de MEK1/2 como el inhibidor de ERK1/2 bloqueaban parcialmente la supervivencia inducida por CCR7 (**figura 21**). Por tanto, confirmamos a nivel funcional como MEK1/2 y ERK1/2 podía modular los efectos pro-apoptóticos de AMPK.

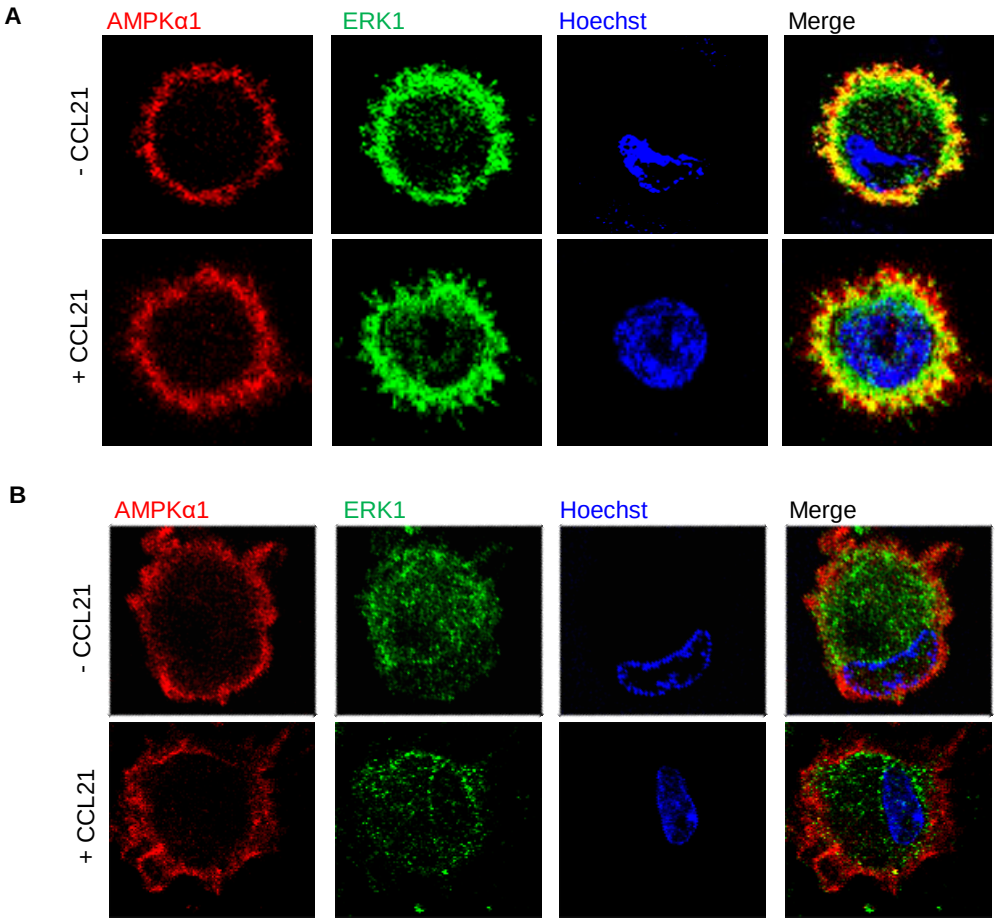

Figura 22: ERK1/2 y AMPK colocalizan en el citoplasma de las CDs. A: CDs humanas en RPMI con 0,1% BSA adheridas sobre cristales recubiertos de poliornitina fueron estimuladas o no 5 min con CCL21. A continuación, las células fueron fijadas con paraformaldehido, permeabilizadas y marcadas con anticuerpos anti ERK1 y anti AMPKα1 o anti MEK1 y anti AMPKα1. Las tinciones fueron analizadas por microscopia confocal, realizando fotos en el plano z cada 1 µm. Se muestra la proyección máxima de células representativas para cada tratamiento y tinción.

6- ERK y AMPK están asociados

Una vez establecida la ruta bioquímica que controla la inhibición de AMPK inducida por CCR7 estudiamos si MEK1/2 y ERK1/2 pudieran estar induciendo la fosforilación de AMPK mediante una interacción directa entre estas moléculas.

En primer lugar, realizamos inmunofluorescencias dobles de ERK1/2 y AMPK y de MEK1/2 y AMPK en CDs humanas estimuladas o no con CCL21. La **figura 22** muestra como ERK1/2 colocaliza con AMPK en el citoplasma de las CDs independientemente de que hayan sido estimuladas o no. En cambio, MEK1/2 no colocaliza con AMPK en ninguno de los dos casos.

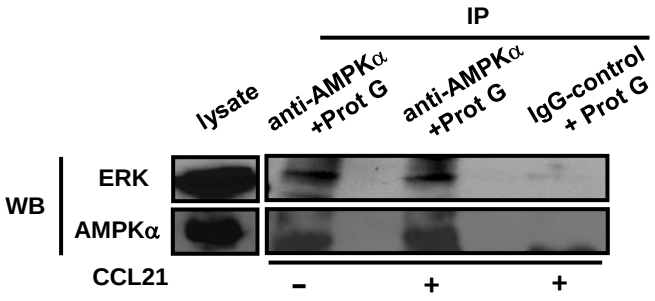

Figura 23: ERK1/2 co-inmunoprecipita con AMPK. Un mismo número de CDs fueron estimuladas 5 min con CCL21 para, a continuación, realizar una inmunoprecipitación con un anticuerpo anti AMPK o anti Gγ5, en el control negativo. Los inmuno-precipitados se analizaron por Western Blot con anticuerpos anti ERK1 y anti AMPK. Como control positivo de expresión se usó un lisado

Puesto que las inmunofluorescencias no tienen resolución suficiente para determinar si dos proteínas interaccionan decidimos realizar una inmunoprecipitación de AMPK que podría mostrar si esta quinasa asociaba con ERK. Inmunoprecipitamos el AMPK endógeno de CDs estimuladas o no con CCL21 durante 5 minutos y posteriormente analizamos por Western Blot la presencia de ERK1 en los inmunoprecipitados. Como control negativo incluimos un tercer punto en el que se realizó la inmunoprecipitación con un anticuerpo anti Gγ5. La **figura 23** muestra como ERK1 efectivamente co-inmunoprecipita con AMPK, indicando que ambos forman parte de un mismo complejo de señalización.

Para averiguar si dentro de ese complejo de señalización AMPK y ERK pudieran estar en contacto directo decidimos emplear la técnica de PLA (Proximity Ligation Assay). El tratamiento de las muestras mediante esta técnica permite detectar proteínas que se encuentran a menos de 40 nm mediante el análisis de la fluorescencia de la muestra. Aunque la técnica se describe con más detalle en la sección de materiales y métodos, esta se basa en el marcaje de la muestra con anticuerpos primarios contra las dos proteínas de interés y el marcaje de estos anticuerpos primarios con unas sondas que generan fluorescencia exclusivamente cuando las dos proteínas de interés se encuentran a menos de 40 nm.

En este caso realizamos el experimento con anticuerpos anti ERK1 y anti AMPKα1 en CDs estimuladas o no con CCL21. Como control positivo realizamos el experimento empleando anticuerpos anti MEK1 y anti ERK1 y como control negativo empleamos CDs que fueron incubadas con uno solo de los anticuerpos. En la **figura 24** se puede apreciar como cuando las CDs son estimuladas con CCL21 se genera una señal fluorescente roja en el interior de las CDs, indicando que ERK1 y AMPK se encuentran a menos de 40 nm de distancia.

En resumen, los resultados sugieren que ERK1/2 regula la actividad de AMPK en un complejo de señalización del que ambas quinasas forman parte.

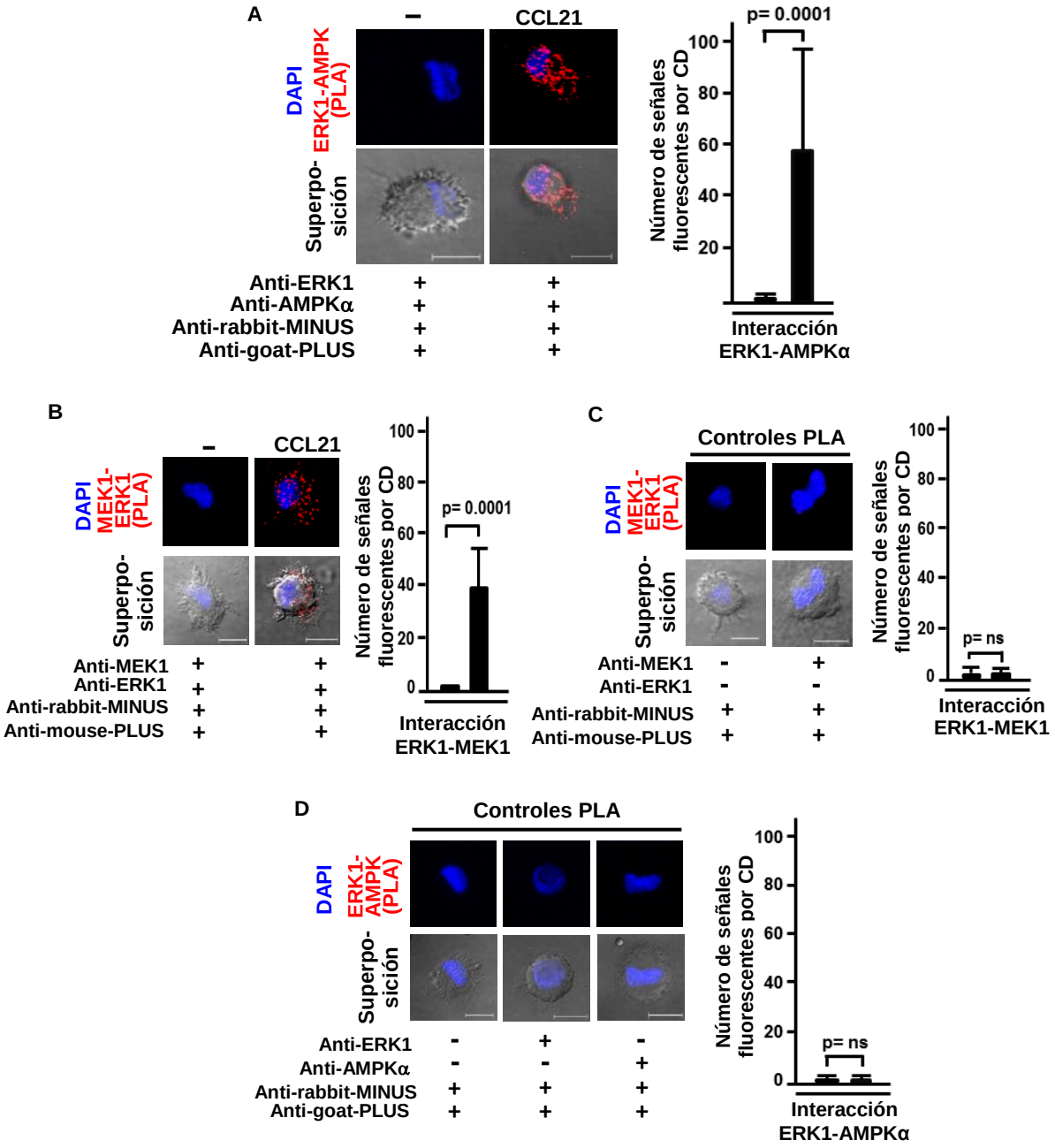

Figura 24: AMPK interacciona con ERK1/2. A: CDs humanas en RPMI/0,1% BSA adheridas sobre cristales recubiertos de poliornitina fueron estimuladas o no 5 min CCL21. A continuación, fueron fijadas, permeabilizadas, bloqueadas y marcadas con anticuerpos anti ERK1 y anti AMPKα1. Posteriormente fueron marcadas con las sondas PLA anti rabbit-MINUS y anti goat-PLUS. Se muestran las imágenes representativas de las proyecciones máximas de la señal de las sondas y del Hoechst 33342 y de su superposición con las imágenes del DIC, así como la cuantificación de la señal obtenida por célula. **B:** Control positivo. CDs tratadas como en el apartado A con la diferencia de que fueron teñidas con anti ERK1 y anti MEK1 y de que las sondas empleadas fueron anti rabbit-MINUS y anti mouse-PLUS. **C:** Control negativo del apartado B. CDs tratadas y marcadas como en el apartado B con la diferencia de que fueron marcadas solo con uno de los anticuerpos primarios o con ninguno. **D:** Control negativo del apartado A. Las CDs fueron tratadas y marcadas como en el apartado A pero con uno solo de los anticuerpos primario o con ninguno de ellos. Las barras de las escalas equivalen a 20 µm. Los resultados muestran el valor de la media ± SD .

DISCUSION

DISCUSIÓN

Para que se desencadene una respuesta inmunológica adaptativa las CDs maduras deben migrar desde los tejidos periféricos hasta los ganglios linfáticos y una vez allí, activar a los linfocitos T. El receptor de quimioquinas CCR7 guía la migración de las CDs hasta los ganglios linfáticos siguiendo un gradiente de sus dos ligandos CCL19 y CCL21. CCR7 no solo regula la quimiotaxis en las CDs, sino que también regula otras funciones de estas células, incluyendo la velocidad migratoria, la citoarquitectura, la endocitosis, la maduración y la supervivencia [11, 65, 68]. Previamente, se ha descrito cómo CCR7 induce supervivencia activando la ruta de PI3K y Akt. La activación de Akt induce supervivencia mediante la activación del factor de transcripción NF-kB que induce un aumento de expresión de Bcl-xl, un miembro pro-supervivencia de la familia Bcl2. Al mismo tiempo, Akt inhibe la activación de GSK3 y del factor de transcripción FOXO1, lo que permite mantener bajos los niveles de expresión de la proteína pro-apoptótica Bim [69, 70].

Con el objetivo de conocer con más detalle los mecanismos que regulan la supervivencia de las CDs decidimos analizar el papel de la quinasa AMPK. Esta proteína puede promover la supervivencia o la apoptosis dependiendo del estímulo y del tipo celular. Por ejemplo, durante el desarrollo de los linfocitos T, se ha visto que en timocitos doble positivo AMPK induce supervivencia, mientras que en células hepáticas su activación prolongada induce apoptosis [164, 178]. Otro ejemplo de la dualidad de esta enzima es su papel en neuronas, donde su activación crónica y prolongada induce apoptosis mientras que ante situaciones de carencia temporales de energía induce supervivencia [165].

En el caso de las CDs humanas, mediante el empleo de dos activadores farmacológicos de AMPK (AICAR y A769662) comprobamos que en estas células AMPK induce muerte celular. Estos resultados fueron corroborados con el empleo de un siRNA específico de AMPK que mostró como la reducción de los niveles de AMPK induce un descenso a la mitad en la mortalidad de las CDs.

Aunque la apoptosis es el tipo de muerte celular programada más estudiada analizamos si AMPK pudiera estar induciendo algún otro tipo de muerte celular. AMPK tiene un conocido papel en la regulación de la autofagia y, de hecho, son varios los trabajos que muestran que AMPK puede inducir muerte de tipo autofágica [183, 184]. Además, AMPK puede inducir la formación del inflamasoma, un complejo proteico que se forma durante el desarrollo de la muerte piroptótica [185]. Para esclarecer qué tipo de muerte celular podría inducirse por la activación de AMPK estudiamos más en profundidad sus características. Se trata de una muerte

que está mediada por caspasas, ya que por un lado la activación de AMPK induce la activación de la caspasa 3, y, por otro, el pretratamiento de las CDs con el inhibidor de caspasas Z-VAD-MNK protege a las CDs de la muerte inducida por AMPK. Además, la muerte que experimentan las CDs en respuesta a la activación de AMPK incluye un proceso de picnosis del núcleo y de fragmentación del ADN. Todo ello nos lleva a concluir que se trata de una muerte apoptótica.

La apoptosis puede ser intrínseca (mitocondrial) o extrínseca (dependiente de receptores de muerte), dependiendo del origen de los estímulos que la inducen. Se ha observado que, en células de cáncer de mama privadas de estrógenos, AMPK puede mediar ambos tipos de apoptosis, tanto intrínseca como extrínseca, es por ello que decidimos examinar cuál de ellas estaba siendo activada en las CDs [163]. Para ello analizamos la activación de la caspasa 8, la caspasa iniciadora que media la apoptosis extrínseca. Sin embargo, no observamos activación de dicha caspasa ni 24 ni 33 horas después de la activación de AMPK, a pesar de que sí se observa activación de la caspasa 3 (caspasa efectora) a las 33 horas. Todo ello nos lleva a sugerir que AMPK induce una apoptosis de tipo intrínseco en las CDs.

Finalmente validamos estos resultados en CDs de ratón. Primero observamos mediante experimentos in vitro que la activación de AMPK induce picnosis y fragmentación nuclear de igual manera que en las CDs humanas. Después, usando un modelo in vivo en el que se empleó un inhibidor de caspasas fluorescente para detectar las CDs apoptóticas comprobamos que el activador de AMPK (A769662) también inducía apoptosis en las CDs localizadas en los ganglios poplíteos de los ratones.

Otro de los objetivos de esta tesis doctoral fue describir los mecanismos empleados por AMPK para regular la apoptosis de las CDs. Estudios anteriores en nuestro laboratorio habían mostrado como la activación de la ruta de GSK3 y FOXO1 en las CDs inducen apoptosis mediante un aumento de la expresión de Bim, un miembro pro-apoptótico de la familia Bcl2 [71]. Puesto que los miembros de esta ruta eran buenos candidatos para ser mediadores de los efectos pro-apoptóticos de AMPK, se analizó el comportamiento del factor de transcripción FOXO1 en respuesta a la activación de AMPK. Cuando CDs transfectadas con un plásmido FOXO1-GFP fueron estimuladas con los activadores farmacológicos de AMPK se observó que la activación de AMPK induce una potente translocación de FOXO1 al núcleo. Además, la movilización de FOXO1 hacia el núcleo va acompañada de un aumento considerable de los niveles Bim. Todo ello permite sugerir que AMPK facilita la movilización de FOXO1 desde el citoplasma al núcleo, donde activa la maquinaria de apoptosis celular mediante, al menos, la inducción de la expresión de la proteína pro-apoptótica Bim. Esta no es la primera vez que se describe cómo AMPK regula la

actividad de los FOXOs, ya que, por ejemplo, estudios in vitro en células HEK293T muestran que AMPK puede activar a FOXO3 fosforilandolo directamente en varios residuos [186]. Nuestros resultados también están en línea con otros estudios que muestran que en la apoptosis inducida por estradiol en células de cáncer de mama AMPK también activa la vía FOXO3-Bim como mecanismo de inducción de la apoptosis [163].

Por otro lado, existen trabajos que demuestran que en células HEK293 y en HTC116 AMPK puede regular la actividad de mTORC1 estimulando la actividad de su inhibidor TSC2 [187, 188]. AMPK también es capaz de fosforilar e inhibir directamente a Raptor, uno de los componentes del complejo mTORC1 [188, 189]. Además, estudios en células de cáncer de mama y de neuroblastoma demuestran que AMPK puede inducir la muerte celular a través de la inhibición de la actividad de mTORC1 [190, 191]. Puesto que la estimulación de CCR7 en las CDs induce activación del complejo mTORC1, y, además, está activación de mTORC1 está mediada por los componentes del módulo de inducción de la supervivencia de CCR7 en las CDs, este complejo se presentaba como un buen candidato para ser regulado por AMPK. Mediante el uso de rapamicina, un inhibidor de mTORC1, pudimos corroborar que mTORC1, al igual que sus quinasas reguladoras induce supervivencia en las CDs. En concordancia con esos resultados, también observamos que la activación de AMPK con AICAR y A769662 inhibe la actividad de mTORC1. Por tanto, analizando ambos resultados en su conjunto se puede sugerir que AMPK inhibe a mTORC1 y bloquea la señalación pro-supervivencia que este complejo favorece para potenciar la apoptosis de las CDs.

La proteína Bcl-xl es un miembro inductor de supervivencia de la familia Bcl2. Bcl-xl se sobreexpresa en respuesta a la estimulación de CCR7, lo cual puede conducir a extender la supervivencia de las CDs[69]. Existen estudios en células de cáncer de ovario tratadas con hispidulina que relacionan la apoptosis mediada por la activación de AMPK con el descenso en los niveles de Bcl-xl en estas células [192]. Es por ello que decidimos comprobar si AMPK pudiera estar inhibiendo la expresión de Bcl-xl como un mecanismo adicional para promover la apoptosis en CDs. Sin embargo, esta hipótesis fue descartada ya que los experimentos de activación de AMPK con sus dos activadores farmacológicos no dieron lugar a cambios en los niveles de Bcl-xl.

Otro de los principales objetivos de este trabajo fue analizar el mecanismo mediante el cual CCR7 regula la actividad de AMPK. En este sentido, vimos que la estimulación de CCR7 con CCL21 provoca un rápido proceso de fosforilación de AMPK en la Ser485, que conduce a la inhibición de esta quinasa, al mismo tiempo que induce desfosforilación en la Thr172, un residuo que mantiene a la quinasa activa Thr172 e

inhibición de su actividad. Estudios previos han mostrado que AMPK es capaz de autofosforilarse en la Ser485 por lo que contemplamos la posibilidad de que el incremento en los niveles de fosforilación observados en esta serina fuera debido a dicho proceso de autofosforilación [132]. Sin embargo, nuestros experimentos con un inhibidor farmacológico de AMPK descartaron esta opción y confirmaron que la fosforilación era inducida por una molécula regulada por CCR7. Los efectos inhibitorios de CCR7 sobre AMPK también fueron observados en CDs de ratón y con la quimioquina CCL19, el segundo ligando de CCR7.

Todos estos resultados son consistentes con el papel desrito para CCR7 como receptor inductor de supervivencia en las CDs maduras. Como se mencionó previamente, CCR7 promueve supervivencia a través de la activación de la quinasa Akt [69]. A su vez, una vez activada, Akt induce la fosforilación de FOXO que provoca su translocación desde el núcleo al citoplasma, evitando de esta manera que FOXO active la transcripción de Bim y lleve a cabo sus efectos pro-apoptóticos [71]. Por tanto, tras la estimulación de CCR7, la inhibición de la actividad de AMPK, evita que esta quinasa, que estimula la translocación de FOXO al núcleo y la expresión de Bim, lleve a cabo un efecto opuesto al de Akt. Además, la inhibición de la actividad de AMPK también evita que esta quinasa también bloquee los efectos inductores de supervivencia de mTORC1. Todo ello, favorece y potencia la capacidad de CCR7 de aumentar la supervivencia de las CDs.

Además de conocer los mecanismos que AMPK emplea para inducir apoptosis estábamos interesados en analizar los mecanismos que median la inhibición de AMPK inducida por CCR7. En primer lugar, comprobamos que la inhibición de AMPK inducida por CCR7 está mediada por las subunidades βγ de la proteína G, así como por la subunidad αi. Este resultado encaja perfectamente con el modelo de señalización de CCR7 que ha sido estudiado hasta ahora ya que las subunidad Gαi y Gβγ ya han sido implicadas en la regulación de la mayoría de las funciones reguladas por CCR7 como son la supervivencia, la quimiotaxis, o la citoarquitectura [65, 69].

Previamente se ha descrito que en diferentes tipos celulares las quinasas Akt, S6K y PKA pueden fosforilar directamente a AMPK en la Ser485 [132, 136, 181]. Además, también se ha descrito en CDs maduras que CCR7 estimula la actividad de dos de ellas (Akt y S6K) y que dicha activación está mediada por Gαi y Gβγ [69]. Además, tanto Akt como S6K forman parte de la ruta de señalización que media la inducción de supervivencia inducida por CCR7. Todo ello nos inducía a pensar que pudiera ser una de estas quinasas la responsable de fosforilar a AMPK en la Ser485 en respuesta a la activación de CCR7. Sin embargo, sorprendentemente, cuando se emplearon 3 inhibidores farmacológicos que inhiben la ruta de PI3K-Akt-S6K a diferentes niveles, en ningún caso la fosforilación de AMPK inducida por CCR7 en las CDs resultó

alterada. Por tanto, se puede concluir que ni Akt, ni S6K están implicadas en la inhibición de AMPK inducida por CCR7. Además, los experimentos con los activadores de PKA también mostraron que no hay relación entre la actividad de PKA y los niveles de fosforilación de AMPK en la Ser485 en las CDs.

En su lugar, los experimentos con dos inhibidores de MEK1/2 y tres inhibidores de ERK1/2 revelaron que tras la estimulación de CCR7, son las quinasas MEK1/2 y ERK1/2 las encargadas de mediar la fosforilación de AMPK en la Ser485. Trabajos previos muestran que en células de melanoma ERK1/2 puede bloquear la activación de AMPK mediante la inhibición de LKB1, la principal quinasa activadora de AMPK. En estas células se ha visto cómo ERk1/2 es capaz de inhibir la actividad de LKB1 induciendo su fosforilación en dos serinas inhibitorias, una de ellas es fosforilada directamente por el propio ERK1/2 y la otra es fosforilada por p90Rsk, una diana de ERK [182]. En el trabajo que aquí se presenta se contempló la posibilidad de que ERK1/2 inhibiera también en las CDs la actividad de LKB1 como mecanismo complementario a la inhibición directa de AMPK por fosforilación en la Ser485. Sin embargo, los resultados sugieren que CCR7 no induce la fosforilación en esta posición inhibidora de LKB1 ni que su nivel de fosforilación este regulado por ERK1/2.

Los datos de las inmunofluorescencias, el PLA y la co-inmunoprecipitación señalan que ERK1/2 forma parte de un complejo de señalización que incluye a AMPK. Tras la estimulación de CCR7, ambas moléculas parecen aproximarse hasta quedar a una distancia que permite su interacción, suficiente para que ERK1/2 pudiera fosforilar a AMPK. Por lo tanto, tomados en su conjunto, los resultados sugieren que ERK1/2 estaría induciendo la inhibición de AMPK de una manera directa.

Estos resultados además parecen ser específicos de este tipo celular y de este receptor ya que, por ejemplo, estudios en células de la granulosa muestran que la estimulación de su receptor FSH induce proliferación celular mediante la fosforilación e inhibición de AMPK en la Ser485, sin embargo, al contrario de lo que ocurre con CCR7 en las CDs, esta inhibición no es dependiente de MEK1/2 y ERK1/2 [193]. Por otro lado, es interesante comentar que existen otros estudios que muestran la relación inversa entre ERK1/2 y AMPK, es decir, que AMPK se encuentra regulando la actividad de ERK1/2. Además, resulta curioso que, en unos casos, como es en la proliferación de los queratinocitos, AMPK induce la inhibición de ERK [194]. En cambio, en células infectadas con el circovirus porcino de tipo 2 AMPK activa a ERK1/2 como parte de la señalización inducida por el virus para activar la autofagia [195]. Además, en este último caso también se observó, igual que en el presente trabajo, que AMPK y ERK co-inmunoprecipitan y forman parte de un mismo complejo molecular. Todos estos datos ponen de manifiesto la complicada relación que existe entre ERK1/2 y AMPK, y como se trata de un caso más donde los mecanismos de regulación entre

estas dos moléculas dependen del contexto. Todo ello evidencia la imposibilidad de extrapolar los resultados obtenidos individualmente para cada caso y la importancia de conocer en detalle los mecanismos específicos empleados por cada receptor en cada tipo de celular.

Los resultados obtenidos también indican que MEK1/2 y ERK1/2 pueden inducir supervivencia de las CDs. Hasta la fecha MEK1/2 y ERK1/2 solo habían sido implicados en el módulo regulador de la quimiotaxis inducida por CCR7, pero habían sido descartados como moléculas reguladoras de la supervivencia. Probablemente ello se debe a que en comparación con Akt, su aportación en la inducción de la supervivencia es mucho menor. De hecho, en los estudios aquí presentados de inhibición de la supervivencia inducida por CCL21, se ve que el inhibidor de Akt bloquea completamente los efectos de CCL21. En cambio, los inhibidores de MEK1/2 y ERK1/2 solo bloquean parcialmente la supervivencia inducida por CCR7. En este sentido, los experimentos de inducción de apoptosis con los activadores de AMPK también muestran como su capacidad de inducción de apoptosis es menor que la observada con el inhibidor de Akt. Además, anteriormente, estos experimentos de análisis de la supervivencia en respuesta a CCL21 se realizaron durante cortos periodos de tiempo, nunca sobrepasando las 10 horas de experimento. En cambio, en este trabajo, para poder detectar los efectos de la inhibición de MEK1/2 y ERK1/2 sobre la supervivencia fue necesario alargar los experimentos mucho más tiempo, analizándolos pasadas las 24 o incluso las 40 horas desde el inicio de los mismos [69]. Por tanto, estos resultados muestran que CCR7 emplea, además de la ruta dependiente de Akt, el eje de señalización MEK-ERK-AMPK como vía complementaria para estimular la supervivencia de las CDs maduras.

En el esquema de la **figura 25** se presenta el modelo que resume los resultados obtenidos en este trabajo y cómo éstos quedan englobados dentro del entramado de las rutas de señalización que activa la estimulación del receptor CCR7. En este esquema se puede apreciar cómo los resultados obtenidos conectan los módulos previamente descritos de regulación de la quimiotaxis y la supervivencia. Por tanto, la idea que se tenía anteriormente de que los módulos actuaban de manera completamente independiente unos de otros ahora cambia. Al menos los módulos inductores de quimiotaxis y supervivencia sí están conectados y AMPK se constituye como una molécula responsable de la comunicación entre los dos módulos.

Alteraciones en la correcta regulación de la supervivencia de las CDs pueden desencadenar diversas patologías. Ello lo demuestra el hecho de que ratones con CDs con una longevidad aumentada presentan una mayor activación de sus células linfoides y pueden acabar desarrollando síntomas de autoinmunidad [195, 196]. Además, el aumento artificial de la apoptosis de las CDs en ratones puede provocar un estado

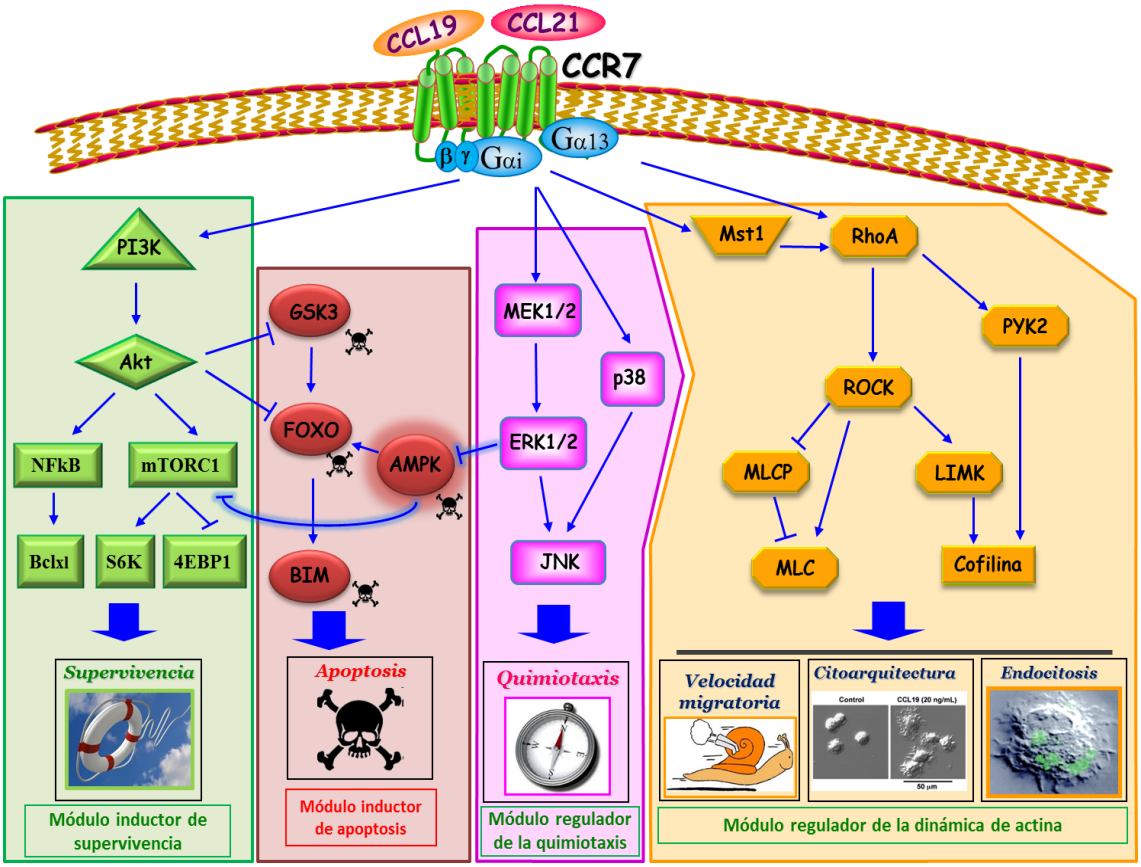

Figura 25: Esquema actualizado de CCR7 y sus rutas de señalización. *La estimulación de CCR7 con CCL19 o CCL21 induce un aumento de la supervivencia, la quimiotaxis, la endocitosis, la velocidad migratoria y cambios en la citoarquitectura de las CDs. Previamente se había descrito que CCR7 regula la quimiotaxis mediante la activación de MEK1/2 y ERK1/2 y que promueve supervivencia activando la ruta de PI3K-AktmTORC-S6K. Los nuevos resultados muestran que AMPK puede inducir apoptosis en las CDs mediante la inhibición del complejo anti-apoptótica mTORC1. Además, AMPK induce la translocación del factor de transcripción FOXO1 al núcleo desde donde puede inducir la expresión de la proteína pro-apoptótica Bim. La activación de CCR7 induce la inhibición de AMPK mediante la estimulación de su fosforilación en la Ser485, evitando que esta quinasa lleve a cabo sus efectos pro-apoptóticos. Además, la inhibición de AMPK inducida por CCR7 está mediada por la vía de Gαi/Gβγ-MEK1/2-ERK1/2 pero no por la ruta de Akt ni S6K como había sido descrito anteriormente en otros tipos celulares. De esta manera, AMPK queda como nexo de unión entre la ruta reguladora de la quimiotaxis y la ruta reguladora de la supervivencia.*

de inmunodepresión debido a que se produce una excesiva activación de la respuesta inmune adaptativa [197, 198]. En este sentido, en algunas patologías en humanos, como es el caso del síndrome linfoproliferativo humano de tipo II, se han detectado pacientes que presentan anomalías en la regulación de la apoptosis de sus CDs [35].

Todo ello constata la importancia de alcanzar un conocimiento preciso de los mecanismos que regulan la apoptosis y la supervivencia de las CDs para poder modularlos y conseguir una respuesta inmune adecuada, ayudando, entre otras cosas, a mitigar los efectos de este tipo de patologías.

Los resultados expuestos en esta tesis doctoral, por tanto, añaden un nuevo componente al conjunto de mecanismos dependientes de CCR7 que promueven supervivencia en las CDs y señalan a AMPK como una nueva molécula susceptible de ser una potencial nueva diana terapéutica. Además, el hecho de que los efectos pro-apoptóticos de AMPK y de que su regulación por parte de CCR7 sean reproducibles no solo en las CDs humanas sino también en las CDs de ratón sugiere que los funciones y mecanismos aquí descritos se encuentran conservados entre estas dos especies de mamíferos.

CONCLUSIONES

CONCLUSIONES

- AMPK juega un papel pro-apoptótico en las CDs tanto en los experimentos in vitro con CDs humanas como en el modelo in vivo de ratón en los ganglios poplíteos.
- La apoptosis inducida por AMPK en las CDs es de tipo intrínseco t se caracteriza por ser dependiente de caspasa, estimular la activación de la caspasa 3 e inducir picnosis y fragmentación nuclear.
- AMPK induce apoptosis mediante al menos dos mecanismos:
    1. Inhibiendo la actividad pro-supervivencia del complejo mTORC1.
    2. Promoviendo la translocación al núcleo del factor de transcripción FOXO1 que induce un aumento de los niveles de la proteína pro-apoptótica Bim.
- La estimulación de CCR7 induce un rápido incremento de fosforilación AMPK en la posición inhibitoria Ser485. Ello se ve acompañado de una disminución de su actividad y de los niveles de la fosforilación activadora en la Thr172.
- La fosforilación de AMPK en la Ser485 en las CDs no está mediada por PKA, Akt o S6K como había sido descrito hasta ahora en otros tipos celulares, sino por las quinasas MEK y ERK.
- MEK/ERK pueden regular la supervivencia de las CDs maduras
- ERK y AMPK parecen ser componentes de un complejo de señalización puesto que ERK es capaz de controlar la fosforilación de AMPK.
- La inhibición de AMPK inducida por CCR7 facilita la supervivencia de las CDs inducida por CCR7.

BIBLIOGRAFIA

BIBLIOGRAFIA

1. Dudek, A.M., Martin, S., Garg, A.D. & Agostinis, P. Immature, Semi-Mature, and Fully Mature Dendritic Cells: Toward a DC-Cancer Cells Interface That Augments Anticancer Immunity. *Frontiers in immunology* **4**, 438 (2013).
2. Vivier, E. *et al.* Innate or adaptive immunity? The example of natural killer cells. *Science* **331**, 44-49 (2011).
3. Netea, M.G., Quintin, J. & van der Meer, J.W. Trained immunity: a memory for innate host defense. *Cell host & microbe* **9**, 355-361 (2011).
4. Lutz, M.B. & Schuler, G. Immature, semi-mature and fully mature dendritic cells: which signals induce tolerance or immunity? *Trends in immunology* **23**, 445-449 (2002).
5. Sallusto, F. *et al.* Rapid and coordinated switch in chemokine receptor expression during dendritic cell maturation. *European journal of immunology* **28**, 2760-2769 (1998).
6. Dieu, M.C. *et al.* Selective recruitment of immature and mature dendritic cells by distinct chemokines expressed in different anatomic sites. *The Journal of experimental medicine* **188**, 373-386 (1998).
7. Banchereau, J. & Steinman, R.M. Dendritic cells and the control of immunity. *Nature* **392**, 245-252 (1998).
8. Banchereau, J., Steinman, R.M. Dendritic cells and the control of immunity. *Nature Reviews Immunology* **392**, 245-252 (1998).
9. Steinman, R.M. The dendritic cell system and its role in immunogenicity. *Annu Rev Immunol* **9**, 271-296 (1991).
10. Platt, C.D. *et al.* Mature dendritic cells use endocytic receptors to capture and present antigens. *Proceedings of the National Academy of Sciences of the United States of America* **107**, 4287-4292 (2010).
11. Yanagihara, S., Komura, E., Nagafune, J., Watarai, H. & Yamaguchi, Y. EBI1/CCR7 is a new member of dendritic cell chemokine receptor that is up-regulated upon maturation. *J Immunol* **161**, 3096-3102 (1998).
12. Sozzani, S. *et al.* Differential regulation of chemokine receptors during dendritic cell maturation: a model for their trafficking properties. *J Immunol* **161**, 1083-1086 (1998).
13. Cyster, J.G. Chemokines and cell migration in secondary lymphoid organs. *Science* **286**, 2098-2102 (1999).
14. Forster, R., Davalos-Misslitz, A.C. & Rot, A. CCR7 and its ligands: balancing immunity and tolerance. *Nat Rev Immunol* **8**, 362-371 (2008).
15. Mempel, T.R., Henrickson, S.E. & Von Andrian, U.H. T-cell priming by dendritic cells in lymph nodes occurs in three distinct phases. *Nature* **427**, 154-159 (2004).
16. Prindull, G. Apoptosis in the embryo and tumorigenesis. *Eur J Cancer* **31A**, 116-123 (1995).
17. Kerr, J.F., Wyllie, A.H. & Currie, A.R. Apoptosis: a basic biological phenomenon with wide-ranging implications in tissue kinetics. *British journal of cancer* **26**, 239-257 (1972).
18. Savill, J. & Fadok, V. Corpse clearance defines the meaning of cell death. *Nature* **407**, 784-788 (2000).
19. Kurosaka, K., Takahashi, M., Watanabe, N. & Kobayashi, Y. Silent cleanup of very early apoptotic cells by macrophages. *J Immunol* **171**, 4672-4679 (2003).
20. Boatright, K.M. *et al.* A unified model for apical caspase activation. *Molecular cell* **11**, 529-541 (2003).
21. Galluzzi, L. *et al.* Molecular definitions of cell death subroutines: recommendations of the Nomenclature Committee on Cell Death 2012. *Cell death and differentiation* **19**, 107-120 (2012).
22. Kroemer, G., Galluzzi, L. & Brenner, C. Mitochondrial membrane permeabilization in cell death. *Physiological reviews* **87**, 99-163 (2007).
23. Li, P. *et al.* Cytochrome c and dATP-dependent formation of Apaf-1/caspase-9 complex initiates an apoptotic protease cascade. *Cell* **91**, 479-489 (1997).
24. Li, L.Y., Luo, X. & Wang, X. Endonuclease G is an apoptotic DNase when released from mitochondria. *Nature* **412**, 95-99 (2001).

25. Siddiqui, W.A., Ahad, A. & Ahsan, H. The mystery of BCL2 family: Bcl-2 proteins and apoptosis: an update. *Archives of toxicology* **89**, 289-317 (2015).
26. Wang, X., Xing, D., Liu, L. & Chen, W.R. BimL directly neutralizes Bcl-xL to promote Bax activation during UV-induced apoptosis. *FEBS letters* **583**, 1873-1879 (2009).
27. Kamath, A.T., Henri, S., Battye, F., Tough, D.F. & Shortman, K. Developmental kinetics and lifespan of dendritic cells in mouse lymphoid organs. *Blood* **100**, 1734-1741 (2002).
28. Chen, M. & Wang, J. Programmed cell death of dendritic cells in immune regulation. *Immunological reviews* **236**, 11-27 (2010).
29. Hildeman, D., Jorgensen, T., Kappler, J. & Marrack, P. Apoptosis and the homeostatic control of immune responses. . *Curr. Opin. Immunol.* **19**, 516-521 (2007).
30. Kushwah, R. & Hu, J. Dendritic cell apoptosis: regulation of tolerance versus immunity. . *J. Immunol.* **185**, 795-782 (2010).
31. Chen, M., Huang, L. & J., W. Deficiency of Bim in dendritic cells contributes to overactivation of lymphocytes and autoimmunity. *Blood* **109**, 4360-4367 (2007).
32. Hou, W.S. & Van Parijs, L. A Bcl-2-dependent molecular timer regulates the lifespan and immunogenicity of dendritic cells. *Nat. Immunol.* **5**, 583-589 (2004).
33. Nopora, A. & Brocker, T. Bcl-2 controls dendritic cell longevity in vivo *J. Immunol.* **169**, 3006-3014 (2002).
34. Ohnmacht, C. *et al.* Constitutive ablation of dendritic cells breaks self-tolerance of CD4 T cells and results in spontaneous fatal autoimmunity. *J Exp Med.* **206**, 549-559 (2009).
35. Wang, J. *et al.* Inherited human Caspase 10 mutations underlie defective lymphocyte and dendritic cell apoptosis in autoimmune lymphoproliferative syndrome type II. *Cell* **98**, 47-58 (1999).
36. Tinsley, K.W. *et al.* Sepsis induces apoptosis and profound depletion of splenic interdigitating and follicular dendritic cells. *J Immunol* **171**, 909-914 (2003).
37. Kushwah, R. & Hu, J. Dendritic cell apoptosis: regulation of tolerance versus immunity. *J Immunol* **185**, 795-802 (2010).
38. Munoz, L.M. *et al.* Receptor oligomerization: a pivotal mechanism for regulating chemokine function. *Pharmacology & therapeutics* **131**, 351-358 (2011).
39. Allen, S.J., Crown, S.E. & Handel, T.M. Chemokine: receptor structure, interactions, and antagonism. *Annual review of immunology* **25**, 787-820 (2007).
40. Chemokine/chemokine receptor nomenclature. *Journal of leukocyte biology* **70**, 465-466 (2001).
41. Weber, M. *et al.* Interstitial dendritic cell guidance by haptotactic chemokine gradients. *Science* **339**, 328-332 (2013).
42. Vassileva, G. *et al.* The reduced expression of 6Ckine in the plt mouse results from the deletion of one of two 6Ckine genes. *The Journal of experimental medicine* **190**, 1183-1188 (1999).
43. Comerford, I. *et al.* A myriad of functions and complex regulation of the CCR7/CCL19/CCL21 chemokine axis in the adaptive immune system. *Cytokine & growth factor reviews* **24**, 269-283 (2013).
44. Carlsen, H.S., Haraldsen, G., Brandtzaeg, P. & Baekkevold, E.S. Disparate lymphoid chemokine expression in mice and men: no evidence of CCL21 synthesis by human high endothelial venules. *Blood* **106**, 444-446 (2005).
45. Sallusto, F. *et al.* Distinct patterns and kinetics of chemokine production regulate dendritic cell function. *European journal of immunology* **29**, 1617-1625 (1999).
46. Britschgi, M.R., Favre, S. & Luther, S.A. CCL21 is sufficient to mediate DC migration, maturation and function in the absence of CCL19. *European journal of immunology* **40**, 1266-1271 (2010).
47. Schumann, K. *et al.* Immobilized chemokine fields and soluble chemokine gradients cooperatively shape migration patterns of dendritic cells. *Immunity* **32**, 703-713 (2010).
48. Heinzel, K., Benz, C. & Bleul, C.C. A silent chemokine receptor regulates steady-state leukocyte homing in vivo. *Proceedings of the National Academy of Sciences of the United States of America* **104**, 8421-8426 (2007).
49. Bunting, M.D. *et al.* CCX-CKR deficiency alters thymic stroma impairing thymocyte development and promoting autoimmunity. *Blood* **121**, 118-128 (2013).
50. Hildebrandt, J.D. Role of subunit diversity in signaling by heterotrimeric G proteins. *Biochemical pharmacology* **54**, 325-339 (1997).

51. Oldham, W.M. & Hamm, H.E. Structural basis of function in heterotrimeric G proteins. *Quarterly reviews of biophysics* **39**, 117-166 (2006).
52. Kohout, T.A. & Lefkowitz, R.J. Regulation of G protein-coupled receptor kinases and arrestins during receptor desensitization. *Molecular pharmacology* **63**, 9-18 (2003).
53. Krupnick, J.G. & Benovic, J.L. The role of receptor kinases and arrestins in G protein-coupled receptor regulation. *Annual review of pharmacology and toxicology* **38**, 289-319 (1998).
54. Pitcher, J.A., Freedman, N.J. & Lefkowitz, R.J. G protein-coupled receptor kinases. *Annual review of biochemistry* **67**, 653-692 (1998).
55. Zidar, D.A., Violin, J.D., Whalen, E.J. & Lefkowitz, R.J. Selective engagement of G protein coupled receptor kinases (GRKs) encodes distinct functions of biased ligands. *Proceedings of the National Academy of Sciences of the United States of America* **106**, 9649-9654 (2009).
56. Campbell, J.J. *et al.* Unique subpopulations of CD56+ NK and NK-T peripheral blood lymphocytes identified by chemokine receptor expression repertoire. *J Immunol* **166**, 6477-6482 (2001).
57. Menning, A. *et al.* Distinctive role of CCR7 in migration and functional activity of naive- and effector/memory-like Treg subsets. *European journal of immunology* **37**, 1575-1583 (2007).
58. Muller, A. *et al.* Involvement of chemokine receptors in breast cancer metastasis. *Nature* **410**, 50-56 (2001).
59. Liu, Y. *et al.* Correlation effect of EGFR and CXCR4 and CCR7 chemokine receptors in predicting breast cancer metastasis and prognosis. *Journal of experimental & clinical cancer research : CR* **29**, 16 (2010).
60. Hopken, U.E. *et al.* CCR7 deficiency causes ectopic lymphoid neogenesis and disturbed mucosal tissue integrity. *Blood* **109**, 886-895 (2007).
61. Forster, R. *et al.* CCR7 coordinates the primary immune response by establishing functional microenvironments in secondary lymphoid organs. *Cell* **99**, 23-33 (1999).
62. Forster, R., Davalos-Misslitz, A.C. & Rot, A. CCR7 and its ligands: balancing immunity and tolerance. *Nature reviews. Immunology* **8**, 362-371 (2008).
63. Schneider, M.A., Meingassner, J.G., Lipp, M., Moore, H.D. & Rot, A. CCR7 is required for the in vivo function of CD4+ CD25+ regulatory T cells. *The Journal of experimental medicine* **204**, 735-745 (2007).
64. Davalos-Misslitz, A.C. *et al.* Generalized multi-organ autoimmunity in CCR7-deficient mice. *European journal of immunology* **37**, 613-622 (2007).
65. Riol-Blanco, L. *et al.* The chemokine receptor CCR7 activates in dendritic cells two signaling modules that independently regulate chemotaxis and migratory speed. *J Immunol* **174**, 4070-4080 (2005).
66. Yanagawa, Y. & Onoe, K. CCL19 induces rapid dendritic extension of murine dendritic cells. *Blood* **100**, 1948-1956 (2002).
67. Marsland, B.J. *et al.* CCL19 and CCL21 induce a potent proinflammatory differentiation program in licensed dendritic cells. *Immunity* **22**, 493-505 (2005).
68. Yanagawa, Y. & Onoe, K. CCR7 ligands induce rapid endocytosis in mature dendritic cells with concomitant up-regulation of Cdc42 and Rac activities. *Blood* **101**, 4923-4929 (2003).
69. Sanchez-Sanchez, N. *et al.* Chemokine receptor CCR7 induces intracellular signaling that inhibits apoptosis of mature dendritic cells. *Blood* **104**, 619-625 (2004).
70. Torres-Bacete, J., Delgado-Martin, C., Gomez-Moreira, C., Simizu, S. & Rodriguez-Fernandez, J.L. The Mammalian Sterile 20-like 1 Kinase Controls Selective CCR7-Dependent Functions in Human Dendritic Cells. *J Immunol* **195**, 973-981 (2015).
71. Escribano, C., Delgado-Martin, C. & Rodriguez-Fernandez, J.L. CCR7-dependent stimulation of survival in dendritic cells involves inhibition of GSK3beta. *J Immunol* **183**, 6282-6295 (2009).
72. Hawkins, P.T., Jackson, T.R. & Stephens, L.R. Platelet-derived growth factor stimulates synthesis of PtdIns(3,4,5)P3 by activating a PtdIns(4,5)P2 3-OH kinase. *Nature* **358**, 157-159 (1992).
73. Lemmon, M.A. Phosphoinositide recognition domains. *Traffic* **4**, 201-213 (2003).
74. Alessi, D.R. *et al.* Mechanism of activation of protein kinase B by insulin and IGF-1. *The EMBO journal* **15**, 6541-6551 (1996).
75. Leslie, N.R., Biondi, R.M. & Alessi, D.R. Phosphoinositide-regulated kinases and phosphoinositide phosphatases. *Chemical reviews* **101**, 2365-2380 (2001).
76. Sarbassov, D.D., Guertin, D.A., Ali, S.M. & Sabatini, D.M. Phosphorylation and regulation of Akt/PKB by the rictor-mTOR complex. *Science* **307**, 1098-1101 (2005).

77. Mahajan, K. & Mahajan, N.P. PI3K-independent AKT activation in cancers: a treasure trove for novel therapeutics. *Journal of cellular physiology* **227**, 3178-3184 (2012).
78. Cross, D.A., Alessi, D.R., Cohen, P., Andjelkovich, M. & Hemmings, B.A. Inhibition of glycogen synthase kinase-3 by insulin mediated by protein kinase B. *Nature* **378**, 785-789 (1995).
79. Grimes, C.A. & Jope, R.S. The multifaceted roles of glycogen synthase kinase 3beta in cellular signaling. *Progress in neurobiology* **65**, 391-426 (2001).
80. Biggs, W.H., 3rd, Meisenhelder, J., Hunter, T., Cavenee, W.K. & Arden, K.C. Protein kinase B/Akt-mediated phosphorylation promotes nuclear exclusion of the winged helix transcription factor FKHR1. *Proceedings of the National Academy of Sciences of the United States of America* **96**, 7421-7426 (1999).
81. Matsuzaki, H., Daitoku, H., Hatta, M., Tanaka, K. & Fukamizu, A. Insulin-induced phosphorylation of FKHR (Foxo1) targets to proteasomal degradation. *Proceedings of the National Academy of Sciences of the United States of America* **100**, 11285-11290 (2003).
82. Brunet, A. *et al.* Akt promotes cell survival by phosphorylating and inhibiting a Forkhead transcription factor. *Cell* **96**, 857-868 (1999).
83. Fu, Z. & Tindall, D.J. FOXOs, cancer and regulation of apoptosis. *Oncogene* **27**, 2312-2319 (2008).
84. Dijkers, P.F., Medema, R.H., Lammers, J.W., Koenderman, L. & Coffer, P.J. Expression of the pro-apoptotic Bcl-2 family member Bim is regulated by the forkhead transcription factor FKHR-L1. *Current biology : CB* **10**, 1201-1204 (2000).
85. Baldwin, A.S., Jr. The NF-kappa B and I kappa B proteins: new discoveries and insights. *Annual review of immunology* **14**, 649-683 (1996).
86. Neumann, M. *et al.* RelA/p65 is a molecular target for the immunosuppressive action of protein kinase A. *The EMBO journal* **14**, 1991-2004 (1995).
87. Vermeulen, L., De Wilde, G., Van Damme, P., Vanden Berghe, W. & Haegeman, G. Transcriptional activation of the NF-kappaB p65 subunit by mitogen- and stress-activated protein kinase-1 (MSK1). *The EMBO journal* **22**, 1313-1324 (2003).
88. Dibble, C.C. & Cantley, L.C. Regulation of mTORC1 by PI3K signaling. *Trends in cell biology* **25**, 545-555 (2015).
89. Hara, K. *et al.* Raptor, a binding partner of target of rapamycin (TOR), mediates TOR action. *Cell* **110**, 177-189 (2002).
90. Sancak, Y. *et al.* PRAS40 is an insulin-regulated inhibitor of the mTORC1 protein kinase. *Molecular cell* **25**, 903-915 (2007).
91. Kim, D.H. *et al.* GbetaL, a positive regulator of the rapamycin-sensitive pathway required for the nutrient-sensitive interaction between raptor and mTOR. *Molecular cell* **11**, 895-904 (2003).
92. Peterson, T.R. *et al.* DEPTOR is an mTOR inhibitor frequently overexpressed in multiple myeloma cells and required for their survival. *Cell* **137**, 873-886 (2009).
93. Mills, J.R. *et al.* mTORC1 promotes survival through translational control of Mcl-1. *Proceedings of the National Academy of Sciences of the United States of America* **105**, 10853-10858 (2008).
94. Bhaskar, P.T. *et al.* mTORC1 hyperactivity inhibits serum deprivation-induced apoptosis via increased hexokinase II and GLUT1 expression, sustained Mcl-1 expression, and glycogen synthase kinase 3beta inhibition. *Molecular and cellular biology* **29**, 5136-5147 (2009).
95. Fischmann, T.O. *et al.* Crystal structures of MEK1 binary and ternary complexes with nucleotides and inhibitors. *Biochemistry* **48**, 2661-2674 (2009).
96. Ohren, J.F. *et al.* Structures of human MAP kinase kinase 1 (MEK1) and MEK2 describe novel noncompetitive kinase inhibition. *Nature structural & molecular biology* **11**, 1192-1197 (2004).
97. Catalanotti, F. *et al.* A Mek1-Mek2 heterodimer determines the strength and duration of the Erk signal. *Nature structural & molecular biology* **16**, 294-303 (2009).
98. Zheng, C.F. & Guan, K.L. Activation of MEK family kinases requires phosphorylation of two conserved Ser/Thr residues. *The EMBO journal* **13**, 1123-1131 (1994).
99. Alessi, D.R. *et al.* Identification of the sites in MAP kinase kinase-1 phosphorylated by p74raf-1. *The EMBO journal* **13**, 1610-1619 (1994).
100. Frost, J.A. *et al.* Cross-cascade activation of ERKs and ternary complex factors by Rho family proteins. *The EMBO journal* **16**, 6426-6438 (1997).
101. Eblen, S.T., Slack, J.K., Weber, M.J. & Catling, A.D. Rac-PAK signaling stimulates extracellular signal-regulated kinase (ERK) activation by regulating formation of MEK1-ERK complexes. *Molecular and cellular biology* **22**, 6023-6033 (2002).

102. Rossomando, A.J., Dent, P., Sturgill, T.W. & Marshak, D.R. Mitogen-activated protein kinase kinase 1 (MKK1) is negatively regulated by threonine phosphorylation. *Molecular and cellular biology* **14**, 1594-1602 (1994).
103. Brunet, A., Pages, G. & Pouyssegur, J. Growth factor-stimulated MAP kinase induces rapid retrophosphorylation and inhibition of MAP kinase kinase (MEK1). *FEBS letters* **346**, 299-303 (1994).
104. Eblen, S.T. *et al.* Mitogen-activated protein kinase feedback phosphorylation regulates MEK1 complex formation and activation during cellular adhesion. *Molecular and cellular biology* **24**, 2308-2317 (2004).
105. Roskoski, R., Jr. ERK1/2 MAP kinases: structure, function, and regulation. *Pharmacological research : the official journal of the Italian Pharmacological Society* **66**, 105-143 (2012).
106. Khokhlatchev, A.V. *et al.* Phosphorylation of the MAP kinase ERK2 promotes its homodimerization and nuclear translocation. *Cell* **93**, 605-615 (1998).
107. Chuderland, D., Konson, A. & Seger, R. Identification and characterization of a general nuclear translocation signal in signaling proteins. *Molecular cell* **31**, 850-861 (2008).
108. Owens, D.M. & Keyse, S.M. Differential regulation of MAP kinase signalling by dual-specificity protein phosphatases. *Oncogene* **26**, 3203-3213 (2007).
109. Robinson, M.J., Stippec, S.A., Goldsmith, E., White, M.A. & Cobb, M.H. A constitutively active and nuclear form of the MAP kinase ERK2 is sufficient for neurite outgrowth and cell transformation. *Current biology : CB* **8**, 1141-1150 (1998).
110. Brunet, A. *et al.* Nuclear translocation of p42/p44 mitogen-activated protein kinase is required for growth factor-induced gene expression and cell cycle entry. *The EMBO journal* **18**, 664-674 (1999).
111. Schaeffer, H.J. *et al.* MP1: a MEK binding partner that enhances enzymatic activation of the MAP kinase cascade. *Science* **281**, 1668-1671 (1998).
112. Wunderlich, W. *et al.* A novel 14-kilodalton protein interacts with the mitogen-activated protein kinase scaffold mp1 on a late endosomal/lysosomal compartment. *The Journal of cell biology* **152**, 765-776 (2001).
113. Vaidyanathan, H. *et al.* ERK MAP kinase is targeted to RSK2 by the phosphoprotein PEA-15. *Proceedings of the National Academy of Sciences of the United States of America* **104**, 19837-19842 (2007).
114. Formstecher, E. *et al.* PEA-15 mediates cytoplasmic sequestration of ERK MAP kinase. *Developmental cell* **1**, 239-250 (2001).
115. Rose, B.A., Force, T. & Wang, Y. Mitogen-activated protein kinase signaling in the heart: angels versus demons in a heart-breaking tale. *Physiological reviews* **90**, 1507-1546 (2010).
116. Thornton, C., Snowden, M.A. & Carling, D. Identification of a novel AMP-activated protein kinase beta subunit isoform that is highly expressed in skeletal muscle. *The Journal of biological chemistry* **273**, 12443-12450 (1998).
117. Stapleton, D. *et al.* Mammalian AMP-activated protein kinase subfamily. *The Journal of biological chemistry* **271**, 611-614 (1996).
118. Cheung, P.C., Salt, I.P., Davies, S.P., Hardie, D.G. & Carling, D. Characterization of AMP-activated protein kinase gamma-subunit isoforms and their role in AMP binding. *The Biochemical journal* **346 Pt 3**, 659-669 (2000).
119. Wu, J. *et al.* Chemoproteomic analysis of intertissue and interspecies isoform diversity of AMP-activated protein kinase (AMPK). *The Journal of biological chemistry* **288**, 35904-35912 (2013).
120. Oakhill, J.S. *et al.* beta-Subunit myristoylation is the gatekeeper for initiating metabolic stress sensing by AMP-activated protein kinase (AMPK). *Proceedings of the National Academy of Sciences of the United States of America* **107**, 19237-19241 (2010).
121. Xiao, B. *et al.* Structural basis for AMP binding to mammalian AMP-activated protein kinase. *Nature* **449**, 496-500 (2007).
122. Townley, R. & Shapiro, L. Crystal structures of the adenylate sensor from fission yeast AMP-activated protein kinase. *Science* **315**, 1726-1729 (2007).
123. Hardie, D.G. & Ashford, M.L. AMPK: regulating energy balance at the cellular and whole body levels. *Physiology (Bethesda)* **29**, 99-107 (2014).
124. Davies, S.P., Helps, N.R., Cohen, P.T. & Hardie, D.G. 5'-AMP inhibits dephosphorylation, as well as promoting phosphorylation, of the AMP-activated protein kinase. Studies using bacterially

expressed human protein phosphatase-2C alpha and native bovine protein phosphatase-2AC. *FEBS letters* **377**, 421-425 (1995).

125. Gowans, G.J., Hawley, S.A., Ross, F.A. & Hardie, D.G. AMP is a true physiological regulator of AMP-activated protein kinase by both allosteric activation and enhancing net phosphorylation. *Cell metabolism* **18**, 556-566 (2013).
126. Suter, M. *et al.* Dissecting the role of 5'-AMP for allosteric stimulation, activation, and deactivation of AMP-activated protein kinase. *The Journal of biological chemistry* **281**, 32207-32216 (2006).
127. Xiao, B. *et al.* Structure of mammalian AMPK and its regulation by ADP. *Nature* **472**, 230-233 (2011).
128. Shaw, R.J. *et al.* The tumor suppressor LKB1 kinase directly activates AMP-activated kinase and regulates apoptosis in response to energy stress. *Proceedings of the National Academy of Sciences of the United States of America* **101**, 3329-3335 (2004).
129. Hawley, S.A. *et al.* Calmodulin-dependent protein kinase kinase-beta is an alternative upstream kinase for AMP-activated protein kinase. *Cell metabolism* **2**, 9-19 (2005).
130. Momcilovic, M., Hong, S.P. & Carlson, M. Mammalian TAK1 activates Snf1 protein kinase in yeast and phosphorylates AMP-activated protein kinase in vitro. *The Journal of biological chemistry* **281**, 25336-25343 (2006).
131. Hurley, R.L. *et al.* Regulation of AMP-activated protein kinase by multisite phosphorylation in response to agents that elevate cellular cAMP. *The Journal of biological chemistry* **281**, 36662-36672 (2006).
132. Horman, S. *et al.* Insulin antagonizes ischemia-induced Thr172 phosphorylation of AMP-activated protein kinase alpha-subunits in heart via hierarchical phosphorylation of Ser485/491. *The Journal of biological chemistry* **281**, 5335-5340 (2006).
133. Hawley, S.A. *et al.* Phosphorylation by Akt within the ST loop of AMPK-alpha1 down-regulates its activation in tumour cells. *The Biochemical journal* **459**, 275-287 (2014).
134. Hardie, D.G. AMPK: positive and negative regulation, and its role in whole-body energy homeostasis. *Current opinion in cell biology* **33C**, 1-7 (2014).
135. (!!! INVALID CITATION !!!).
136. Djouder, N. *et al.* PKA phosphorylates and inactivates AMPKalpha to promote efficient lipolysis. *The EMBO journal* **29**, 469-481 (2010).
137. Warden, S.M. *et al.* Post-translational modifications of the beta-1 subunit of AMP-activated protein kinase affect enzyme activity and cellular localization. *The Biochemical journal* **354**, 275-283 (2001).
138. Mitchelhill, K.I. *et al.* Posttranslational modifications of the 5'-AMP-activated protein kinase beta1 subunit. *The Journal of biological chemistry* **272**, 24475-24479 (1997).
139. Sanz, P., Rubio, T. & Garcia-Gimeno, M.A. AMPKbeta subunits: more than just a scaffold in the formation of AMPK complex. *The FEBS journal* **280**, 3723-3733 (2013).
140. Celenza, J.L. & Carlson, M. A yeast gene that is essential for release from glucose repression encodes a protein kinase. *Science* **233**, 1175-1180 (1986).
141. Polge, C. & Thomas, M. SNF1/AMPK/SnRK1 kinases, global regulators at the heart of energy control? *Trends in plant science* **12**, 20-28 (2007).
142. Russell, R.R., 3rd, Bergeron, R., Shulman, G.I. & Young, L.H. Translocation of myocardial GLUT-4 and increased glucose uptake through activation of AMPK by AICAR. *The American journal of physiology* **277**, H643-649 (1999).
143. Marsin, A.S. *et al.* Phosphorylation and activation of heart PFK-2 by AMPK has a role in the stimulation of glycolysis during ischaemia. *Current biology : CB* **10**, 1247-1255 (2000).
144. Carling, D. & Hardie, D.G. The substrate and sequence specificity of the AMP-activated protein kinase. Phosphorylation of glycogen synthase and phosphorylase kinase. *Biochimica et biophysica acta* **1012**, 81-86 (1989).
145. Aschenbach, W.G. *et al.* Effect of AICAR treatment on glycogen metabolism in skeletal muscle. *Diabetes* **51**, 567-573 (2002).
146. Davies, S.P., Sim, A.T. & Hardie, D.G. Location and function of three sites phosphorylated on rat acetyl-CoA carboxylase by the AMP-activated protein kinase. *European journal of biochemistry / FEBS* **187**, 183-190 (1990).
147. Sullivan, J.E. *et al.* Inhibition of lipolysis and lipogenesis in isolated rat adipocytes with AICAR, a cell-permeable activator of AMP-activated protein kinase. *FEBS letters* **353**, 33-36 (1994).

148. Henin, N., Vincent, M.F., Gruber, H.E. & Van den Berghe, G. Inhibition of fatty acid and cholesterol synthesis by stimulation of AMP-activated protein kinase. *FASEB journal : official publication of the Federation of American Societies for Experimental Biology* **9**, 541-546 (1995).
149. Luiken, J.J. *et al.* Contraction-induced fatty acid translocase/CD36 translocation in rat cardiac myocytes is mediated through AMP-activated protein kinase signaling. *Diabetes* **52**, 1627-1634 (2003).
150. Shearer, J. *et al.* AMP kinase-induced skeletal muscle glucose but not long-chain fatty acid uptake is dependent on nitric oxide. *Diabetes* **53**, 1429-1435 (2004).
151. Browne, G.J., Finn, S.G. & Proud, C.G. Stimulation of the AMP-activated protein kinase leads to activation of eukaryotic elongation factor 2 kinase and to its phosphorylation at a novel site, serine 398. *The Journal of biological chemistry* **279**, 12220-12231 (2004).
152. Bolster, D.R., Crozier, S.J., Kimball, S.R. & Jefferson, L.S. AMP-activated protein kinase suppresses protein synthesis in rat skeletal muscle through down-regulated mammalian target of rapamycin (mTOR) signaling. *The Journal of biological chemistry* **277**, 23977-23980 (2002).
153. Shaw, R.J. *et al.* The LKB1 tumor suppressor negatively regulates mTOR signaling. *Cancer cell* **6**, 91-99 (2004).
154. Zheng, B. & Cantley, L.C. Regulation of epithelial tight junction assembly and disassembly by AMP-activated protein kinase. *Proceedings of the National Academy of Sciences of the United States of America* **104**, 819-822 (2007).
155. Williams, T., Courchet, J., Viollet, B., Brenman, J.E. & Polleux, F. AMP-activated protein kinase (AMPK) activity is not required for neuronal development but regulates axogenesis during metabolic stress. *Proceedings of the National Academy of Sciences of the United States of America* **108**, 5849-5854 (2011).
156. Amato, S. *et al.* AMP-activated protein kinase regulates neuronal polarization by interfering with PI 3-kinase localization. *Science* **332**, 247-251 (2011).
157. Steinberg, G.R. & Kemp, B.E. AMPK in Health and Disease. *Physiological reviews* **89**, 1025-1078 (2009).
158. Egan, D.F. *et al.* Phosphorylation of ULK1 (hATG1) by AMP-activated protein kinase connects energy sensing to mitophagy. *Science* **331**, 456-461 (2011).
159. Kim, J., Kundu, M., Viollet, B. & Guan, K.L. AMPK and mTOR regulate autophagy through direct phosphorylation of Ulk1. *Nature cell biology* **13**, 132-141 (2011).
160. Nakada, D., Saunders, T.L. & Morrison, S.J. Lkb1 regulates cell cycle and energy metabolism in haematopoietic stem cells. *Nature* **468**, 653-658 (2010).
161. Durante, P., Gueuning, M.A., Darville, M.I., Hue, L. & Rousseau, G.G. Apoptosis induced by growth factor withdrawal in fibroblasts overproducing fructose 2,6-bisphosphate. *FEBS letters* **448**, 239-243 (1999).
162. Saberi, B. *et al.* Regulation of H(2)O(2)-induced necrosis by PKC and AMP-activated kinase signaling in primary cultured hepatocytes. *American journal of physiology. Cell physiology* **295**, C50-63 (2008).
163. Chen, H., Wang, J.P., Santen, R.J. & Yue, W. Adenosine monophosphate activated protein kinase (AMPK), a mediator of estradiol-induced apoptosis in long-term estrogen deprived breast cancer cells. *Apoptosis : an international journal on programmed cell death* **20**, 821-830 (2015).
164. Meisse, D. *et al.* Sustained activation of AMP-activated protein kinase induces c-Jun N-terminal kinase activation and apoptosis in liver cells. *FEBS letters* **526**, 38-42 (2002).
165. Weisova, P. *et al.* Role of 5'-adenosine monophosphate-activated protein kinase in cell survival and death responses in neurons. *Antioxidants & redox signaling* **14**, 1863-1876 (2011).
166. Guigas, B. *et al.* 5-Aminoimidazole-4-carboxamide-1-beta-D-ribofuranoside and metformin inhibit hepatic glucose phosphorylation by an AMP-activated protein kinase-independent effect on glucokinase translocation. *Diabetes* **55**, 865-874 (2006).
167. Daignan-Fornier, B. & Pinson, B. 5-Aminoimidazole-4-carboxamide-1-beta-D-ribofuranosyl 5'-Monophosphate (AICAR), a Highly Conserved Purine Intermediate with Multiple Effects. *Metabolites* **2**, 292-302 (2012).
168. Scott, J.W. *et al.* Thienopyridone drugs are selective activators of AMP-activated protein kinase beta1-containing complexes. *Chemistry & biology* **15**, 1220-1230 (2008).
169. Goransson, O. *et al.* Mechanism of action of A-769662, a valuable tool for activation of AMP-activated protein kinase. *The Journal of biological chemistry* **282**, 32549-32560 (2007).

170. Sanders, M.J. *et al.* Defining the mechanism of activation of AMP-activated protein kinase by the small molecule A-769662, a member of the thienopyridone family. *The Journal of biological chemistry* **282**, 32539-32548 (2007).
171. Xiao, B. *et al.* Structural basis of AMPK regulation by small molecule activators. *Nature communications* **4**, 3017 (2013).
172. Scott, J.W. *et al.* Small molecule drug A-769662 and AMP synergistically activate naive AMPK independent of upstream kinase signaling. *Chemistry & biology* **21**, 619-627 (2014).
173. Jin, J. *et al.* AMPK inhibitor Compound C stimulates ceramide production and promotes Bax redistribution and apoptosis in MCF7 breast carcinoma cells. *Journal of lipid research* **50**, 2389-2397 (2009).
174. Bain, J. *et al.* The selectivity of protein kinase inhibitors: a further update. *The Biochemical journal* **408**, 297-315 (2007).
175. Iwatsubo, K. *et al.* Prevention of heart failure in mice by an antiviral agent that inhibits type 5 cardiac adenylyl cyclase. *American journal of physiology. Heart and circulatory physiology* **302**, H2622-2628 (2012).
176. Soderberg, O. *et al.* Direct observation of individual endogenous protein complexes in situ by proximity ligation. *Nature methods* **3**, 995-1000 (2006).
177. Gomez-Cabanas, L. *et al.* Detecting apoptosis of leukocytes in mouse lymph nodes. *Nature protocols* **9**, 1102-1112 (2014).
178. Cao, Y. *et al.* The serine/threonine kinase LKB1 controls thymocyte survival through regulation of AMPK activation and Bcl-XL expression. *Cell research* **20**, 99-108 (2010).
179. Stein, S.C., Woods, A., Jones, N.A., Davison, M.D. & Carling, D. The regulation of AMP-activated protein kinase by phosphorylation. *The Biochemical journal* **345 Pt 3**, 437-443 (2000).
180. Riccardi, C. & Nicoletti, I. Analysis of apoptosis by propidium iodide staining and flow cytometry. *Nature protocols* **1**, 1458-1461 (2006).
181. Dagon, Y. *et al.* p70S6 kinase phosphorylates AMPK on serine 491 to mediate leptin's effect on food intake. *Cell metabolism* **16**, 104-112 (2012).
182. Zheng, B. *et al.* Oncogenic B-RAF negatively regulates the tumor suppressor LKB1 to promote melanoma cell proliferation. *Molecular cell* **33**, 237-247 (2009).
183. Aryal, P. *et al.* Baicalein induces autophagic cell death through AMPK/ULK1 activation and downregulation of mTORC1 complex components in human cancer cells. *The FEBS journal* **281**, 4644-4658 (2014).
184. Ji, H.T., Chien, L.T., Lin, Y.H., Chien, H.F. & Chen, C.T. 5-ALA mediated photodynamic therapy induces autophagic cell death via AMP-activated protein kinase. *Molecular cancer* **9**, 91 (2010).
185. Liao, K.C. & Mogridge, J. Activation of the Nlrp1b inflammasome by reduction of cytosolic ATP. *Infection and immunity* **81**, 570-579 (2013).
186. Greer, E.L. *et al.* The energy sensor AMP-activated protein kinase directly regulates the mammalian FOXO3 transcription factor. *The Journal of biological chemistry* **282**, 30107-30119 (2007).
187. Inoki, K., Zhu, T. & Guan, K.L. TSC2 mediates cellular energy response to control cell growth and survival. *Cell* **115**, 577-590 (2003).
188. Agarwal, S., Bell, C.M., Rothbart, S.B. & Moran, R.G. AMP-activated Protein Kinase (AMPK) Control of mTORC1 Is p53- and TSC2-independent in Pemetrexed-treated Carcinoma Cells. *The Journal of biological chemistry* **290**, 27473-27486 (2015).
189. Gwinn, D.M. *et al.* AMPK phosphorylation of raptor mediates a metabolic checkpoint. *Molecular cell* **30**, 214-226 (2008).
190. Fumarola, C. *et al.* Effects of sorafenib on energy metabolism in breast cancer cells: role of AMPK-mTORC1 signaling. *Breast cancer research and treatment* **141**, 67-78 (2013).
191. Lennon, J.C. *et al.* Involvement of AMP-activated protein kinase in mediating pyrrolo-1,5-benzoxazepine-induced apoptosis in neuroblastoma cells. *Investigational new drugs* (2016).
192. Yang, J.M. *et al.* Hispidulin sensitizes human ovarian cancer cells to TRAIL-induced apoptosis by AMPK activation leading to Mcl-1 block in translation. *Journal of agricultural and food chemistry* **58**, 10020-10026 (2010).
193. Kayampilly, P.P. & Menon, K.M. Follicle-stimulating hormone inhibits adenosine 5'-monophosphate-activated protein kinase activation and promotes cell proliferation of primary granulosa cells in culture through an Akt-dependent pathway. *Endocrinology* **150**, 929-935 (2009).

194. Shen, C.H. *et al.* Phosphorylation of BRAF by AMPK impairs BRAF-KSR1 association and cell proliferation. *Molecular cell* **52**, 161-172 (2013).
195. Zhu, B. *et al.* Porcine circovirus type 2 induces autophagy via the AMPK/ERK/TSC2/mTOR signaling pathway in PK-15 cells. *Journal of virology* **86**, 12003-12012 (2012).
196. Chen, M., Huang, L. & Wang, J. Deficiency of Bim in dendritic cells contributes to overactivation of lymphocytes and autoimmunity. *Blood* **109**, 4360-4367 (2007).
197. Ohnmacht, C. *et al.* Constitutive ablation of dendritic cells breaks self-tolerance of CD4 T cells and results in spontaneous fatal autoimmunity. *The Journal of experimental medicine* **206**, 549-559 (2009).
198. Hildeman, D., Jorgensen, T., Kappler, J. & Marrack, P. Apoptosis and the homeostatic control of immune responses. *Current opinion in immunology* **19**, 516-521 (2007).

ANEXOS

ANEXO 1: ABREVIATURAS Y ACRÓNIMOS

4EBP1: eukaryotic translation initiation factor 4E-Binding Protein 1

ACC: Acetyl-CoA Carboxisalasa

ADN: Ácido DesoxiriboNucleico

ADP: Adenosine DiPhosphate

Akt: AK strain Thymoma

Akti: inhibidor de Akt

AMPK: AMP-activated protein Kinase

AMP: Adenosine MonoPhosphate

cAMP: cyclic AMP

Apaf-1: Apoptosis Protease-inducing Factor 1

Asp: Aspartico

ATP: Adenosine TriPhosphate

Bax: BCL2-associated X protein

Bad: Bcl-2-Associated Death promoter

Bcl-2: B cell lymphoma 2

Bcl-xL: B cell lymphoma extra large

Bid: BH3 Interacting Domain death agonist

Bim: Bcl-2 interacting mediator of death

BSA: Bovine Serum Albumin

Boo: Bcl-2 homolog Of Ovary

Br cAMP: Bromo cAMP

CAMKK2: Calcium/Calmodulin-dependent protein Kinase Kinase 2

CCL: Chemokine (CC motif) Ligand

CCR: Chemokine (CC motif) Receptor

CDs: Células Dendríticas

CDi: Célula Dendrítica Inmadura

CDm: Célula Dendrítica Madura

CREB: cAMP Response Element-Binding

CXCL: Chemokine (CXC motif) Ligand

CXCR: Chemokine (CXC motif) Receptor

DAMPS: Danger-Associated Molecular Patterns

DEPTOR: DEP domain-containing mTOR-interacting protein

Desv. Est.: Desviación estándar

Dib cAMPK: Dibutiril cAMP

DN: Doble negativo

DUSP: Dual-Specificity Phosphatase

ECL: Enhanced ChemiLuminescence

EDTA: EthyleneDiamineTetraacetic Acid

Erk1/2: Extracellular signal-Regulated Kinase ½

FASL: Fas Lingando

FBS: Fetal Bovine Serum

FoxO: Forkhead box class O

FYVE: Fab 1, YOTB, Vac and EEA1 domain

GBP: GSK3 Binding Protein

GDP: Guanine DiPhosphate

GFP: Green Fluorescent Protein

GLUT4: GLUcose Transporter type 4

GM-CSF: Granulocyte/Macrophage Colony-Stimulating Factor

GPCR: G protein-coupled Receptor

GRK: G protein-coupled Receptor Kinase

GSK: Glycogen Synthase Kinase

GTP: Guanine TriPhosphate

IFN: InterFeroN

Ig: Inmunoglobulina

IκB: Inhibitor of nfF-kappa-B protein

IL: InterLeukin

iNOS: inducible Nitric Oxide Synthase

IP: Yoduro de Propidio

JNK: c-Jun N-terminal Kinase

KDa: Kilodalton

KID: Kinase Insert Domain

KO: Knockout

KSR: Kinase Suppressor of Ras

LKB1: Liver Kinase B1

LIMK: LIM Domain Kinase

LPS: Lipopolisacárido

MACS: Magnetic-Activated Cell Sorting

MAPK: Mitogen-Activated Protein Kinase

MEK: MAPKinase-Erk Kinase

MHC: Major Histocompatibility Complex

MLC: Myosin Light-Chain

MLCP: MLC phosphatase

MNK: MAP kinase iNtegrating Kinase

MOMP: permeabilización de la membrana externa mitocondrial

MP-1: MEK Partner-1

MSK: Mitogen- and Stress-activated protein Kinase-1

MST1: Mammalian Sterile20-like 1

mTOR: Mechanistic Target Of Rapamycin

mTORC: Mechanistic Target Of Rapamycin (mTOR) Complex

NF-κB: Nuclear Factor-κB

NK: Natural Killer

p70S6K: 70 kDa ribosomal protein S6Kinase

p90rsk: 90-kDa ribosomal S6 kinase

PAGE: PolyAcrylamide Gel Electrophoresis

PAK1: P-21-Activated Kinase-1

PBS: Phosphate-Buffered Saline

PDK1: Phosphoinositide-Dependent

protein Kinase 1

PH: Pleckstrin Homology

PI: PhosphatidylInositol

PIP: PhosphatidylInositol Phosphate

PI3K: PhosphatidylInositol 3-kinase

PKA: Protein Kinase A

PKC: Protein Kinase C

PLA: Proximity ligation assay

PRAS40: Proline-Rich Akt Substrate of 40 kDa

PTX: Pertussis Toxin

PX: P40phoX domain

PYK2: Proline-rich tyrosine Kinase 2

RAPTOR: Regulatory-Associated Protein of mTOR

Raf: Rapidly Accelerated Fibrosarcoma

RHD: Rel Homology Domain

RhoA: Ras HOmolog gene family, member A

ROCK: Rho-associated protein Kinase

ROS: Reactive Oxigen Species

SDS: Sodium Dodecyl Sulfate

Ser: SERina

siRNA: small interfering Ribonucleic Acid

SR-FLIVO: Sulforhodamine-[Val-Ala-Asp-fluoromethylketone (VAD-FMK)]

TAK1: Transforming growth factor β-Activated Kinase 1

TBS: Tris-Buffered Saline

TBST: Tris-Buffered Saline Tween

TCR: T Cell Receptor

Thr: Treonina

TLR: Toll Like Receptor

TNF: Tumor Necrosis Factor

TRAIL: TNF-Related Apoptosis-Inducing Ligand

TSC: Tuberose Sclerosis Complex

Tyr: Tirosina

ZMP: 5-amino-4-imidazolecarboxamide riboside 5'-MonoPhosphate

ANEXO 2: PUBLICACIONES CIENTÍFICAS

Gómez-Cabañas L, Delgado-Martín C, ***López-Cotarelo P****, Escribano-Diaz C, Alonso-C LM, Riol-Blanco L, Rodríguez-Fernández JL. Detecting apoptosis of leukocytes in mouse lymph nodes. (2014). Nature Protocols. Vol 9: p. 1102–1112.*

López-Cotarelo P*, Escribano-Díaz C, González-Bethencourt IL, Gómez-Moreira C, Deguiz ML, Torres-Bacete J, Gómez-Cabañas L, Fernández-Barrera J, Delgado-Martín C, Mellado M, Regueiro JR, Miranda-Carús ME, Rodríguez-Fernández JL. A novel MEK-ERK-AMPK signalling axis controls chemokine receptor CCR7-dependent survival in human mature dendritic cells. (2015). J. BIOL. CHEM. Vol. 290: p. 827-840.*

Cascio G, Martín-Cófreces NB, Rodríguez-Frade JM, ***López-Cotarelo P****, Criado G, Pablos JL, Rodríguez-Fernández JL, Sánchez-Madrid F, Mellado M. CXCL12 Regulates through JAK1 and JAK2 Formation of Productive Immunological Synapses. (2015). Journal Immunology. Vol.194 no.11: p. 5509-19.*

Detecting apoptosis of leukocytes in mouse lymph nodes

Laura Gómez-Cabañas[1,3], Cristina Delgado-Martín[1,3], Pilar López-Cotarelo[1], Cristina Escribano-Diaz[1], Luis M Alonso-C[2], Lorena Riol-Blanco[1,4] & José Luis Rodríguez-Fernández[1]

[1]Centro de Investigaciones Biológicas. Consejo Superior de Investigaciones Científicas, Madrid, Spain. [2]Centro de Microscopía y Citometría, Universidad Complutense, Madrid, Spain. [3]These authors contributed equally to this work. [4]Present address: Department of Microbiology and Immunobiology, Harvard Medical School, Boston, Massachusetts, USA. Correspondence should be addressed to J.L.R.-F. (rodrifer@cib.csic.es).

Published online 17 April 2014; doi:10.1038/nprot.2014.078

Although there are multiple methods for analyzing apoptosis in cultured cells, methodologies for analyzing apoptosis *in vivo* are sparse. In this protocol, we describe how to detect apoptosis of leukocytes in mouse lymph nodes (LNs) via the detection of apoptotic caspases. We have previously used this protocol to study factors that modulate dendritic cell (DC) survival in LNs; however, it can also be used to analyze other leukocytes that migrate to the LNs. DCs labeled with a fluorescent cell tracker are subcutaneously injected in the posterior footpads of mice. Once the labeled DCs reach the popliteal LN (PLN), the animals are intravenously injected with FLIVO, a permeant fluorescent reagent that selectively marks active caspases and consequently apoptotic cells. Explanted PLNs are then examined under a two-photon microscope to look for the presence of apoptotic cells among the DCs injected. The protocol requires 6–6.5 h for preparation and analysis plus an additional 34–40 h to allow apoptosis of the injected DCs in the PLN.

INTRODUCTION

Importance of apoptosis in the immune system

Apoptosis, or programmed cell death, has a key role during development and the maintenance of cell homeostasis[1]. In the immune system, defective apoptosis of leukocytes has important effects on the immune response, leading, in some cases, to autoimmune diseases[2,3]. This is exemplified in the case of DCs, antigen-presenting cells that bridge the innate and adaptive arms of the immune system[4]. The control of the survival of DC is particularly important in the LNs, where antigen-loaded DCs activate T cells displaying cognate T cell receptors[4]. It has been observed that moderate increases in the survival of DCs (i.e., their longevity), leads to improvement in the quality of the immune response[2,5]; however, mice depleted of DCs or mice that present abnormally long-lived DCs develop autoimmune diseases[2,6–9]. Therefore, knowledge of the mechanisms that regulate DC, and other leukocyte, survival is important in order to develop strategies that allow the modulation of the immune response.

Methods to measure apoptosis of leukocytes in LNs

Although many protocols have been developed to study apoptosis in cell culture[10–13], fewer methods are available to study it in the more complex *in vivo* context, in which cells are exposed to multiple stimuli that could modulate the effects observed in *in vitro* experiments. Transferase-mediated dUTP nick-end labeling (TUNEL), or methods based on it[14], is probably the most popular technique used to detect apoptotic cells *in vivo*. TUNEL staining takes advantage of the fact that apoptosis results in the generation of double-stranded fragments of DNA with free 3′-hydroxyl termini. In the TUNEL assay, the terminal deoxynucleotidyl transferase (TdT) enzyme catalyzes the incorporation of labeled dUTP, which can be subsequently visualized by using different strategies[14], for example, tissue sections of the LNs or organs of interest can be stained with TUNEL to detect apoptotic cells. Although TUNEL is a good method for measuring apoptosis, it has a high sensitivity to tissue processing, which can lead to problems of sensitivity and specificity[15]. Furthermore, free 3′-hydroxyl termini are not always exclusively seen in apoptotic cells, but they have been observed on DNA in necrotic cells, cells undergoing gene transcription or DNA repair, and cells damaged by mechanical forces[15–19]. As a result of these drawbacks, it is recommended that TUNEL staining be complemented with an additional approach to confirm apoptosis[15,20].

Another common method for detecting apoptosis of leukocytes in secondary lymphatic regions of mouse, including LN and spleen, involves the preparation of cell suspensions that are subsequently analyzed by flow cytometry for the presence of apoptotic markers on the membrane. One of the most commonly studied markers is phosphatydilserine, which translocates from the inner side of the plasma membrane to the outer layer during apoptosis, and which is detected by analyzing its binding to annexin V[21,22]. A drawback of this method is that to obtain cell suspensions in lymphoid organs considerable mechanical stress is required, which may induce proteases and/or the secretion of proapoptotic cytokines, which could in turn result in the artifactual estimation of the number of apoptotic cells.

A third strategy to evaluate apoptosis *in vivo* involves the use of Hoechst to stain apoptotic cells[20,23]. Hoechst staining is a simple and inexpensive method for fluorescence detection in culture cells of the condensed (pyknotic) or fragmented chromatin that is typical of apoptotic cells. Kidney cell apoptosis has been analyzed *in vivo* by injecting a solution of Hoechst through the tail vein of rats[20,23]. This method allows the staining of the nucleus of the kidney cells, which can be subsequently analyzed by two-photon microscopy either in the anesthetized living animals[20,23] or in explanted kidneys. We have used a slightly modified version of this method to study apoptosis of DCs in mouse PLNs (L.R.-B., C.D.-M., L.M.A.-C., and J.L.R.-F., unpublished data). The leukocytes were first labeled with the fluorescent intravital fluorescent dye 5-chloromethylfluorescein diacetate (CMFDA) to allow their subsequent tracking, and then they were injected in the

footpads to allow their migration to the PLN (see below). Mice were then intravenously (i.v.) injected with a solution of Hoechst to stain the injected CMFDA-DCs. The PLNs were subsequently explanted and fixed to analyze the morphology of the nucleus of the injected DCs by two-photon microscopy. However, in our hands, this method did not distinguish apoptotic DCs unambiguously. For example, it was difficult to distinguish apoptotic DCs with condensed nuclei from small DCs with small nuclei (L.R.-B., C.D.-M., L.M.A.-C., and J.L.R.-F., unpublished data).

Fluorochrome-labeled inhibitors of caspase (FLICA)-based methods allow the detection of apoptotic leukocytes in the LNs

An important hallmark of the apoptotic process is the activation of caspases, a group of proteases that cleave vital cell substrates and cause cell death[24]. Given the drawbacks of the methods that are available for *in vivo* analysis of apoptosis mentioned above, we decided to analyze apoptosis of leukocytes in the LNs by using FLICA reagents. FLICA reagents selectively bind and label caspases that are activated during apoptosis. When caspases are activated during apoptosis, a cysteine residue, which is required for the activity of these proteases, is displayed in their active centers[24–28]. FLICA reagents include three components: an inhibitor, which selectively binds the active center of the caspase; a reactive fluoromethylketone (FMK) component, which forms an irreversible thio-methyl ketone link with the cysteine at the active center of the enzyme; and a fluorophore, which allows the visualization of the cells that bind the reagent (**Fig. 1**). It is noteworthy that FLICA-based reagents only bind active caspases but not the inactive pro-caspases, implying that these reagents selectively label apoptotic cells (**Fig. 1**). In our protocol, we use an FLICA-based reagent called FLIVO. This reagent, apart from the FMK component, includes the peptide-based, poly-caspase-binding–inhibitor probe (Val-Ala-Asp(OMe), which contains an O-methylation in the Aspartic residue that provides enhanced stability and cell permeability to the inhibitor. It has been shown that the Val-Ala-Asp(OMe)-FMK inhibitor binds irreversibly to the apoptotic caspases-1, -3, -4, -5, -6, -7, -8 and -9 (ref. 29). FLIVO includes either the red fluorophore sulforhodamine B (SR)-FLIVO (λ_{abs} 565 nm; λ_{em} >600 nm) or the green fluorophore carboxyfluorescein (FAM)-FLIVO (λ_{abs} 492 nm; λ_{em} 520 nm). As FLIVO reagents are cell permeant, they can be i.v. injected into living mice, in which they can selectively bind to cells displaying active caspases, resulting in the trapping of the (green or red) FLIVO fluorescence signal within these cells (**Fig. 1**). Nonapoptotic cells, which lack caspase activity, are not stained because FLIVO reagents leak out from cells (**Fig. 1**).

We use the FLICA-based protocol described here to analyze the apoptosis of DCs in the LNs of mice according to the following basic strategy. The DCs are first labeled with the fluorescent cell tracker CMFDA to allow their subsequent tracking, and then they are subcutaneously (s.c.) injected in the posterior footpads of mice, which allows these cells to readily migrate to the PLN[30,31]. Once the DCs are positioned in the PLN, we inject SR-FLIVO and allow the product to bind to the apoptotic CMFDA-DCs. Subsequently, the PLNs are explanted and the CMFDA-DCs are examined by two-photon microscopy to search for the presence of the fluorescent FLIVO labeling and therefore potential apoptosis. Obviously, the same procedure can be carried out by injecting DCs with a red intravital fluorescent dye such as seminaphtorhodafluor-1 (SNARF-1) and subsequently injecting the green FAM-FLIVO to detect apoptotic SNARF-1–DCs.

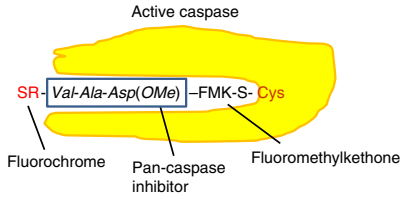

Figure 1 | Cartoon showing the FLICA-based strategy used to detect apoptotic leukocytes. FLIVO, the FLICA-based agent depicted, includes a red fluorochrome (SR), a peptide-based polycaspase inhibitor (Val-Ala-Asp(OMe)), which binds the active center of the caspases 1, -3, -4, -5, -6, -7, -8 and -9, and a reactive FMK group that forms an irreversible thio-methyl ketone link with the cysteine located in the active center of the caspases.

Applications of the protocol

An important advantage of the FLICA-based protocol is its relative unambiguity with respect to determining the effects of different treatments on leukocyte survival. Although the ability of FLIVO to detect apoptotic leukocytes is similar to that of the well-established Hoechst staining (**Fig. 2**), in contrast to the latter, which relies on the correct evaluation of the apoptotic morphology of the nucleus, the fluorescent nature of FLIVO makes the analysis of the staining with this reagent less ambiguous in terms of distinguishing the apoptotic DCs. The protocol is particularly useful and the results are relatively simple to analyze for experiments in which it is not necessary to assess the absolute percentage of apoptotic cells, but rather to assess the relative effects of different treatments or pharmacological agents with respect to a control. In this regard, by using FLIVO, we have previously shown that both immunological synapse formation and the stimulation of chemokine receptor CXCR4 protect DCs from apoptosis in LNs and that the activation of the kinase GSK3-β induces apoptosis in the DCs in these organs[31–33]. Although so far we have used the FLICA-based protocol mostly to study the survival of DCs *in vivo*, this protocol can also be used to study other leukocytes that migrate to the LNs. In this regard, the protocol can be used to study any cell type that expresses the chemokine receptor CCR7, which is responsible for driving leukocytes and other cells to the LNs[34]. The cell types that migrate to the LNs include B cells, naive and central memory T cells, NK cells and some types of monocytes and macrophages. By using this protocol, we have shown that, within the PLN, CD4 T cells are less prone to undergoing apoptosis when compared with DCs[31]. Notably, some metastatic cells, including melanoma, non-small lung cancer, gastric cancer and esophageal cancer also express CCR7 and/or CXCR4 and can migrate to the LNs, which implies that the survival of these cells or their apoptosis in response to different treatments can also be readily analyzed by using this strategy. As it has been shown that migratory monocyte-derived human DCs are able to migrate to mouse PLNs[35,36], it is even possible to use a xenograft model and inject human DCs into mice to accrue information on the influence of different stimuli on the survival of the human leukocytes in mouse PLNs.

FLICA-based staining methods can also be used to analyze the survival of leukocytes or other cells types, not only in mice

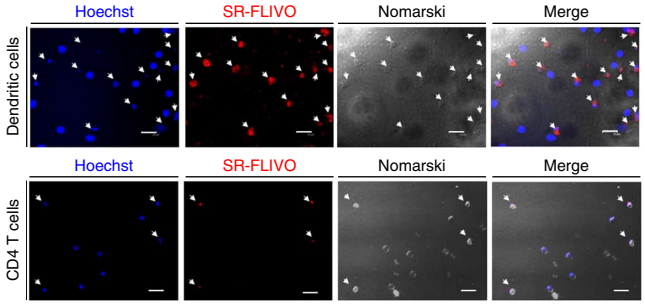

Figure 2 | Hoechst and FLIVO staining of apoptotic leukocytes. DC and CD4 T cells were left for 18 and 30 h, respectively, in serum-free medium. Subsequently, the cells were allowed to adhere onto poly-L-lysine–coated coverslips for 30 min. The cells were then stained with SR-FLIVO (0.5 µg/ml) for 45 min and then fixed and stained with Hoechst 33342 (4 µm) for an additional 30 min. After extensive washing first with PBS and subsequently with water, the coverslips were mounted for fluorescence microscope observation. Small arrows indicate apoptotic cells. As observed, all DCs or CD4 T cells that are identified as apoptotic upon SR-FLIVO staining are also apoptotic according to Hoechst 33342 staining. Consistently, those cells that do not incorporate SR-FLIVO also display the typical live cell nucleus after Hoechst staining. Nomarski images of each field are also shown. Scale bars, 25 µm.

but also in other species, provided that the cells to be studied use caspase-mediated mechanisms of apoptosis, and that they can be tracked, either by labeling with intravital markers or by other alternative strategies for subsequent analysis by two-photon microscopy. Recently, taking advantage of the fact that SR-FLIVO can cross the blood-brain barrier, this reagent has been used to analyze the apoptosis of neurons in the brain of a mouse model of Huntington's disease[37]. However, this method differed from the present protocol, as sections of mouse brain were used to analyze, by confocal microscopy, the amount of SR-FLIVO staining in the neurons of the animals[37]. Here we present an updated version of our *Protocol Exchange* FLIVO staining protocol[38]. Although the basic protocol is similar, this protocol incorporates further detail intended to facilitate the use of this protocol and to show its advantages to study apoptosis of DCs and other leukocytes in the LNs.

Experimental design

The protocol can be divided into six sequential sections: preparation of splenic DCs (Steps 1–13); labeling with fluorescent intravital markers and injection of DCs in mice (Steps 14–20); i.v. injection of FLIVO to stain the apoptotic DCs (Step 21); extraction and preparation of the PLN (Steps 22–26); visualization and scanning of the DCs in the PLN by using two-photon optics (Step 27); and tracking and analysis of FLIVO-stained intravital marker-labeled DCs in the PLN (Steps 28 and 29).

Figure 3 | Two-photon microscopy analysis of CMFDA-DCs showing SR-FLIVO staining in explanted LNs. (**a**) Experimental protocol. A total of 2 × 10^6 CMFDA-labeled splenic DCs (CMFDA-DCs) were s.c. injected in the footpads of recipient mice. After 34 h, the animals were i.v. injected in the tail vein with SR-FLIVO to stain apoptotic DCs in the PLN. After an additional 2 h, the PLNs were extracted, fixed and subjected to two-photon analysis. (**b**) LN optical sections showing the injected CMFDA-DCs, SR-FLIVO–stained DCs (SR-FLIVO) and merged images (CMFDA-DCs/SR-FLIVO). (**c**) The profile quantification tool provided by the LCS was used to obtain graphs with the profiles of intensities of SR-FLIVO along lineal regions of interest (ROI). MA of the SR-FLIVO intensity profiles of DC#1, DC#2 and DC#3 are shown. Maximum amplitude of the CMFDA-DC intensity profiles of DC#1, DC#2 and DC#3 are shown to identify the CMFDA-DCs injected. Animals were treated according to Animal Care Committee guidelines of the Centro de Investigaciones Biológicas.

Preparation of the leukocytes. Although the protocol presented below focuses on DCs, alternative protocols can be substituted for this section to extract and purify other types of leukocytes. For instance, T cells can be obtained from suspensions of different secondary LNs, including inguinal, cervical, axillary splenic and intestinal LNs. Higher number of cells can be used, and consequently more experiments can be performed, by using leukocyte lines. For example, it is possible to obtain a high number of DCs derived from bone marrow precursors in the presence of granulocyte macrophage colony-stimulating factor (GM-CSF)[39]. By using this protocol after purification of the DCs, we usually obtain 4–5 × 10^6 DCs per spleen (obtained from C57BL/6 mice). Considering that 1–2 × 10^6 labeled DCs per footpad should be injected, authors should assess, according to the experiment that they want to carry out, the number of animals that they require. The DCs obtained from the C57BL/6 mice are injected in the same strain of mice. Note that in this protocol we do not use collagenase. Although this may result in a lower yield of cells, because we were measuring apoptosis we wanted to avoid the potential effects that treatment with this enzyme could exert on the viability of the DCs.

Labeling with fluorescent intravital markers and injection of the leukocytes into mice. Before injecting the leukocytes into mice, they should be labeled with suitable fluorescent markers to allow their tracking in the PLN. In this regard, it is necessary to select the fluorescent tracker to be used by taking into consideration that its emission wavelengths need to be clearly distinguishable from those of the FLIVO, which will be subsequently used to

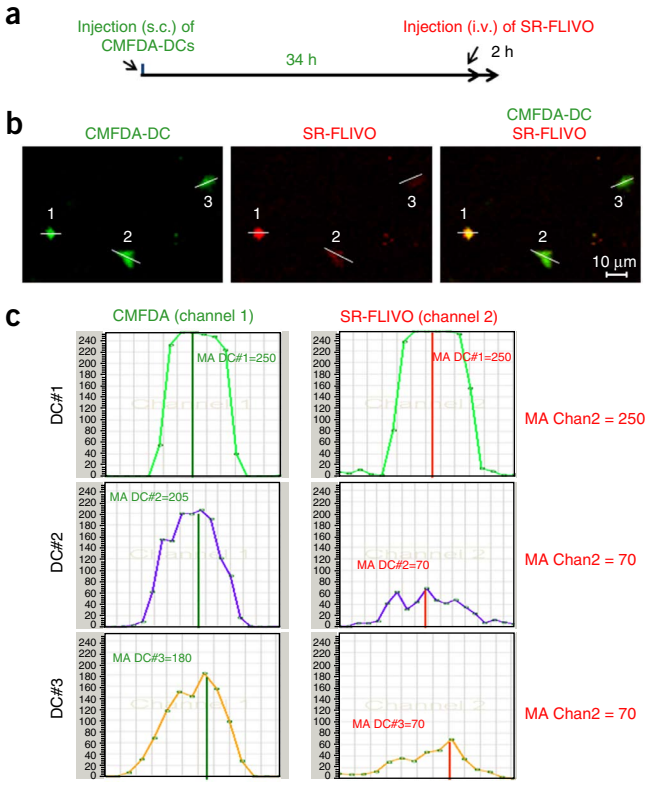

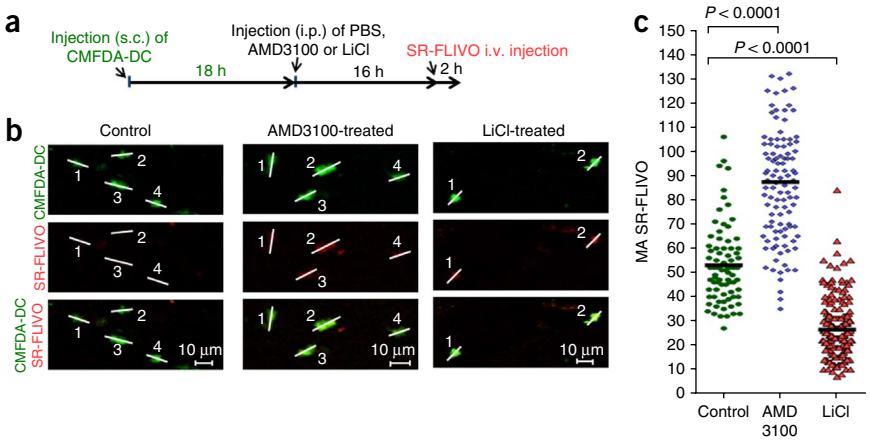

Figure 4 | Effects of pharmacological agents on the survival of DCs in the PLN. (**a**) Experimental protocol. A total of 2 × 10^6 CMFDA-labeled splenic DCs (CMFDA-DCs) were injected in the footpads of recipient mice. After 18 h, the animals were injected i.p. with 50 µmoles of NaCl (control), dissolved in 50 µl of distilled, deionized water, with AMD3100 (4 mg/kg) dissolved in 50 µl of PBS or with 50 µmol of LiCl dissolved in 50 µl of distilled, deionized water. After an additional 16 h, the animals were i.v. injected in the tail vein with SR-FLIVO to stain apoptotic CMFDA-DCs in the PLN. After an additional 2 h, the PLNs were extracted, fixed and subjected to two-photon analysis. (**b**) CMFDA-DC, SR-FLIVO and merged CMFDA-DC/SR-FLIVO staining of a two-photon confocal plane with three cells. (**c**) The stacks of optical images obtained from the PLNs were examined with the LCS, and the MA values of the SR-FLIVO channel were obtained. In the figure, it is represented the MA of the SR-FLIVO-channel measured in the CMFDA-DCs observed in the PLNs of untreated controls, AMD3100-treated or LiCl-treated animals. Data are presented as maximum intensity of SR-FLIVO for each individual DC in a LN. As the SR-FLIVO values of the DCs were similar in the NaCl-injected and PBS-injected animals (i.e., the controls of the LiCl- and the AMD3100-injected animals, respectively), for simplicity we use as controls the SR-FLIVO values of the DCs obtained from the PLNs of the PBS-injected animals. A representative experiment is shown; between 114 and 380 DCs were examined. Significance of differences between the two series of results was assessed with Student's *t* test. Animals were treated according to Animal Care Committee guidelines of the Centro de Investigaciones Biológicas.

analyze apoptotic DCs within the PLN. We normally label the DCs either with the green emitters CMFDA or with carboxyfluorescein succinimidyl ester (CFSE), which enables us to use the red emitter SR-FLIVO to detect the apoptotic CMFDA-DCs in the PLN. When the DCs are labeled with red or orange emitters, e.g., SNARF-1 or 5-(and-6)-(((4-chloromethyl)benzoyl)amino)tetramethylrhodamine (CMTMR), it is convenient to use green emitter FAM-FLIVO to detect the degree of apoptosis in the PLN.

In this protocol, it is also important to inject the cells in a site that ensures their efficient migration to the PLN. In the case of cells that access to the PLN through the lymphatics, e.g., DCs, the cells are injected in the posterior footpads from where they efficiently migrate to the PLN, through the afferent lymphatics, attracted by CCL19 and CCL21, which are the two ligands of the chemokine receptor CCR7 (see below). Thus, the DCs are usually co-injected in the footpad with lipopolysaccharide (LPS) (1 mg/ml), which induces rapid maturation of these cells and also expression of CCR7 (refs. 34,40,41). When the leukocytes under study access the PLN preferentially through the high endothelial veins (HEV), instead of the afferent lymphatics (this occurs, for example, with plasmacytoid DCs naive T cells and central memory T cells), these cells have to be injected i.v. to ensure that they enter the PLN efficiently. When using albino laboratory strains of mice, the tail vein can be easily located, and therefore it is a convenient i.v. route of injection; however, the identification of the tail vein can be problematic in other strains, such as the C57BL/6 mice, which have a dark skin. When using these animals, an alternative is to use the periorbital venous sinus route of injection, which is considered to be easier to perform and less stressful for the animals[42,43]. However, as this route of injection is not allowed in some jurisdictions, it is important to ensure that the specific protocol being used conforms to all relevant governmental and institutional regulations.

It is important to inject an appropriate number of cells. When performing s.c. injection of DCs in the footpads, it is necessary to administer 1–2 × 10^6 DCs to get a sufficient number of these cells in the PLN[40]. Previous studies indicate that injecting more than 2 × 10^6 DCs results in a decline in the number of cells that reach the PLN[40]. As mice footpads are relatively small, it is not convenient to inject more than 50 µl in each footpad. In our experience, independently of the volume injected, there is always some leakage of DCs, and we usually find labeled cells in the spleen (C.D.-M., L.R.-B. and J.L.R.-F., unpublished results). In the case of the lymphocytes, up to 5–10 × 10^6 cells can be injected into the tail vein (in a volume of 100–200 µl) or into the periorbital venous sinus (generally in a volume of 30–50 µl).

If animals are going to be subjected to treatments to analyze the survival of the leukocytes, it is important to ensure that the cells are positioned in the PLN before subjecting the animals to the treatment. This is important because leukocytes are migratory cells, and if the pharmacological agents used inhibit their motility they will not reach the PLN. For instance, we have observed that the pharmacological inhibition of the kinase GSK3-β blocks the motility of DCs (C.E.-D. and J.L.R.-F., unpublished results), implying that these cells should be treated with inhibitors of GSK3 only after they are positioned in the PLN[33]. Furthermore, it is important to consult the bibliography and/or to perform pilot experiments to ascertain the time that it takes for the leukocyte cell of interest to be positioned in the PLN.

In our experience, we detect DCs in the PLN from 6 h after injecting the cells in the footpads; however, it takes ~18 h to observe a substantial number of DCs in the PLN, implying that the treatment with pharmacological inhibitors, or other treatment that may affect the survival of the DCs, should start at least 18 h after injecting the cells. Furthermore, as we have observed that the injected splenic-derived DCs become largely apoptotic in the LNs after 48 h, 34–40 h from the initial injection of the DCs is the optimal time window to analyze the effect of a pharmacological agent on the apoptosis of the DCs in the PLN. We have observed that during this 6-h period (i.e., from 34 to 40 h) there is moderate but not complete apoptosis of the DCs in the PLN, which enables us to readily detect whether a treatment stimulates or inhibits apoptosis of the injected DCs. Therefore, we usually treat the animals with pharmacological inhibitors at 18 h, by injecting the drug i.p. and then allowing the drug to exert its effect for an additional 18–22 h.

In these experiments, we usually inject FLIVO i.v. at 34–38 h and allow this reagent to label the apoptotic DCs for another 1–2 h. When testing the effects of pharmacological inhibitors on DC survival *in vivo*, it is important to include positive controls. In this regard, we have used mice treated with AMD3100, an inhibitor of the chemokine receptor CXCR4 that induces apoptosis in DCs, as a positive control[32]; however, it is possible to use other agents, including inhibitors of the kinase Akt that are known to induce apoptosis of DCs[32–34]. It is also possible to inject mice with agents that induce survival of DCs to test the sensibility of the system. In this regard, we have shown that injection of LiCl and inhibitor IX, two pharmacological agents that inhibit the kinase GSK3-β reduce the apoptosis of DCs in the PLN[33]. In summary, by using the strategy indicated above, we ensure that when the animals are killed the pharmacological inhibitors have exerted their effects for 35–40 h and that we are able to detect their effects on the apoptosis of the DCs inside the PLN.

In the case of the T cells, we observe that after i.v. injection they rapidly migrate to the PLN and it is possible to observe numerous T cells in these areas 1 h after injection (results not shown and ref. 30). Furthermore, unlike DCs, which are known to terminate their life cycle at the LNs[31], T cells are continuously transiting from one LN to another under normal conditions. It has been also shown that, in the absence of inflammation, their time of permanence in the LNs can vary from a few hours to days[44,45]. When T cells recognize, through their TCRs, DCs that present cognate antigens, they can establish long-term interaction with DCs (up to 36 h) inside the LNs, after which the T cells become activated[30,44,45]. In summary, all these considerations, i.e., route of entrance to the LNs and thus the site of injection, the time of permanency of the leukocytes in the LNs and the life span of the leukocytes in the LNs have to be taken into account when planning experiments.

Intravenous injection of FLIVO. FLIVO works better when it is injected i.v. As indicated by the manufacturer, it does not work well when it is injected i.p. Use the tail-vein route of injection or, alternatively, the periorbital venous sinus route of injection, if it is allowed by governmental and institutional regulations. To ensure that excess FLIVO is washed out of cells, mice should be killed 1–2 h after FLIVO has been injected.

Visualization and scanning of the DCs in the LNs with two-photon optics. Before proceeding to an exhaustive scan of the whole PLN with a two-photon microscopy, it is advisable to confirm, via confocal microscopy, that the labeled DCs have reached these organs. Although a confocal microscope does not provide the large depth penetration of a two-photon microscope, it allows imaging deep enough to know whether the injected CFSE-DCs reached the LNs. This enables exhaustive scanning to be reserved only when labeled DCs are found in the PLN.

Detection and analysis of SR-FLIVO-stained DCs in the PLN. When studying the apoptosis of leukocytes in the PLN by using FLIVO staining, there are two possible options for how to analyze and present the data. One possibility is to measure the absolute percentage of apoptotic DCs under different conditions. Alternatively, it is possible to carry out a comparative analysis of the average SR-FLIVO staining in leukocytes from control and treated LNs. The evaluation of the absolute level of apoptotic DCs in the PLN is cumbersome and time consuming because it requires a fine calibration to determine the intensity at which single DCs are considered unambiguously apoptotic. Therefore, we usually carry out, and recommend, a comparative analysis because it is easier to perform, and it yields equally scientifically meaningful information. For this purpose, we obtain the average FLIVO staining of the DCs in the PLN (measured as maximum amplitude of each single SR-FLIVO-stained DCs) in treated and control animals (**Figs. 3** and **4**).

Limitations

A limitation of the protocol is that it requires the use of a multiphoton microscope; however, this is an instrument that is available in most research centers. The protocol that we describe is also limited in that instead of analyzing endogenous cells, leukocytes have to be isolated, labeled and injected in mice. However, most studies on the migration of leukocytes in the LNs and in other organs during recent years have resorted to this adoptive-transfer strategy with impressive results[46]. To circumvent the need to inject leukocytes, knock-in mice with leukocytes that express selectively fluorescent proteins can be used. For example, in the recently described *Zbtb46*$^{gfp/+}$ transgenic mice[47], the promoter of the transcription factor Zbtb46, which is selectively expressed in DCs, controls the expression of GFP, implying that in these mice only the DCs express GFP. In addition, the CD4-GFP transgenic mice[48] express the GFP protein selectively in CD4 T cells. Therefore, the *Zbtb46*$^{gfp/+}$ and CD4-GFP transgenic mice can be used to analyze the apoptosis of endogenous DCs and CD4 T cells, respectively, by using the red-emission version of FLIVO (SR-FLIVO).

An additional limitation is that as PLN macrophages may phagocytose some of the apoptotic cells, the number of apoptotic DCs detected with FLIVO may represent the net balance between the DCs that reach the PLN and the cells that could be phagocytosed. It is important also to be aware that although FLIVO reagents, owing to the presence of the pan-caspase inhibitor moieties, are able to detect with high specificity the activation of caspases and therefore apoptosis, they lack the specificity to discriminate between activation of particular caspases. Finally, the protocol has the limitation that it only detects caspase-dependent apoptosis, which is detected in cells by the pan-caspase inhibitor, and thus caspase-independent types of cell death are not detected.

MATERIALS

REAGENTS

- *Mice*. We extract DCs from the spleens of 2–3-month-old C57BL/6 mice and then inject the purified DCs into recipient mice of the same strain and age **! CAUTION** Experiments involving live rodents must conform to all relevant governmental and institutional regulations.
- PBS/EDTA solution (see Reagent Setup)
- BSA fraction V (Roche, cat. no. 735086)
- LPS from *Escherichia coli* 0111:B4 (Sigma, cat. no. L3024; see Reagent Setup)
- MACS buffer (see Reagent Setup)

- Anti-CD11c (N418), magnetic microbeads (Miltenyi Biotec, cat. no. 130-052-001). This solution can be stored for several weeks at 4 °C
- CMFDA (Molecular Probes, cat. no. C7025; see Reagent Setup)
- SNARF-1 (seminaphtorhodafluor1) (Molecular Probes, cat. no. C1272; see Reagent Setup)
- Paraformaldehyde solution (Santa Cruz Biotechnology, cat. no. sc-281692; see Reagent Setup). ! CAUTION This compound is toxic; handle it as a suspected carcinogen. Dispose of this waste according to appropriate guidelines.
- Complete medium (see Reagent Setup)
- Green carboxyfluorescein (FAM)-FLIVO (FAM, λ_{abs} 492 nm; λ_{em} 520 nm), (cat. no. 981) or red sulforhodamine B (SR)-FLIVO (SR, λ_{abs} 565 nm; λ_{em} >600 nm) (cat. no. 983) (ImmunoChemistry Technologies)
- Fluorescence antifading reagent (Invitrogen. Molecular Probes, cat. no. P36930). This reagent can be stored at −20 °C for several months
- DMSO
- RPMI
- FCS
- Sterile water

EQUIPMENT

- Tweezers
- Scissors
- U-100 insulin micro-fine syringes, 0.5 ml (BD, cat. no. 320927)
- Cell strainers (BD Falcon, cat. no. 352360)
- Refrigerated centrifuge
- LS separation columns (Miltenyi Biotec, cat. no. 130-042-401)
- QuadroMACS separator (including QuadroMACS separation unit (cat. no. 130-090-976) and 1 MACS MultiStand (Miltenyi Biotec, cat. no. 130-042-303)
- Coverslips, 22 × 22 mm (Menzel-Gläser, cat. no. BB022022A1)
- Cell incubator
- Leica confocal inverted microscope (TCS-SP2 AOBS spectral system) equipped with a wide-band mode–locked Ti:sapphire two-photon excitation laser (Mai Tai, Spectra-Physics)
- Two-sided tape (e.g., Scotch tape)

REAGENT SETUP

FLIVO reagent Reconstitute the FLIVO reagent according to the manufacturer's instructions. Briefly, dissolve a vial including 131 µg of lyophilized FLIVO in 50 µl of DMSO to obtain 2.6 mg/ml (wt/vol) FLIVO, which forms a 12× FLIVO stock solution. Divide the stock to small aliquots and store it, protected from the light, at −20 °C or below. Avoid repeated freeze/thaw cycles. This reagent is stable for at least 1 year. On the day of injection, dissolve 1 volume of the 12× FLIVO stock solution in sterile PBS to yield a 1× (vol/vol) FLIVO solution (corresponding to ~0.26 mg/ml). Prepare sufficient 1× FLIVO solution for the injection experiment, and discard the remaining solution because the diluted reagent gets hydrolyzed and loses its activity after 1 d.

PBS/EDTA solution PBS/EDTA solution is 5 mM EDTA in PBS. This solution can be stored for several weeks at 4 °C.

LPS from *E. coli* Prepare a 2-mg/ml stock solution in sterile water. Divide it into small aliquots and store it at −20 °C . Avoid repeated freeze/thaw cycles. After thawing, this solution can be stored for several weeks at 4 °C.

MACS buffer Combine 0.5% (wt/vol) BSA and 2 mM EDTA in PBS. This solution can be stored for several weeks at 4 °C.

CMFDA Prepare a 5 mM stock in DMSO. Divide the stock into aliquots and store it at −20 °C, protected from light, for at least 6 months. Avoid repeated freeze/thaw cycles.

SNARF1 Prepare a 5 mM stock in DMSO. Divide the stock into aliquots and store it at −20 °C, protected from light, for several months. Avoid repeated freeze/thaw cycles.

Paraformaldehyde solution Paraformaldehyde solution is 4% (wt/vol) paraformaldehyde in PBS. Divide the solution into aliquots and store it at −20 °C. Under these conditions, this reagent can be stored for several months. Once it is thawed, paraformaldehyde solution can be stored for 2–3 d at 4 °C. ! CAUTION This compound is toxic; handle it as a suspected carcinogen. Dispose of this waste according to appropriate guidelines.

Complete medium Complete medium is 10% (vol/vol) FCS in RPMI. This medium can be stored for several weeks at 4 °C.

EQUIPMENT SETUP

PLN mount We mount the PLN in a custom-made setting. Make an ~0.5-mm-thick layer composed of two-sided tape (Scotch tape). Punch a small circular hole with a diameter large enough to fit the two halves of the PLN in the center of the latter. Stick the 0.5-mm-thick two-sided tape layer onto a coverslip.

PROCEDURE

Preparation of splenic DCs ● TIMING 1.5 h

1| Kill C57BL/6 mice by cervical dislocation.

! CAUTION All experiments involving animals must be carried out according to institutional and national guidelines.

2| Extract the spleens. To do this, first sterilize the skin of the mouse with ethanol. Next, use tweezers and scissors to cut through the skin below the rib cage on the left side of the abdomen. Identify the spleen and extract it by using scissors and tweezers. Place the spleen in a Petri dish containing PBS, and trim away the fatty tissue carefully.

3| Use tweezers to hold the spleen. Inject the PBS/EDTA solution into this organ via a syringe until the color of the organ becomes clearer (usually it is necessary to inject 1.5–2 ml of PBS/EDTA solution). This treatment facilitates the subsequent disaggregation of the spleen. Collect the fluid that exits the spleens. This fluid will be mixed with the cell suspension obtained from Step 4.

4| Place the spleen on a cell strainer and use the plunger of a syringe to disaggregate the spleens. Simultaneously pour 5–6 ml of PBS/EDTA solution over the spleen.

5| Collect the cellular suspension with splenic cells that has gone through the strainer and mix it with the fluid obtained from Step 3. Count the cells and centrifuge them at 290*g* for 5 min at 4 °C.

6| Resuspend the cellular pellet in cold MACS buffer, and add the required volume of anti-CD11c Miltenyi magnetic microbeads (20 µl/10^8 DCs).

7| Incubate the cells with beads for 20 min at 4 °C.

8| Add cold MACS buffer up to a volume of 10 ml.

9| Centrifuge the cells at 290*g* for 5 min at room temperature (21–24 °C). Suspend the cells in 3 ml of cold MACS buffer.

10| Insert the Miltenyi LS column into a magnetic MACS separator. Equilibrate the column by passing 3 ml of MACS buffer. Apply the 3-ml cell suspension labeled with anti-CD11c Miltenyi magnetic microbeads from Step 9 onto the equilibrated LS column.
? TROUBLESHOOTING

11| Collect the unlabeled cells that pass through the columns. Wash the LS column three times with 3 ml of MACS buffer. This is the unlabeled cell fraction that should be discarded.

12| Remove the column from the separator and place it in a new collection tube.

13| Pipette 5 ml of MACS buffer onto the LS column and flush out the fraction with the magnetically labeled cells by applying a plunger. The cell fraction obtained is the DC fraction. Count the viable cells obtained in the DC fraction by performing a trypan blue staining.

Labeling with fluorescent intravital markers and injection of DCs in mice ● TIMING 57 min
▲ **CRITICAL** Steps 14–20 describe the labeling of the DCs with the green emitter CMFDA. If this is done, mice should be injected with the red emitter SR-FLIVO. Please note that the protocol also works well when the DCs are labeled with SNARF-1, or other red emitter trackers; however, in this case, mice should be injected with the green emitter FAM-FLIVO to detect the apoptotic DCs.
14| Centrifuge DCs (from Step 13) at 290*g* for 5 min and suspend them in 0.1% (wt/vol) BSA in PBS to obtain a final concentration of 10^7 DCs per ml.

15| Add CMFDA to the DC suspension to obtain a final concentration of 5 μM CMFDA (CMFDA stock should be used at a 1:1,000 dilution).

16| Incubate the cells for 40 min at 37 °C in the incubator.

17| Add two volumes of cold complete medium to quench staining and incubate the cells for 5 min on ice.

18| Centrifuge the cells for 5 min at 290*g* at 4 °C. Discard the supernatant and resuspend the pellet with RPMI. Centrifuge the cells again for 5 min at 290*g* at 4 °C and resuspend the pellet in a small volume of RPMI. Count viable DCs by using trypan blue staining, and then dilute the cells in RPMI at a concentration of 20–100 $\times 10^6$ DCs per ml, depending on the number and volume of DCs to be injected in the next step.
▲ **CRITICAL STEP** In this step, it is important to perform a trypan blue staining to check for the number and viability of the DCs obtained.
? TROUBLESHOOTING

19| Inject 20–50 μl of the suspension of CMFDA-DCs (1–2 × 10^6 DCs) in RPMI, including LPS (1 μg/ml), in each of the two posterior footpads of the mouse.
▲ **CRITICAL STEP** It is important to inject 1–2 × 10^6 DCs to ensure a sufficient number of DCs in the PLN. Avoid air bubbles before injecting the animals.
▲ **CRITICAL STEP** Ensure that the DCs are injected along with LPS to induce the expression of the chemokine receptor CCR7, which will drive the DCs to the PLN.

20| Return the mice to the cages. Ensure that the animals have enough food and, especially, water.
▲ **CRITICAL STEP** During this step, the injected DCs will migrate through the afferent lymphatic vessels to the PLN.
As indicated above, after 18 h, most injected DCs will have entered in the PLN. In the next steps, we explain the general procedure that can be used to detect apoptotic DCs in the PLN by using the FLIVO method. Authors should adapt their protocol according to the needs of their experiment (see above the section Experimental Design). See also **Figures 3** and **4** and ANTICIPATED RESULTS for examples on the type of experiments that can be performed.

Intravenous injection of FLIVO ● TIMING ~1 min per mouse

▲ **CRITICAL** It is important to establish, by performing pilot experiments, the correct time at which to proceed to injection of FLIVO. Injection of FLIVO should only be performed at a time point at which most labeled DCs (or other leukocyte types under study) are in the PLN.

21| Use a U-100 insulin syringe to i.v. inject each animal with 8 µg of FLIVO, i.e., 30.76 µl from the 1× FLIVO solution (0.26 mg/ml). (Inject red SR-FLIVO or green FAM-FLIVO if CMFDA- or SNARF-1–labeled DCs, respectively, were previously injected.)

▲ **CRITICAL STEP** Avoid forming bubbles in the syringe to prevent injecting air into the animals.

▲ **CRITICAL STEP** We have injected 6–8 µg of different batches of FLIVO (SR-FLIVO or FAM-FLIVO) to C57BL/6 mice with optimal results. Perform pilot experiments by using pharmacological agents that induce apoptosis of the injected DCs in the PLN (e.g., treatment with AMD3100 induces the apoptosis of DCs in the PLN; **Fig. 4**), or other leukocytes studied, to assess the optimal amount of FLIVO that should be injected.

? TROUBLESHOOTING

Extraction and preparation of the PLN ● TIMING 15 min per LN

22| Kill the animals by cervical dislocation.

23| To isolate the PLN, first sterilize the skin of the mouse with ethanol. Make an incision with scissors at the knee to expose the popliteal fossa where the PLN locate. Use tweezers to extract the PLN and place it in a Petri dish containing PBS. Under a magnification glass (10×), quickly trim away carefully the larger pieces of fatty tissue.

! CAUTION The PLN is very small (1–1.5 mm) and its identification can be difficult. It is necessary to get advice from a trained operator when the extraction is performed for the first time.

24| Fix the PLN with paraformaldehyde solution for at least 60 min at 4 °C (or at least 30 min at room temperature) and then immerse them in PBS. During the fixation, protect the PLN from light.

▲ **CRITICAL STEP** After fixation, ensure that all of the fat is trimmed to prevent interference with the multiphoton analysis.

▲ **CRITICAL STEP** Allow sufficient fixation time with paraformaldehyde solution to ensure that the PLN is not too soft.

? TROUBLESHOOTING

■ **PAUSE POINT** Fixed PLN can be suspended in PBS and kept at 4 °C, protected from the light, and analyzed at a later date. The samples can be kept under these conditions for 1 week.

25| By using a sharp razor blade and a 10× magnification glass, transversally cut the PLN along the longest axis of the organ into two halves. Slice the PLN as cleanly as possible for easier observation.

26| Mount the two halves of the PLN into the small circular hole in the tape layer of the PLN mount. Immerse the two pieces of PLN in fluorescence mounting medium. Finally, taking care to avoid air bubbles, seal the sandwich that includes the LNs with a second glass coverslip.

? TROUBLESHOOTING

■ **PAUSE POINT** The mounted PLN can be kept at 4 °C and analyzed at a later date. The samples can be kept under these conditions for up to 2 months.

Visualization and scanning of the CMFDA-DCs in the PLN with two-photon optics ● TIMING 20–30 min per stack

27| It is advisable to check with a confocal microscope that the PLN contains CMFDA-labeled DCs. If this is the case, proceed to analyze these organs under a two-photon microscope by using a 20× magnification oil-immersion objective (1.20 numerical aperture). We use a Leica confocal inverted microscope. Use the appropriate wavelength and spectral detection. Optimal two-photon excitation of the three fluorochromes is achieved at 856-nm wavelength, and spectral detection is at 510–540 nm (for CMFDA and FAM- FLIVO) and 560–600 nm (for SNARF-1 and SR- FLIVO). Configure the detector slits to minimize cross talk between channels. Scan the LNs thoroughly from both sides of the coverslip up to a depth of 200–300 µm with a *z* spacing of 2 µm and save as optical section stacks.

? TROUBLESHOOTING

■ **PAUSE POINT** The images obtained can be analyzed at a later date.

Tracking and analysis of SR-FLIVO–labeled CMFDA-DCs in the PLN ● TIMING 2–3 h per LN

28| Use the Leica confocal software (LCS) to examine the optical section stacks obtained in Step 27. Quantify the amount of SR-FLIVO incorporated by the CMFDA-DCs (or the FAM-FLIVO incorporated by SNARF-1–labeled DCs if the DCs were labeled before with this tracker). Try to analyze more than 100 DCs and ideally examine 200–300 DCs. Use the LCS profile quantification tool to manually trace a lineal region of interest in each cell that is subjected to analysis. Subsequently, obtain graphs displaying the intensity profiles of CMFDA/SR- FLIVO (or SNARF-1/FAM-FLIVO pair intensity). **Figure 3** shows an example of how this analysis is carried out.

▲ CRITICAL STEP It is important to check for leakage between the SR-FLIVO and CMFDA channels (or the FAM-FLIVO and the SNARF-1 channels when this pair is used).

29| Measure the value of maximum amplitude of the SR-FLIVO. This value is measured automatically by the LCS, and it provides an index of the incorporation of SR-FLIVO and consequently yields information on the degree of apoptosis of the DCs analyzed. When we inject the mice with the amount of SR-FLIVO recommended in this protocol, we rarely observe FLIVO channel background signal (i.e., SR-FLIVO labeling in areas where there are no CMFDA-DCs). However, if SR-FLIVO channel background is observed, it is necessary to subtract this value from the maximum amplitude of the SR-FLIVO value of each CMFDA-DC.
▲ CRITICAL STEP When you are comparing the survival of DCs in the PLNs of control and treated animals, it is important to analyze the maximum amplitude of the SR-FLIVO in a large number of leukocytes. Analyze three or four mice for each condition and scan more than 100 DCs (ideally 200–300 DCs per PLN). Statistical differences in SR-FLIVO maximum amplitudes when comparing control and treated animals are analyzed by Student's *t* test.

? TROUBLESHOOTING

Step 10: after applying the cell suspension, the column becomes blocked
Clumps present in the cell suspension applied could be responsible for blocking the column. If clumps are observed, remove them from the column. Clumps can also be removed before loading the column, by passing the cell suspension through a sterile 30-μm nylon mesh.

Try not to saturate the column. Do not use more than four spleens to obtain the cell suspensions that will be passed through the column. Alternatively, use a larger column.

If the column is blocked in the absence of clumps, apply the plunger supplied with the column and push the cell suspension gently through the column. If the cell suspension is still not able to pass through the column, remove the column from the magnetic separator, and use the plunger to flush out the cell suspension from the column. Subsequently, use the cell suspension in a new column.

Step 18: no leukocytes are found in this step
This can happen for several reasons. Washes after centrifugation may result in loss of leukocytes. Use conical-bottom tubes instead of round-bottom tubes to improve the recovery after the centrifugation. In Step 13, check that the columns used for the experiment work properly. For this purpose, confirm that the DC fraction flushed out from the column contains cells by examining the samples obtained under a microscope.

Step 21: i.v. injection in the mouse tail vein becomes problematic
This is a problem that can be experienced in dark-skinned C57BL/6 mice. To avoid this problem, use a mouse restrainer when injecting in the tail vein. If it is absolutely necessary, use the periorbital venous sinus route of injection. Ensure that this route of injection conforms to all relevant governmental and institutional regulations.

Step 24: LNs are too soft
Soft LNs indicate that the fixation of the PLN was not performed properly. To solve this problem, prepare a fresh fixation solution or increase the fixation time.

Step 26: air bubbles form when mounting on the coverslips
Air bubbles prevent the immersion of the PLN in the mounting medium and therefore should be avoided. To prevent this problem, push the coverslip gently with tweezers to push air bubbles out; otherwise, they will interfere with observations by two-photon microscopy.

Step 27: no labeled DCs are found in the PLN
To prevent this problem, ensure that a correct number of DCs are injected in Step 19. DCs are usually found in the T cell region; therefore, ensure that this region is analyzed by two-photon microscopy. If you are working with leukocytes different from DCs, it is important to perform pilot experiments to assess the time that it takes the leukocytes to migrate and get positioned in the PLN.

This problem can also occur when you are performing experiments in which the animals are treated with pharmacological compounds. Rule out the possibility that the pharmacological agents could block the migration of the leukocytes to the PLN by treating the mice with the pharmacological agents only when the leukocytes are already positioned in the PLN.

Step 27: high nonspecific staining under two-photon microscopy
Injection of an excessive amount of FLIVO can result in high nonspecific staining. In DCs it is important to inject 6–8 μg of FLIVO, but not higher amounts. High nonspecific staining can be also due to an inappropriate washout of FLIVO. To prevent this from happening, after i.v. injection of this reagent it is convenient to wait for 1–2 h before killing the animals.

Step 27: the leukocytes are not stained with FLIVO in the PLN
If apoptosis is expected in the leukocytes under study and these cells do not take the FLIVO reagent, check that the injection was administered correctly. After i.v. injection of FLIVO, at least 1 h is necessary to allow the reagent to stain the cells. To ensure that the FLIVO reagent is not spoiled, perform positive controls in *in vitro* experiments by using leukocytes treated with a reagent known to induce apoptosis.

● **TIMING**
Steps 1–13, preparation of splenic DCs: ~1.5 h (spleen extraction: 30 min; disaggregation of spleen: 30 min; magnetic labeling and separation: 30 min)
Steps 14–20, labeling with fluorescent intravital markers and injection of DCs in mice: 57 min (labeling: 55 min; s.c. injection of DC in the two posterior footpads: 1 min per footpad)
Step 21, intravenous injection of FLIVO to stain apoptotic DCs: 1 min per mouse
Steps 22–26, extraction and preparation of the PLN: 15 min per PLN
Step 27, visualization of DCs in the PLN with two-photon optics: 20–30 min per stack (each stack includes 100–150 confocal planes)
Steps 28 and 29, tracking of the CMFDA-DCs and detection and analysis of SR-FLIVO-labeled DCs: 2–3 h per LN

ANTICIPATED RESULTS

We have largely used the FLICA-based technique described in this report to analyze the apoptosis of DCs in the PLN[31–33]. **Figure 3** shows the results that were obtained in a representative experiment. As indicated in the experimental protocol (**Fig. 3a**), SR-FLIVO was i.v. administered 34 h after the s.c. injection of the CMFDA-DCs in the posterior footpads of the mice. After 2 h, to allow SR-FLIVO to label the apoptotic CMFDA-DCs in the PLN, the mice were killed and the PLNs were extracted, fixed and mounted for subsequent analysis of the apoptosis of the CMFDA-DCs in the PLN by two-photon microscopy. **Figure 3b** shows a small section that includes three CMFDA-DCs, which were observed in two-photon confocal microscopic analysis of the PLN. The lines traced on the CMFDA-DCs depict the lineal regions of interest that were analyzed by using the LCS. As shown in **Figure 3c**, the analysis of the profiles of CMFDA channel of these cells confirmed that they were CMFDA-labeled DCs. The maximum amplitude (MA) values obtained from the analysis of the profiles of the SR-FLIVO-stained CMFDA-DCs showed that out of the three CMFDA-DCs observed only DC#1 displays a high intensity of SR-FLIVO, indicating that this cell is more apoptotic. A representation of the individual MA, obtained from all the SR-FLIVO profiles of a population of CMFDA-DCs in the PLN, provides an indication of the relative apoptosis in this population of DCs under the conditions studied (**Fig. 4**).

As discussed in the INTRODUCTION, this protocol is particularly useful for comparing the effects of different pharmacologic agents on the survival of DCs. **Figure 4** shows the results of one of these experiments. CMFDA-DCs were injected in the posterior footpads of the C57BL/6 mice, and after 18 h the animals were injected i.p. either with the CXCR4 inhibitor AMD3100 or with the GSK3-β inhibitor LiCl for an additional 16 h. Subsequently, the animals were injected with SR-FLIVO for 2 h to stain all apoptotic CMFDA-DCs. In our experience, the window from 34–40 h is a convenient time to inject SR-FLIVO and to analyze the apoptosis of DCs labeled with fluorescent trackers in the PLN, because prior experiments indicate that at 34–40 h there is a moderate degree of apoptosis in the control, untreated CMFDA-DCs positioned in the PLN. This information allows the analysis of whether the pharmacological agents used are able to increase or reduce the apoptosis of the DCs in the PLN compared with untreated CMFDA-DCs. After 2 h (i.e., 36–42 h from the onset of the experiment), the animals are killed and the PLN can be explanted and analyzed by two-photon microscopy. After staining with SR-FLIVO as indicated in the protocol, an analysis of the average MA profiles of ~300 SR-FLIVO–stained DCs in the control, the AMD3100-treated and LiCl-treated CMFDA-DCs indicated that CXCR4 induces survival and GSK3-β induces apoptosis in DCs in the PLN. We normally compare the average SR-FLIVO staining among the treatments. This strategy allows the determination of whether a receptor or a signaling molecule is proapoptotic or antiapoptotic.

ACKNOWLEDGMENTS We acknowledge the criticism of O. Criado and J. Torres Bacete. This study is supported by grants awarded by Ministerio de Educación y Ciencia (SAF2005-00801), Ministerio de Economía y Competitividad (SAF2011-23890), RIER (RETICS Program/Instituto de Salud Carlos III) (RD08/0075) and Consejería de Educación y Empleo from Comunidad de Madrid (Raphyme, S2010/BMD-2350). L.G.-C. was supported by a Formación de Profesorado Universitario (FPU) scholarship (Ministerio de Educación y Ciencia). P.L.-C. was supported by a Formación de Personal Investigador (FPI) scholarship (Ministerio de Economía y Competitividad). C.E.-D. was the recipient of an I3P fellowship (Consejo Superior de Investigaciones Científicas-Fondo Social Europeo). C.D.-M. was partially supported by an FPI fellowship conferred by the Ministerio de Educación y Ciencia (Spain) and by a contract associated with grant no. RD08/0075 (RIER). L.R.-B. was partially supported by a scholarship associated with grant no. PI021058.

AUTHOR CONTRIBUTIONS L.G.-C., C.D.-M., P.L.-C. and C.E.-D. performed the experiments. L.G.-C., C.D.-M., P.L.-C., C.E.-D., L.M.A.-C., L.R.-B. and J.L.R.-F. analyzed the data. J.L.R.-F. wrote the manuscript with input from all authors.

COMPETING FINANCIAL INTERESTS The authors declare no competing financial interests.

1. Taylor, R.C., Cullen, S.P. & Martin, S.J. Apoptosis: controlled demolition at the cellular level. *Nat. Rev. Mol. Cell Biol.* **9**, 231–241 (2008).

2. Hildeman, D., Jorgensen, T., Kappler, J. & Marrack, P. Apoptosis and the homeostatic control of immune responses. *Curr. Opin. Immunol.* **19**, 516–521 (2007).
3. Maniati, E., Potter, P., Rogers, N.J. & Morley, B.J. Control of apoptosis in autoimmunity. *J. Pathol.* **214**, 190–198 (2008).
4. Ueno, H. *et al.* Dendritic cell subsets in health and disease. *Immunol. Rev.* **219**, 118–142 (2007).
5. Kushwah, R. & Hu, J. Dendritic cell apoptosis: regulation of tolerance versus immunity. *J. Immunol.* **185**, 795–802 (2010).
6. Chen, M., Huang, L. & Wang, J. Deficiency of Bim in dendritic cells contributes to overactivation of lymphocytes and autoimmunity. *Blood* **109**, 4360–4367 (2007).
7. Hou, W.S. & Van Parijs, L. A Bcl-2–dependent molecular timer regulates the lifespan and immunogenicity of dendritic cells. *Nat. Immunol.* **5**, 583–589 (2004).
8. Ohnmacht, C. *et al.* Constitutive ablation of dendritic cells breaks self-tolerance of CD4 T cells and results in spontaneous fatal autoimmunity. *J. Exp. Med.* **206**, 549–559 (2009).
9. Nopora, A. & Brocker, T. Bcl-2 controls dendritic cell longevity *in vivo*. *J. Immunol.* **169**, 3006–3014 (2002).
10. Dong, H.P., Kleinberg, L., Davidson, B. & Risberg, B. Methods for simultaneous measurement of apoptosis and cell surface phenotype of epithelial cells in effusions by flow cytometry. *Nat. Protoc.* **3**, 955–964 (2008).
11. Troiano, L. *et al.* Multiparametric analysis of cells with different mitochondrial membrane potential during apoptosis by polychromatic flow cytometry. *Nat. Protoc.* **2**, 2719–2727 (2007).
12. Logue, S.E., Elgendy, M. & Martin, S.J. Expression, purification and use of recombinant annexin V for the detection of apoptotic cells. *Nat. Protoc.* **4**, 1383–1395 (2009).
13. Riccardi, C. & Nicoletti, I. Analysis of apoptosis by propidium iodide staining and flow cytometry. *Nat. Protoc.* **1**, 1458–1461 (2006).
14. Loo, D.T. *In situ* detection of apoptosis by the TUNEL assay: an overview of techniques. *Methods Mol. Biol.* **682**, 3–13 (2011).
15. Jerome, K.R., Vallan, C. & Jaggi, R. The TUNEL assay in the diagnosis of graft-versus-host disease: caveats for interpretation. *Pathology* **32**, 186–190 (2000).
16. Ansari, B., Coates, P.J., Greenstein, B.D. & Hall, P.A. *In situ* end-labelling detects DNA strand breaks in apoptosis and other physiological and pathological states. *J. Pathol.* **170**, 1–8 (1993).
17. Kanoh, M. *et al.* Significance of myocytes with positive DNA *in situ* nick end-labeling (TUNEL) in hearts with dilated cardiomyopathy: not apoptosis but DNA repair. *Circulation* **99**, 2757–2764 (1999).
18. Sloop, G.D. *et al.* Histologic sectioning produces TUNEL reactivity. A potential cause of false-positive staining. *Arch. Pathol. Lab. Med.* **123**, 529–532 (1999).
19. Kockx, M.M., Muhring, J., Knaapen, M.W. & de Meyer, G.R. RNA synthesis and splicing interferes with DNA *in situ* end labeling techniques used to detect apoptosis. *Am. J. Pathol.* **152**, 885–888 (1998).
20. Kelly, K.J., Sandoval, R.M., Dunn, K.W., Molitoris, B.A. & Dagher, P.C. A novel method to determine specificity and sensitivity of the TUNEL reaction in the quantitation of apoptosis. *Am. J. Physiol. Cell Physiol.* **284**, C1309–C1318 (2003).
21. Mannering, S.I., Zhong, J. & Cheers, C. T-cell activation, proliferation and apoptosis in primary *Listeria monocytogenes* infection. *Immunology* **106**, 87–95 (2002).
22. Bahl, K., Huebner, A., Davis, R.J. & Welsh, R.M. Analysis of apoptosis of memory T cells and dendritic cells during the early stages of viral infection or exposure to toll-like receptor agonists. *J. Virol.* **84**, 4866–4877 (2010).
23. Dunn, K.W. *et al.* Functional studies of the kidney of living animals using multicolor two-photon microscopy. *Am. J. Physiol. Cell Physiol.* **283**, C905–C916 (2002).
24. Shi, Y. Mechanisms of caspase activation and inhibition during apoptosis. *Mol. Cell* **9**, 459–470 (2002).
25. Bedner, E., Smolewski, P., Amstad, P. & Darzynkiewicz, Z. Activation of caspases measured *in situ* by binding of fluorochrome-labeled inhibitors of caspases (FLICA): correlation with DNA fragmentation. *Exp. Cell Res.* **259**, 308–313 (2000).
26. Darzynkiewicz, Z., Bedner, E., Smolewski, P., Lee, B.W. & Johnson, G.L. Detection of caspases activation *in situ* by fluorochrome-labeled inhibitors of caspases (FLICA). *Methods Mol. Biol.* **203**, 289–299 (2002).
27. Grabarek, J., Amstad, P. & Darzynkiewicz, Z. Use of fluorescently labeled caspase inhibitors as affinity labels to detect activated caspases. *Human Cell* **15**, 1–12 (2002).
28. Pozarowski, P. *et al.* Interactions of fluorochrome-labeled caspase inhibitors with apoptotic cells: a caution in data interpretation. *Cytometry A* **55**, 50–60 (2003).
29. Garcia-Calvo, M. *et al.* Inhibition of human caspases by peptide-based and macromolecular inhibitors. *J. Biol. Chem.* **273**, 32608–32613 (1998).
30. Mempel, T.R., Henrickson, S.E. & von Andrian, U.H. T-cell priming by dendritic cells in lymph nodes occurs in three distinct phases. *Nature* **427**, 154–159 (2004).
31. Riol-Blanco, L. *et al.* Immunological synapse formation inhibits, via NF-κB and FOXO1, the apoptosis of dendritic cells. *Nat. Immunol.* **10**, 753–760 (2009).
32. Delgado-Martin, C., Escribano, C., Pablos, J.L., Riol-Blanco, L. & Rodriguez-Fernandez, J.L. Chemokine CXCL12 uses CXCR4 and a signaling core formed by bifunctional Akt, extracellular signal-regulated kinase (ERK)1/2, and mammalian target of rapamycin complex 1 (mTORC1) proteins to control chemotaxis and survival simultaneously in mature dendritic cells. *J. Biol. Chem.* **286**, 37222–37236 (2011).
33. Escribano, C., Delgado-Martin, C. & Rodriguez-Fernandez, J.L. CCR7-dependent stimulation of survival in dendritic cells involves inhibition of GSK3β. *J. Immunol.* **183**, 6282–6295 (2009).
34. Sanchez-Sanchez, N., Riol-Blanco, L. & Rodriguez-Fernandez, J.L. The multiple personalities of the chemokine receptor CCR7 in dendritic cells. *J. Immunol.* **176**, 5153–5159 (2006).
35. Briley-Saebo, K.C. *et al.* Longitudinal tracking of human dendritic cells in murine models using magnetic resonance imaging. *Magn. Reson. Med.* **64**, 1510–1519 (2010).
36. Rey-Gallardo, A., Delgado-Martin, C., Gerardy-Schahn, R., Rodriguez-Fernandez, J.L. & Vega, M.A. Polysialic acid is required for neuropilin-2a/b-mediated control of CCL21-driven chemotaxis of mature dendritic cells and for their migration *in vivo*. *Glycobiology* **21**, 655–662 (2011).
37. Ju, T.C. *et al.* Nuclear translocation of AMPK-1 potentiates striatal neurodegeneration in Huntington's disease. *J. Cell Biol.* **194**, 209–227 (2011).
38. Delgado-Martin, C., Riol-Blanco, L., Alonso-C., L.M. & Rodriguez-Fernandez, J.L. A protocol to detect apoptotic dendritic cells in murine lymph nodes using multiphoton microscopy. *Protoc. Exchange* doi:10.1038/nprot.2009.133 (2009).
39. Zanoni, I., Ostuni, R. & Granucci, F. Generation of mouse bone marrow-derived dendritic cells (BM-DCs). *Protoc. Exchange* doi:10.1038/nprot.2009.137 (2009).
40. Martin-Fontecha, A. *et al.* Regulation of dendritic cell migration to the draining lymph node: impact on T lymphocyte traffic and priming. *J. Exp. Med.* **198**, 615–621 (2003).
41. Riol-Blanco, L. *et al.* The chemokine receptor CCR7 activates in dendritic cells two signaling modules that independently regulate chemotaxis and migratory speed. *J. Immunol.* **174**, 4070–4080 (2005).
42. Steel, C.D., Stephens, A.L., Hahto, S.M., Singletary, S.J. & Ciavarra, R.P. Comparison of the lateral tail vein and the retro-orbital venous sinus as routes of intravenous drug delivery in transgenic mouse models. *Lab. Anim.* **37**, 26–32 (2008).
43. Yardeni, T., Eckhaus, M., Morris, H.D., Huizing, M. & Hoogstraten-Miller, S. Retro-orbital injection in mice. *Lab. Anim.* **40**, 155–160 (2011).
44. Willard-Mack, C.L. Normal structure, function, and histology of lymph nodes. *Toxicol. Pathol.* **34**, 409–424 (2006).
45. Bajenoff, M. *et al.* Highways, byways and breadcrumbs: directing lymphocyte traffic in the lymph node. *Trends Immunol.* **28**, 346–352 (2007).
46. Germain, R.N., Robey, E.A. & Cahalan, M.D. A decade of imaging cellular motility and interaction dynamics in the immune system. *Science* **336**, 1676–1681 (2012).
47. Satpathy, A.T. *et al. Zbtb46* expression distinguishes classical dendritic cells and their committed progenitors from other immune lineages. *J. Exp. Med.* **209**, 1135–1152 (2012).
48. Hofmann, U. *et al.* Activation of $CD4^+$ T lymphocytes improves wound healing and survival after experimental myocardial infarction in mice. *Circulation* **125**, 1652–1663 (2012).

THE JOURNAL OF BIOLOGICAL CHEMISTRY VOL. 290, NO. 2, pp. 827–840, January 9, 2015

A Novel MEK-ERK-AMPK Signaling Axis Controls Chemokine Receptor CCR7-dependent Survival in Human Mature Dendritic Cells*

Received for publication, July 14, 2014, and in revised form, October 31, 2014 Published, JBC Papers in Press, November 25, 2014, DOI 10.1074/jbc.M114.596551

Pilar López-Cotarelo[‡1], Cristina Escribano-Díaz[‡2], Ivan Luis González-Bethencourt[‡], Carolina Gómez-Moreira[‡3], María Laura Deguiz[‡], Jesús Torres-Bacete[‡4], Laura Gómez-Cabañas[‡5], Jaime Fernández-Barrera[‡6], Cristina Delgado-Martín[‡7], Mario Mellado[§], José Ramón Regueiro[¶], María Eugenia Miranda-Carús[‖], and José Luis Rodríguez-Fernández[‡8]

From the [‡]CIB/CSIC (Centro de Investigaciones Biológicas, Consejo Superior de Investigaciones Científicas), 28040 Madrid, the [§]CNB/CSIC (Centro Nacional de Biotecnología/Consejo Superior de Investigaciones Cientificas,) 28049 Madrid, the [¶]School of Medicine, Universidad Complutense, 28040 Madrid, and the [‖]Department of Rheumatology, Hospital La Paz, 28046 Madrid, Spain

Background: Chemokine receptor CCR7 promotes survival in mature dendritic cells (mDCs).
Results: Activated AMP-dependent kinase (AMPK) induces apoptosis in mDCs; CCR7 uses the kinases MEK1/2-ERK1/2 to regulate phosphorylation of AMPK on Ser-485 and consequently its inhibition.
Conclusion: CCR7 uses a novel MEK1/2-ERK1/2-AMPK signaling axis to induce survival in mDCs.
Significance: AMPK is a potential target to regulate mDC-mediated immune responses.

Chemokine receptor CCR7 directs mature dendritic cells (mDCs) to secondary lymph nodes where these cells regulate the activation of T cells. CCR7 also promotes survival in mDCs, which is believed to take place largely through Akt-dependent signaling mechanisms. We have analyzed the involvement of the AMP-dependent kinase (AMPK) in the control of CCR7-dependent survival. A pro-apoptotic role for AMPK is suggested by the finding that pharmacological activators induce apoptosis, whereas knocking down of AMPK with siRNA extends mDC survival. Pharmacological activation of AMPK also induces apoptosis of mDCs in the lymph nodes. Stimulation of CCR7 leads to inhibition of AMPK, through phosphorylation of Ser-485, which was mediated by $G_i/G\beta\gamma$, but not by Akt or S6K, two kinases that control the phosphorylation of AMPK on Ser-485 in other settings. Using selective pharmacological inhibitors, we show that CCR7-induced phosphorylation of AMPK on Ser-485 is mediated by MEK and ERK. Coimmunoprecipitation analysis and proximity ligation assays indicate that AMPK associates with ERK, but not with MEK. These results suggest that in addition to Akt-dependent signaling mechanisms, CCR7 can also promote survival of mDCs through a novel MEK1/2-ERK1/2-AMPK signaling axis. The data also suggest that AMPK may be a potential target to modulate mDC lifespan and the immune response.

Mature dendritic cells (mDCs)[9] are potent antigen-presenting cells that stimulate naive T cells in the lymph nodes (1). It has been shown that the longevity of mDCs importantly affects the immune response. In this regard, both mice depleted of mDCs and mice that present aberrant long lived mDCs develop autoimmune diseases (2–6). However, between these two extremes, it is observed that the immune response improves as the longevity of the mDCs increases (3, 7). The aforementioned results suggest that obtaining information on the mechanisms that regulate mDC survival can be very useful to develop strategies to modulate the longevity of these cells and improve the immune response.

Chemokine receptor CCR7 (ligands CCL19 and CCL21) directs mDCs to the lymph nodes (LNs), attracted first by CCL21, which is expressed in the lymphatic vessels that lead to the LNs, and then by both CCL19 and CCL21, which are both expressed by stromal cells in the LNs (8, 9). Apart from directing the migration of mDCs, CCR7 also promotes survival in

* This work was supported by grants awarded by the Ministerio de Educación y Ciencia (SAF2005-00801), Ministerio de Ciencia e Innovación (SAF2008-01468), Ministerio de Economía y Competitividad (SAF2011-23890), Ministerio de Economía y Competitividad (SAF2011-23890), RIER (RETICS Program/Instituto de Salud Carlos III) (RD08/0075), and Consejería de Educación y Empleo from Comunidad de Madrid (Raphyme, S2010/BMD-2350).
[1] Supported by an FPI scholarship (Ministerio de Economía y competitividad).
[2] Recipient of an I3P contract (Consejo Superior de Investigaciones Científicas-Fondo Social Europeo).
[3] Supported by a contract associated with Grant Raphyme S2010/BMD-2350 (Consejería de Educación y Empleo, Comunidad de Madrid).
[4] Recipient of a JAEdoc contract (Consejo Superior de Investigaciones Científicas-Fondo Social Europeo).
[5] Supported by an FPU scholarship (Ministerio de Educación y Ciencia).
[6] Supported by scholarship I3P intro (Ministerio de Educación y Ciencia).
[7] Partially supported by an FPI fellowship, conferred by the Ministerio de Educación y Ciencia (Spain), and by a contract associated with grant RD08/0075 (RIER).
[8] To whom correspondence should be addressed: Centro de Investigaciones Biológicas, Consejo Superior de Investigaciones Científicas. C/Ramiro de Maeztu, 9, 28040 Madrid, Spain. Tel.: 34-91-8373112, Ext. 4302; Fax: 34-34-91-5360436; E-mail: rodrifer@cib.csic.es.

[9] The abbreviations used are: mDC, mature dendritic cell; ACC, acetyl coenzyme A carboxylase; mTOR, mammalian target of rapamycin; mTORC, mTOR complex; PTX, pertussis toxin; LN, lymph node; PLN, popliteal LN; FOXO, Forkhead box class O; AMPK, AMP-dependent kinase; S6K, S6 kinase; AICAR, 5-aminoimidazole-4-carboxamide ribonucleotide; CFSE, carboxyfluorescein diacetate succinimidyl ester; PLA, proximity ligation assay; DMSO, dimethyl sulfoxide; SR, sulforhodamine B; Z, benzyloxycarbonyl; VAD-FMK, Val-Ala-Asp(OMe)-fluoromethyl ketone; OMe, O-methyl ester; Akti, Akt1/2 inhibitor; RAPA, rapamycin; Abs, antibodies; p, phospho.

these cells (10–12), although the signaling mechanisms that regulate the latter function are starting to be defined. Previously, we showed that CCR7-regulated survival in mDCs is mediated by the G_i family of G proteins and the kinase Akt (10, 11). This kinase promotes survival through activation of the transcription factor NFκB and inhibition of several pro-apoptotic targets, including the transcription factors FOXO1/3 and the kinase GSK3β (10–12).

AMP-dependent kinase (AMPK) is considered a molecular sensor of cellular energy status (13, 14). Under conditions of low cellular energy status, AMPK becomes activated, resulting in the stimulation of ATP-producing (catabolic) pathways and the inhibition of ATP-consuming (anabolic) processes (13, 14), which together lead to the recovery of the ATP/ADP ratio of the cell. Recently, it has emerged that AMPK may also promote survival (*e.g.* Ref. 15) or apoptosis (*e.g.* Ref. 16) depending on the cell type. AMPK is activated upon phosphorylation of Thr-172, which is located on the activation loop of the catalytic α-subunit of the kinase (17), and it is inhibited by phosphorylation of Ser-485/491 (AMPKα1 on Ser-485 and AMPKα2 on Ser-491) (18–20). Phosphorylation of Ser-485/491 blocks the activity of AMPK, even when Thr-172 is phosphorylated, suggesting that phosphorylation of the aforementioned Ser residues exerts a dominant inhibitory role on activity of AMPK (21). It has been shown that the kinases Akt (18, 22, 23) or S6K (21) can inhibit AMPK by directly phosphorylating Ser-485/491 in different cell types. Herein we have studied whether the kinase AMPK plays a role in the regulation of the survival of mDCs. We show, first, that AMPK can play pro-apoptotic roles in mDCs both *in vitro* and *in vivo*; second, we show that the stimulation of CCR7 in mDCs leads to a rapid inhibition of AMPK through the phosphorylation of Ser-485; third, we show that MEK/ERK mediate the CCR7-dependent inhibition of AMPK; and fourth, we show that ERK, but not MEK, interacts with AMPK. Together, these results indicate that CCR7 can contribute to extend the survival of mDCs through the novel MEK1/2-ERK1/2-AMPK signaling axis. These results also suggest that the kinase AMPK may be a potential target to modulate the immune response.

EXPERIMENTAL PROCEDURES

Reagents and Materials—CCL19, CCL21 and TNFα were from PeproTech (Rocky Hill, NJ). GM-CSF and IL4 were purchased from ImmunoTools. Fluorescent dye carboxyfluorescein diacetate succinimidyl ester (CFSE) was obtained from Molecular Probes. FLIVO™ is Val-Ala-Asp(OMe)-fluoromethyl ketone (VAD-FMK). Sulforhodamine B (SR)-FLIVO (SR, λ_{abs} 565 nm; λ_{em} >600 nm), a form of FLIVO conjugated to sulforhodamine B, was obtained from Immunochemistry Technologies, LLC. Z-VAD-FMK was obtained from Enzo (Life Sciences). LY294002, Akt1/2 inhibitor, pertussis toxin, Hoechst 33342, propidium iodide, and the anti-α-tubulin antibodies were from Sigma. Compound C (24), UO126 and PD0325901, and ERK activation inhibitor peptide II, were from Calbiochem (Nottingham, UK). Rapamycin, KU0063794, Gallein, A769662 and FR180204 were obtained from Tocris Bioscience (Bristol, UK). CAY10561 was from Cayman Chemicals (Ann Harbor, MI). The anti-Bim antibody was from Affinity Bioreagents (Golden, CO). The MEK1, β-actin, 4E-BP1, ERK1, ERK2, and anti-AMPKα1 antibodies were from Santa Cruz Biotechnology Inc. (Santa Cruz, CA). The anti-Akt1, anti Bcl-$_{xL}$, anti-AMPKα, the anti-TSC2, anti-mTOR, anti-phospho-MEK1/2 (Ser-217/221), anti-phospho-ERK1/2 (Thr-202/Tyr-204 in ERK1, Thr-185/Tyr-187 in ERK2), anti-phospho-Akt1 (Ser-473), anti-phospho-AMPKα1 (Ser-485), anti-phospho-AMPKα (Thr-172), anti-phospho-TSC2 (Thr-1462), anti-phospho-mTOR (Ser-2448) and anti-phospho-4EBP1 (Thr-37/46), anti-phospho-p70-S6K (Thr-389), and anti-p70-S6K antibodies were from Cell Signaling Technology (Beverly, MA). The anti-phospho-acetyl CoA-carboxylase (Ser-79) was from Millipore. The anti-cleave caspase 3 was form Biorbyt (Cambridge, UK).

Mice—C57BL/6 mice (8–10 weeks) were maintained in the animal facility at the Centro de Investigaciones Biológicas and treated according to Animal Care Committee guidelines.

Purification of Murine DCs and Labeling of the Cells with Fluorescent Cell Trackers—Murine DCs were purified (97% $CD11c^+$) from spleens of donor mice using magnetic beads (Miltenyi) following the manufacturer's protocol. DCs used in the *in vivo* studies were labeled for 30 min at 37 °C with 2.5 μM of the fluorescent cell tracker probe CFSE in 0.1% BSA in PBS.

Cells and Culture Conditions—Human peripheral blood mononuclear cells were isolated from buffy coats from normal donors over a Lymphoprep (Nycomed, Norway). Monocytes were purified using anti-CD14 magnetic beads (Miltenyi) following the manufacturer's protocol and then induced to differentiate to DCs by adding GM-CSF and IL4 for 7 days as indicated previously (10, 11, 25–27). The DCs were induced to mature by adding TNFα as indicated previously (10, 11, 25–27).

Assays of Apoptotic Damage in Vitro—An equal number of live mDCs (determined by exclusion on trypan blue staining) were incubated in 0.1% BSA or 10% FCS in RPMI in the presence or absence of AMPK activators. Subsequently, the mDCs were harvested and plated for 40 min on polyornithine-coated coverslips. Apoptotic nuclear morphology was assessed using Hoechst 33342 staining as indicated previously (10, 11, 25, 26) or by analyzing the loss of nuclear DNA content by flow cytometry using propidium iodide as indicated elsewhere (28, 29).

Cell Lysis and Western Blot Analysis—To reduce the basal levels of activity of the molecules analyzed, mDCs (100×10^3 cells) were maintained in 0.1% BSA/RPMI for 30 min before starting the stimulation with chemokines. Mature DCs were then stimulated with chemokines for the indicated periods of time. The stimulation was terminated by solubilizing the cells in SDS-PAGE sample buffer (100 mM Tris/HCl, pH 6.8, 0.05 mM sodium orthovanadate, 3% SDS, 1 mM EDTA, 2% 2-β-mercaptoethanol, 5% glycerol) and boiled and then fractionated by SDS-PAGE and transferred to nitrocellulose membranes. After blocking with 5% nonfat milk protein in TBST (TBS plus 0.1% Tween 20), pH 7.5, membranes were incubated with the indicated antibodies in TBST and visualized with the appropriate HRP-conjugated secondary antibodies (Santa Cruz Biotechnology) and an ECL substrate (Pierce) detection system. Quantification of the blots was performed using MultiGauge software from Fujifilm.

Immunoprecipitation—Mature DC (~50×10^6 DCs) were dissolved in lysis buffer A (1% Nonidet P-40, 100 mM NaCl, 1 mM EDTA, 0.5 μM vanadate, and 20 mM Hepes, pH 7.4, includ-

ing a protease inhibition mixture (Sigma), and subjected to immunoprecipitation with anti-AMPKα antibody in the presence of TrueBlot™ anti-rabbit Ig agarose beads (TrueBlot™, eBioscience, San Diego, CA). Immunoprecipitates were washed five times in lysis buffer and then boiled in SDS-PAGE sample buffer supplemented with 50 mM dithiothreitol. After SDS-PAGE and transfer to nitrocellulose, the primary antibody step was followed by incubation with a horseradish peroxidase-conjugated antibody that recognizes native rabbit IgG (TrueBlot™, eBioscience).

SiRNAs and Nucleofections—Random control and AMPKα1 siRNAs were obtained from Santa Cruz Biotechnology. The siRNAs were transfected into mDCs by using nucleofection technology (Amaxa Biosystems) according to the manufacturer's instructions.

Proximity Ligation Assay (PLA)—The assay was performed on mDC seeded onto polyornithine-coated coverslips. The mDCs were treated with CCL21 and fixed in 4% paraformaldehyde. Staining with primary antibodies was performed as in conventional immunofluorescence. However, instead of using fluorescently labeled secondary antibodies, a PLA was carried following the manufacturer's instructions (30) (Duolink II *in situ* PLA detection kit, Olink Bioscience). Briefly, samples were incubated with secondary antibodies conjugated with DNA probes (MINUS and PLUS DNA probes). Probes were hybridized and ligated, followed by amplification of the DNA template in a rolling circle amplification reaction. A detection solution was added to identify amplified DNA. Finally, coverslips with the cells were prepared using mounting medium that includes DAPI to stain the nuclei. The coverslips were analyzed with a confocal microscope, and the interactions among ERK and AMPK proteins, detected as distinct fluorescent spots inside each DC, were subsequently quantified.

Two-photon Microscopy and Analysis of Apoptotic CFSE-labeled Dendritic Cells in the Lymph Nodes—The method has been described in detail previously (10, 25, 26, 31). Briefly, CFSE-labeled splenic mDCs (10^8 mDCs/ml) were dissolved in 20 μl of RPMI and injected subcutaneously along with LPS (1 μg/ml) into the hind footpad of recipient C57BL/6 mice (2×10^6 mDCs per footpad). After 36 h, when the mDCs have already reached the popliteal LNs (PLNs) (26, 32), treated or control animals were injected intraperitoneally, respectively, with the AMPK activator A769662 (3.6 mg/25 g of mice in DMSO) or with vehicle control DMSO. 40.5 h after initiation of the experiment, the mice were injected intravenously with SR-FLIVO (SR, λ_{abs} 565 nm; λ_{em} >600 nm), and after an additional 1 h, the mice were sacrificed, and the popliteal LNs were extracted from the mice and subsequently subjected to two-photon confocal analysis to visualize among the injected CFSE-mDCs those that present SR-FLIVO staining (see "Results"). Two-photon microscopy and analysis of apoptotic CFSE-DCs in the LNs was performed as described previously (31).

Statistics—Data are expressed as mean ± S.D., and significance of differences between two series of results was assessed using the Student's *t* test. Values of $p < 0.05$ were considered significant, and *ns* indicates non-significant differences.

RESULTS

AMPK Promotes Apoptosis in Mature Dendritic Cells in Vitro—To determine whether AMPK could regulate apoptosis in mDCs, we maintained the cells in complete medium in the absence or in the presence of the selective AMPK activators A769662 or AICAR. A769662 is a direct allosteric activator of AMPK (36). AICAR is an agent that is transported into cells where it is phosphorylated to form the AMP-mimetic *S*-aminoimidazole-4-carboxamida ribonucleoside monophosphate (ZMP), which activates AMPK without altering the intracellular levels of AMP or ATP (33) (Fig. 1*A*). Western blotting analysis using antibodies that recognize a phosphorylated/active AMPKα (p-AMPK (Thr-172)), or phosphorylated acetyl coenzyme A carboxylase (ACC) (p-ACC (Ser 79)), which is a direct target of active AMPK (34), confirmed that the treatment of mDCs with A769662 or AICAR induced activation of AMPK (Fig. 1*A*, *panel a*). We treated the mDCs with the AMPK activators and then measured the percentage of apoptosis by staining the nuclei of the cells with Hoechst 33342. DCs treated with Akti1/2, a potent inhibitor of the pro-survival kinase Akt (10, 11, 25), were used as positive controls of apoptosis. As shown in Fig. 1*A*, *panels b* and *c*, mDCs treated with pharmacological activators of AMPK displayed increased percentage of apoptosis. Similar results were obtained when, instead of Hoechst staining, apoptosis was measured by analyzing the loss of nuclear DNA content typical of apoptotic cells by flow cytometry using propidium iodide as label (28, 29) (Fig. 1*A*, *panel d*) or the activation of caspase-3, another well known apoptotic marker (Fig. 1*A*, *panel e*). When the pharmacological activators of AMPK were used to induce apoptosis in mDCs that had been pretreated with Z-VAD-FMK, a general caspase inhibitor, the effects of the AMPK activators on the apoptosis of the cells were abrogated, indicating that these agents induce caspase-dependent cell death (Fig. 1*B*). Finally, to corroborate that AMPK played pro-apoptotic roles in DCs, we reduced AMPK levels using siRNA (Fig. 1*C*, *panel a*). When DCs with normal or reduced levels of AMPK were shifted to 0.1% BSA/RPMI for 24 h and then stained with Hoechst 33342, it was observed that the mDCs that displayed reduced levels of AMPK (Fig. 1*C*, *panel b*) also presented a reduced percentage of apoptosis. Together, these results indicate that AMPK can promote apoptosis in mDCs.

We analyzed potential mechanisms whereby active AMPK could induce apoptosis in DCs. Previously, we reported that the kinase GSK3β may induce apoptosis in DCs by promoting the translocation to the nucleus of the transcription factor FOXO (10), which controls the expression of the pro-apoptotic Bcl2 family member Bim (10, 25, 26, 35). We tested whether similarly active AMPK could also promote the translocation of FOXO and induce overexpression of Bim in DCs. For this purpose, we transfected the DCs with FOXO1-GFP and then induced activation of AMPK by stimulating the DCs with AICAR or A769662. As shown in Fig. 2*A*, these agents induced a significant increase in the number of DCs that displayed FOXO-GFP in the nucleus. Consistent with these results, the stimulation of DCs with AICAR or A769662 also caused an increase in Bim levels in the DCs (Fig. 2*B*). In similar experi-

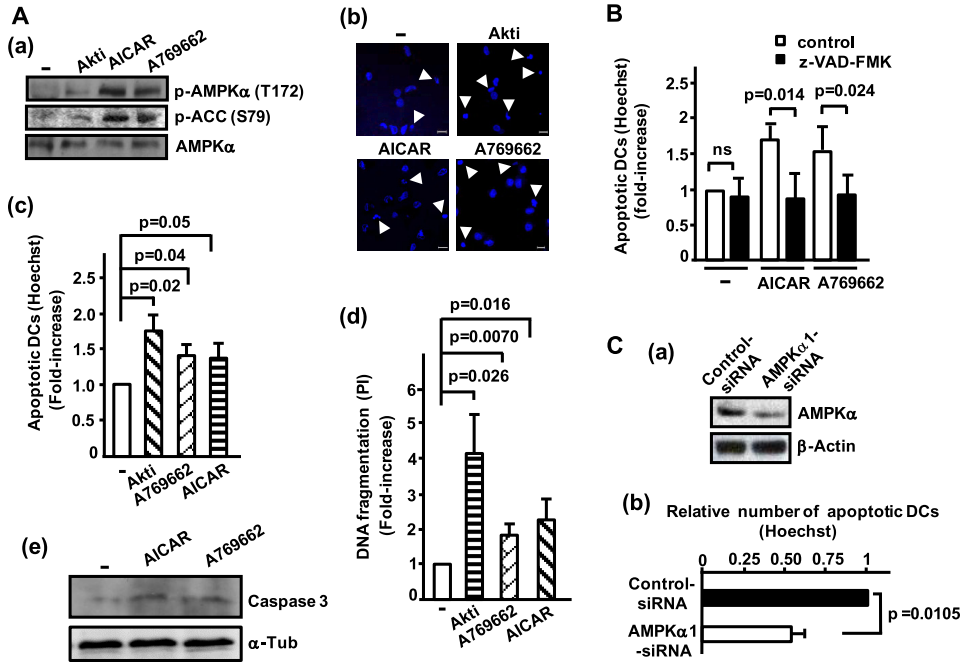

FIGURE 1. **AMPK induces apoptosis in dendritic cells.** *A*, *panel a*, DCs were suspended in 10% FCS in RPMI and then incubated for 24 h either in this medium alone (−) or in this medium plus Akti (5 μM), AICAR (1 mM), or A769662 (25 μM). Aliquots of DCs were subjected to a Western blotting analysis with Abs against phospho-AMPKα (Thr-172), phospho-ACC, or total AMPKα. *Panel b*, photographs taken from representative samples of the Hoechst 33342 stained DCs treated as in *panel a*. *Arrowheads* indicate apoptotic cells, showing condensed or fragmented nuclei. *Panel c*, DCs were suspended in 10% FCS in RPMI and then incubated in medium alone (−) or in medium plus Akti, AICAR, or A769662, as in *panel a*. The number represents -fold increase in the number of apoptotic DCs, determined by Hoechst 33342 staining, with respect to the control untreated DCs kept in 10% FCS in RPMI, which was considered as 1. Results shown represent the mean ± S.D. ($n = 4$). *Panel d*, the cells were treated or not with Akti, AICAR, or A769662 as in *panel b*. The number represents -fold increase in the number of DCs that presented DC fragmentation upon propidium iodide (*PI*) staining with respect to control untreated DCs kept in 10% FCS in RPMI. Results shown represent the mean ± S.D. ($n = 6$). *Panel e*, the DCs were suspended in 10% FCS in RPMI and then incubated for 33 h either in this medium alone (−) or in this medium plus AICAR or A769662 as in *panel a*. Aliquots of DCs were subjected to a Western blotting analysis with an antibody against caspase-3. The blots were probed with an antibody against α-tubulin to show equal loading. A representative experiment out of two performed is shown. *B*, DCs were suspended in 0.1% BSA in RPMI and then incubated for 40 h either in this medium alone (−) or in medium including AICAR (1 mM) or A769662 (25 μM), either in the absence (*control*) or in the presence of 10 μg/ml pan caspase inhibitor z-VAD-FMK. The apoptotic DCs observed in medium alone (−) untreated with z-VAD-FMK were given an arbitrary value of 1, and the -fold increase of apoptosis in the other samples was referred to this value. Results shown represent the mean ± S.D. ($n = 5$). *ns* indicates non-significant differences. *C*, mDCs were nucleofected either with random siRNA (control siRNA) or with a siRNA specific for AMPK (AMPKα1 siRNA). *Panel a*, 36 h after nucleofection, mDCs were washed in RPMI, and then an equal number of live DCs, determined by trypan blue exclusion, were subjected to Western blotting with an anti-AMPKα antibody. To confirm equal loading, the blots were reprobed with an antibody reacting with β-actin. *Panel b*, samples of DCs nucleofected either with control or with AMPKα1 siRNA were washed in RPMI, and then an equal number of live DCs, determined by trypan blue exclusion, were transferred to 0.1% BSA in RPMI for an additional 24 h. At the end of this period, the DCs were stained with Hoechst. The number of apoptotic DCs observed in the control siRNA nucleofected DCs was given an arbitrary value of 1, and the number of apoptotic DCs observed in AMPK siRNA-transfected DCs was referred to this value. Results shown represent the mean ± S.D. ($n = 3$).

ments, we did not observe any change in the expression of the pro-survival Bcl2 member Bcl-$_{xL}$ (not shown). Together, these results suggest that AMPK could induce apoptosis in DCs by promoting translocation of pro-apoptotic FOXO1 to the nucleus, which up-regulates the expression of the pro-apoptotic Bim.

Because it has been shown that AMPK inhibits the kinase mammalian target of rapamycin complex 1 (mTORC1) (36, 37), and mTORC1 has been shown to mediate the pro-survival signaling of the kinase Akt (38), we hypothesized that active AMPK may induce apoptosis by interfering with the pro-survival signaling induced from mTORC1 in DCs. To test this concept first, we analyzed whether mTORC1 plays a pro-survival role in DCs. Inhibition of mTORC1 by treating the DCs with the highly selective inhibitor rapamycin (RAPA) induces apoptosis, indicating that mTORC1 promotes survival in these cells (Fig. 2*C*). Next we studied whether CCR7 could also induce activation of mTORC1. As shown in Fig. 2*D*, simulation of CCR7 with CCL21 induces phosphorylation/inhibition of the mTORC upstream inhibitory molecule TSC2 and an increase in the phosphorylation of 4EBP1, a direct downstream target of mTORC (Fig. 2*D*), together indicating that CCR7 induces activation of mTORC1. Finally, we analyzed whether active AMPK could inhibit CCR7-dependent activation of mTORC1 (Fig. 2*E*). The treatment of the DCs with A769662 or AICAR, which, as indicated by the elevated levels of active/phosphorylated AMPK (Thr-172), induced activation of AMPK (Fig. 2*E*), also inhibited mTORC1 activity, as indicated by the reduction in the phosphorylation of 4EBP1 (Fig. 2*E*). Together, these results indicate that in DCs, active AMPK may also promote apoptosis by inhibiting mTORC1.

Stimulation of CCR7 Receptor Induces Phosphorylation/Inhibition of AMPK—As we have shown previously that stimulation of CCR7 protects mDCs from apoptosis (10, 11), we hypothesized that this receptor could also induce inhibition of pro-apoptotic AMPK in these cells. To test this hypothesis, the mDCs were treated with CCL21 for various times and then lysed in sample buffer. Subsequently, we examined the activity of AMPK using an antibody that recognizes the phosphorylated/inactive form of AMPKα1 (p-Ser-485). Stimulation with

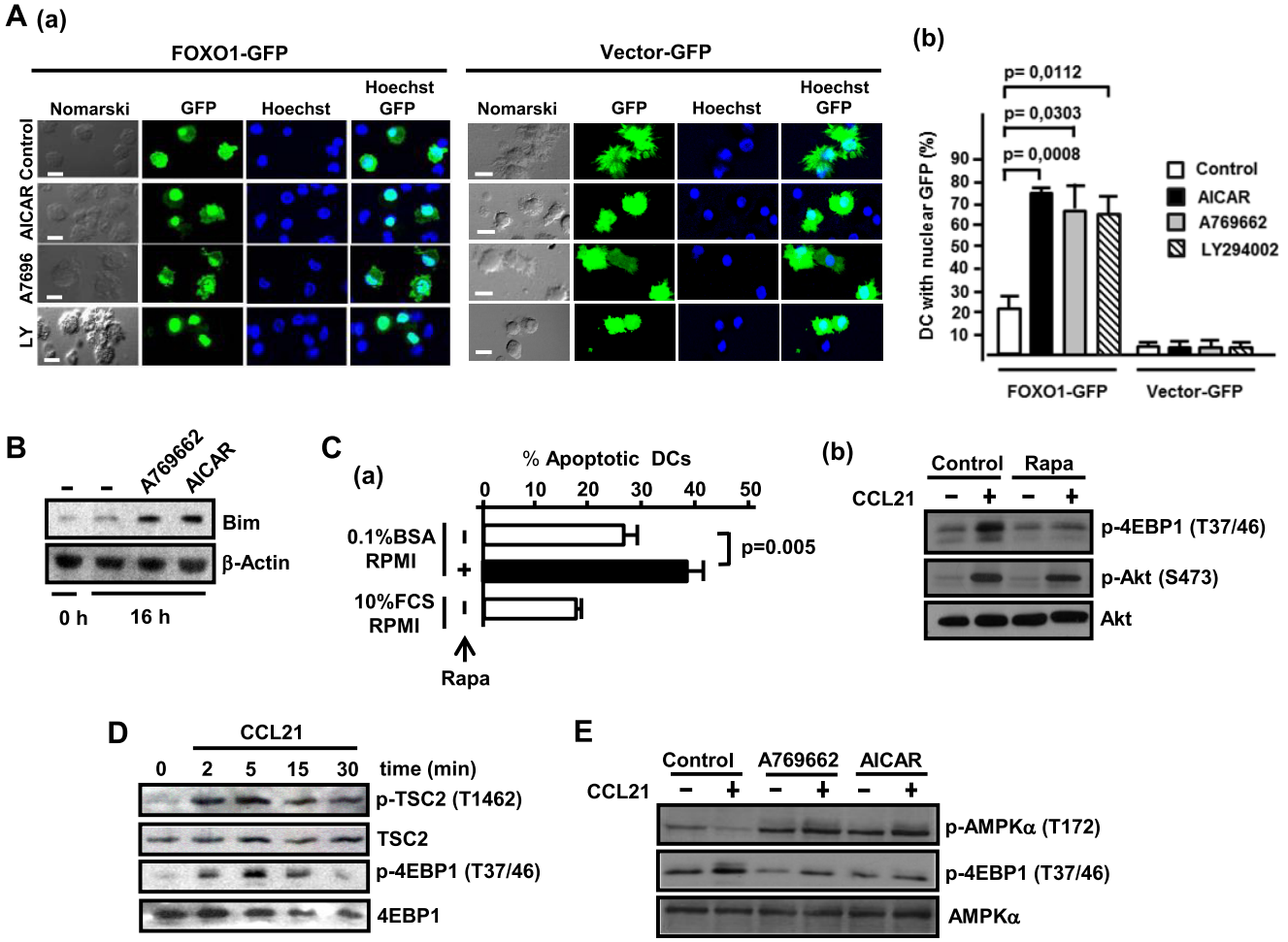

FIGURE 2. **Active AMPK may promote apoptosis by inducing translocation of FOXO1 to the nucleus and by inhibiting mTORC1.** *A*, *panel a*, the DCs were transfected with vector or FOXO1-GFP, and 6 h after transfection, the cells were resuspended in 10% FCS RPMI and then either kept untreated (*Control*) or treated with AICAR (1 mM), A769662 (25 μM), or LY294002 (*LY*, 100 μM) for an additional 2.5 h. Subsequently, the DCs were plated onto polyornithine-coated coverslips, fixed, permeabilized, and stained with Hoechst 33342. The DCs were examined with a fluorescence microscope. *Scale bar* represents 20 μm. *Panel b*, bar diagram representing the percentage of vector- or FOXO1-GFP-transfected DCs with GFP staining concentrated in the nucleus. Results shown represent the mean ± S.D. ($n = 3$). *B*, DCs were suspended in 0.1% BSA in RPMI and then kept untreated (−) or stimulated with A769662 (25 μM) or AICAR (1 mM) for 16 h. Aliquots of the DCs were subjected to a Western blot with an Ab against Bim. Blots were reprobed with an antibody reacting with β-actin to show equal loading (a representative experiment is shown). *C*, *panel a*, the DCs were suspended in 0.1% BSA in RPMI and then treated (+) or not (−) for 40 h with RAPA (100 nM). DCs maintained in 10% FCS in RPMI were used as negative controls. The DCs were plated on polyornithine-coated coverslips, fixed, and stained with Hoechst, and the apoptotic cells were examined as indicated under "Experimental Procedures." Results shown represent the mean ± S.D. ($n = 3$). *Panel b*, to confirm that RAPA inhibited mTORC1, aliquots of the control or RAPA-treated DCs from *panel a* were stimulated (+) or not (−) with CCL21 (15 nM). Subsequently, the DCs were lysed and analyzed by SDS-PAGE, followed by Western blotting. The blots were analyzed with Abs against phosphorylated 4EBP1 (Thr-37/46) or phosphorylated Akt (Ser-473). To show equal loading, the membranes were reprobed with an Ab against Akt. *D*, DCs (100,000 cells), suspended in 0.1% BSA in RPMI, were stimulated for the indicated times with CCL21 (15 nM) and then lysed and analyzed by SDS-PAGE, followed by Western blotting with Abs against phosphorylated TSC2 (Thr-1462) or phosphorylated 4EBP1 (Thr-37/46). To show equal loading, the membranes were reprobed with Abs against total 4EBP1. A representative experiment out of three performed is shown. *E*, the DCs were suspended in 0.1% BSA in RPMI and then kept untreated (*Control*) or treated with A769662 (25 μM) or AICAR (1 mM) for 60 min. Subsequently, the DCs were stimulated (+) or not (−) with CCL21 (15 nM) and then lysed and analyzed by SDS-PAGE, followed by Western blotting. The blots were analyzed with Abs against phosphorylated 4EBP1 (Thr-37/46) or phosphorylated AMPKα (Thr-172). To show equal loading, the membranes were reprobed with an Ab against AMPKα.

CCL21 (Fig. 3*A*) or CCL19 (not shown) induced inactivation of AMPK, which remained at relatively high levels until 60 min and only decayed after 120 min (Fig. 3*A*). Consistent with these results, stimulation of CCR7 caused also a reduction of the phosphorylation of the AMPK substrate ACC (Fig. 3*B*). When we used an antibody that recognizes the active form of AMPK (p-Thr-172), it was observed that stimulation of CCR7 also led to reduced levels of this active form of AMPK (Fig. 3*B*). Finally, the treatments of the mDCs with Compound C, a selective inhibitor of AMPK (24), blunted the phosphorylation of the active form of AMPK (p-Thr-172) (Fig. 3*C*, *panel a*), but failed to affect the CCR7-induced phosphorylation of Ser-485 on AMPK (Fig. 3*C*, *panel b*). Because AMPK activity is completely blunted after the treatment with Compound C, these results indicate that upon stimulation of CCR7, the phosphorylation of AMPK on Ser-485 was not due to an autophosphorylation event, but to the activity of an upstream kinase. In summary, these experiments indicate that stimulation of CCR7 in mDC causes phosphorylation on Ser-485 and inhibition of AMPK, which is mediated by an upstream kinase.

Activation of AMPK Induces Apoptosis of Murine DCs in the Lymph Nodes—We studied whether active AMPK could also play a pro-apoptotic role in the LNs, the setting where DCs present antigens to naive T-cells during the initiation of the

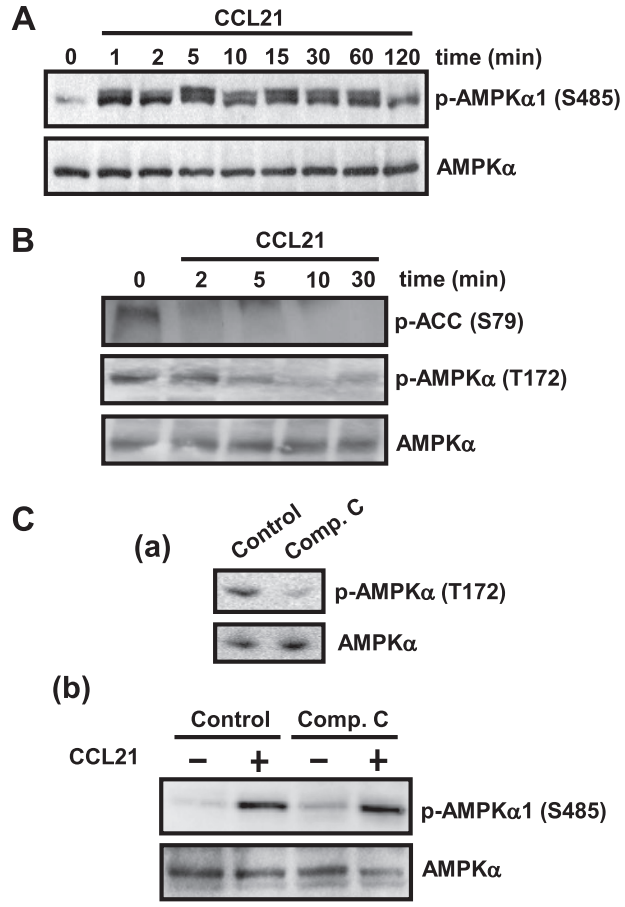

FIGURE 3. **Stimulation of CCR7 induces phosphorylation/inhibition of AMPK.** *A*, DCs (100,000 cells), suspended in 0.1% BSA in RPMI, were stimulated for the indicated times with CCL21 (15 nM) and then lysed and analyzed by SDS-PAGE, followed by Western blotting with Abs against phosphorylated/inhibited AMPKα1 (Ser-485). To show equal loading, the membranes were reprobed with Abs against total AMPKα. A representative experiment out of three performed is shown. *B*, DCs (100,000 cells), suspended as in *A*, were stimulated with CCL21 for the indicated times and then extracted and subjected to a Western blotting with Ab against phospho-ACC (Ser-79) and against phosphorylated/active AMPKα (Thr-172). To show equal loading, the membrane was reprobed with an Ab against total AMPKα. A representative experiment out of three performed is shown. *C*, *panel a*, DCs, suspended as in *panel a*, were either untreated (*Control*) or treated with AMPK inhibitor Compound C (*Comp. C*, 20 μM) for 60 min. Control and Compound C-treated DCs were stimulated with CCL21 (15 nM) for 5 min, and subsequently, lysed and subjected to Western blot analysis with Abs against phospho-AMPKα (Thr-172) and AMPKα. A representative experiment out of three performed is shown. *Panel b*, aliquots of the control or Compound C-treated samples, stimulated or not with CCL21, were used to analyze the activity of AMPK using the anti-phosphorylated AMPKα1 (Ser-485) antibody. To show equal loading, the membrane was reprobed with an Ab against total AMPKα.

immune response. Before performing the experiment *in vivo*, we first analyzed whether the treatment with AMPK activators also induced apoptosis in the splenic mDCs *in vitro*. Treatment with AICAR and A769662 significantly enhanced the activity of AMPK (Fig. 4*A*, *panel a*) and the apoptosis of the cells (Fig. 4*A*, *panel b*), indicating that active AMPK is also pro-apoptotic in splenic mDCs in culture. Furthermore, stimulation of splenic mDCs with murine CCL19 or CCL21 also induced, as in human mDCs, phosphorylation of AMPK on Ser-485 (Fig. 4*B*).

As it is known that conventional mDCs that arrive from peripheral tissues to the LNs become largely apoptotic in these regions (26, 39), we studied whether activators of AMPK could enhance the percentage of apoptotic mDCs inside the PLNs, which would indicate that active AMPK plays pro-apoptotic roles in these cells *in vivo*. For this purpose, C57BL/6 mice were injected subcutaneously in the hind footpad with CFSE-labeled splenic DCs. After 36 h, a time at which, as we previously demonstrated (26), there are a significant number of CFSE-labeled DCs positioned in the PLNs, the mice were injected intraperitoneally with 100 μmol of A769662. Control animals were injected with the same amount of vehicle (Fig. 4*C*, *panel a*). After an additional 4.5 h, the animals were injected intravenously with SR-FLIVO, a poly-caspase binding inhibitor probe (VAD-FMK) conjugated to a fluorescent dye that binds irreversibly to apoptotic caspases and allows the detection of apoptotic cells *in vivo* (10, 25, 26, 31). 1 h after the injection of SR-FLIVO, the mice were sacrificed, and the PLNs were obtained and analyzed by two-photon microscopy. In these experiments, if AMPK is pro-apoptotic, an enhanced SR-FLIVO staining in the mDCs in the PLNs obtained from the A769662-treated animals would be expected when compared with the vehicle-treated controls. Consistent with this prediction, mice injected with A769662 displayed a significant increase in the percentage of SR-FLIVO-labeled CFSE-DCs, indicating that active AMPK plays pro-apoptotic roles in the mDCs *in vivo* (Fig. 4*C*, *panels b* and *c*). We also observed induction of apoptosis in the DCs inside the PLNs when the mice were injected with AICAR (not shown). In summary, the prior experiments indicate that active AMPK promotes apoptosis of mDCs both *in vivo* and *in vitro*.

CCR7-dependent Inhibition of AMPK in mDCs Is Mediated by G_i and Gβγ, but Not by PI3K/Akt or S6K—In the next experiments, we studied the signaling pathway that could regulate the phosphorylation/inhibition of AMPK downstream of CCR7. As the G_i protein family of G proteins and the Gβγ dimers associated to these proteins mediate CCR7-dependent survival in mDCs (10, 11), we tested their involvement in the control of CCR7-dependent inhibition of AMPK. G_i-mediated signaling was blocked by treating the mDCs with the selective inhibitor pertussis toxin (PTX), and Gβγ-mediated signaling was blocked by treating the cells with Gallein (40). The observed inhibition of the CCR7-dependent phosphorylation of ERK1/2 (Fig. 5*A*, *panels a* and *b*), two kinases known to be regulated by G_i and Gβγ (10, 27), indicated that both PTX and Gallein efficiently blocked their targets. The treatment with PTX or Gallein also blunted the CCR7-induced phosphorylation of AMPK on Ser-485 (Fig. 5*A*, *panels a* and *b*), indicating that G_i and Gβγ regulate the phosphorylation of AMPK on Ser-485 downstream of CCR7.

Stimulation of CCR7 induces activation of Akt in mDCs (10, 11, 41), which is also controlled by the G_i family of proteins (10, 11). As Akt mediates the phosphorylation of Ser-485 on AMPK in a variety of cell types (18, 22, 23, 42), we analyzed whether it could also play a similar role downstream of CCR7 in mDCs. Surprisingly, the blocking of the activity of Akt, with the PI3K inhibitor LY294002 (Fig. 5*B*, *panel a*) or with the selective Akt inhibitor Akti1/2 (43) (Fig. 5*B*, *panel b*), failed to affect CCR7-dependent phosphorylation of AMPK on Ser-485, indicating that Akt does not mediate CCR7-dependent inhibition of AMPK in mDCs. Further emphasizing that Akt and AMPK are

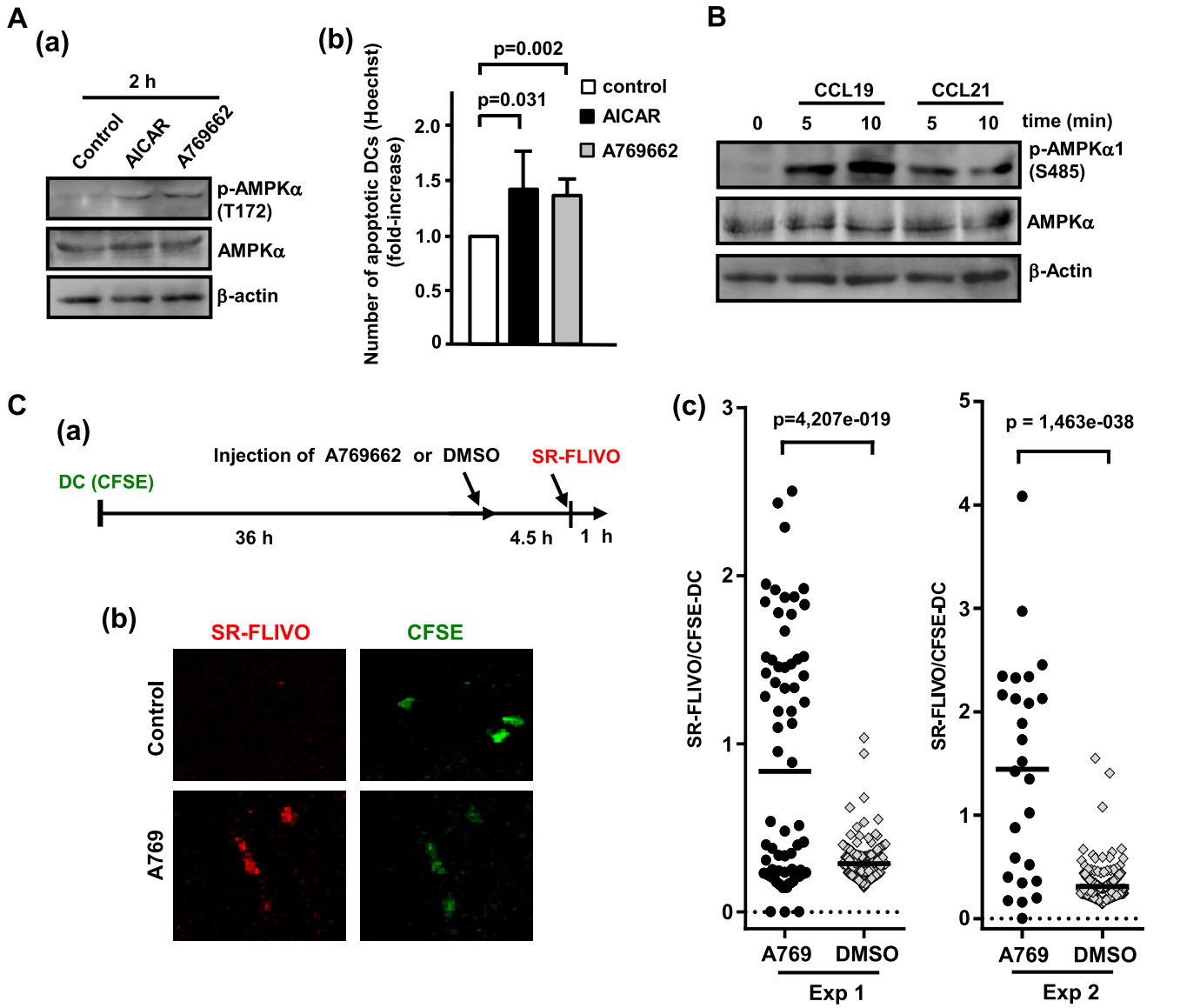

FIGURE 4. **Activation of AMPK increases the apoptosis of dendritic cells *in vitro* and in the lymph nodes.** *A*, *panel a*, splenic mDCs (500,000 cells) suspended in 10% FCS in RPMI were kept unstimulated (*Control*) or stimulated for the indicated times with AICAR (1 mM) or A769662 (25 μM) and then lysed and analyzed by SDS-PAGE, followed by Western blotting with Abs against phospho-AMPKα (Thr-172), total AMPKα and β-actin. A representative experiment out of five performed is shown. *Panel b*, aliquots of the splenic DCs treated as in *panel a* for 2 h were fixed and stained with Hoechst 33342 to detect apoptotic DCs. The number represents the -fold increase in the number of apoptotic DCs respect to the number of apoptotic DCs observed in the controls that was considered as 1. Results represent the mean ± S.D. ($n = 6$ experiments). *B*, splenic DCs (500,000 cells) suspended in 0.1% BSA in RPMI were stimulated for the indicated times with murine CCL19 or CCL21 (both at 15 nM) and then lysed and analyzed by SDS-PAGE, followed by Western blotting with Abs against phospho-AMPKα1 (Ser-485), total AMPKα, and β-actin. A representative experiment out of five performed is shown. *C*, *panel a*, experimental protocol. 2×10^6 CFSE-labeled splenic DCs were injected in the footpads of recipient mice. After 36 h, the animals were injected intraperitoneally with 100 μmol of A769662 or a similar volume of vehicle DMSO. After an additional 4.5 h, mice were injected (intravenously) with SR-FLIVO to stain apoptotic DCs in the LNs. After 1 h, the popliteal LNs were extracted, fixed, and subjected to two-photon analysis. *Panel b*, representative SR-FLIVO staining displayed by CFSE-labeled DCs obtained from the LNs of animals treated either with A769662 or with DMSO. The LNs of the mice were extracted and studied by two-photon microscopy as indicated under "Experimental Procedures." *Panel c*, the stacks of optical images of the LNs were examined with the Leica confocal software, and the values of the maximum amplitude of the SR-FLIVO and CFSE channel were obtained as indicated previously (see "Experimental Procedures"). Data from two experiments are presented. The data are represented as maximum intensity of SR-FLIVO over maximum intensity of CFSE for each individual DC in an LN. For A769662-treated animals, 74 DCs were analyzed in Experiment 1 (*Exp 1*), and 26 DCs were analyzed in Experiment 2 (*Exp 2*); for DMSO vehicle-treated animals, 171 DCs were analyzed in Experiment 1 (*Exp 1*), and 237 DCs were analyzed in Experiment 2(*Exp 2*).

independently regulated, the inhibition of AMPK, by treating the mDCs with Compound C, did not affect the CCR7-dependent phosphorylation of Akt (not shown).

Stimulation of CCR7 also induces activation of the mammalian target of rapamycin complex 1 (mTORC1) (Fig. 5*C*), which promotes survival in mDCs (Fig. 2*C*). Recently, it has been shown that S6K, a molecule that is regulated by mTORC1 (44), may also directly phosphorylate AMPK on Ser-485 (21). Therefore, we studied whether inhibition of S6K could block CCR7-dependent phosphorylation of AMPK on Ser-485. To inhibit S6K, we treated the mDCs with pharmacological agents that block either Akt (Akti) or mTORC1 (RAPA or KU0063794), both upstream regulators of S6K (44) (Fig. 5*D*). To analyze S6K activity, we used an antibody that recognizes a phosphorylated/

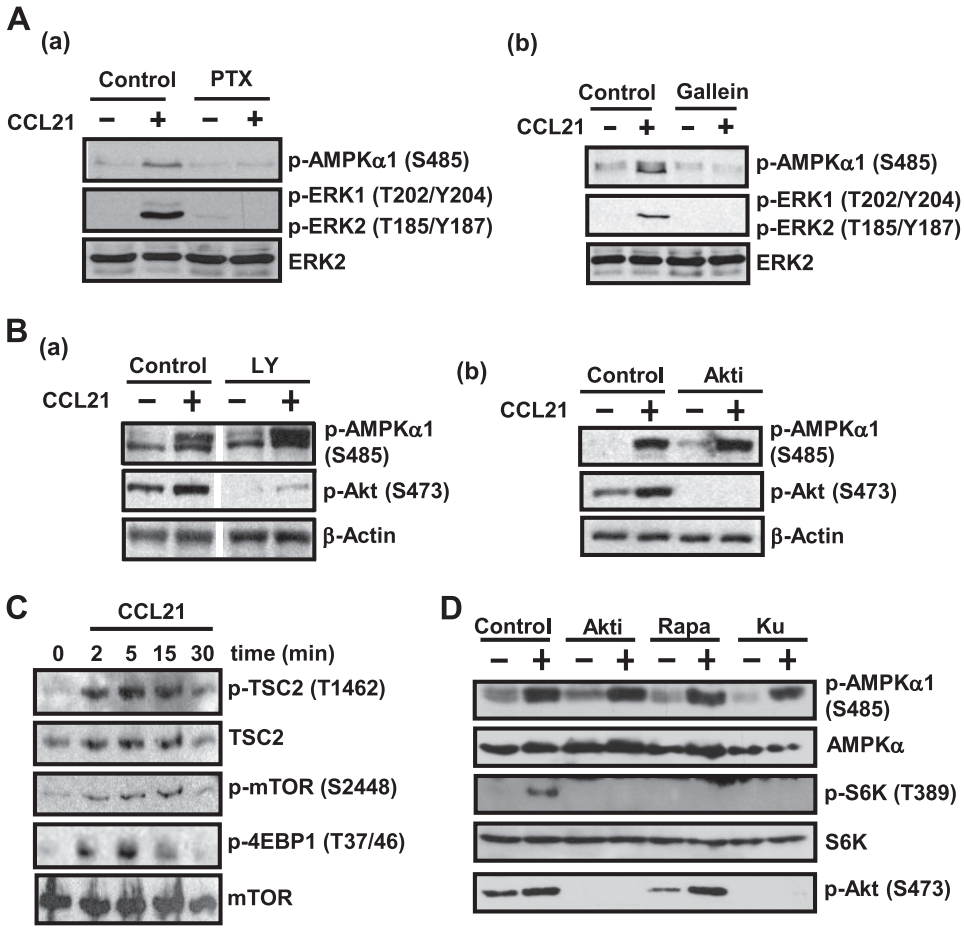

FIGURE 5. **Signaling downstream of CCR7 regulating the phosphorylation of AMPKα1 on serine 485.** *A*, *panel a*, DCs (100,000 cells) in complete medium were either kept untreated (*Control*) or treated with PTX (100 ng/ml) for 180 min. Subsequently, the DCs were washed and suspended in 0.1% BSA in RPMI. Control and PTX-treated DCs were stimulated with CCL21 (15 nM) for 5 min and subsequently lysed and subjected to Western blotting with the Ab against phosphorylated AMPKα1 (Ser-485) or phosphorylated ERK1/2 (Thr-202/Tyr-204 ERK1/Thr-185/Tyr-187 ERK2). ERK2 levels show equal loading of the gels. A representative experiment out of three performed is shown. *Panel b*, DCs, untreated or pretreated with the Gβγ inhibitor Gallein (40) for 15 min, were stimulated or not with CCL21 for 5 min and then lysed, and aliquots were subjected to Western blotting with an Ab against phosphorylated AMPKα1 (Ser-485) and phosphorylated ERK1/2 as in *panel a*. ERK2 levels show equal loading of the gels. A representative experiment out of three performed is shown. *B*, DCs suspended in 0.1% BSA in RPMI were either left untreated (*Control*) or pretreated for 60 min with the PI3K inhibitor LY294002 (*LY*, 100 μM, 60 min) (*panel a*) or Akti (5 μM) (*panel b*). The DCs were subsequently stimulated or not with CCL21 (15 nM) for 5 min and then lysed, and aliquots were subjected to Western blot with the Ab against phosphorylated/inhibited AMPKα1 (Ser-485) or against phosphorylated/active Akt1 (Ser-473). β-Actin levels show equal loading of the gels. A representative experiment out of three performed is shown. *C*, DCs (100,000 cells), suspended in 0.1% BSA in RPMI, were stimulated for the indicated times with CCL21 (15 nM) and then lysed and analyzed by SDS-PAGE, followed by Western blotting with Abs against phosphorylated TSC2 (Thr-1462), phosphorylated mTOR (Ser-2448), or phosphorylated 4EBP1 (Thr-37/46). To show equal loading, the membranes were reprobed with Abs against total TSC2 and mTOR. *D*, DCs suspended in 0.1% BSA in RPMI were either left untreated (*Control*) or pretreated for 60 min with Akti (5 μM), RAPA (100 nM), or KU0063794 (*Ku*) (500 nM). The DCs were subsequently stimulated or not with CCL21 (15 nM) for 5 min. The DCs were then lysed and analyzed by Western blotting with Abs against phosphorylated/inactive AMPKα1 (Ser-485), phosphorylated/active S6K (Thr-389), and phosphorylated/active Akt (Ser-473). Membranes were also probed with antibodies that recognize total S6K and AMPKα.

active form of this kinase (p-S6K (Thr-389)). Treatment of the mDCs with the inhibitors Akti1/2 (43), rapamycin (43, 45), and Ku (46), to inhibit Akt, mTORC1 and mTORC1/2, respectively, blunted, as expected, the activation of S6K. However, despite strong inhibition of S6K, the CCR7-dependent phosphorylation of AMPK on Ser-485 was not affected (Fig. 5*D*). These results indicate that Akt, mTORC1, mTORC2, and S6K do not mediate CCR7-dependent inhibition of AMPK in mDCs (see model in Fig. 9).

CCR7-dependent Inhibition of AMPK in DCs Is Mediated by MEK/ERK—Upon stimulation of the mDCs with CCL21, we observed similar kinetics in the activation of the kinases MEK1/2/ERK1/2 and phosphorylation of AMPK on Ser-485 (Fig. 6*A*). Therefore, we studied whether MEK1/2/ERK1/2 could mediate the phosphorylation of AMPK on Ser-485 downstream of CCR7. Treatment of the cells with UO126 (Fig. 6*B*) or PD03255901 (Fig. 6*C*), two potent and selective inhibitors of MEK1/2 (45) and, consequently of ERK1/2, the only known downstream targets of MEK1/2 (47), blunted CCR7-dependent phosphorylation of AMPK, indicating that MEK1/2 regulates the phosphorylation of AMPK on Ser-485 downstream of CCR7. In the next experiments, we studied whether ERK1/2 could also regulate AMPK phosphorylation on Ser-485. Our attempts to reduce the expression of ERK1 or ERK2 in mDCs using siRNAs were unsuccessful. Although the siRNAs used readily blunted ERK1 and ERK2 expression in HL-60 cells, we were unable to reduce the levels of these two kinases in mDCs (not shown). Therefore, we decided to use two pharmacological inhibitors to block ERK1/2 activity, namely, CAY10561 (Fig. 7*A*) and FR180204 (Fig. 7*B*). CAY10561 displays a high selec-

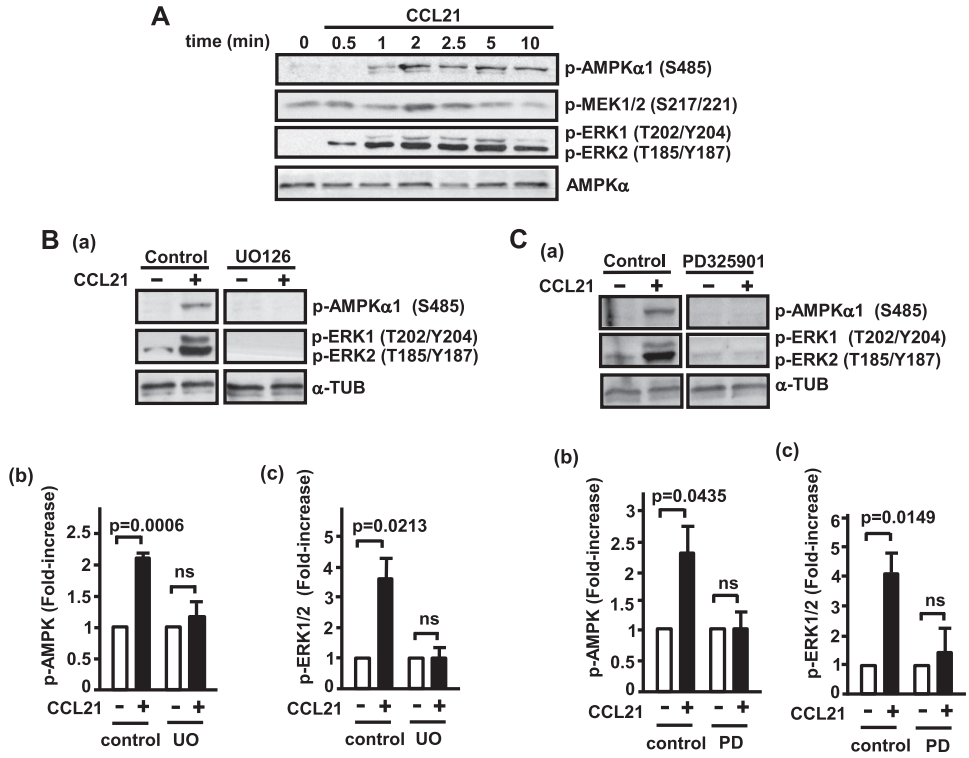

FIGURE 6. **CCR7-dependent phosphorylation/inhibition of AMPK is mediated by MEK.** *A*, DCs (100,000 cells) suspended in 0.1% BSA in RPMI were stimulated for the indicated times with CCL21 (15 nM) and then lysed and analyzed by SDS-PAGE, followed by Western blotting with Abs against phosphorylated AMPKα1 (Ser-485), MEK1/2 (Ser-217/221), or ERK1/2 (Thr-202/Thr-204 ERK1/Thr-185/Tyr-187 ERK2). To show equal loading, the membranes were reprobed with an Ab against AMPKα. A representative experiment out of three performed is shown. *B*, *panel a*, DCs suspended in 0.1% BSA in RPMI were either left untreated (*Control*) or pretreated with UO126 (2.5 μM, 60 min). The mDCs were subsequently stimulated or not with CCL21 for 5 min and then lysed, and the aliquots were subjected to Western blot with an antibody against phosphorylated/inactive AMPKα1 (Ser-485) or phosphorylated active ERK1/2 (Thr-202/Tyr-204 ERK1/Thr-185/Tyr-187 ERK2). α-Tubulin (*α-TUB*) levels show equal loading of the gels. A representative experiment out of three performed is shown. *Panel b*, -fold increase in the phosphorylation of AMPK in control and UO126 (*UO*)-treated mDCs, upon stimulation with CCL21. In both control and UO126-treated DCs, the degree of phosphorylation of the unstimulated DCs was given an arbitrary value of 1, and -fold increase in the CCL21-stimulated mDCs was represented. *Panel c*, similar to *panel b* with the difference that -fold increase in phosphorylation of ERK1/2 was examined. *C*, *panel a*, the experiments were performed as described in *B*, with the only difference that the DCs were treated with PD325901 (1 μM, 60 min). *Panels b* and *c*, similar to *panels b* and *c* in *B*, with the only difference that PD325901 was used. *ns* indicates non-significant differences.

tivity against ERK when tested against a panel of 184 related kinases (48, 49), and FR180 displays a high selectivity against ERK when tested against eight related kinases (50). As shown in Fig. 7, *A* and *B*, although the effects of CAY10561 and FR180 displayed higher variability when compared with the effects of the MEK1/2 inhibitors, both agents blocked CCR7-dependent phosphorylation of AMPK1a on Ser-485. Therefore, these results indicate that ERK1/2 can mediate the effects of MEK1/2 to induce inhibition of AMPK. As the pharmacological blocking of MEK1/2 and ERK1/2 prevents the phosphorylation/inhibition of AMPK, which plays pro-apoptotic roles, we predicted that treatment of the mDCs with the inhibitor would reduce the pro-survival effects induced by stimulation of CCR7. As shown in Fig. 7*C*, as expected, the pretreatment of the mDCs with the inhibitors of MEK1/2 or ERK1/2 reduced the pro-survival effects induced by the stimulation of CCR7, although at an extent slightly lower than that induced by inhibition of Akt.

ERK Associates to AMPK—As active MEK/ERK are required to observe phosphorylation of AMPK on Ser-485 downstream of CCR7, we studied the possibility that these molecules could associate to AMPKα in mDCs. We immunoprecipitated the endogenous AMPKα from cultures of mDCs and then carried out a Western blotting to analyze for the presence of ERK1 or MEK1 in the immunoprecipitates. As shown in Fig. 8*A*, we observed that AMPKα and ERK1 interacted both in unstimulated and in CCL21-stimulated mDCs, suggesting that these two proteins are able to associate, directly or indirectly, constitutively. In contrast, we did not detect MEK1 in the AMPKα immunoprecipitates (not shown). Because direct or indirect protein-protein associations cannot be discriminated by immunoprecipitation, to study whether AMPKα and ERK1 could interact directly each other, we performed a PLA (51, 52). This is a novel microscopy technique that allows detecting, with high specificity and sensitivity, close proximity between two proteins (<40 nm), suggesting direct interactions between these two molecules (30, 51, 52). The mDCs were plated on polyornithine-coated dishes, and then they were stimulated with CCL21 and finally subjected to a PLA analysis. Negative controls where single antibodies against ERK1 (Fig. 8*B*, *panel a*), AMPK1α (Fig. 8*B*, *panel a*), or MEK1 (Fig. 8*B*, *panel b*) were used showed no PLA fluorescence. Interestingly, we observed PLA fluorescence signal between the pair ERK1/AMPKα only in CCL21-stimulated mDCs, but not in unstimulated mDCs, suggesting that stimulation of CCR7 induces proximity between these two kinases (Fig. 8*B*, *panel c*). Consistent with immunoprecipitation results, we did not observe PLA fluorescent signal between the pair MEK1/AMPKα (not shown). Analysis of the interaction between ERK1 and MEK1, which was

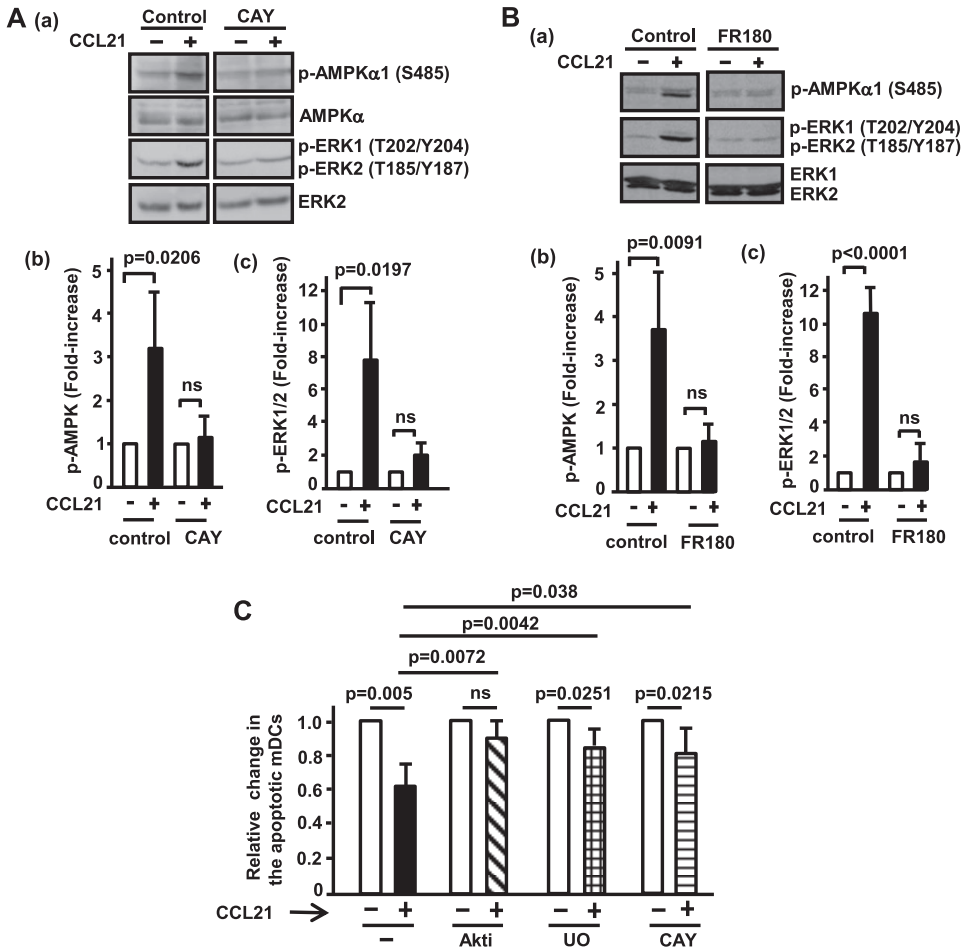

FIGURE 7. **CCR7-dependent phosphorylation/inhibition of AMPK is mediated by ERK.** *A*, *panel a*, DCs suspended in 0.1% BSA in RPMI were either left untreated (*Control*) or pretreated with CAY10561 (*CAY*, 20 μM, 2,5 h). The DCs were stimulated with CCL21 (15 nM) for 5 min and then lysed, and aliquots were subjected to Western blot with antibodies against phosphorylated/inactive AMPKα1 (Ser-485), total AMPKα, phosphorylated active ERK1/2 (Thr-202/Tyr-204 ERK1/Thr-185/Tyr-187 ERK2), or total ERK2. A representative experiment out of five performed is shown. *Panel b*, -fold increase in AMPK phosphorylation in control and CAY10561-treated mDCs, upon stimulation with CCL21. In both control and CAY10561-treated DCs, the degrees of phosphorylation of the unstimulated DCs were given an arbitrary value of 1, and the -fold increase in the CCL21-stimulated mDCs was represented. *Panel c*, similar to *panel b* with the difference that -fold increase in phosphorylation of Erk1/2 was examined. In *panels b* and *c*, the results represent the mean $\pm$ S.D. ($n = 5$ experiments). *ns* indicates non-significant differences. *B*, *panel a*, experiments were performed as described in *A*, with the differences that FR180 (100 μM, 60 min) was used and that anti-total ERK1/2 shows equal loading of the gels. A representative experiment out of three performed is shown. *Panel b*, similar to *panel b* in *A*, with the difference that -fold increase in AMPK phosphorylation was examined in the presence of FR180 as indicated in *panel a* in *B*. *Panel c*, experiments similar to *panel c* in *A* with the difference that -fold increase in phosphorylation of Erk1/2 was examined in the presence of FR180 as indicated in *panel a* in *B*. In *panels b* and *c*, the results represent the mean $\pm$ S.D. ($n = 3$ experiments). *ns* indicates non-significant differences. *C*, relative number of apoptotic DCs in unstimulated ($-$) and CCL21-stimulated DCs ($+$), after treating the mDCs with Akti, the MEK1/2 inhibitor UO126 (*UO*), or the ERK1/2 inhibitor CAY10561 (*CAY*). Results represent the mean $\pm$ S.D. ($n = 5$ experiments).

used as a positive control, also showed intense PLA fluorescence in the stimulated, but not in the unstimulated, mDCs (Fig. 8*B*, *panel d*). In summary, these results show that ERK and AMPK may be part of a similar protein complex, and in this complex, active ERK may control the phosphorylation of AMPK on Ser-485.

DISCUSSION

CCR7 directs mDCs to the LNs where the initiation of the immune response takes place. Previously, we showed that in addition to chemotaxis, CCR7 can promote survival in mDCs through the kinase Akt (10–12), which controls survival by inducing activation of NFκB and inhibition of FOXO1/3 and GSK3β (10–12). To get further insights on the mechanisms used by CCR7 to induce survival in mDCs, herein we have analyzed the involvement of the kinase AMPK in this process. Our results indicate that in mDCs, AMPK can play pro-apoptotic roles *in vitro* and *in vivo*.

The phenotypical features presented by the DCs that die after inducing activation of AMPK suggest that this kinase may induce an apoptotic type of death. In this regard, AMPK-dependent death is inhibited by the pan-caspase inhibitor z-VAD-FMK; it associates to caspase 3 activation, to the fragmentation of the nucleus, and to the increase in the expression of the pro-apoptotic Bcl2 family member Bim. Our results indicate that AMPK may promote apoptosis, at least partially, by inducing translocation to the nucleus of FOXO1, a transcription factor that plays pro-apoptotic roles in mDCs through the regulation of the expression of Bim (10, 25, 26), and by inhibiting mTORC1, a kinase complex controlled by CCR7 that also induces survival in mDCs (10, 26). In other cell types, AMPK has also been shown to be able to promote apoptosis using these two mechanisms (36, 53, 54).

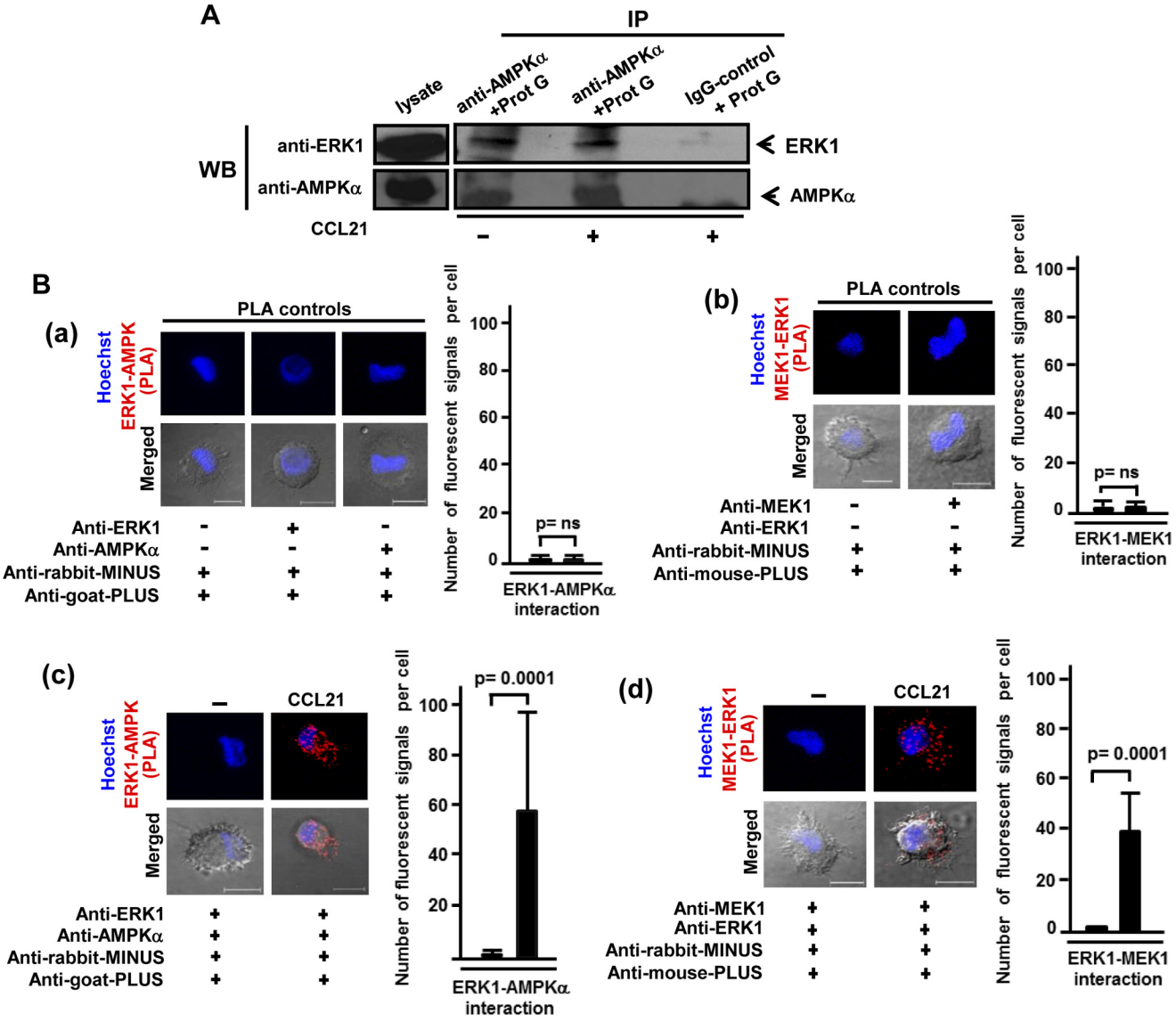

FIGURE 8. **AMPKα interacts with ERK1.** *A*, equal number of DCs, stimulated (+) or not (−) with CCL21 (15 nM), were subjected to immunoprecipitation (*IP*) with anti-AMPKα antibody or with IgG control, and subsequently, the immunoprecipitates were separated by SDS-PAGE, followed by Western blotting (*WB*) with anti-ERK1 or anti-AMPKα antibodies. A lysate of DCs was used as positive control. Aliquots of the lysates used to immunoprecipitate AMPK were analyzed for Western blotting for the presence of β-actin to demonstrate equal amount of proteins immunoprecipitated (not shown). *B*, interaction between ERK1 and AMPKα in mDCs was detected as fluorescent signals using the PLA. *Panels a* and *b*, PLA negative controls performed by labeling the DCs only with the anti-ERK1 or anti-AMPKα antibodies plus the anti-rabbit MINUS and the anti-goat PLUS (*panel a*) and the anti-MEK1 antibody and the anti-rabbit MINUS and the anti-mouse PLUS probes (*panel b*). Nomarski images and nuclei stained with Hoechst 33342 are also shown. *Scale bar*, 10 μm. In *panels a* and *b*, the number of fluorescent signals per cell was also quantified. At least 40 cells per field were counted. Results represent the mean ± S.D. ($n = 3$ experiments). *Panel c*, PLA fluorescent staining, indicating interaction between ERK1 and AMPKα, after CCL21 stimulation. *Panel d*, positive control. PLA fluorescent staining between MEK1 and ERK1 upon CCL21 stimulation is shown. Nomarski images and nuclei stained with Hoechst 33342 are also shown. *Scale bar*, 10 μm. In *panels c* and *d*, the number of fluorescent signals per cell was also quantified. At least 40 cells per field were counted. Results represent the mean ± S.D. ($n = 3$ experiments). *ns* indicates non-significant differences.

Consistent with its pro-survival role of the chemokine receptor CCR7 (11), we observed that its stimulation induces a rapid phosphorylation/inhibition of pro-apoptotic AMPK on Ser-485 (18–21). This inhibition of AMPK may promote DC survival through the effects that can be exerted on FOXO and mTORC1. Previously, we showed that stimulation of CCR7 induces activation of Akt, which, upon phosphorylating nuclear FOXO, induces its translocation to the cytoplasm (10, 11), preventing this factor from exerting pro-apoptotic effects through Bim. However, in contrast to Akt, active AMPK promotes, as shown above, the translocation of FOXO to the nucleus of DCs, from where it can regulate apoptosis. Thus, CCR7-mediated inhibition of AMPK may prevent this kinase from opposing the effects of Akt on FOXO, facilitating the complete translocation of FOXO to the cytoplasm. Moreover, CCR7-dependent inhibition of AMPK may also be able to prevent this kinase from inhibiting the pro-survival effects exerted by mTORC1. Thus, CCR7-mediated inhibition of AMPK may contribute to the extended survival of the DCs.

These results suggest that downstream of CCR7, the kinases MEK/ERK, but not Akt or S6K, mediate the phos-

phorylation of AMPK on Ser-485. Our results also indicate that ERK and AMPK may be components of a signaling complex where active ERK controls the phosphorylation of AMPK on Ser-485. Interestingly, these data contrast with prior results, obtained in other cell types, where it has been indicated that AMPK promotes inhibition of ERK (55–58), pointing out context-dependent differences in the mechanisms used by these two molecules to regulate each other. Previously, it has also been shown that infection of PK-15 cells with porcine circovirus type 2 (PCV2) also promotes interaction between AMPK and ERK (58). To the best of our knowledge, our work is the first study indicating that MEK/ERK can mediate the inhibition of AMPK by regulating Ser-485 phosphorylation.

The results obtained also indicate that MEK/ERK can regulate mDC survival. Until now, we had overlooked a role for MEK/ERK as regulators of CCR7-dependent survival in mDCs, probably due to the relatively less important role of these kinases as regulators of this function when compared with Akt. In most early experiments, the effects of MEK/ERK on mDC survival were analyzed after relatively short periods (6–10 h). Under these conditions, the effects of interfering with MEK/ERK on survival were negligible when compared with those induced by Akt inhibition. Only when apoptosis was analyzed after longer treatment with ERK1/2 inhibitors (24–40 h) did MEK/ERK emerge as a regulator of mDC survival, although still less potent than Akt. In Fig. 9, we present a model that summarizes the results obtained regarding the signaling mechanisms involved in the phosphorylation/inhibition of AMPK.

The results indicating that MEK/ERK, but not Akt, control AMPK phosphorylation on Ser-485 were unexpected for several reasons. First, we have shown previously that Akt is a key mediator of CCR7-dependent survival in mDCs (10, 11). Second, CCR7-mediated activation of Akt and phosphorylation of AMPK on Ser-485 were both mediated by G_i, suggesting that the CCR7-G_i-Akt axis may regulate the phosphorylation of AMPK. Third, Akt inhibits AMPK by directly phosphorylating Ser-485 on AMPK in several other cell types (18, 22, 23, 42). However, despite these prior results, we observe that inhibition of Akt or S6K, another kinase involved recently in the regulation of the phosphorylation of AMPK on Ser-485 (21), failed to block the phosphorylation of this residue upon stimulation of CCR7. In contrast, inhibition of MEK or its direct target ERK blocked CCR7-dependent phosphorylation of AMPK on Ser-485. Therefore, MEK/ERK emerge as novel regulators of the phosphorylation/inhibition of AMPK and, consequently, the survival of mDCs in addition to Akt. Interestingly MEK-ERK dependent phosphorylation of AMPK on Ser-485 seems cell- and/or receptor-specific because in granulosa cells, MEK/ERK inhibition was ineffective in preventing the FSH-mediated phosphorylation of AMPK on Ser-485 (22). These disparate results regarding the roles of Akt, S6K, and MEK/ERK on the phosphorylation of Ser-485 emphasize the combinatorial character of the signaling pathways and the importance of a detailed knowledge of the specific pathways used by specific receptors in each cell type. In summary, the data presented herein indicate that CCR7 may use the MEK-AMPK axis, in addition to Akt-dependent mechanisms (10–12), to promote survival in mDCs. These results add a novel component to the array of signals relayed from CCR7 to promote the survival of mDCs and provide new potential targets to modulate the function of these cells in the immune system.

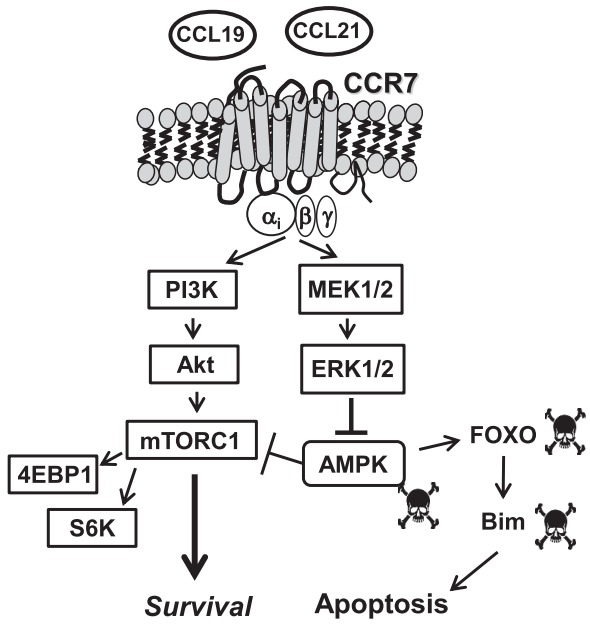

FIGURE 9. **CCR7-stimulated phosphorylation-inhibition of AMPK.** Stimulation of CCR7 with CCL19 or CCL21 induces $G_i G\beta\gamma$-mediated activation of the kinases MEK1/2/ERK1/2. CCR7 also induces activation of the PI3K/Akt/mTORC1/4EBP1 and S6K pathways, which promote survival in mDCs. Active AMPK induces apoptosis in mDCs by inhibiting the pro-survival effects of mTORC1 and by promoting translocation of the transcription factor FOXO to the nucleus, where it can control the expression of the pro-apoptotic Bcl2 family member Bim. Stimulation of CCR7 regulates, through the $G_i G\beta\gamma$/MEK1/2-ERK1/2 pathway (and independently of the PI3K/Akt/mTORC1pathway), the phosphorylation of the kinase AMPK on Ser-485, which results in the inhibition of this kinase and the consequent dampening of its pro-apoptotic effects. Therefore, CCR7 promotes survival in DCs through Akt-dependent mechanisms described previously (10–12) and by promoting MEK/ERK-dependent inhibition of AMPK.

Acknowledgments—We acknowledge P. Lastres for help with the cytometer and discussions and Génesis Andrea Altuve Urbina and Cristina Ruano Domínguez for expert technical assistance. We acknowledge Jill Suttles (University of Louisville School of Medicine) for kindly supplying reagents.

REFERENCES

1. Ueno, H., Klechevsky, E., Morita, R., Aspord, C., Cao, T., Matsui, T., Di Pucchio, T., Connolly, J., Fay, J. W., Pascual, V., Palucka, A. K., and Banchereau, J. (2007) Dendritic cell subsets in health and disease. *Immunol. Rev.* **219,** 118–142
2. Chen, M., Huang, L., and Wang, J. (2007) Deficiency of Bim in dendritic cells contributes to overactivation of lymphocytes and autoimmunity. *Blood* **109,** 4360–4367
3. Hildeman, D., Jorgensen, T., Kappler, J., and Marrack, P. (2007) Apoptosis and the homeostatic control of immune responses. *Curr. Opin. Immunol.* **19,** 516–521
4. Hou, W. S., and Van Parijs, L. (2004) A Bcl-2-dependent molecular timer regulates the lifespan and immunogenicity of dendritic cells. *Nat. Immunol.* **5,** 583–589
5. Nopora, A., and Brocker, T. (2002) Bcl-2 controls dendritic cell longevity *in vivo*. *J. Immunol.* **169,** 3006–3014

6. Ohnmacht, C., Pullner, A., King, S. B., Drexler, I., Meier, S., Brocker, T., and Voehringer, D. (2009) Constitutive ablation of dendritic cells breaks self-tolerance of CD4 T cells and results in spontaneous fatal autoimmunity. *J. Exp. Med.* **206,** 549–559
7. Kushwah, R., and Hu, J. (2010) Dendritic cell apoptosis: regulation of tolerance *versus* immunity. *J. Immunol.* **185,** 795–802
8. Randolph, G. J., Ochando, J., and Partida-Sánchez, S. (2008) Migration of dendritic cell subsets and their precursors. *Annu. Rev. Immunol.* **26,** 293–316
9. Comerford, I., Harata-Lee, Y., Bunting, M. D., Gregor, C., Kara, E. E., and McColl, S. R. (2013) A myriad of functions and complex regulation of the CCR7/CCL19/CCL21 chemokine axis in the adaptive immune system. *Cytokine Growth Factor Rev.* **24,** 269–283
10. Escribano, C., Delgado-Martín, C., and Rodríguez-Fernández, J. L. (2009) CCR7-dependent stimulation of survival in dendritic cells involves inhibition of GSK3β. *J. Immunol.* **183,** 6282–6295
11. Sánchez-Sánchez, N., Riol-Blanco, L., de la Rosa, G., Puig-Kröger, A., García-Bordas, J., Martín, D., Longo, N., Cuadrado, A., Cabañas, C., Corbí, A. L., Sánchez-Mateos, P., and Rodríguez-Fernández, J. L. (2004) Chemokine receptor CCR7 induces intracellular signaling that inhibits apoptosis of mature dendritic cells. *Blood* **104,** 619–625
12. Sánchez-Sánchez, N., Riol-Blanco, L., and Rodríguez-Fernández, J. L. (2006) The multiple personalities of the chemokine receptor CCR7 in dendritic cells. *J. Immunol.* **176,** 5153–5159
13. Hardie, D. G. (2011) AMP-activated protein kinase: an energy sensor that regulates all aspects of cell function. *Genes Dev.* **25,** 1895–1908
14. Hardie, D. G., Ross, F. A., and Hawley, S. A. (2012) AMPK: a nutrient and energy sensor that maintains energy homeostasis. *Nat. Rev. Mol. Cell Biol.* **13,** 251–262
15. Ido, Y., Carling, D., and Ruderman, N. (2002) Hyperglycemia-induced apoptosis in human umbilical vein endothelial cells: inhibition by the AMP-activated protein kinase activation. *Diabetes* **51,** 159–167
16. Campàs, C., Lopez, J. M., Santidrián, A. F., Barragán, M., Bellosillo, B., Colomer, D., and Gil, J. (2003) Acadesine activates AMPK and induces apoptosis in B-cell chronic lymphocytic leukemia cells but not in T lymphocytes. *Blood* **101,** 3674–3680
17. Woods, A., Vertommen, D., Neumann, D., Turk, R., Bayliss, J., Schlattner, U., Wallimann, T., Carling, D., and Rider, M. H. (2003) Identification of phosphorylation sites in AMP-activated protein kinase (AMPK) for upstream AMPK kinases and study of their roles by site-directed mutagenesis. *J. Biol. Chem.* **278,** 28434–28442
18. Horman, S., Vertommen, D., Heath, R., Neumann, D., Mouton, V., Woods, A., Schlattner, U., Wallimann, T., Carling, D., Hue, L., and Rider, M. H. (2006) Insulin antagonizes ischemia-induced Thr^{172} phosphorylation of AMP-activated protein kinase α-subunits in heart via hierarchical phosphorylation of $Ser^{485}/^{491}$. *J. Biol. Chem.* **281,** 5335–5340
19. Hurley, R. L., Barré, L. K., Wood, S. D., Anderson, K. A., Kemp, B. E., Means, A. R., and Witters, L. A. (2006) Regulation of AMP-activated protein kinase by multisite phosphorylation in response to agents that elevate cellular cAMP. *J. Biol. Chem.* **281,** 36662–36672
20. Pulinilkunnil, T., He, H., Kong, D., Asakura, K., Peroni, O. D., Lee, A., and Kahn, B. B. (2011) Adrenergic regulation of AMP-activated protein kinase in brown adipose tissue *in vivo*. *J. Biol. Chem.* **286,** 8798–9809
21. Dagon, Y., Hur, E., Zheng, B., Wellenstein, K., Cantley, L. C., and Kahn, B. B. (2012) p70S6 kinase phosphorylates AMPK on serine 491 to mediate leptin's effect on food intake. *Cell Metab.* **16,** 104–112
22. Kayampilly, P. P., and Menon, K. M. (2009) Follicle-stimulating hormone inhibits adenosine 5′-monophosphate-activated protein kinase activation and promotes cell proliferation of primary granulosa cells in culture through an Akt-dependent pathway. *Endocrinology* **150,** 929–935
23. Kovacic, S., Soltys, C. L., Barr, A. J., Shiojima, I., Walsh, K., and Dyck, J. R. (2003) Akt activity negatively regulates phosphorylation of AMP-activated protein kinase in the heart. *J. Biol. Chem.* **278,** 39422–39427
24. Zhou, G., Myers, R., Li, Y., Chen, Y., Shen, X., Fenyk-Melody, J., Wu, M., Ventre, J., Doebber, T., Fujii, N., Musi, N., Hirshman, M. F., Goodyear, L. J., and Moller, D. E. (2001) Role of AMP-activated protein kinase in mechanism of metformin action. *J. Clin. Invest.* **108,** 1167–1174
25. Delgado-Martín, C., Escribano, C., Pablos, J. L., Riol-Blanco, L., and Rodríguez-Fernández, J. L. (2011) Chemokine CXCL12 uses CXCR4 and a signaling core formed by bifunctional Akt, extracellular signal-regulated kinase (ERK)1/2, and mammalian target of rapamycin complex 1 (mTORC1) proteins to control chemotaxis and survival simultaneously in mature dendritic cells. *J. Biol. Chem.* **286,** 37222–37236
26. Riol-Blanco L, Delgado-Martín, C., Sánchez-Sánchez, N., Alonso-C, L. M., Gutiérrez-López, M. D., Del Hoyo, G. M., Navarro, J., Sánchez-Madrid, F., Cabañas, C., Sánchez-Mateos, P., and Rodríguez-Fernández, J. L. (2009) Immunological synapse formation inhibits, via NF-κB and FOXO1, the apoptosis of dendritic cells. *Nat. Immunol.* **10,** 753–760
27. Riol-Blanco, L., Sánchez-Sánchez, N., Torres, A., Tejedor, A., Narumiya, S., Corbí, A. L., Sánchez-Mateos, P., and Rodríguez-Fernández, J. L. (2005) The chemokine receptor CCR7 activates in dendritic cells two signaling modules that independently regulate chemotaxis and migratory speed. *J. Immunol.* **174,** 4070–4080
28. Nicoletti, I., Migliorati, G., Pagliacci, M. C., Grignani, F., and Riccardi, C. (1991) A rapid and simple method for measuring thymocyte apoptosis by propidium iodide staining and flow cytometry. *J. Immunol. Methods* **139,** 271–279
29. Riccardi, C., and Nicoletti, I. (2006) Analysis of apoptosis by propidium iodide staining and flow cytometry. *Nat. Protoc.* **1,** 1458–1461
30. Söderberg, O., Gullberg, M., Jarvius, M., Ridderstråle, K., Leuchowius, K. J., Jarvius, J., Wester, K., Hydbring, P., Bahram, F., Larsson, L. G., and Landegren, U. (2006) Direct observation of individual endogenous protein complexes *in situ* by proximity ligation. *Nat. Methods* **3,** 995–1000
31. Gómez-Cabañas, L., Delgado-Martín, C., López-Cotarelo, P., Escribano-Diaz, C., Alonso-C, L. M., Riol-Blanco, L., and Rodríguez-Fernández, J. L. (2014) Detecting apoptosis of leukocytes in mouse lymph nodes. *Nat. Protoc* **9,** 1102–1112
32. Mempel, T. R., Henrickson, S. E., and Von Andrian, U. H. (2004) T-cell priming by dendritic cells in lymph nodes occurs in three distinct phases. *Nature* **427,** 154–159
33. Corton, J. M., Gillespie, J. G., Hawley, S. A., and Hardie, D. G. (1995) 5-Aminoimidazole-4-carboxamide ribonucleoside: a specific method for activating AMP-activated protein kinase in intact cells? *Eur. J. Biochem.* **229,** 558–565
34. Winder, W. W., and Hardie, D. G. (1996) Inactivation of acetyl-CoA carboxylase and activation of AMP-activated protein kinase in muscle during exercise. *Am. J. Physiol.* **270,** E299–E304
35. Gilley, J., Coffer, P. J., and Ham, J. (2003) FOXO transcription factors directly activate *bim* gene expression and promote apoptosis in sympathetic neurons. *J. Cell Biol.* **162,** 613–622
36. Inoki, K., Zhu, T., and Guan, K. L. (2003) TSC2 mediates cellular energy response to control cell growth and survival. *Cell* **115,** 577–590
37. Gwinn, D. M., Shackelford, D. B., Egan, D. F., Mihaylova, M. M., Mery, A., Vasquez, D. S., Turk, B. E., and Shaw, R. J. (2008) AMPK phosphorylation of raptor mediates a metabolic checkpoint. *Mol. Cell* **30,** 214–226
38. Hung, C. M., Garcia-Haro, L., Sparks, C. A., and Guertin, D. A. (2012) mTOR-dependent cell survival mechanisms. *Cold Spring Harb. Perspect. Biol.* **4,** a008771
39. Kamath, A. T., Henri, S., Battye, F., Tough, D. F., and Shortman, K. (2002) Developmental kinetics and lifespan of dendritic cells in mouse lymphoid organs. *Blood* **100,** 1734–1741
40. Lehmann, D. M., Seneviratne, A. M., and Smrcka, A. V. (2008) Small molecule disruption of G protein $\beta\gamma$ subunit signaling inhibits neutrophil chemotaxis and inflammation. *Mol. Pharmacol.* **73,** 410–418
41. Iijima, N., Yanagawa, Y., Clingan, J. M., and Onoé, K. (2005) CCR7-mediated c-Jun N-terminal kinase activation regulates cell migration in mature dendritic cells. *Int. Immunol.* **17,** 1201–1212
42. Beauloye, C., Marsin, A. S., Bertrand, L., Krause, U., Hardie, D. G., Vanoverschelde, J. L., and Hue, L. (2001) Insulin antagonizes AMP-activated protein kinase activation by ischemia or anoxia in rat hearts, without affecting total adenine nucleotides. *FEBS Lett.* **505,** 348–352
43. Bain, J., Plater, L., Elliott, M., Shpiro, N., Hastie, C. J., McLauchlan, H., Klevernic, I., Arthur, J. S., Alessi, D. R., and Cohen, P. (2007) The selectivity of protein kinase inhibitors: a further update. *Biochem. J.* **408,** 297–315
44. Foster, K. G., and Fingar, D. C. (2010) Mammalian target of rapamycin (mTOR): conducing the cellular signaling symphony. *J. Biol. Chem.* **285,**

14071–14077
45. Davies, S. P., Reddy, H., Caivano, M., and Cohen, P. (2000) Specificity and mechanism of action of some commonly used protein kinase inhibitors. *Biochem. J.* **351,** 95–105
46. García-Martínez, J. M., Moran, J., Clarke, R. G., Gray, A., Cosulich, S. C., Chresta, C. M., and Alessi, D. R. (2009) Ku-0063794 is a specific inhibitor of the mammalian target of rapamycin (mTOR). *Biochem. J.* **421,** 29–42
47. Kolch, W. (2005) Coordinating ERK/MAPK signalling through scaffolds and inhibitors. *Nat. Rev. Mol. Cell Biol.* **6,** 827–837
48. Aronov, A. M., Baker, C., Bemis, G. W., Cao, J., Chen, G., Ford, P. J., Germann, U. A., Green, J., Hale, M. R., Jacobs, M., Janetka, J. W., Maltais, F., Martinez-Botella, G., Namchuk, M. N., Straub, J., Tang, Q., and Xie, X. (2007) Flipped out: structure-guided design of selective pyrazolylpyrrole ERK inhibitors. *J. Med. Chem.* **50,** 1280–1287
49. Hatzivassiliou, G., Liu, B., O'Brien, C., Spoerke, J. M., Hoeflich, K. P., Haverty, P. M., Soriano, R., Forrest, W. F., Heldens, S., Chen, H., Toy, K., Ha, C., Zhou, W., Song, K., Friedman, L. S., Amler, L. C., Hampton, G. M., Moffat, J., Belvin, M., and Lackner, M. R. (2012) ERK inhibition overcomes acquired resistance to MEK inhibitors. *Mol. Cancer Ther.* **11,** 1143–1154
50. Ohori, M., Kinoshita, T., Okubo, M., Sato, K., Yamazaki, A., Arakawa, H., Nishimura, S., Inamura, N., Nakajima, H., Neya, M., Miyake, H., and Fujii, T. (2005) Identification of a selective ERK inhibitor and structural determination of the inhibitor-ERK2 complex. *Biochem. Biophys. Res. Commun.* **336,** 357–363
51. Fredriksson, S., Gullberg, M., Jarvius, J., Olsson, C., Pietras, K., Gústafsdóttir, S. M., Ostman, A., and Landegren, U. (2002) Protein detection using proximity-dependent DNA ligation assays. *Nat. Biotechnol.* **20,** 473–477
52. Weibrecht, I., Leuchowius, K. J., Clausson, C. M., Conze, T., Jarvius, M., Howell, W. M., Kamali-Moghaddam, M., and Söderberg, O. (2010) Proximity ligation assays: a recent addition to the proteomics toolbox. *Expert Rev. Proteomics* **7,** 401–409
53. Greer, E. L., Oskoui, P. R., Banko, M. R., Maniar, J. M., Gygi, M. P., Gygi, S. P., and Brunet, A. (2007) The energy sensor AMP-activated protein kinase directly regulates the mammalian FOXO3 transcription factor. *J. Biol. Chem.* **282,** 30107–30119
54. Mihaylova, M. M., and Shaw, R. J. (2011) The AMPK signalling pathway coordinates cell growth, autophagy and metabolism. *Nat. Cell Biol.* **13,** 1016–1023
55. Du, J., Guan, T., Zhang, H., Xia, Y., Liu, F., and Zhang, Y. (2008) Inhibitory crosstalk between ERK and AMPK in the growth and proliferation of cardiac fibroblasts. *Biochem. Biophys. Res. Commun.* **368,** 402–407
56. Hwang, S. L., Jeong, Y. T., Li, X., Kim, Y. D., Lu, Y., Chang, Y. C., Lee, I. K., and Chang, H. W. (2013) Inhibitory cross-talk between the AMPK and ERK pathways mediates endoplasmic reticulum stress-induced insulin resistance in skeletal muscle. *Br. J. Pharmacol.* **169,** 69–81
57. Shen, C. H., Yuan, P., Perez-Lorenzo, R., Zhang, Y., Lee, S. X., Ou, Y., Asara, J. M., Cantley, L. C., and Zheng, B. (2013) Phosphorylation of BRAF by AMPK impairs BRAF-KSR1 association and cell proliferation. *Mol. Cell* **52,** 161–172
58. Zhu, B., Zhou, Y., Xu, F., Shuai, J., Li, X., and Fang, W. (2012) Porcine circovirus type 2 induces autophagy via the AMPK/ERK/TSC2/mTOR signaling pathway in PK-15 cells. *J. Virol.* **86,** 12003–12012

CXCL12 Regulates through JAK1 and JAK2 Formation of Productive Immunological Synapses

Graciela Cascio,* Noa B. Martín-Cófreces,† José Miguel Rodríguez-Frade,* Pilar López-Cotarelo,‡,§ Gabriel Criado,¶ José L. Pablos,¶ José Luis Rodríguez-Fernández,‡,§ Francisco Sánchez-Madrid,† and Mario Mellado*

The adaptive immune response requires interaction between T cells and APC to form a specialized structure termed the immune synapse (IS). Although the TCR is essential for IS organization, other factors such as chemokines participate in this process. In this study, we show that the chemokine CXCL12-mediated signaling contributes to correct IS organization and therefore influences T cell activation. CXCR4 downregulation or blockade on T cells caused defective actin polymerization at the contact site with APC, altered microtubule-organizing center polarization and the IS structure, and reduced T cell/APC contact duration. T cell activation was thus inhibited, as shown by reduced expression of CD25 and CD69 markers and of IL-2 mRNA levels. The results indicate that, through Gi and JAK1 and 2 kinases activation, CXCL12 signaling cooperates to build the IS and to maintain adhesive contacts between APC and T cells, required for continuous TCR signaling. ***The Journal of Immunology*****, 2015, 194: 5509–5519.**

Adaptive immune responses are initiated through interaction between naive Ag-specific T cells and Ag-bearing dendritic cells (DC) in the lymph node. A specialized structure, termed the immune synapse (IS), is formed at the T cell–APC contact site. This occurs immediately after TCR activation and is implicated in the induction of T cell proliferation, cytokine production, and lytic granule release (1). The IS is characterized by protein segregation, signaling compartmentalization, and bidirectional information exchange through soluble and membrane-bound transmitters. The TCR and associated proteins congregate in the central area (central supramolecular activation cluster; cSMAC), whereas integrins reorganize in a surrounding external ring called the peripheral SMAC (pSMAC) (2). IS formation also requires participation of the actin cytoskeleton, which forms a ring in the pSMAC.

Although TCRs are essential for IS organization, a number of other surface receptors such as adhesion molecules and costimulatory receptors also have important roles in SMAC formation and in cell cross-talk. Interaction between LFA-1 and the ICAMs precedes mature synapse development and facilitates signaling events that promote T cell activation (3, 4).

Chemokine receptors are also recruited to the IS (5, 6), which suggests that chemokines can help T cells to interpret the context of Ag presentation. During T cell activation, the chemokines CCL5 and CXCL12 enhance T cell proliferation and cytokine production (5, 7, 8), which indicates that chemokines might act as soluble immunotransmitters at the IS and help to activate T cells. Signals relayed from the active TCR trigger integrin activation at the IS, and there is evidence that chemokines cooperate in this process. Chemokine-mediated integrin activation is essential for cell extravasation (9, 10), and chemokines in the IS can reinforce T cell–APC attraction and prevent premature separation, thus facilitating T cell activation (11, 12). Chemokine-induced LFA-1 activation leads to rapid recruitment of microtubule-organizing center (MTOC) and mitochondria to the APC, which amplifies TCR-induced Ca^{2+} signaling at the nascent immunological synapse (13).

Regulation of integrin activation depends on a wide variety of signaling proteins (14). Signaling through small GTPases is currently the best-studied mechanism of chemokine-induced integrin activation (15, 16). Recent evidence nonetheless indicates that JAKs also participate in the control of chemokine-induced integrin activation (10, 17) and might modulate the activation hierarchy of the small GTPases.

Using CXCL12 and its receptor CXCR4 as a model, we assessed the precise role of chemokine-mediated signaling in T cell activation during IS formation. After downregulation of CXCR4 expression, after treatment with the CXCR4-specific binding site inhibitor AMD3100 or pertussis toxin (PTx), or after drug inhibition or

*Departamento de Inmunología y Oncología, Centro Nacional de Biotecnología/Consejo Superior de Investigaciones Cientificas, E-28049 Madrid, Spain; †Servicio de Inmunología, Instituto de Investigación Sanitaria Hospital Universitario de la Princesa, Universidad Autónoma de Madrid, E-28006 Madrid, Spain; ‡Departamento de Biología Vascular e Inflamación, Fundación Centro Nacional de Investigaciones Cardiovasculares-Carlos III, E-28029 Madrid, Spain; §Centro de Investigaciones Biológicas/Consejo Superior de Investigaciones Cientificas, E-28040 Madrid, Spain; and ¶Grupo de Enfermedades Inflamatorias y Autoinmunes, Instituto de Investigación Sanitaria Hospital 12 de Octubre, E-28041 Madrid, Spain

Received for publication September 23, 2014. Accepted for publication March 23, 2015.

This work was supported in part by the Ministerio de Ciencia e Innovación (Grant SAF 2011-27370), the Redes Telemáticas de Investigación en Red Program (Grants RD12/0009/009, RD12/0009/001, and R12/0009/006; Red de Inflamación y Enfermedades Reumáticas and Grant RD12/0042/0056; Red de Investigación Cardiovascular), and the Gobierno Regional de Madrid (Grant S2010/BMD-2350; Rheumatoid Arthritis: Physiopathology Mechanisms). Optical microscopy was conducted at the Unidad de Microscopía Confocal (Centro Nacional de Biotecnología/Consejo Superior de Investigaciones Cientificas) at the Hospital de la Princesa and at the Unidad de microscopía y dinámica de la imagen (Madrid, Spain), which is funded by the Ministerio de Ciencia e Innovación de España and by the Pro Centro Nacional de Investigaciones Cardiovasculares Foundation.

Address correspondence and reprint requests to Dr. Mario Mellado, Departamento de Inmunología y Oncología, Centro Nacional de Biotecnología/Consejo Superior de Investigaciones Cientificas, Darwin 3, Cantoblanco, E-28049 Madrid, Spain. E-mail address: mmellado@cnb.csic.es

The online version of this article contains supplemental material.

Abbreviations used in this article: BM-DC, bone marrow–derived DC; cSMAC, central supramolecular activation cluster; DC, dendritic cell; GAG, glycosaminoglycan; IS, immune synapse; MFI, mean fluorescence intensity; MTOC, microtubule-organizing center; pSMAC, peripheral SMAC; PTx, pertussis toxin; siRNA, small interfering RNA; siTyk2, siRNA pool for Tyk2; wt, wild-type.

downregulation of JAK1/2 expression, OT-II CD4$^+$ T cells showed defective IS formation when cocultured with OVA peptide–loaded bone marrow–derived DC (BM-DC). These T cells also showed reduced F-actin accumulation as well as defects in MTOC polarization to the contact site and in IS formation. Time-lapse videomicroscopy analysis showed significantly reduced mean contact duration, reflected as T cell activation defects. Our results indicate that whereas T cell–APC interactions are Ag dependent (18, 19), these Ag-specific interactions coincide with Ag-independent, chemokine-promoted adhesive contacts between these cells, which help to build a productive immune synapse.

Materials and Methods

Mice

Male and female 3- to 5-mo-old C57BL/6 mice were purchased from Harlan Laboratories. OVA-specific TCR-transgenic mice (OT-II) were donated by Dr. C. Ardavín (Centro Nacional de Biotecnología, Madrid, Spain) and Cxcl12^{Gagtm} mice by Dr. F. Arenzana (Institut Pasteur, Paris, France). The phenotype of OT-II mouse offspring was confirmed by flow cytometry using anti–Vα2 TCR Ab (BD Pharmingen). Cxcl12$^{Gagtm/wt}$ and Cxcl12$^{Gagtm/Gagtm}$ mice were genotyped by PCR amplification on genomic DNA with specific primers (20). Mice were housed in pathogen-free conditions at the animal facility at the Centro Nacional de Biotecnología/Consejo Superior de Investigaciones Cientificas. All animal experiments were approved by the appropriate ethics committees and carried out according to national and European Union guidelines.

Abs and reagents

For Western blot assays, we used the following Abs: anti-JAK1, -Tyk2 (Santa Cruz Biotechnology), -JAK2 (Upstate Biotechnology), –Vav-1 mAb (Cell Signaling Technology), –ZAP-70 mAb (BD Pharmingen), –P-Tyr (Promega), –β-tubulin mAb, and -CXCL12 mAb (Sigma-Aldrich). HRP-labeled anti-mouse and -rabbit Ig (DakoCytomation) were used as secondary Abs. Cell purity was assessed by flow cytometry using anti–B220-FITC and –Gr1-PECy7 (Beckman Coulter), –CD4-PECy5 and –CD3-APC mAb (BioLegend), and –CD11c-PE (eBioscience). Surface marker expression was determined by flow cytometry using anti–CD69-PE and –CD25-PE mAb (BioLegend) and anti–CXCR4-biotin mAb (BD Pharmingen). CXCL12 was purchased from PeproTech. CellTrace CFSE and seminaphtharhodafluor-1 were obtained from Molecular Probes. Ruxolitinib and tofacitinib were donated by Prof. P. Cohen (MRC Protein Phosphorylation Unit, University of Dundee, Dundee, Scotland).

Cell culture and small interfering RNA nucleofection

CD4$^+$ naive T cells were obtained from OT-II mouse spleen and lymph nodes and purified by negative selection with a mouse T cell negative isolation kit (MACS; Miltenyi Biotec); T cell purity was routinely >97%. Freshly isolated murine OT-II CD4$^+$ T cells were nucleofected (mouse T cell Nucleofector kit; Amaxa) with a mixture of four individual small interfering RNA (siRNA) duplexes (ON-TARGETplus SMARTpool siRNA; Dharmacon) for the target sequences on JAK1 (5′-GAAAAUGAAUUGAGUCGAU-3′; 5′-GAAAUCACCCACAUUGUAA-3′; 5′-CGCAUGAGGUUC UACUUUA-3′; 5′-GCACAGGGACAGUAUGAUU-3′), JAK2 (5′-AAUAGGAGACUUCGGAUUA-3′; 5′-GAAUUGUAACUGUCCAUAA-3′; 5′-GAACUUAGCUCAUUAAAAG-3′; 5′-GAAUUUAUGCGAA UGAUUG-3′), Tyk2 (5′-UGACAGAAUUCGUAGAACA-3′; 5′-GAACCUCUAUUUUCGAAUG-3′; 5′-CAAGGACCAUGUGUAUGA-3′; 5′-CCUGAUGGAUCCGUUUGUA-3′), and CXCR4 (5′-GAACCGA UCAGUGUGAGUA-3′; 5′-GUGUAAGGCUGUCCAUAUC-3′; 5′-GUGUUUCAAUUCCAGCAUA-3′; 5′-AAACGUCCAUUUCAAUAGG-3′) or siRNA control (ON-TARGETplus Nontargeting Pool D-001810-10; Dharmacon) to ensure silencing specificity. Nucleofection efficiency was controlled with fluorescence-labeled siRNA duplex siGLO Green indicator (Dharmacon) as a positive control. Nucleofected naive OT-II CD4$^+$ T cells were incubated (24 h, 37°C) in the medium supplied with the Nucleofector kit and murine IL-7 (25 U/ml; Cell Signaling Technology).

BM-DC differentiation

BM-DC were obtained from bone marrow cell suspensions treated with erythrocyte lysis buffer and then cultured in 150-mm petri dishes in complete RPMI 1640 medium supplemented with 10% FCS and 20 ng/ml rGM-CSF (PeproTech) (21). Immature BM-DC were collected at day 8, and purity was evaluated by flow cytometry using anti–CD11c-FITC and –MHCII-PE Ab (BD Pharmingen). Batches with >95% purity were used for maturation with LPS (1 μg/ml, 12 h, 37°C).

Flow cytometry analysis

Cells were plated in V-bottom 96-well plates (2.5 × 10^5 cells/well) and incubated (30 min, 4°C) with 50 μl/well anti–CD3-allophycocyanin and –CD25-PE or anti–CD69-PE (all from BioLegend) for determination of T cell activation. When needed, anti-CXCL12 mAb, followed by goat anti-mouse IgG-Cy3 or anti–CXCR4-Biotin mAb, followed of avidin-PE were used. Cell-bound fluorescence was determined in a Gallios flow cytometer (Beckman Coulter).

In vitro induction of IS formation between DC and CD4 T cells

IS formation between mouse BM-DC and OT-II CD4$^+$ T cells was induced as reported previously (22, 23). Briefly, matured BM-DC (1 μg/ml LPS, 12 h, 37°C) were loaded with OVA$_{323–339}$-peptide (5 μM, 30 min, 37°C; GenScript) and mixed in complete medium (RPMI 1640 medium, 10% FCS) with CD4$^+$ T cells (1:5 DC:CD4$^+$ T cells). Cells were centrifuged (120 × *g*, 2 min) in a conical tube and incubated in complete medium (15–30 min, 37°C) to foster IS formation. When necessary, T cells were pretreated with PTx (0.2 μg/ml, 120 min, 37°C; Sigma-Aldrich), AMD3100 (10 μM, 30 min, 37°C; Sigma-Aldrich), ruxolitinib (1 μM, 60 min, 37°C), or tofacitinib (1 μM, 60 min, 37°C) before mixing with BM-DC. For AMD3100, ruxolitinib, and tofacitinib treatments, drug levels were maintained throughout the experiment.

Quantitative image analysis of conjugate formation and F-actin accumulation

Conjugation was scored visually by counting under a confocal microscope, with at least 50 random T cells scored as conjugates only if they contacted no more than one CMAC-labeled BM-DC and no other T cell contacted the scored T cell. F-Actin accumulation at the IS was detected by staining with phalloidin–Alexa 488, and images were analyzed with ImageJ software (National Institutes of Health, Bethesda, MD). Using region of interest of the same area for all measurements, we quantified the signal generated by 1) the BM-DC/T cell contact area (IS), 2) the area of BM-DC membrane not in contact with the T cell (B), 3) an area of the T cell membrane not in contact with the BM-DC (T), and 4) the background. We subtracted the background signal from other measurements, then measured F-actin accumulation at the IS relative to the rest of the T cell using the formula (IS − B)/T. Results were expressed as the percentage of T cells with accumulated F-actin at the contact with DC. Statistical significance was calculated using a two-tailed Student *t* test.

Analysis of IS architecture

Cell conjugates were observed under a confocal laser scanning unit (TCS SP5; Leica) attached to an inverted epifluorescence microscope (DMI6000; Leica) fitted with an HCX PL APO ×40/1.40-0.6 oil objective. Images were acquired and processed with confocal software (LCS; Leica) or WCIF ImageJ (http://rsbweb.nih.gov/ij/) to obtain a three-dimensional analysis and maximal projections of T cell–bead contact. Figures were composed with Adobe Photoshop.

Analysis of CD3ζ, protein kinase Cθ, talin, and CXCR4 accumulation

OT-II CD4$^+$ T cells were nucleofected as above with siRNA pools for JAK1+JAK2 (siJAK1,2) or siRNA pool control (Dharmacon). These cells, alone or treated with AMD3100 (10 μM, 30 min, 37°C) or PTx (0.2 μg/ml, 120 min, 37°C), were conjugated to anti-CD3–coated latex beads or to isotype control–coated latex beads (Sigma-Aldrich) for 20 min, alone or with CXCL12 (50 nM). Cells were then fixed and stained with appropriate Abs, and the IS was analyzed by confocal imaging. We assumed that background signal is homogeneous in the latex beads. To quantify the fluorescence distribution ratio, individual IS were processed with the "Synapse Measures" plugin for ImageJ (http://rsbweb.nih.gov/ij/) (for a detailed description of Synapse Measures, including the algorithms used, see Ref. 24). To analyze talin and CXCR4 distribution at the IS-like complex, three-dimensional reconstructions of the area were generated with the Leica software. Mean fluorescence intensity (MFI) per area was calculated with a Matlab routine for pSMAC and cSMAC regions from three independent experiments (at least 24 cells were measured per experimental condition). Mean values from the pSMAC/cSMAC ratio of MFI per area were calculated.

T cell activation and proliferation

OT-II CD4$^+$ T cells were labeled with CellTrace Violet (0.5 μM, 30 min, 37°C; Molecular Probes) and added to plates containing OVA peptide–loaded BM-DC (3 × 10^4 DC/6 × 10^4 T cells). Cells were

cocultured in RPMI 1640 medium with 10% FCS (24, 48, or 72 h), and proliferation was determined by flow cytometry using dye dilution evaluation in a Gallios flow cytometer (Beckman Coulter). The percentage of dividing cells was calculated using Flowjo (Tree Star). T cell activation was evaluated in parallel at indicated time points using anti–CD3-allophycocyanin and –CD25-PE or anti–CD69-PE mAb in flow cytometry, as above.

Immunoprecipitation and Western blot analysis

CXCL12 (50 nM)-activated OT-II CD4$^+$ T cells (5×10^6) were lysed in 200 μl detergent buffer (1% Nonidet P-40, 50 mM Tris-HCl [pH 8], 150 mM NaCl, 0.5 mM EDTA, 10 mM sodium pyrophosphate, 1 mM PMSF, 10 μg/ml aprotinin, 10 μg/ml leupeptin, and 10 mM sodium orthovanadate; 30 min, 4˚C) and immunoprecipitated using anti-PTyr Ab (1 μg/sample; Promega), and cell extracts were analyzed in Western blot, as described previously (25). When needed, densitometry analyses were performed using ImageJ.

Rho GTPase activation assays

Rho GTPase activity was determined in T cell lysates using RhoA activation assay kits (BK124; Cytoskeleton). T cells were stimulated with CXCL12 (50 nM; various times), and the reaction was terminated by adding ice-cold PBS and centrifugation ($470 \times g$, 5 min, 4˚C); lysis and GTPase activity were measured following G-LISA kit protocols.

Quantitative real-time PCR

IL-2 mRNA levels were analyzed by quantitative real-time PCR with specific primers. Cells (3×10^5) were lysed, and RNA was extracted using the RNeasy micro kit (Qiagen) with DNase treatment to digest residual genomic DNA. Equal RNA amounts were reverse transcribed using a reverse transcription system (Promega). cDNA was determined by semiquantitative real-time PCR with the LightCycler480 SybrGreen I Master kit (Roche Diagnostics) using specific primer pairs (IL-2, 5′-CACTTCAAGCTCTACAGCGGA-3′ and 5′-AAAATTTGAAGGTGAGCATCC-3′; β-actin, 5′-GGCACCACACCTTCT-ACAATG-3′ and 5′-TGGATGGCTACGTACATGG CTG-3′). Samples were

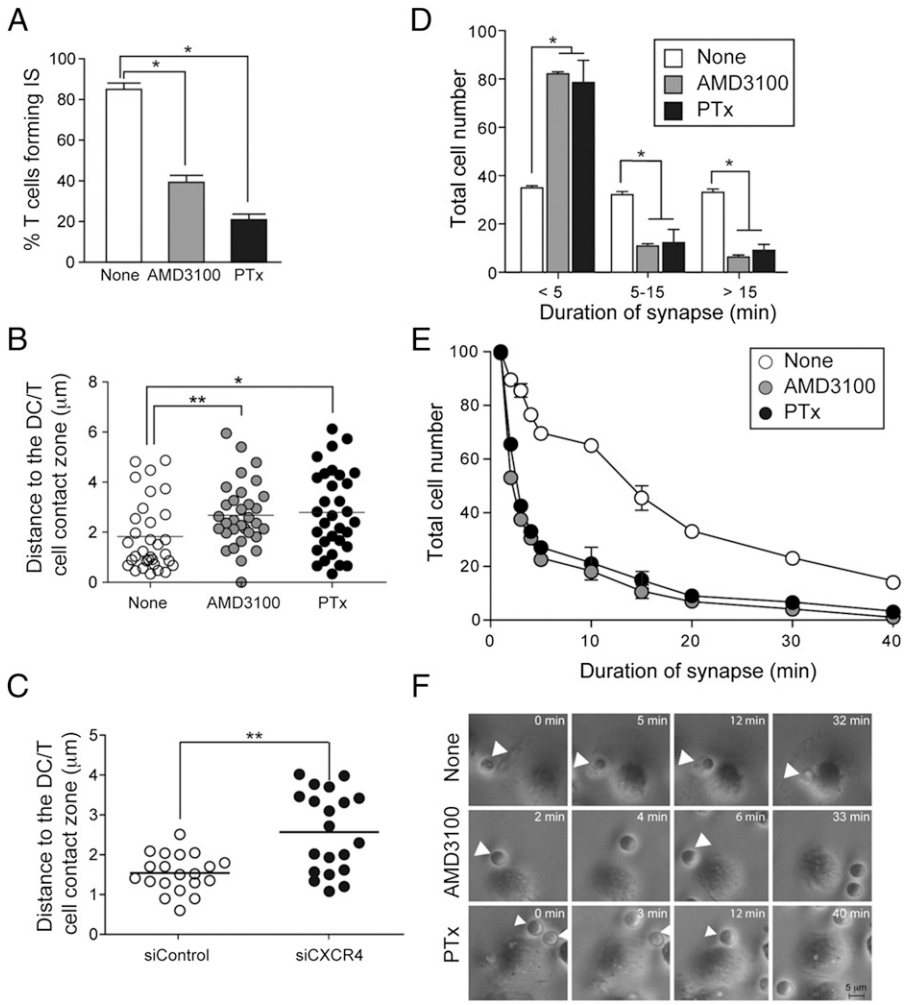

FIGURE 1. CXCR4 blockade alters IS formation. (**A**) Conjugates of OT-II CD4$^+$ T cells, alone or treated with AMD3100 or PTx and OVA peptide–pulsed BM-DC, were paraformaldehyde fixed. F-Actin polymerization was detected using phalloidin–Alexa 488 and quantified, and results were expressed as the percentage of T cells showing accumulated protein at the cell–cell contact site. *$p \leq 0.05$, nonparametric test. (**B**) Conjugates as in (A) were stained with anti–γ-tubulin mAb followed by Cy3-goat anti-mouse IgG Ab. Quantitation of MTOC translocation measured as the distance (in micrometers) of the MTOC to the DC/T cell contact zone. Data shown are pooled from two independent experiments. *$p \leq 0.05$, **$p \leq 0.01$, nonparametric test. (**C**) Conjugates of siControl or siCXCR4 OT-II CD4$^+$ T cells with OVA peptide–pulsed BM-DC were paraformaldehyde fixed, stained with anti–γ-tubulin, then quantified, and expressed as in (B). Data shown are pooled from three independent experiments. **$p \leq 0.01$, nonparametric test. (**D**) BM-DC were incubated with OVA peptide and seeded onto fibronectin-coated coverslips. OT-II CD4$^+$ T cells, alone or treated with AMD3100 or PTx, were added to the chambers. Contacts between T cells and DC were monitored by time-lapse videomicroscopy (40 min), and the contact times of individual DC–T cell pairs were measured. T cell–DC interactions were classified into three categories based on duration of the interaction: short (<5 min), medium (5–15 min), and long (>15 min). Data pooled from three independent experiments shown the percentage of each category (mean ± SD). *$p \leq 0.05$, nonparametric test. (**E**) Cells as in (D) were monitored by time-lapse videomicroscopy and 200 BM-DC/OT-II CD4$^+$ T conjugates for each condition monitored for 40 min. A representative experiment is shown of three performed. (**F**) Representative images of distinct time frames from the video recordings (Supplemental Videos 1–3). Arrows indicate T cell/BM-DC contacts. Scale bar, 5 μm.

analyzed in duplicate and normalized to β-actin using ABI 7900HT SDS 2.3 software.

Immunofluorescence

The conjugates (5×10^4 OVA peptide–loaded BM-DC/2.5×10^5 OT-II $CD4^+$ T cells) were plated on coverslips precoated with poly-L-lysine (20 μg/ml, overnight, 4˚C; Sigma-Aldrich) and cultured (30 min, 37˚C). Cells were washed in cold TBS and fixed with 2% paraformaldehyde (10 min, 37˚C) and then permeablized with 0.2% Triton X-100 in TBS (10 min, 37˚C). After washing with TBS with 1% BSA, 0.1% goat serum, and 0.05% Tween 20 to avoid nonspecific binding, cells were stained with anti-Ptyr mAb (Millipore) or –γ-tubulin (Sigma-Aldrich) (60 min, 37˚C), followed by Cy3-goat anti-mouse IgG (3.5 μg/ml, 45 min, 37˚C; Jackson ImmunoResearch Laboratories). When necessary, cells were stained with Alexa 488–phalloidin (60 min, 37˚C; Sigma-Aldrich). Coverslips were mounted on slides with Fluoromount G medium (Southern Biotechnology Associates), and fluorescence was evaluated using the Olympus IX81 microscope with a PLAPON 40 × 03 objective (aperture 1:40) and FV10-ASW 1.6 software. When needed, MFI was determined using ImageJ64 software; staining intensity is shown as a percentage of total MFI versus MFI at the cell–cell contact site.

Time-lapse videomicroscopy

OVA peptide–loaded BM-DC (5×10^4 cells) cells were added to fibronectin-coated glass chambers (10 μg/ml, 4˚C, overnight; Nunc Lab-Tek), placed on a 37˚C stage of a laser-scanning fluorescence microscope (AMI 6000B; Leica), and allowed to settle (60 min). We then added 2.5×10^5 OT-II $CD4^+$ T cells. Images were acquired every 30 s before, during, and after T cell addition. Videos were analyzed with image analysis software (Adobe Photoshop CS5).

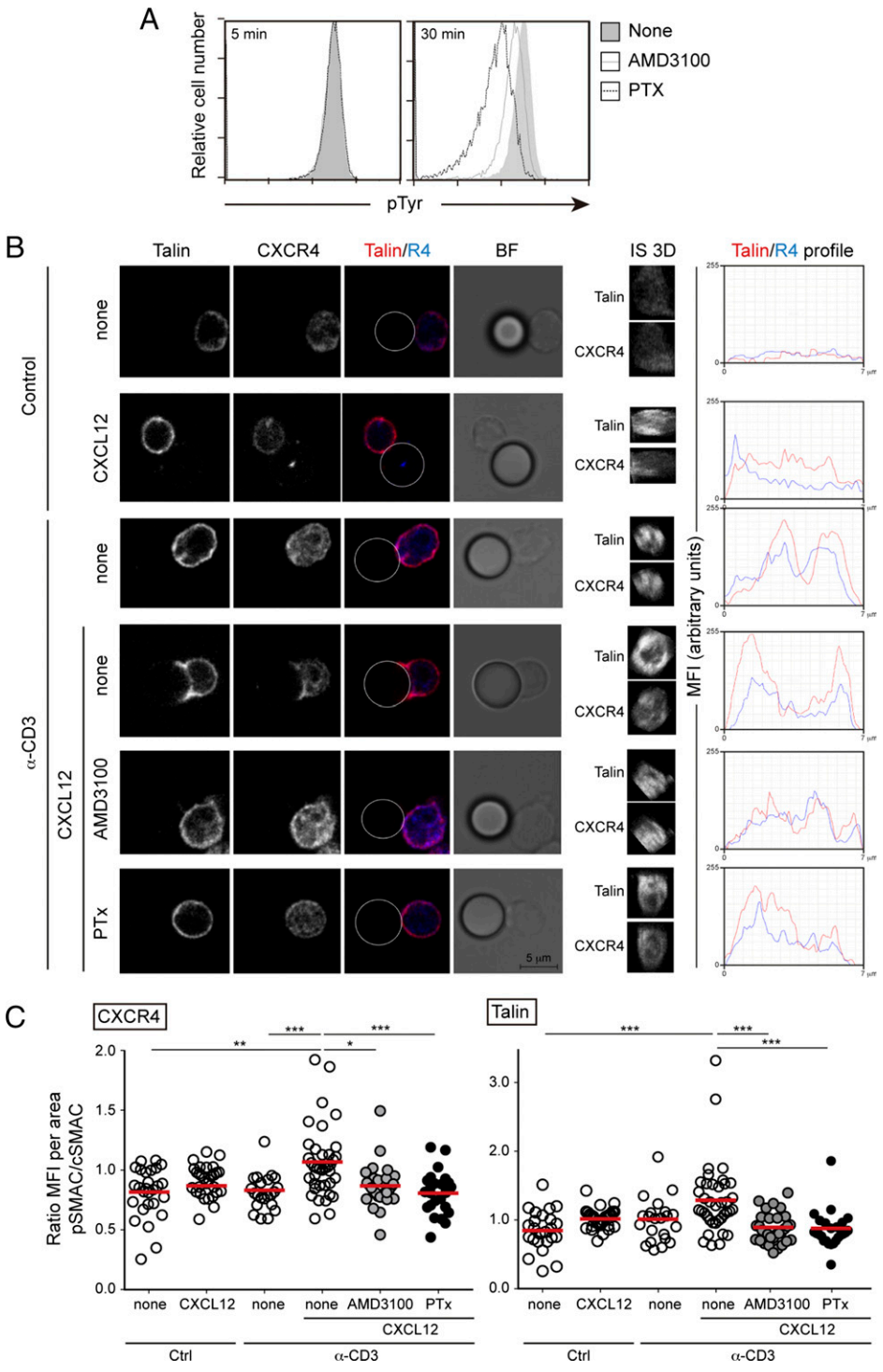

FIGURE 2. CXCR4 inhibition triggers defective IS organization. (**A**) Conjugates of OT-II $CD4^+$ T cells, alone or treated with AMD3100 or PTx and OVA peptide–pulsed BM-DC, were paraformaldehyde fixed, permeabilized, stained with anti–CD4-FITC and -PTyr mAb, followed by Cy3-goat anti-mouse IgG Ab and evaluated by flow cytometry. The figure shows Ptyr staining on $CD4^+$ T cells. A representative experiment is shown of four performed. (**B**) OT-II $CD4^+$ T cells were isolated and pretreated with AMD3100 or PTx or untreated. Cells were conjugated to anti-CD3–coated beads (CD3) or control isotype (Ctrl); where indicated, CXCL12 was added at the initiation of bead conjugation. Cells were allowed to conjugate (30 min), fixed, and stained for the indicated proteins. *Left*, A single slice from a confocal Z-stack. *Right*, Three-dimensional reconstruction of the IS-like area for talin and CXCR4. Histograms show protein distribution in the merge image of the IS-like reconstruction (red, talin; blue, CXCR4). (**C**) Ratio of MFI per area calculated at the pSMAC relative to the cSMAC for CXCR4 and talin at the IS-like area. MFI per area was calculated using a Matlab routine for image analysis. Data were analyzed with a one-way ANOVA with a Kruskal–Wallis test, followed by Dunn's posttest. Means are also shown. $*p \leq 0.05$, $**p \leq 0.01$, $***p \leq 0.001$.

Statistical analysis

Statistical analysis was performed with Prism software (GraphPad) using the non-parametric Student *t* test. Multiple comparisons were analyzed with a one-way ANOVA, followed by the Tukey posttest or Dunn's posttest, where needed.

Results

CXCR4 inhibition impairs IS formation

CXCR4 is recruited to the pSMAC at the IS (6), and its ligand, CXCL12, is secreted by bone marrow stroma cells and endothelial cells (26), among other cell types (27, 28). Using FACS and immunofluorescence techniques, we detected CXCL12 bound to the surface of BM-DC but not on naive OT-II T cells (Supplemental Fig. 1A). To assess the effect of CXCR4/CXCL12 blockade on IS formation, naive OT-II CD4$^+$ T cells were pretreated with AMD3100 (10 μM, 30 min, 37˚C) or PTx (0.2 μg/ml, 120 min, 37˚C) and used to form conjugates with OVA peptide–loaded BM-DC (ratio 5:1, 30 min, 37˚C). Phalloidin staining showed that whereas 87.5 ± 3.5% of untreated OT-II CD4$^+$ T cells showed cytoskeletal rearrangement at the IS contact zone, F-actin accumulation was greatly reduced in T cells treated with AMD3100 (39.7 ± 2.5%) or PTx (20.3 ± 1.5%) (Fig. 1A). Because MTOC translocation toward the contact zone is a hallmark of IS formation (29), we tested for γ-tubulin in the BM-DC/T cell conjugates (Supplemental Fig. 1B). Quantitative analysis showed that AMD3100 or PTx treatment significantly reduced MTOC translocation (Fig. 1B).

To confirm these observations, we used nucleofected OT-II CD4$^+$ T cells with an siRNA pool for CXCR4 (siCXCR4) or control (siControl). Flow cytometry analysis using anti-CXCR4 mAb showed a marked reduction in CXCR4 expression at the cell surface (~85%; Supplemental Fig. 1C). We thus formed conjugates using siCXCR4 and siControl cells and OVA peptide–loaded BM-DC and stained for γ-tubulin as above. The results indicated significant alteration in MTOC translocation to the contact zone in CXCR4-deficient cells (Fig. 1C).

We next determined the effect of AMD3100 and PTx treatments on BM-DC/T cell conjugation dynamics time-lapse videomicroscopy. The majority of untreated T cells formed medium-lived (5–15 min) and long-lived (>15 min) contacts, whereas drug treatments significantly increased the proportion of short-lived (<5 min) contacts (Fig. 1D). Mean contact duration of untreated OT-II CD4$^+$ T cells with BM-DC (14 ± 1 min) was significantly longer than with AMD3100- or PTx-treated T cells (4 ± 0.3 and 4.5 ± 0.2 min, respectively; Fig. 1E, 1F, Supplemental Videos 1–3).

CXCR4 blockade promotes defective IS function

TCR engagement induces phosphorylation and relocation of specific signaling proteins that interact with the TCR-CD3 complex

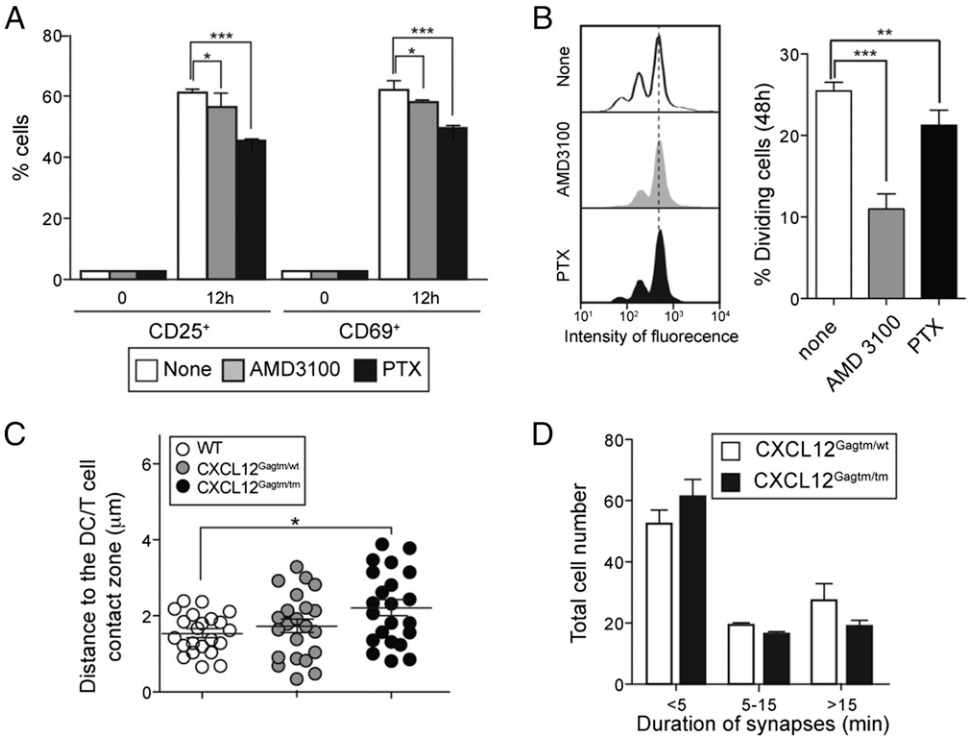

FIGURE 3. CXCR4 inhibition promotes defective T cell activation. (**A**) Conjugates of OT-II CD4$^+$ T cells, alone or treated with AMD3100 or PTx and OVA peptide–pulsed BM-DC, were cultured (12 h, 37˚C), costained with anti–CD3-APC and with anti–CD25-PE or –CD69-PE mAb and evaluated by flow cytometry. Results are shown as a percentage of T cells (mean ± SD). Data are pooled from two independent experiments. *$p \leq 0.05$, ***$p \leq 0.001$, nonparametric test. (**B**) OT-II CD4$^+$ T cells were labeled with CellTrace violet and then untreated or treated with AMD3100 or PTx before forming conjugates with OVA peptide–pulsed BM-DC. Conjugates were cultured (48 h, 37˚C) and T cell proliferation determined following dye dilution by flow cytometry (*left*). Quantitative analysis of T cell proliferation using data from three independent experiments (*right*). Results are shown as a percentage of T cells (mean ± SD). **$p \leq 0.01$, ***$p \leq 0.001$, nonparametric test. (**C**) Conjugates of OT-II CD4$^+$ T cells with OVA peptide–pulsed BM-DC obtained from wt, Cxcl12$^{Gagtm/wt}$, or Cxcl12$^{Gagtm/Gagtm}$ mice were fixed, permeabilized, and stained with anti–γ-tubulin mAb, followed by Cy3-goat anti-mouse IgG Ab. The figure shows the quantitation of MTOC translocation measured as in Fig. 1B. Data are pooled from two independent experiments. *$p \leq 0.05$, nonparametric test. (**D**) BM-DC as in (C) were incubated with OVA peptide and seeded onto fibronectin-coated coverslips. OT-II CD4$^+$ T cells were added to chambers. Contacts between T cells and DC were monitored by time-lapse videomicroscopy (40 min), and contact times of individual DC–T cell pairs were measured. DC–T cell interactions were classified as in Fig. 1D. Data pooled from two independent experiments shown as the percentage for each category (mean ± SD).

(30). To assess the role of chemokines in DC-triggered signaling events during IS formation, we analyzed phosphotyrosine staining as a T cell activation marker. Untreated or AMD3100- or PTx-treated naive OT-II CD4$^+$ T cells were incubated with OVA peptide–loaded BM-DC for various times; cells were fixed, permeabilized, stained for PTyr, and evaluated by FACS. Treatment with either drug clearly reduced anti-PTyr staining in CD4$^+$ T cells (Fig. 2A).

We then analyzed in detail the contribution of CXCL12 to the IS structure. OT-II CD4$^+$ T cells were conjugated with anti–CD3-coated latex beads (31), alone or in the presence of soluble CXCL12 (50 nM), and cells were stained for specific IS markers (CD3ζ for cSMAC; talin and CXCR4 for pSMAC) (Fig. 2B, 2C, Supplemental Fig. 1D). We found partial colocalization of talin and CXCR4 in a ring-shaped structure, as shown in three-dimensional reconstitution (Fig. 2B); this colocalization was reinforced by CXCL12 addition, as indicated by the coincidence of red and blue lines in the histograms in Fig. 2B. Talin and CXCR4 redistribution at the pSMAC was clearly increased in the presence of CXCL12 (pSMAC/cSMAC ratio $>$ 1; graphs in Fig. 2C). CXCL12 treatment similarly increased the anti–CD3-triggered IS localization ratio of CD3ζ (Supplemental Fig. 1D). These CXCL12-mediated effects were reduced by treatment of OT-II CD4$^+$ T cells with AMD3100 or PTx (Fig. 2B, 2C, Supplemental Fig. 1D).

We compared the in vitro activation of drug-treated CD4$^+$ cells in the OVA peptide–loaded BM-DC system. Flow cytometry analysis showed that AMD3100 and PTx treatment reduced the stimulatory effect on both CD25 and CD69 expression markers (Fig. 3A, Supplemental Fig. 2A). We therefore used untreated and AMD3100- or PTx-treated live cell tracker–labeled OT-II CD4$^+$ T cells to form conjugates with OVA peptide–loaded BM-DC and determined their ability to proliferate. Flow cytometry detection of cell tracker dilution after 48-h coculture showed lower proliferation of drug-treated T cells (Fig. 3B). These results indicate that CXCL12 binding to CXCR4 in T cells is an important element for IS formation and that blockade of this interaction alters conjugate formation and stability and thus T cell activation.

To determine whether the CXCL12 effect requires chemokine binding to glycosaminoglycans (GAG) on the BM-DC surface, we

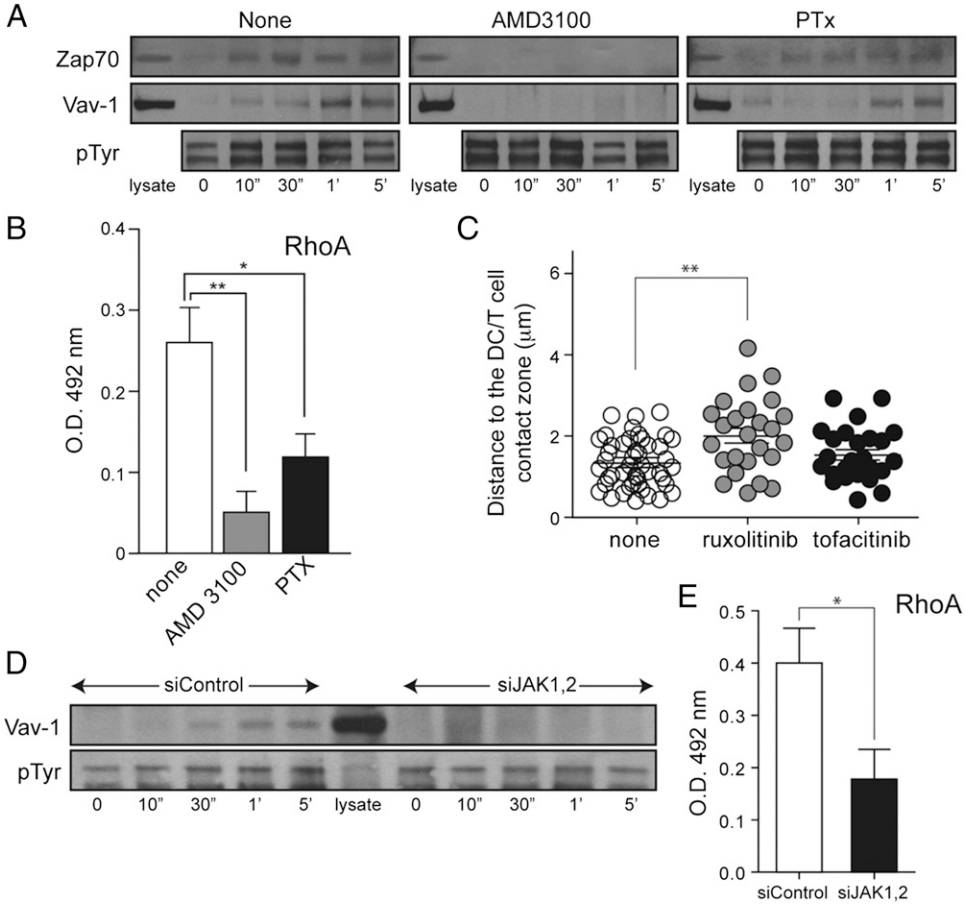

FIGURE 4. CXCL12-triggered Vav-1 and RhoA activation is involved in IS formation. (**A**) OT-II CD4$^+$ T cells, alone or treated with AMD3100 or PTx, were activated with CXCL12 at indicated times, immunoprecipitaed with anti-PTyr Ab, and cell extracts analyzed by Western blot using anti-Zap70 (*top*) or anti–Vav-1 (*middle*) Ab. As protein loading control, the membrane was reblotted with anti-Ptyr Ab (*bottom*). OT-II CD4$^+$ T cell lysate was used as positive control. Data are from one representative experiment of three performed. (**B**) OT-II CD4$^+$ T cells as in (A) were stimulated with CXCL12 (50 nM, 30 s), lysed, and evaluated for RhoA GTPase activity using G-LISA. Data show mean ± SD (n = 3 experiments). *$p \leq 0.05$, **$p \leq 0.01$, nonparametric test. (**C**) Conjugates of OT-II CD4$^+$ T cells, untreated or treated with ruxolitinib or tofacitinib, with OVA peptide–pulsed BM-DC, were fixed, permeabilized, and stained with anti–γ-tubulin mAb, followed by Cy3-goat anti-mouse IgG Ab. The figure shows quantitation of MTOC translocation measured as in Fig. 1B. Data are pooled from two independent experiments. **$p \leq 0.01$, nonparametric test. (**D**) siControl and siJAK1,2 OT-II CD4$^+$ T cells were activated with CXCL12 and immunoprecipitated with anti-PTyr Ab, and cell extracts were analyzed by Western blot using anti–Vav-1 Ab. As protein loading control, the membrane was reblotted with anti-PTyr Ab. OT-II CD4$^+$ T cell lysate was used as positive control. Data shown are from one representative experiment of two performed. (**E**) siControl and siJAK1,2 OT-II CD4$^+$ T cells were stimulated with CXCL12 (50 nM, 30 s), lysed, and evaluated for RhoA GTPase as in (B). Data show mean ± SD (n = 4 experiments). *$p \leq 0.05$, nonparametric test.

prepared BM-DC from Cxcl12$^{Gagtm/Gagtm}$ mice, which bear a mutated CXCL12 gene (*Cxcl12Gagtm*) (Supplemental Fig. 2B) that precludes CXCL12 interaction with heparin sulfate structures but does not affect CXCR4-dependent CXCL12 cell signaling (20). Conjugates of OVA peptide–loaded Cxcl12$^{Gagtm/Gagtm}$ BM-DC with OT-II CD4$^+$ T cells (ratio 1:5, 30 min, 37˚C) showed a small but significant reduction in MTOC translocation toward the contact zone that was not detected when we used BM-DC from Cxcl12$^{Gagtm/wt}$ mice (Fig. 3C). In addition, time-lapse videomicroscopy analysis of conjugation dynamics showed similar levels of short-, medium-, and long-lived contacts compared with those for wild-type (wt) BM-DC (Fig. 3D). These results concur with those using anti-CD3–coated beads and soluble CXCL12, suggesting that in vitro CXCL12–mediated IS stabilization does not require chemokine binding to GAG.

CXCL12-mediated effects on IS formation require Rho/Vav activation

Integrin activation is an essential step in IS stabilization (32); it is triggered by TCR engagement and chemokine binding to their receptors (33, 34), which require ZAP-70 phosphorylation and Rho small GTPase activation (16, 35). In static adhesion assays, CXCL12 stimulation induced OT-II CD4$^+$ T cell adhesion to ICAM-1 and potentiated that triggered by anti-CD3 stimulation (Supplemental Fig. 2C). To evaluate the CXCL12-mediated signaling cascades involved, we used OT-II CD4$^+$ T cells, untreated or treated with AMD3100 (10 μM, 30 min, 37˚C) or PTx (0.2 μg/ml, 120 min, 37˚C). CXCL12 promoted rapid ZAP-70 phosphorylation and RhoA activation; AMD3100 treatment notably decreased both processes, which were reduced to a lesser extent by PTx (Fig. 4A, *top*, 4B). The nucleotide exchange factor (GEF) Vav is also

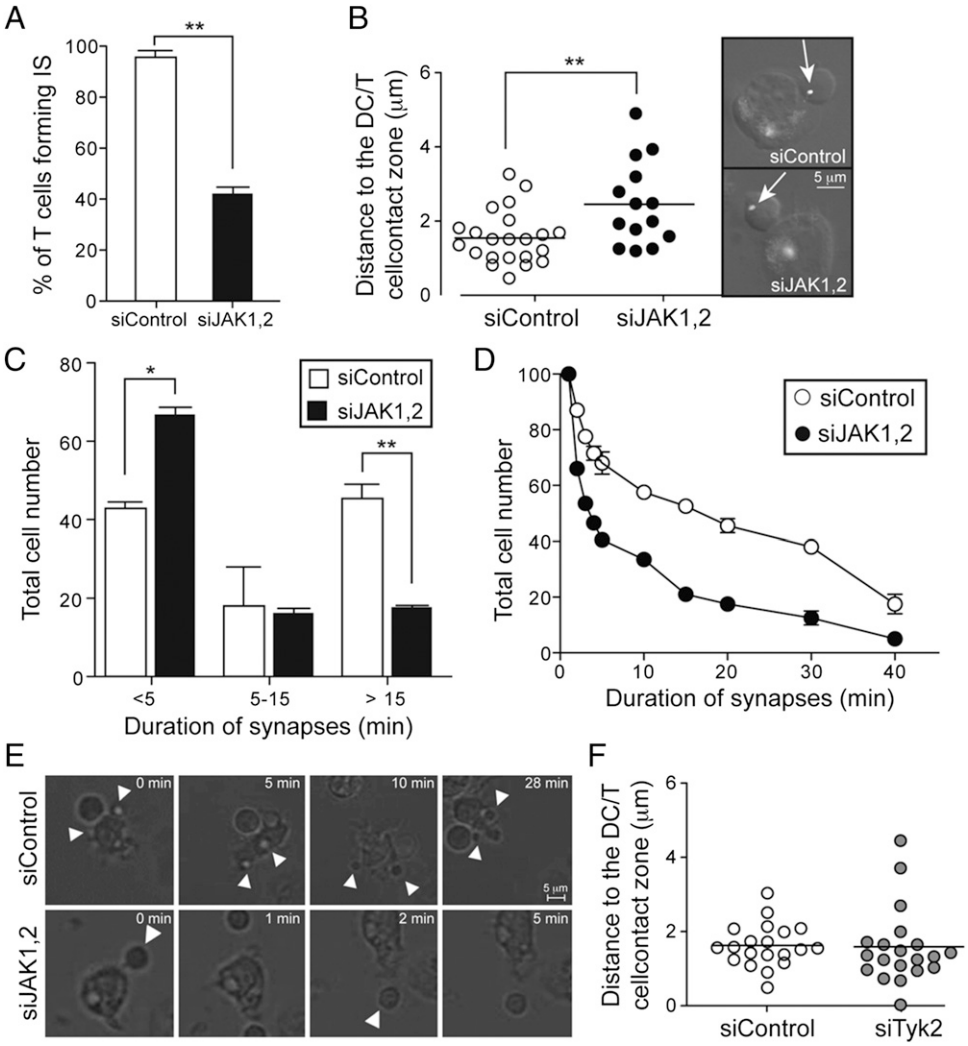

FIGURE 5. CXCL12-triggered JAK activation is involved in IS formation. (**A**) Conjugates of siControl or siJAK1,2 OT-II CD4$^+$ T cells with OVA peptide–pulsed BM-DC were paraformaldehyde fixed. F-Actin polymerization was detected using phalloidin–Alexa 488 and expressed as in Fig. 1A. $^{**}p \leq 0.01$, nonparametric test. (**B**) Conjugates as in (A) were stained with anti–γ-tubulin mAb, followed by Cy3-goat anti-mouse IgG Ab. Arrows indicate MTOC position. Scale bar, 5 μm. The figure also shows quantitation of MTOC translocation measured as the distance (in micrometers) of the MTOC to the DC/T cell contact zone. Data shown are pooled from two independent experiments. $^{**}p \leq 0.01$, nonparametric test. (**C**) BM-DC were incubated with OVA peptide and seeded onto fibronectin-coated coverslips. siControl or siJAK1,2 OT-II CD4$^+$ T cells were added to chambers. Contacts between T cells and DC were monitored by time-lapse videomicroscopy (40 min), and contact times of individual DC–T cell pairs were measured and classified as in Fig. 1D. Data pooled from three independent experiments show the percentage for each category (mean ± SD). $^{*}p \leq 0.05$, $^{**}p \leq 0.01$, nonparametric test. (**D**) Cells as in (C) were monitored by time-lapse videomicroscopy, and 200 BM-DC/OT-II CD4$^+$ T conjugates for each condition were monitored for 40 min. A representative experiment is shown of three performed. (**E**) Representative images of distinct time frames from the video recordings (Supplemental Videos 4, 5). Arrows indicate T cell/BM-DC contacts. Scale bar, 5 μm. (**F**) Conjugates of siControl or siTyk2 OT-II CD4$^+$ T cells with OVA peptide–pulsed BM-DC were paraformaldehyde fixed, stained with anti–γ-tubulin, quantified, and expressed as in (B). Data shown are pooled from two independent experiments.

associated with CXCL12-mediated LFA-1 activation (16). We found that, in CXCL12-activated CD4$^+$ T cells, Vav-1 was phosphorylated. This activation was abolished by AMD3100 treatment and was not blocked in PTx-treated cells (Fig. 4A, *middle*). A recent report suggests G protein–independent CXCL12 mediated Vav-1 phosphorylation, which links Rho small GTPase and integrin activation in a pathway that entails rapid CXCL12-mediated JAK activation (17). We thus tested the effect of specific JAK inhibitors on IS formation, including ruxolitinib, which blocks JAK1 and JAK2 activity (36) and tofacitinib, which inhibits JAK3 (37). We calibrated drug concentrations in a CXCL12-triggered OT-II CD4$^+$ T cell migration assay. Whereas ruxolitinib treatment (1.0 μM, 60 min, 37˚C) reduced cell migration by 50%, tofacitinib had no effect at any concentration tested (0.3, 1.0, or 3.0 μM, 60 min, 37˚C) (Supplemental Fig. 3A). We thus formed conjugates using untreated, ruxolitinib (1 μM)-, or tofacitinib (1 μM)-treated OT-II CD4$^+$ T cells, and OVA peptide–loaded BM-DC. γ-Tubulin staining showed significantly less MTOC translocation to the contact zone only in ruxolitinib-treated cells (Fig. 4C).

To rule out nonspecific effects because of the use of chemical inhibitors, we performed the remaining experiments using nucleofected OT-II CD4$^+$ T cells with siRNA pools for JAK1/2 (siJAK1,2) or controls (siControl) (10). Western blot analysis confirmed a sharp reduction in protein levels for both kinases (>60%; Supplemental Fig. 3B) in siJAK1,2 T cells. We also observed abrogation of CXCL12-mediated Vav-1 phosphorylation (Fig. 4D) and reduced Rho activation (Fig. 4E) in the siJAK1,2 T cells.

Naive OT-II CD4$^+$ T cells with reduced JAK levels show altered IS

To confirm the role of JAK in chemokine-mediated stabilization of the IS, we formed conjugates using siJAK1,2 OT-II CD4$^+$ T cells and OVA peptide–loaded BM-DC (30 min, 5:1 ratio, 37˚C). Whereas phalloidin staining showed F-actin accumulation cytoskeletal rearrangement at the contact zone in 94.7 ± 2.5% of siControl OT-II CD4$^+$ cells, F-actin accumulation was reduced in JAK-deficient CD4$^+$ T cells (41.3 ± 3.0%) (Fig. 5A). γ-Tubulin staining indicated a significant alteration in MTOC translocation to the contact zone in JAK-deficient cells (Fig. 5B). Finally, time-lapse videomicroscopy analysis (Supplemental Videos 4, 5) showed that JAK1/2 deficiency significantly increased the percentage of

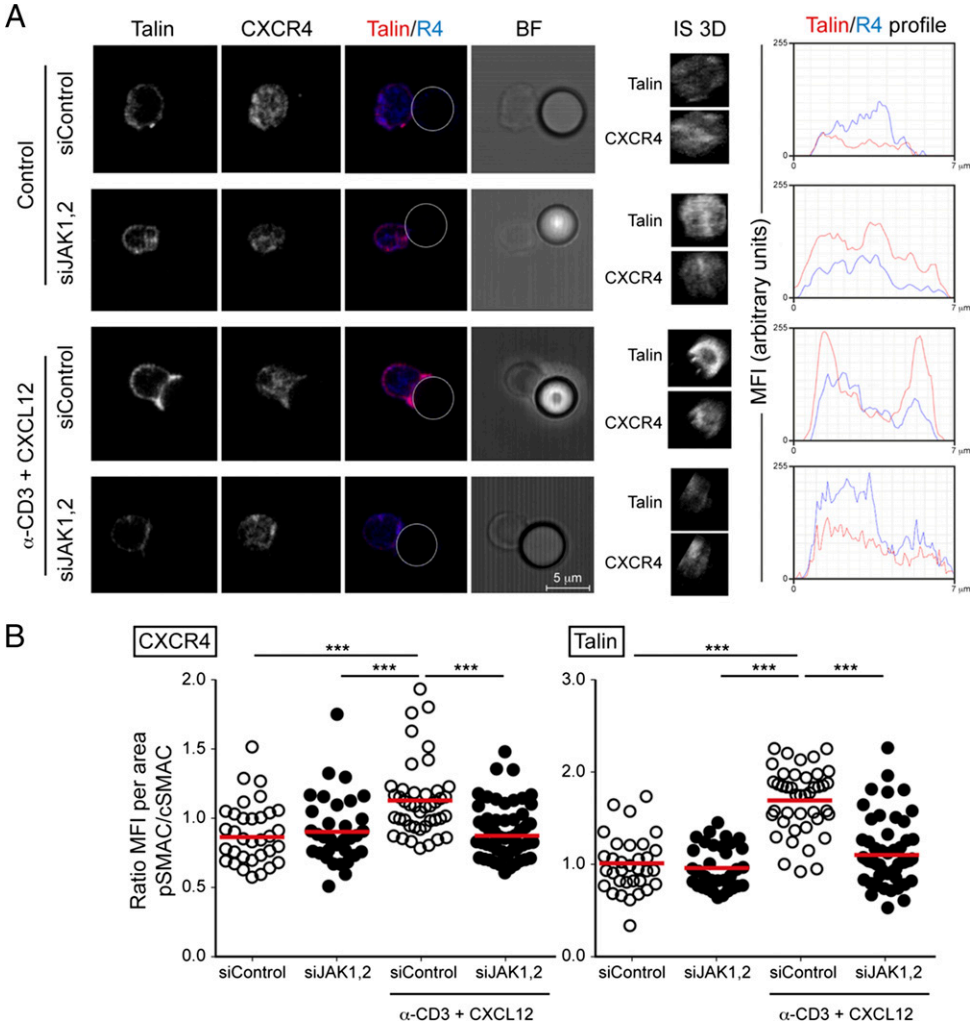

FIGURE 6. JAK contributes to IS architecture. (**A**) siControl and siJAK1/2 OT-II CD4$^+$ T cells were conjugated with anti-CD3–coated beads (CD3) or control isotype (control); CXCL12 was added where indicated and processed as in Fig. 3B. *Right*, A single slice from a confocal Z-stack showing the focus plane of the IS-like area for talin, CXCR4, and merge (talin/CXCR4). *Left*, Three-dimensional reconstruction of the IS-like area for talin and CXCR4. Histograms show protein distribution in the merged image of the IS-like reconstruction (red, talin; blue, CXCR4). (**B**) Ratio of MFI per area calculated at the pSMAC relative to the cSMAC for CXCR4 and talin at the IS-like area. MFI per area was calculated using Matlab for image analysis. Data were analyzed with a one-way ANOVA with a Kruskal–Wallis test, followed by Dunn's posttest. Means are also shown. ***$p \leq 0.001$.

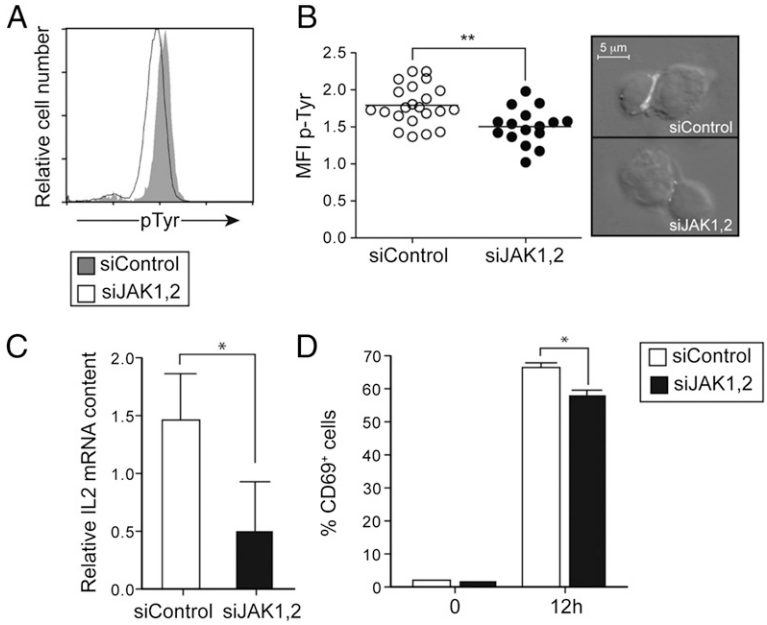

FIGURE 7. JAK blockade alters IS function. (**A**) Conjugates of siControl or siJAK1,2 OT-II CD4$^+$ T cells and OVA peptide–pulsed BM-DC were paraformaldehyde fixed, permeabilized, stained with anti–CD4-FITC and -PTyr mAb, followed by Cy3-goat anti-mouse IgG Ab, and evaluated by flow cytometry. A representative experiment is shown of three performed. (**B**) Conjugates as in (A) were stained with anti-PTyr, followed by Cy3-goat anti-mouse IgG Ab and evaluated by immunofluorescence (*right*). Scale bar, 5 μm. Quantitation of MFI of Ptyr staining using the ImageJ (*left*). Data shown are pooled from two independent experiments. $^{**}p \leq 0.01$, nonparametric test. (**C**) Quantitative real-time PCR was used to determine relative levels of IL-2 mRNA in siControl or siJAK1,2 OT-II CD4$^+$ T and OVA peptide–pulsed BM-DC conjugates (24 h, 37˚C). $^*p \leq 0.05$, nonparametric test. (**D**) Conjugates of siControl or siJAK1,2 OT-II CD4$^+$ T cells and OVA peptide–pulsed BM-DC were cultured (12 h, 37˚C), costained with anti–CD3-APC mAb and with anti–CD69-PE mAb (*right*), and evaluated by flow cytometry. Results are shown as the percentage of CD69$^+$ cells relative to total T cells (mean ± SD). Data are pooled from two independent experiments. $^*p \leq 0.05$, nonparametric test.

short-lived cell contacts (<5 min; Fig. 5C) and reduced mean contact duration (4 ± 0.3 min; Fig. 5D, 5E). To control biological specificity, we repeated the experiments using OT-II CD4$^+$ T cells nucleofected with a siRNA pool for Tyk2 (siTyk2). These cells showed >90% Tyk2 protein in Western blot with a specific Ab (Supplemental Fig. 3C). siTyk2 cells showed no alteration in MTOC translocation to the contact zone when conjugated with OVA peptide–loaded BM-DC (Fig. 5F).

Detailed analysis of IS structure on siControl and JAK-deficient T cells showed that JAK1 and JAK2 are essential for correct IS formation. siJAK1,2 and siControl OT-II CD4$^+$ T cells were allowed to conjugate with stimulating anti-CD3–coated beads plus soluble CXCL12 (50 nM) (Fig. 6). In the three-dimensional reconstruction of the IS-like area, we observed an increase in talin and CXCR4 colocalization at the pSMAC after CXCL12 addition to the anti-CD3–coated beads (histograms in Fig. 6A). Lack of siJAK1,2 nonetheless prevented correct localization of these molecules; their redistribution at the pSMAC was abolished by JAK1/2 knockdown in the presence of CXCL12 and anti-CD3 (pSMAC/cSMAC ratio < 1; graphs in Fig. 6A, 6B). Similarly, CXCL12 plus anti-CD3–mediated protein kinase Cθ redistribution to the contact site was abolished in siJAK1,2 T cells (Supplemental Fig. 4A). JAK1,2-deficient naive OT-II CD4$^+$ T cells conjugated with BM-DC showed a marked reduction in intracellular PTyr staining when evaluated by flow cytometry and by immunofluorescence (Fig. 7A, 7B). These defects led to reduced T cell activation, as shown by lower IL-2 mRNA (Fig. 7C) as well as CD69 levels (Fig. 7D, Supplemental Fig. 4B). The results indicate that, through both Gi and JAK signaling pathways, CXCL12 regulates integrin activation and IS stabilization.

Discussion

For T cell activation, cell membrane and cytoplasmic proteins must be rearranged to form the immunological synapse (32). IS formation depends on TCR-mediated signals that, in concert with costimulatory signals, cause the T cell cytoskeleton, membrane receptors, and certain signaling effectors to polarize toward the APC/T cell interface. Synapse-associated signaling also leads to spatial segregation into organized clusters of the TCR, CD28, LFA-1, and other surface molecules such as chemokine receptors (2). Some reports regard TCR recognition of specific Ags as the starting point of organelle redistribution and IS formation (38–40), and contact duration is thought to control efficient T cell activation in vivo (41). Although guidance of leukocyte trafficking is the principal role of

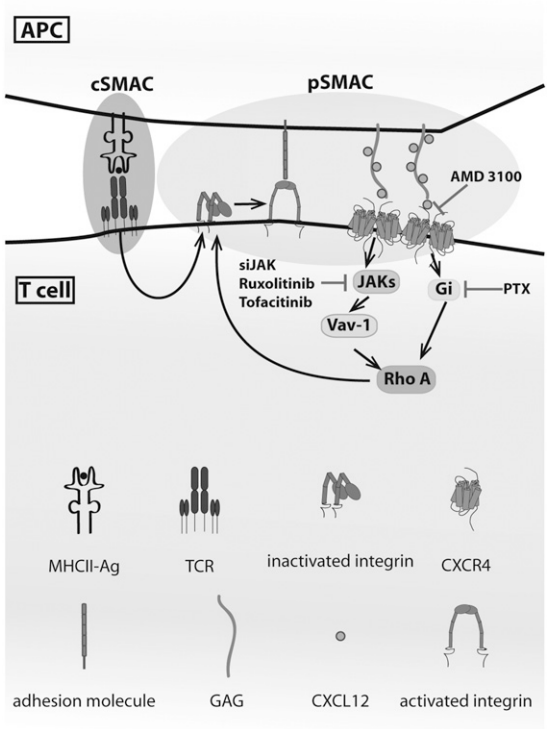

FIGURE 8. CXCL12 signaling contributes to maintenance of IS structure. TCR engagement initiates IS formation and triggers protein segregation and integrin-mediated cell adhesion. CXCL12 is retained at the APC surface by binding to GAG; this increases the local chemokine concentration at the APC:T cell contact site. CXCL12 binding to CXCR4 on T cells thus reinforces integrin activation and their binding to adhesion molecules expressed on the APC surface. The molecular mechanism includes CXCL12-mediated Gi protein and JAK activation. Both signaling pathways converge in RhoA activation, which is via Vav-1 in the case of the JAK. The scheme also indicates the inhibitors used in this study and their targets as well as a reference to cSMAC and pSMAC regions.

chemokines, they also influence T cell recognition of Ag. Chemokines direct T cell tethering to APC, which facilitates scanning and formation of stable Ag-dependent interactions (34). In addition, chemokines promote cell polarization, which increases sensitivity to Ag (42) and costimulate T cell function (5, 43).

In this study, we show that chemokines also influence IS formation and T cell activation. Membrane CXCR4 concentrates in the IS periphery; drebrin has a function in this relocation and in F-actin reorganization (6). When we blocked CXCL12 binding to CXCR4 or its signaling pathways, IS structure and duration as well as T cell activation were altered. We detected CXCL12 at the BM-DC surface but not on OT-II $CD4^+$ T cells. Our in vitro experiments using anti-CD3–coated beads nonetheless indicated that soluble CXCL12 also influences IS formation. The anti-CD3–coated bead model is often used for T cell activation analysis as it provides the geometry of the cell–cell contact with the APC and, because of the control of the stimuli used, permits dissection of the molecular pathways involved (44, 45). Although these experiments were performed in the absence of integrin ligands, we detected CXCR4 and talin in the pSMAC. Anti-CD3 Ab promotes cytoskeletal organization through Vav-1 and talin complexes (46), and Vav-1 is also involved in CXCL12-mediated talin interaction with β_1 integrins (16). Talin binding to the cytosplasmic tails of the integrins is thus one of the inside–outside mechanisms that activates integrins and enables their interaction with adhesion molecules.

IS were also formed between BM-DC prepared from $CXCL12^{Gagtm/Gagtm}$ mice and T cells. These mice have a mutant CXCL12 that cannot interact with GAG (20), impeding its retention at the cell surface. In this mouse model, we nonetheless detected a significant but small defect in MTOC translocation to the contact site, suggesting that soluble CXCL12 is less efficient than GAG-bound CXCL12. Although chemokines act as soluble mediators in vitro, in vivo they are thought to bind GAG at the cell surface (47, 48). These results coincide with data that suggest various roles for chemokines in T cell recognition of APC. Whereas some dominant chemokines such as CCL19 or CCL21 increase T cell motility on DC monolayers (49) and mediate direction and tethering (34), others like CXCL12 might stabilize cell–cell contacts. IS stability is impaired in T cells bearing warts, hypogammaglobulinemia, infections, and myelokathexis syndrome–mutant CXCR4 because of defects in receptor recruitment to the cell–cell contact area (50).

We found defective MTOC translocation in CXCR4-deficient T cells or those with altered CXCR4 function. The MTOC translocation mechanism underlies IS formation, sustains T cell signaling (29), and increases mitochondrial localization at the cell–cell contact site (51). MTOC positioning during T cell activation facilitates correct effector functions such as cytokine secretion (52) and target cell killing (53, 54). T cell treatment with the inhibitors AMD3100 or PTx or with reduced JAK1 and JAK2 expression levels significantly diminished conjugate duration; these defects might explain the IL-2 production defect as well as the reduced T cell activation and proliferation in these conditions. In T cells, CXCR4 interaction with the TCR–CD3 complex induces ZAP-70 and SLP-76 recruitment, ERK pathway activation, and cytokine synthesis (55–57). Blockade of CXCL12-mediated signaling in T cells during IS formation correlated with less cell activation, as indicated by reduced levels of IL-2 mRNA and of activation markers.

LFA-1 is reported to enhance T cell activation (58–60). Cell adhesion amplifies TCR signaling via several mechanisms, including prolonged inositol phospholipid hydrolysis (61), replenishment of intracellular Ca^{2+} stores (61), and cAMP increase (62). Chemokine-mediated integrin activation can thus contribute to IS stabilization. We nonetheless observed that PTx treatment did not completely block CXCL12-mediated RhoA activation and Vav-1 phosphorylation in a key signaling pathway involved in integrin activation by chemokines (16), which suggests G protein–dependent and –independent mechanisms. An earlier study indicated that although chemokines increase basal T cell adhesion to DC, the effect on Ag-pulsed T cells is not PTx sensitive (63). In primary T lymphocytes, we previously showed that chemokines control LFA-1– and VLA-4–mediated cell adhesion, both key processes in T cell homing (10) that involve chemokine-mediated JAK activation. A recent report implicates JAKs in CXCL12-mediated integrin activation and lymphocyte trafficking, via RhoA, Rac1, and Rap1 (17). Our findings now link JAK activation to CXCL12-mediated IS stabilization through the Vav-1/RhoA pathway. We cannot entirely rule out a JAK3 function because our experiments to evaluate the role of this kinase were only performed using a chemical inhibitor, tofacitinib. Our results nonetheless show that JAK1 and JAK2 inhibition or knockdown in T cells altered IS formation, reduced conjugate number, contact duration, and T cell activation.

Adhesion molecules, chemokines, and costimulatory and coinhibitory receptors all take part in the complex process of tuning TCR signaling and T cell activation thresholds. Whereas initiation of integrin-mediated cell adhesion is Ag dependent, our data suggest that through Gi and JAK signaling, CXCL12 helps to maintain the integrin activation at the pSMAC needed for continuous TCR signaling (Fig. 8), a finding with broad implications for cell contact–dependent communication in adaptive immunity.

Acknowledgments

We thank Drs. P. Cohen for the JAK inhibitors and F. Arenzana-Seisdedos for $Cxcl12^{Gagtm}$ mice and C. Bastos for secretarial and C. Mark for editorial assistance.

Disclosures

The authors have no financial conflicts of interest.

References

1. Delon, J., S. Stoll, and R. N. Germain. 2002. Imaging of T-cell interactions with antigen presenting cells in culture and in intact lymphoid tissue. *Immunol. Rev.* 189: 51–63.
2. Monks, C. R., B. A. Freiberg, H. Kupfer, N. Sciaky, and A. Kupfer. 1998. Three-dimensional segregation of supramolecular activation clusters in T cells. *Nature* 395: 82–86.
3. Wülfing, C., M. D. Sjaastad, and M. M. Davis. 1998. Visualizing the dynamics of T cell activation: intracellular adhesion molecule 1 migrates rapidly to the T cell/B cell interface and acts to sustain calcium levels. *Proc. Natl. Acad. Sci. USA* 95: 6302–6307.
4. Montoya, M. C., D. Sancho, G. Bonello, Y. Collette, C. Langlet, H. T. He, P. Aparicio, A. Alcover, D. Olive, and F. Sánchez-Madrid. 2002. Role of ICAM-3 in the initial interaction of T lymphocytes and APCs. *Nat. Immunol.* 3: 159–168.
5. Molon, B., G. Gri, M. Bettella, C. Gómez-Moutón, A. Lanzavecchia, C. Martínez-A, S. Mañes, and A. Viola. 2005. T cell costimulation by chemokine receptors. *Nat. Immunol.* 6: 465–471.
6. Pérez-Martínez, M., M. Gordón-Alonso, J. R. Cabrero, M. Barrero-Villar, M. Rey, M. Mittelbrunn, A. Lamana, G. Morlino, C. Calabia, H. Yamazaki, et al. 2010. F-actin-binding protein drebrin regulates CXCR4 recruitment to the immune synapse. *J. Cell Sci.* 123: 1160–1170.
7. Karpus, W. J., and N. W. Lukacs. 1996. The role of chemokines in oral tolerance: abrogation of nonresponsiveness by treatment with antimonocyte chemotactic protein-1. *Ann. N. Y. Acad. Sci.* 778: 133–144.
8. Taub, D. D., J. R. Ortaldo, S. M. Turcovski-Corrales, M. L. Key, D. L. Longo, and W. J. Murphy. 1996. Beta chemokines costimulate lymphocyte cytolysis, proliferation, and lymphokine production. *J. Leukoc. Biol.* 59: 81–89.
9. Alon, R., and M. L. Dustin. 2007. Force as a facilitator of integrin conformational changes during leukocyte arrest on blood vessels and antigen-presenting cells. *Immunity* 26: 17–27.
10. Pérez-Rivero, G., G. Cascio, S. F. Soriano, A. G. Sanz, J. S. de Guinoa, J. M. Rodríguez-Frade, R. P. Gomariz, B. L. Holgado, C. Cabañas, Y. R. Carrasco, et al. 2013. Janus kinases 1 and 2 regulate chemokine-mediated integrin activation and naïve T-cell homing. *Eur. J. Immunol.* 43: 1745–1757.

11. Shamri, R., V. Grabovsky, J. M. Gauguet, S. Feigelson, E. Manevich, W. Kolanus, M. K. Robinson, D. E. Staunton, U. H. von Andrian, and R. Alon. 2005. Lymphocyte arrest requires instantaneous induction of an extended LFA-1 conformation mediated by endothelium-bound chemokines. *Nat. Immunol.* 6: 497–506.
12. Tybulewicz, V. L. 2002. Chemokines and the immunological synapse. *Immunology* 106: 287–288.
13. Contento, R. L., S. Campello, A. E. Trovato, E. Magrini, F. Anselmi, and A. Viola. 2010. Adhesion shapes T cells for prompt and sustained T-cell receptor signalling. *EMBO J.* 29: 4035–4047.
14. Montresor, A., L. Toffali, G. Constantin, and C. Laudanna. 2012. Chemokines and the signaling modules regulating integrin affinity. *Front. Immunol.* 3: 127.
15. García-Bernal, D., A. Dios-Esponera, E. Sotillo-Mallo, R. García-Verdugo, N. Arellano-Sánchez, and J. Teixidó. 2011. RGS10 restricts upregulation by chemokines of T cell adhesion mediated by α4β1 and αLβ2 integrins. *J. Immunol.* 187: 1264–1272.
16. García-Bernal, D., M. Parmo-Cabañas, A. Dios-Esponera, R. Samaniego, D. Hernán-P de la Ossa, and J. Teixidó. 2009. Chemokine-induced Zap70 kinase-mediated dissociation of the Vav1-talin complex activates $\alpha_4\beta_1$ integrin for T cell adhesion. *Immunity* 31: 953–964.
17. Montresor, A., M. Bolomini-Vittori, L. Toffali, B. Rossi, G. Constantin, and C. Laudanna. 2013. JAK tyrosine kinases promote hierarchical activation of Rho and Rap modules of integrin activation. *J. Cell Biol.* 203: 1003–1019.
18. Henrickson, S. E., T. R. Mempel, I. B. Mazo, B. Liu, M. N. Artyomov, H. Zheng, A. Peixoto, M. P. Flynn, B. Senman, T. Junt, et al. 2008. T cell sensing of antigen dose governs interactive behavior with dendritic cells and sets a threshold for T cell activation. *Nat. Immunol.* 9: 282–291.
19. Skokos, D., G. Shakhar, R. Varma, J. C. Waite, T. O. Cameron, R. L. Lindquist, T. Schwickert, M. C. Nussenzweig, and M. L. Dustin. 2007. Peptide-MHC potency governs dynamic interactions between T cells and dendritic cells in lymph nodes. *Nat. Immunol.* 8: 835–844.
20. Rueda, P., A. Richart, A. Récalde, P. Gasse, J. Vilar, C. Guérin, H. Lortat-Jacob, P. Vieira, F. Baleux, F. Chretien, et al. 2012. Homeostatic and tissue reparation defaults in mice carrying selective genetic invalidation of CXCL12/proteoglycan interactions. *Circulation* 126: 1882–1895.
21. Inaba, K., W. J. Swiggard, R. M. Steinman, N. Romani, G. Schuler, and C. Brinster. 2009. Isolation of dendritic cells. *Curr. Protoc. Immunol.* 86: 3.7.1–3.7.19.
22. Al-Alwan, M. M., G. Rowden, T. D. Lee, and K. A. West. 2001. The dendritic cell cytoskeleton is critical for the formation of the immunological synapse. *J. Immunol.* 166: 1452–1456.
23. Maldonado, R. A., D. J. Irvine, R. Schreiber, and L. H. Glimcher. 2004. A role for the immunological synapse in lineage commitment of CD4 lymphocytes. *Nature* 431: 527–532.
24. Calabia-Linares, C., J. Robles-Valero, H. de la Fuente, M. Perez-Martinez, N. Martín-Cofreces, M. Alfonso-Pérez, C. Gutierrez-Vázquez, M. Mittelbrunn, S. Ibiza, F. R. Urbano-Olmos, et al. 2011. Endosomal clathrin drives actin accumulation at the immunological synapse. *J. Cell Sci.* 124: 820–830.
25. Vila-Coro, A. J., J. M. Rodríguez-Frade, A. Martín De Ana, M. C. Moreno-Ortíz, C. Martínez-A, and M. Mellado. 1999. The chemokine SDF-1α triggers CXCR4 receptor dimerization and activates the JAK/STAT pathway. *FASEB J.* 13: 1699–1710.
26. Nagasawa, T., S. Hirota, K. Tachibana, N. Takakura, S. Nishikawa, Y. Kitamura, N. Yoshida, H. Kikutani, and T. Kishimoto. 1996. Defects of B-cell lymphopoiesis and bone-marrow myelopoiesis in mice lacking the CXC chemokine PBSF/SDF-1. *Nature* 382: 635–638.
27. Kollet, O., S. Shivtiel, Y. Q. Chen, J. Suriawinata, S. N. Thung, M. D. Dabeva, J. Kahn, A. Spiegel, A. Dar, S. Samira, et al. 2003. HGF, SDF-1, and MMP-9 are involved in stress-induced human $CD34^+$ stem cell recruitment to the liver. *J. Clin. Invest.* 112: 160–169.
28. Ponomaryov, T., A. Peled, I. Petit, R. S. Taichman, L. Habler, J. Sandbank, F. Arenzana-Seisdedos, A. Magerus, A. Caruz, N. Fujii, et al. 2000. Induction of the chemokine stromal-derived factor-1 following DNA damage improves human stem cell function. *J. Clin. Invest.* 106: 1331–1339.
29. Martín-Cófreces, N. B., J. Robles-Valero, J. R. Cabrero, M. Mittelbrunn, M. Gordón-Alonso, C. H. Sung, B. Alarcón, J. Vázquez, and F. Sánchez-Madrid. 2008. MTOC translocation modulates IS formation and controls sustained T cell signaling. *J. Cell Biol.* 182: 951–962.
30. Mittelbrunn, M., G. Martínez del Hoyo, M. López-Bravo, N. B. Martín-Cofreces, A. Scholer, S. Hugues, L. Fetler, S. Amigorena, C. Ardavín, and F. Sánchez-Madrid. 2009. Imaging of plasmacytoid dendritic cell interactions with T cells. *Blood* 113: 75–84.
31. Martín-Cófreces, N. B., D. Sancho, E. Fernández, M. Vicente-Manzanares, M. Gordón-Alonso, M. C. Montoya, F. Michel, O. Acuto, B. Alarcón, and F. Sánchez-Madrid. 2006. Role of Fyn in the rearrangement of tubulin cytoskeleton induced through TCR. *J. Immunol.* 176: 4201–4207.
32. Grakoui, A., S. K. Bromley, C. Sumen, M. M. Davis, A. S. Shaw, P. M. Allen, and M. L. Dustin. 1999. The immunological synapse: a molecular machine controlling T cell activation. *Science* 285: 221–227.
33. Mueller, K. L., M. A. Daniels, A. Felthauser, C. Kao, S. C. Jameson, and Y. Shimizu. 2004. Cutting edge: LFA-1 integrin-dependent T cell adhesion is regulated by both ag specificity and sensitivity. *J. Immunol.* 173: 2222–2226.
34. Friedman, R. S., J. Jacobelli, and M. F. Krummel. 2006. Surface-bound chemokines capture and prime T cells for synapse formation. *Nat. Immunol.* 7: 1101–1108.
35. Huang, J., D. Tilly, A. Altman, K. Sugie, and H. M. Grey. 2000. T-cell receptor antagonists induce Vav phosphorylation by selective activation of Fyn kinase. *Proc. Natl. Acad. Sci. USA* 97: 10923–10929.
36. Verstovsek, S., H. Kantarjian, R. A. Mesa, A. D. Pardanani, J. Cortes-Franco, D. A. Thomas, Z. Estrov, J. S. Fridman, E. C. Bradley, S. Erickson-Viitanen, et al. 2010. Safety and efficacy of INCB018424, a JAK1 and JAK2 inhibitor, in myelofibrosis. *N. Engl. J. Med.* 363: 1117–1127.
37. Changelian, P. S., M. E. Flanagan, D. J. Ball, C. R. Kent, K. S. Magnuson, W. H. Martin, B. J. Rizzuti, P. S. Sawyer, B. D. Perry, W. H. Brissette, et al. 2003. Prevention of organ allograft rejection by a specific Janus kinase 3 inhibitor. *Science* 302: 875–878.
38. Mempel, T. R., S. E. Henrickson, and U. H. Von Andrian. 2004. T-cell priming by dendritic cells in lymph nodes occurs in three distinct phases. *Nature* 427: 154–159.
39. Miller, M. J., O. Safrina, I. Parker, and M. D. Cahalan. 2004. Imaging the single cell dynamics of $CD4^+$ T cell activation by dendritic cells in lymph nodes. *J. Exp. Med.* 200: 847–856.
40. Martín-Cófreces, N. B., F. Baixauli, and F. Sánchez-Madrid. 2014. Immune synapse: conductor of orchestrated organelle movement. *Trends Cell Biol.* 24: 61–72.
41. Celli, S., F. Lemaître, and P. Bousso. 2007. Real-time manipulation of T cell-dendritic cell interactions in vivo reveals the importance of prolonged contacts for $CD4^+$ T cell activation. *Immunity* 27: 625–634.
42. Negulescu, P. A., T. B. Krasieva, A. Khan, H. H. Kerschbaum, and M. D. Cahalan. 1996. Polarity of T cell shape, motility, and sensitivity to antigen. *Immunity* 4: 421–430.
43. Flanagan, K., D. Moroziewicz, H. Kwak, H. Hörig, and H. L. Kaufman. 2004. The lymphoid chemokine CCL21 costimulates naive T cell expansion and Th1 polarization of non-regulatory $CD4^+$ T cells. *Cell. Immunol.* 231: 75–84.
44. Ilani, T., C. Khanna, M. Zhou, T. D. Veenstra, and A. Bretscher. 2007. Immune synapse formation requires ZAP-70 recruitment by ezrin and CD43 removal by moesin. *J. Cell Biol.* 179: 733–746.
45. Tsun, A., I. Qureshi, J. C. Stinchcombe, M. R. Jenkins, M. de la Roche, J. Kleczkowska, R. Zamoyska, and G. M. Griffiths. 2011. Centrosome docking at the immunological synapse is controlled by Lck signaling. *J. Cell Biol.* 192: 663–674.
46. Fischer, K. D., Y. Y. Kong, H. Nishina, K. Tedford, L. E. Marengère, I. Kozieradzki, T. Sasaki, M. Starr, G. Chan, S. Gardener, et al. 1998. Vav is a regulator of cytoskeletal reorganization mediated by the T-cell receptor. *Curr. Biol.* 8: 554–562.
47. Middleton, J., A. M. Patterson, L. Gardner, C. Schmutz, and B. A. Ashton. 2002. Leukocyte extravasation: chemokine transport and presentation by the endothelium. *Blood* 100: 3853–3860.
48. Proudfoot, A. E., T. M. Handel, Z. Johnson, E. K. Lau, P. LiWang, I. Clark-Lewis, F. Borlat, T. N. Wells, and M. H. Kosco-Vilbois. 2003. Glycosaminoglycan binding and oligomerization are essential for the in vivo activity of certain chemokines. *Proc. Natl. Acad. Sci. USA* 100: 1885–1890.
49. Kaiser, A., E. Donnadieu, J. P. Abastado, A. Trautmann, and A. Nardin. 2005. CC chemokine ligand 19 secreted by mature dendritic cells increases naive T cell scanning behavior and their response to rare cognate antigen. *J. Immunol.* 175: 2349–2356.
50. Kallikourdis, M., A. E. Trovato, F. Anselmi, A. Sarukhan, G. Roselli, L. Tassone, R. Badolato, and A. Viola. 2013. The CXCR4 mutations in WHIM syndrome impair the stability of the T-cell immunologic synapse. *Blood* 122: 666–673.
51. Baixauli, F., N. B. Martín-Cófreces, G. Morlino, Y. R. Carrasco, C. Calabia-Linares, E. Veiga, J. M. Serrador, and F. Sánchez-Madrid. 2011. The mitochondrial fission factor dynamin-related protein 1 modulates T-cell receptor signalling at the immune synapse. *EMBO J.* 30: 1238–1250.
52. Kupfer, A., T. R. Mosmann, and H. Kupfer. 1991. Polarized expression of cytokines in cell conjugates of helper T cells and splenic B cells. *Proc. Natl. Acad. Sci. USA* 88: 775–779.
53. Kupfer, A., G. Dennert, and S. J. Singer. 1985. The reorientation of the Golgi apparatus and the microtubule-organizing center in the cytotoxic effector cell is a prerequisite in the lysis of bound target cells. *J. Mol. Cell. Immunol.* 2: 37–49.
54. Stinchcombe, J. C., D. C. Barral, E. H. Mules, S. Booth, A. N. Hume, L. M. Machesky, M. C. Seabra, and G. M. Griffiths. 2001. Rab27a is required for regulated secretion in cytotoxic T lymphocytes. *J. Cell Biol.* 152: 825–834.
55. Kremer, K. N., A. Kumar, and K. E. Hedin. 2007. Haplotype-independent costimulation of IL-10 secretion by SDF-1/CXCL12 proceeds via AP-1 binding to the human IL-10 promoter. *J. Immunol.* 178: 1581–1588.
56. Kumar, A., T. D. Humphreys, K. N. Kremer, P. S. Bramati, L. Bradfield, C. E. Edgar, and K. E. Hedin. 2006. CXCR4 physically associates with the T cell receptor to signal in T cells. *Immunity* 25: 213–224.
57. Ticchioni, M., C. Charvet, N. Noraz, L. Lamy, M. Steinberg, A. Bernard, and M. Deckert. 2002. Signaling through ZAP-70 is required for CXCL12-mediated T-cell transendothelial migration. *Blood* 99: 3111–3118.
58. Doucey, M. A., D. F. Legler, M. Faroudi, N. Boucheron, P. Baumgaertner, D. Naeher, M. Cebecauer, D. Hudrisier, C. Rüegg, E. Palmer, et al. 2003. The β_1 and β_3 integrins promote T cell receptor-mediated cytotoxic T lymphocyte activation. *J. Biol. Chem.* 278: 26983–26991.
59. Graf, B., T. Bushnell, and J. Miller. 2007. LFA-1-mediated T cell costimulation through increased localization of TCR/class II complexes to the central supramolecular activation cluster and exclusion of CD45 from the immunological synapse. *J. Immunol.* 179: 1616–1624.
60. Suzuki, J., S. Yamasaki, J. Wu, G. A. Koretzky, and T. Saito. 2007. The actin cloud induced by LFA-1-mediated outside-in signals lowers the threshold for T-cell activation. *Blood* 109: 168–175.
61. Randriamampita, C., G. Boulla, P. Revy, F. Lemaitre, and A. Trautmann. 2003. T cell adhesion lowers the threshold for antigen detection. *Eur. J. Immunol.* 33: 1215–1223.
62. Conche, C., G. Boulla, A. Trautmann, and C. Randriamampita. 2009. T cell adhesion primes antigen receptor-induced calcium responses through a transient rise in adenosine 3′,5′-cyclic monophosphate. *Immunity* 30: 33–43.
63. Bromley, S. K., and M. L. Dustin. 2002. Stimulation of naive T-cell adhesion and immunological synapse formation by chemokine-dependent and -independent mechanisms. *Immunology* 106: 289–298.